Comprehensive Bridge Deck Deterioration Mapping of Nine Bridges by Nondestructive Evaluation Technologies

Final Report
January 2011

Sponsored by
Iowa Highway Research Board (IHRB Project SPR-NDEB(90)--8H-00)
Iowa Department of Transportation
Federal Highway Administration

Disclaimer

The contents of this report reflect the views of the authors, who are responsible for the facts and the accuracy of the information presented herein. The opinions, findings, and conclusions expressed in this publication are those of the authors and not necessarily those of the sponsors.

The sponsors assume no liability for the contents or use of the information contained in this document. This report does not constitute a standard, specification, or regulation. The sponsors do not endorse products or manufacturers. Trademarks or manufacturers' names appear in this report only because they are considered essential to the objectives of the document.

Statement of Non-Discrimination

Federal and state laws prohibit employment and/or public accommodation discrimination on the basis of age, color, creed, disability, gender identity, national origin, pregnancy, race, religion, sex, sexual orientation or veteran's status. If you believe you have been discriminated against, please contact the Iowa Civil Rights Commission at 800-457-4416 or Iowa Department of Transportation's affirmative action officer. If you need accommodations because of a disability to access the Iowa Department of Transportation's services, contact the agency's affirmative action officer at 800-262-0003.

1. Report No. Project SPR-NDEB(90)--8H-00	**2. Government Accession No.**	**3. Recipient Catalog No.**
4 Title and Subtitle Comprehensive Bridge Deck Deterioration Mapping of Nine Bridges by Nondestructive Evaluation Technologies		**5 Report Date** January 2011 **6 Performing Organization Code**
7. Author(s) Nenad Gucunski (PI), Francisco Romero, Sabine Kruschwitz, Ruediger Feldmann, Hooman Parvardeh		**8 Performing Organization Report No.**
9 Performing Organization Name and Address Rutgers, The State University of New Jersey Center for Advanced Infrastructure and Transportation 100 Brett Road, Piscataway, NJ 08854		**10 Work Unit No. (TRAIS)** **11 Contract or Grant No.**
12 Sponsoring Agency Name and Address U.S. Department of Transportation Federal Highway Administration 400 7th Street SW, HIPT-20 Washington, DC 20590 Iowa Highway Research Board Iowa Department of Transportation 800 Lincoln Way Ames, IA 50010		**13 Type of Report and Period Covered** Final Report **14 Sponsoring Agency Code**
15 Supplementary Notes		

16 Abstract

The primary objective of this research was to demonstrate the benefits of NDT technologies for effectively detecting and characterizing deterioration in bridge decks. In particular, the objectives were to demonstrate the capabilities of ground-penetrating radar (GPR) and impact echo (IE), and to evaluate and describe the condition of nine bridge decks proposed by Iowa DOT. The first part of the report provides a detailed review of the most important deterioration processes in concrete decks, followed by a discussion of the five NDT technologies utilized in this project. In addition to GPR and IE methods, three other technologies were utilized, namely: half-cell (HC) potential, electrical resistivity (ER), and ultrasonic surface waves (USW) method. The review includes a description of the principles of operation, field implementation, data analysis, and interpretation; information regarding their advantages and limitations in bridge deck evaluations and condition monitoring are also implicitly provided.. The second part of the report provides descriptions and bridge deck evaluation results from the nine bridges. The results of the NDT surveys are described in terms of condition assessment maps and are compared with the observations obtained from the recovered cores or conducted bridge deck rehabilitation. Results from this study confirm that the used technologies can provide detailed and accurate information about a certain type of deterioration, electrochemical environment, or defect. However, they also show that a comprehensive condition assessment of bridge decks can be achieved only through a complementary use of multiple technologies at this stage,. Recommendations are provided for the optimum implementation of NDT technologies for the condition assessment and monitoring of bridge decks.

17 Key Words bridge deck, concrete, delamination, corrosion, modulus, NDT, GPR, impact echo, half-cell potential, electrical resistivity, surface waves, condition assessment		**18 Distribution Statement**	
19 Security Classification (of this report)	**20 Security Classification (of this page)**	**21 No. of pages** 194	**22 Price**

CONTENTS

LIST OF FIGURES AND TABLES

ACKNOWLEDGMENTS

The authors would like to thank the Iowa Department of Transportation for funding this project. The authors are especially grateful to Sandra Larson, the Iowa DOT's Research Bureau manager, for initiating the project, and to Ahmad Abu-Hawash and Mark Dunn for providing assistance throughout its duration. A number of individuals from Iowa DOT, especially Jerry McClain, Tom Porter and Norbert Kotlers, organized or facilitated excellent conditions for data collection and expeditious coring operations. Their assistance is gratefully acknowledged. Finally, the authors are grateful to Erica Erlanger and Michaela Anderson for their assistance during data collection, analysis and editing of the final report.

EXECUTIVE SUMMARY

The development and implementation of capabilities for the rapid rebuilding, nondestructive inspection and performance monitoring for bridges is even more critical than for most other components of the transportation network. This is especially true for bridge decks, for which providing means for rapid, nondestructive and accurate condition assessment and performance monitoring will make a tremendous difference in the financial resources spent for not only their renewal and also the frequency and duration of traffic interruptions. The data collected from nondestructive testing (NDT) of bridge decks should complement other information in developing a full understanding of its lifecycle costs, deterioration mechanisms, and the effectiveness of preservation techniques at various stages of the aging process, and most importantly, prevent premature and unexpected failure.

The dominant practice by state DOTs in nondestructive evaluation of bridge decks is by visual inspection and use of simple methods like chain drag and hammer sounding. Modern nondestructive evaluation of concrete and concrete bridge decks exploits various physical phenomena (acoustic, seismic, electric, electromagnetic, thermal imaging, etc.) to detect and characterize specific deterioration processes or defects. In general, all the techniques utilize an approach where the objective is to learn about the characteristics of the local medium within a given structure by understanding the response of the medium to the applied excitation.

The primary objective of the conducted research is to demonstrate benefits of the use of NDT technologies in effective detection and characterization of deterioration in bridge decks. The research activity has the following two specific objectives:

1. Demonstrate capabilities of NDT, ground penetrating radar (GPR) and impact echo (IE) in particular, in condition assessment and monitoring of bridge decks, and
2. Evaluate and describe condition of nine bridge decks proposed by Iowa DOT.

This report consists of two main parts. The first part provides a detailed review of most important deterioration processes in concrete decks, followed by the discussion of five NDT technologies utilized in this project. While the proposed plan for the project included evaluation by GPR and IE methods, three other technologies were utilized for the duration of the project, namely: half-cell (HC) potential, electrical resistivity (ER) and ultrasonic surface waves (USW) method. The review includes the description of principles of operation, field implementation, data analysis and interpretation, and implicitly provides information regarding their advantages and limitations in practical bridge deck evaluation and condition monitoring. The second part of the report provides description and results of evaluation of decks of the nine bridges. The results of NDT surveys are described in terms of condition assessment maps and in all cases compared with the observations obtained from the recovered cores or conducted bridge deck rehabilitation.

A number of technologies can provide detailed and accurate information about a certain type of deterioration, electrochemical environment, or defect. For example, impact echo provides reliable and comprehensive delamination detection and characterization with respect to the degree of delamination or other internal damage (cracking/splitting). Or, electrical resistivity and half-cell potential provide accurate and detailed information regarding corrosive environment and presence and intensity of an active corrosion environment. Finally, ground penetrating radar

provides overall deterioration condition mapping, which in many instances correlates well to rebar corrosion or developed delamination, but this technology also can be used to estimate concrete cover, or determine reinforcement and duct layout and depth. However, comprehensive condition assessment of bridge decks, at this stage, can be achieved only through a complementary use of multiple technologies.

One of several very important considerations in the implementation of NDT technologies is that of speed. Evaluation of bridge decks with the NDT technologies used in this project can be conducted at rates of about 2500 to 3000 square feet per work day for a 2 by 2 foot survey grid, where the workday is represented by about 6 hours actual data collection. The ranking of the used NDT technologies by speed would be: GPR, ER, HC, IE and USW. To improve the speed of data collection on bridges where traffic interruptions (lane closures) have to be minimized, the described technologies provide two options. The first option is using multiple devices, which would require larger workforce. The second option is using multiple probes, which is feasible for all technologies. Implementing such measures could probably bring the speed above 7000 square feet per day.

One consideration for further increasing data collection speed which always sacrifices some accuracy would be to use an air-coupled GPR (vehicle deployed system) instead of ground-coupled antennas (sensors). Discussion on some of the differences between air-coupled and ground-coupled GPR methodologies is included both in the main body of the report and the Appendix. For the purpose of this research, both air-coupled and ground-coupled GPR systems were used on several of the Iowa DOT decks, using the most accurate and reliable deployments known for each.

NDT technologies require minimal to advanced training, expertise and experience. Three technologies: GPR, IE and USW require moderate to significant level of training, especially in data analysis and interpretation. Two technologies: HC and ER require minor to moderate level of training. Ease of use in data collection of the presented technologies can be described as moderate to high. Finally, the initial investment for the acquisition of the described technologies, as used for this project, can be described as moderate and on the order of $200,000.

In summary, NDT technologies are powerful tools for comprehensive condition assessment of reinforced concrete elements, and concrete bridge decks in particular. The approach to bridge deck evaluation and monitoring by NDT technologies should be by targeting the use of a group of complementary technologies. The selection of those should be based primarily on the accuracy of information they provide regarding the most important deterioration and defect types. Those technologies should also meet or exceed certain criteria of the Iowa DOT regarding the speed, ease of use and cost. Last, an attempt to incorporate the NDT results requires considering how they can best augment existing visual inspection schedules, ratings and recommendations. This allows the best of existing visual inspections and currently available, multiple NDT technologies to be integrated to improve the decision-making processes involved with asset management.

CHAPTER 1 BACKGROUND

PROBLEM STATEMENT AND RESEARCH OBJECTIVE

Iowa DOT, like many other State DOTs, is faced with the need of identifying and deploying means for rapid, nondestructive and accurate condition assessment and performance monitoring of bridge decks. Finding the right technologies will make a tremendous difference in the financial resources spent for their renewal and frequency and duration of traffic interruptions, especially considering the fact that in most cases bridge deck maintenance and repair constitutes 50-80% of all the expenditures for bridges. The data collected from nondestructive testing (NDT) of bridge decks should complement other information in understanding of its lifecycle costs, deterioration mechanisms, and the effectiveness of preservation techniques at various stages of the aging process, and most importantly, prevent premature and unexpected failure.

One of the biggest challenges of nondestructive evaluation (NDE) of concrete bridge decks, and concrete in general, is that it is more complex than evaluation of metals. It is more complex for several reasons, but primarily due to the composite material nature of concrete and a combination of material preparation and placement variables: batching, mixing and field quality controls; non-uniformity of aggregate supplies; mix design or variations in selection and dosing of admixtures, etc. At the same time, while the nondestructive evaluation of metal members dominantly concentrates on detection, characterization and monitoring of cracks, concrete decks display a whole suite of deterioration processes and defects that require a diverse set of techniques for their detection and monitoring. The complexity of concrete deck evaluation and monitoring and the need for its nondestructive evaluation was best illustrated in a series of SHRP reports in early nineties (S-323, S-325, S-326, S-327, S-330), the NCHRP Synthesis 333 Report on concrete bridge deck performance (2004) and by the recent request for proposals from Strategic Highway Research Program 2 (SHRP 2) "Nondestructive Testing to Identify Concrete Bridge Deck Deterioration." The SHRP 2 RFP clearly points to a consensus of the engineering community that additional effort needs to be placed towards validation of the existing NDE methods for bridge deck evaluation and identification of methods of the future. While there is this need for more methodological and comprehensive validation of NDT technologies, as well as improvement of their speed and resulting interpretation, some of the NDT technologies have been advanced to the level that enables comprehensive evaluation of bridge decks. The proposed work concentrated on bridge deck evaluation by two technologies: ground penetrating radar (GPR) and impact echo (IE). However, three other technologies were deployed in the evaluation, namely: half-cell potential (HCP), electrical resistivity (ER) and ultrasonic surface waves (USW).

There were two main objectives of the project:

1. To demonstrate capabilities of NDT, GPR and IE in particular, in condition assessment and monitoring of bridge decks, and
2. To evaluate and describe condition of the nine bridge decks proposed by Iowa DOT.

The research team approached the proposed evaluation beyond a typical production level bridge deck evaluation. The team utilized the project as a unique opportunity to, in cooperation with Iowa DOT, conduct as detailed and comprehensive as possible evaluation. Such an

evaluation was recognized as having the highest potential benefit to the Iowa DOT for both future selection of technologies of the highest interest, and for raising the confidence level regarding the long term application of the selected technologies in project and network level bridge deck evaluation. Therefore, the conducted work relied on the multi NDT technology data collection, advanced data analysis and interpretation, and wherever it was possible comparisons/validations with cores and comprehensive documentation of the condition found during the deck rehabilitation. As illustrated in Figure 1, the ultimate goal of the project is to demonstrate the use of NDT/NDE technologies that will both motivate and enable Iowa DOT to incorporate them into its evaluation and monitoring practices. That will ultimately contribute to the achievement of broader goals of the agency for a reliable and optimum bridge asset management.

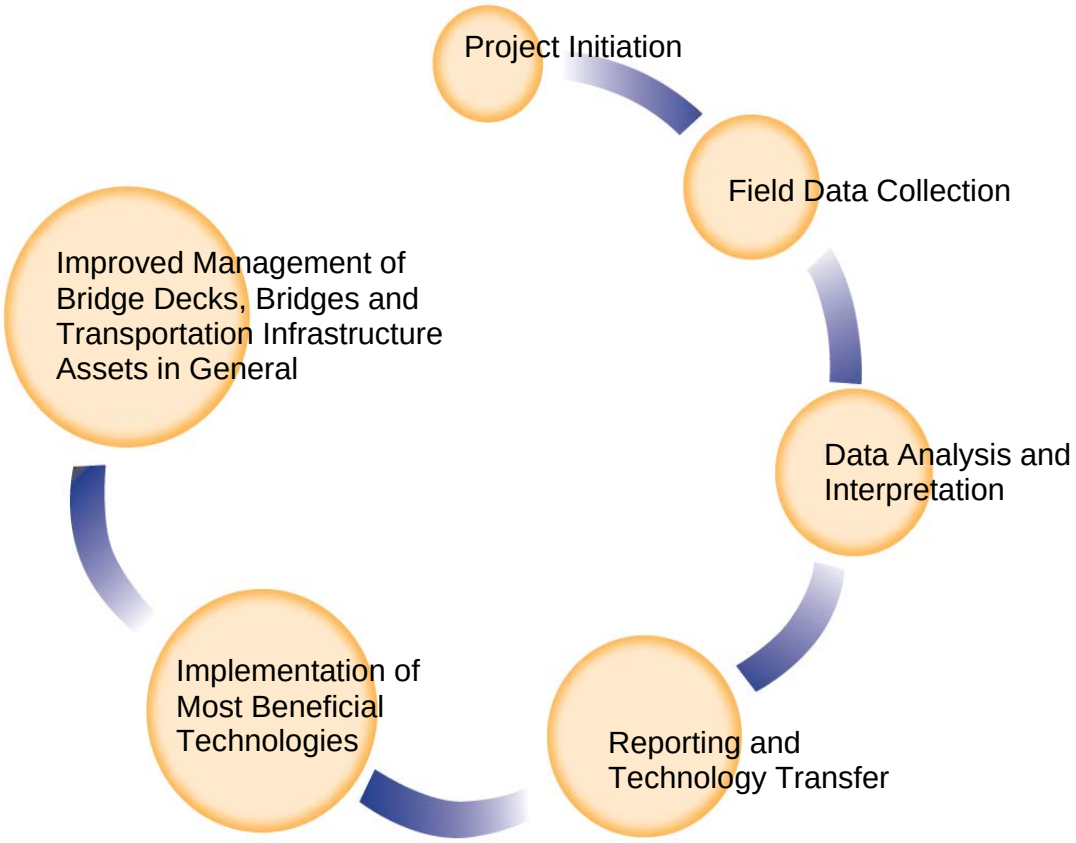

Figure 1. Project contribution to longer lasting and more economically managed bridges.

This report contains a description of the work and results of a comprehensive survey of nine bridge decks in Iowa. The nine bridge decks were investigated for the purpose of determining the location and extent of deteriorated concrete prior to future rehabilitation or replacement. All the decks are Portland cement (PC) concrete decks with or without dense low-slump concrete overlay. The overall work plan for the project is divided into three main tasks, as illustrated by how the report is organized and communicated: The scope of the first task concentrated on providing a brief description of the most common deterioration processes in

concrete bridge decks as well as NDT technologies and techniques used for detection and characterization of these types of deterioration. The scope of the second task included collection, analysis and interpretation of data collected on nine bridge decks. Finally, the third project task involved reporting and dissemination of project results (technology transfer).

CHAPTER 2 RESEARCH APPROACH

GENERAL

The dominant practice by state DOTs in evaluation of bridge decks is by visual inspection and use of simple nondestructive methods like chain drag and hammer sounding. Modern nondestructive evaluation of concrete and concrete bridge decks has its origins in geophysics. A number of techniques introduced exploit various physical phenomena (acoustic or seismic, electric, electromagnetic, thermal, etc.) to detect and characterize specific deterioration processes or defects. In general, all the techniques utilize an approach where the objective is to learn about the characteristics of the medium from the response of the medium to the applied excitation. The following sections provide a review of deterioration processes in concrete decks, followed by the discussion of the most important NDT technologies and techniques for concrete decks. A list is presented in Table 1, showing NDT techniques with their application in defect and deterioration detection used during this project. All the listed techniques are described in terms of their principle of operation, types of defects that can be detected and characterized, and their advantages and limitations with respect to their technical abilities and practical application strengths to meet challenges of transportation agencies. As it will be presented, some of the techniques provide a very good overview of the condition of a deck, while some a very good insight into the causes of the deteriorated condition.

Table 1. NDT Techniques and Their Application in Bridge Deck Deterioration Detection

NDT Method	Defect/Deterioration Applications	Other Applications
Impact Echo (IE)	Deck delamination detection and characterization.	Detection of grouting conditions in ducts.
Ultrasonic Surface Waves (USW)	Measurement of degradation of elastic moduli.	Vertical crack depth estimates.
Ground Penetrating Radar (GPR)	Detection of deterioration caused by corrosion, indirect delamination detection	Deck thickness and concrete cover measurement, rebar and tendon duct location
Eddy Current	Measurement of the concrete cover.	
Half-Cell Potential	Measurement of probability of active rebar corrosion.	
Electrical Resistivity (ER)	Likelihood of corrosive environment; also, demonstrated correlation to corrosion rate.	

Acoustic/Seismic	Electro-Magnetic	Electro-Chemical

For any bridge owner, it will be of interest to be able to assess the condition of a bridge deck at all stages of a particular type of deterioration. This is illustrated in Figure 2 by a typical sequence of rebar corrosion induced delamination and spalling. Also, based on the literature review and the experience of the research team, NDT technologies and procedures most effectively used in identification of deterioration at specific time stages during a deck's degradation are illustrated in the figure. Clearly, a single technology might not always be an answer.

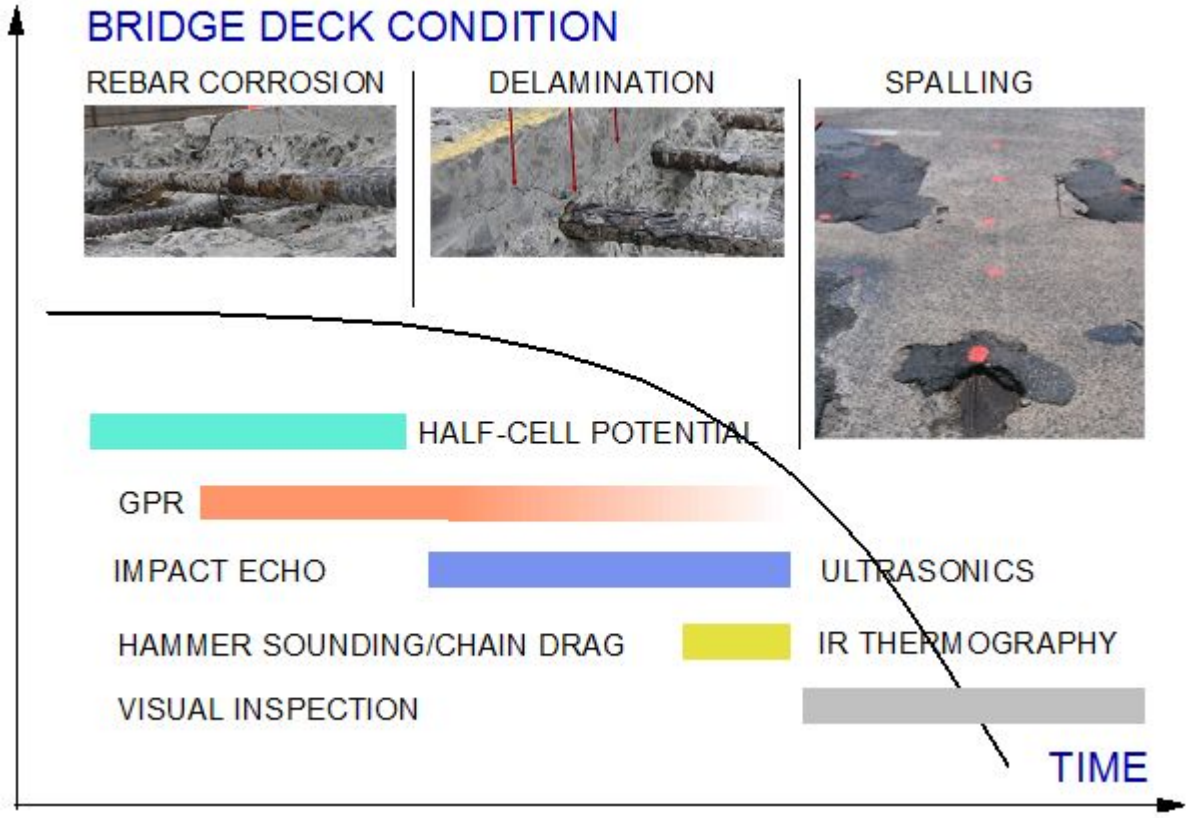

Figure 2. Corrosion induced bridge deck deterioration vs. NDT technologies.

DETERIORATION PROCESSES

Reinforced concrete structures like bridges, highways and other infrastructure facilities experience loss of integrity over time caused by poor initial quality, damage due to deicing salts, overloading, freeze-thaw cycle induced stresses, fatigue and above all corrosion of rebars. According to the Federal Highway Administration (FHWA), the cost of repairing and replacing deteriorating highway bridges in the U.S. is estimated at approximately $100 billion (Lemieux, *et al.*, 2005; El-Safty, 2008).

Different kinds of deterioration that are observed in reinforced concrete structures will be outlined in the following sections. In general, deterioration can be classified into three main categories: chemical, physical and biological. The most frequent phenomena identified by (Bien *et al.,* 2007) are summarized in Table 2.

Table 2: Overview of Degradation Mechanisms (Bien et al., 2007).

Chemical deterioration	Physical deterioration	Biological deterioration
- corrosion - carbonation - alkali-silica reaction - crystallization - leaching - oil and fat influence - salt and acid actions	- creep - fatigue - influence of high temperature - modification of founding conditions - overloading - shrinkage - water penetration	- accumulation of dirt and rubbish - living organisms activity

Deterioration of Bridge Decks

Reinforcing steel embedded in concrete is naturally protected from corrosion by the high alkalinity of the cement-based materials. However, as reinforced concrete structures aged it became apparent that some environments are more severe than originally thought. Depending on construction and design, bridges especially have been observed to have lower service lives and higher maintenance than envisaged (Broomfield *et al.*, 2002). It had been expected that an adequately thick concrete cover itself would be a satisfactory protection against corrosion. Concrete has a very high alkalinity and a pH of around 12.5, which causes the formation of a passive and non-corroding protective oxide film on the steel surface. It can be understood from the equilibrium/pH diagrams that these oxide films with the thickness of a few atomic layers can only exist between pH 9 and 13. Steel alloys or salts solved in the water can change this pH range so that one usually assumes passivity at pH 9.5 or higher.

Rebar Corrosion

ACI 222R (2001) describes the process of corrosion of metals in concrete. During the process, concrete allows electrolytic conduction and hence, the flow of ions from anodes to cathodes. Once the oxide film is destroyed, an electric cell is formed along the steel or between steel bars and the electrochemical process or corrosion begins. Some steel areas along the bar become anodes discharging current in the electric cell and iron goes into solution. Other steel areas receive current so hydroxide ions are formed, known as cathodes. A schematic of the electrical principle is shown in Figure 3.

Chloride ions typically penetrate from the surface into a bridge deck resulting in a higher salt concentration and more negative electrical potential at the top reinforcing steel layer than at the bottom layer. If the electrical potentials between the more negative (anodic) top steel and relatively more positive (cathodic) bottom steel create a current flow, this is referred to as a corrosion macro-cell (Figure 4, a). Likewise, if the concentration of chlorides along one single rebar is not uniform in the top mat, these differences can result in the formation of micro-cells (Figure 4, b).

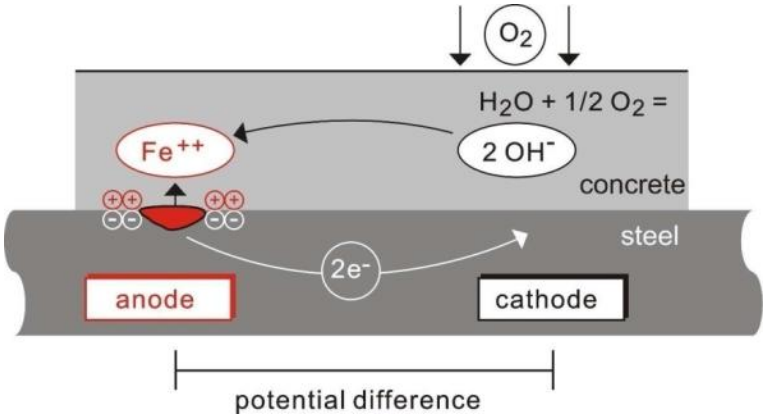

Figure 3. Principle of steel corrosion in concrete with oxygen availability (after Baumann, 2008).

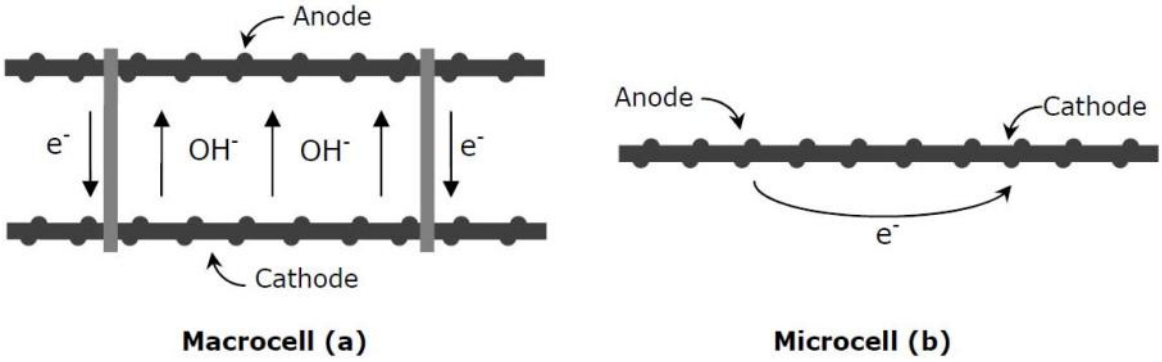

Figure 4: Corrosion in macro-cells (a) and micro-cells (b) (from Pincheira et al., 2008).

Chemically the corrosion process can be divided into anodic and cathodic reactions:

Anodic reaction (oxidation) : $Fe \rightarrow Fe\ 2^{+} + 2e^{-}$

Cathodic reaction (reduction) : $O_2 + 2H_2O + 4e^{-} \rightarrow 4\ OH^{-}$

The iron in the steel reinforcement and abundant hydroxide ions available from calcium hydroxide present in early age concrete form together ferric hydroxide (Fe_2O_3), as part of a thin surface film that tightly adheres to the steel reinforcement. As long as this film is not disturbed, it will keep the steel passive and protected from corrosion in this highly alkaline environment. Once exposed to de-icing salts, chloride ions from these penetrate into the concrete structure, eventually reach the steel and accumulate beyond a concentration level where the protective film is destroyed. The steel begins to actively and continually corrode, when oxygen and moisture are present and continue to be replenished in the steel-concrete interface. Steel reinforcement continues under these conditions to further oxidize and build accumulation of rust, or iron oxide. The consequential deterioration comes from the fact that rust takes up 3 to 4 times more volume than the original material undergoing corrosion. The corrosion process causes internal stress, cracking, delamination and eventually spalling over the reinforcing steel (Nawy, 2008). An example of a severely corroded rebar and delamination of the overlying concrete is shown in Figure 5. Depending on the progress of the deterioration, corroded rebars can have a significantly decreased capacity than sound rebars since splintered grains and pits, within the previously uniform rebar surface and cross-section, are generated during a non-uniform corrosion process.

These newly formed heterogeneities in the rebar cross-section and surface uniformity create stress peaks. Only the remaining sound part of the bar is therefore considered as effective for carrying stress.

Figure 5: Corroded rebar in a deteriorated drill core (left) and delamination in a bore hole in a deck (right).

The two most common steel corrosion processes are the chloride induced pitting corrosion and carbonation. Bridge engineers can often distinguish the two corrosions types after a visual inspection. The locally confined chloride pitting corrosion leaves almost black rust marks. Red or brownish colored rust stains indicate carbonation based corrosion. The rate of corrosion is dependent on numerous factors including the composition of the metal as well as humidity, temperature, water pH, and exposure to pollution and salt. Wet and dry cycles accelerate the corrosion process. Studies have shown that the corrosion rate is the highest during the spring season and lowest during the winter. These rates can vary by a factor of about four or five times during the year (Smith and Virmani, 1996; Page *et al.*, 1996). It is generally important to do corrosion testing on both the reinforcing steel and the concrete. Continuity between reinforcing steel elements also needs be verified as a part of the assessment process.

Epoxy Coated Steel Reinforcement. Many transportation departments started using epoxy-coated steel (ECS) reinforcement in the 1970s. Theoretically, such coatings prevent moisture and salts from reaching the steel and hence, inhibit corrosion. Today epoxy-coated rebars are widely used, however, as many authors outlined, they are not a perfect solution either (Brown, 2002; Clemeña, 2002; Pape and Fanous, 1998; Rosenberg, 1999; Sohanghpurwala and Scannell, 1999 and Wioleta *et al.*, 2000). There are three main reasons for that: a) due to improper fabrication or handling, the coating often gets damaged, b) delaminations or debonding may occur between the coating and the steel, and c) some bridge decks with epoxy coated reinforcing bars have developed an excessive amount of full depth cracks during early curing. As a result, the exposed areas, or the debonded coatings, and the full depth cracks allow chloride ions, moisture and oxygen to reach the steel and start the corrosion process (Chiaw and Harik, 2006).

Effects of Salts. After the 1950s more US states instituted a "bare pavement" policy and the use of deicing salts increased rapidly. Krauss and Rogalla (1996) cited that as much as 2.5 - 5 tons per lane per mile of deicing chemicals have been reportedly used on bridge decks in many US states every year. Moreover, sea water salts in concrete structures near the coast line have a similar deteriorating effect. When dissolved in water sodium chloride forms a highly corrosive solution of sodium ions and chloride ions. The very mobile chloride ions penetrate through the concrete pores and where they reach the reinforcing steel they attack the passive layer. The smaller the attacked area, the higher is the emerging electrical potential drop in this area. The steel gets pitted and can even disintegrate completely. The chloride ions are not consumed during this reaction, but remain fully effective afterwards. Although this damage can also occur without deicing salts, their presence accelerates processes like corrosion of reinforcing steel and surface scaling during freeze-thawing cycles (Guide to Durable Concrete, 1997). Very often material experts are brought for inspection when the damage is already advanced (visible on the surface) due to the spalling effect of iron's corrosion products.

Chloride ions can penetrate the passive film on the reinforcement and combine with iron ions to form a soluble iron chloride complex. This complex can carry the iron into the concrete, where it later gets oxides and forms rust. Nawy (2008) reports that as little as 0.15% water-soluble chloride by weight of cement is sufficient to initiate corrosion of embedded steel under some conditions (Grimm, 1997). This threshold is, however, largely discussed in the literature. Other authors report values of up to 0.40% to be harmful (Bjegovic, 2001). For black unprotected bars, the acceptable amount of salts present is lower than for epoxy coated ones (Clear, 1975 and 1976; Saugues *et al.*, 1995). The cause of the deteriorating impact of chloride ions is that they chemically react with the steel and form iron chloride ($FeCl_3$). In contact with water this turns into iron hydroxide (rust) with a volume three to four times larger than the volume of ordinary steel.

When salt ions in concrete do not penetrate all the way to the steel reinforcement, they are mostly innocuous and only affect the outer appearance of a structure. Salt efflorescence does not impair the mechanical properties or durability of built environment. Water in the pore structure of a concrete object solves soluble salts from the cement and carries them to the surface. When the water evaporates the salts crystallize and build efflorescence. So called primary efflorescence can develop right from the mixing water. Secondary efflorescence can develop months later after water ingress along cracks or joints. Usually they form uniform stains and scaling, where the salts accumulate. When salts crystallize within the pore space, it is often referred to as crypto- or subefflorescence. This process can be very damaging and often cause scaling and spalling. However, as long as the scaling process does not expose the rebar, it does not actually impair the mechanical properties of a structure. Still, they give by all means indications about possible damage and an increased open porosity (cracks).

Even though chlorides are usually understood to be the biggest concern for salt induced corrosion, it must be noted that there are also a number of publications on sulfate related problems. Sulfates also exist in both seawater and deicing agents. They are equally aggressive and have actually just as detrimental effect on concrete as chlorides. Traditionally, engineers have viewed sulfate attack as a problem mostly associated with substructure, industrial environment and maritime locations (Vittery and Pearson-Kirk, 2008). By using a special sulfate

resisting concrete they thought they could easily prevent this problem. But, researchers have shown that even "sulfate resistant" Portland cements (SRPC), that have very high absorption and porosity properties, are just as vulnerable as conventional cements. Sulfate attack of concrete normally takes two different forms, chemical and physical. Initially the sulfate attacks concrete chemically, altering the microstructure of concrete and pore size distribution of the matrix. The by-products of these reactions are volumetrically larger than the original materials, thereby causing expansive stresses (cracks) within the concrete. This cracking thus increases the rate of sulfate entry into the concrete therefore accelerating the rate of deterioration. This combined chemical and physical attack results in a progressive loss of strength and mass with time.

Concrete Deterioration

Concrete deterioration occurs in most cases due to physical and only to a lesser extent due to chemical alterations of the structure (Braml and Keuser, 2009). Chemical attacks can be divided into solving ones, for example after a contact with bases, salts or organic fats, or expanding ones, where the attacking compounds crack the concrete after chemical reactions, as described in the previous sections. The most prominent example of physical impairment is freeze and thaw deterioration.

Freeze and Thaw. The medium to high use of deicing substances in the winter introduces about 1kg of salts into $1m^2$ of a horizontal bridge deck area used for traffic. Even though other deicing agents have been investigated, none has been found that does not harm the concrete in any way and is just as effective. The main freeze-thaw related damage mechanisms are hydraulic pressure increase, temperature shock and freezing of single concrete layers. The repeated freezing and thawing of the topmost layers damages the concrete structure. When water freezes in concrete it will expand around 9% in volume and generate hydraulic pressures in the capillaries and pores of the cement paste and aggregates. Once the pressure exceeds the tensile strength of the concrete, it will rupture and, if exposed to several freeze-thaw cycles, ultimately cause extensive deterioration in the form of cracking, scaling or crumbling (Figure 6).

Deicing salts decrease the freezing point of water and let ice and snow melt. This salt induced melting process draws warmth from the concrete (chills it) and can act like a cold shock. The pore water freezes and creates internal tensile stresses at the concrete surface on the order of 1-4 N/mm^2. If these stresses exceed the tensile strength properties of concrete, it cracks (first) at the microscale. The more the composite structure of the concrete gets damaged, the more it loses its compressive strength properties. The resistance of hardened concrete to freezing water deterioration has been significantly improved by the use of entrained air. Air entrainment prevents frost damage and today is required for all concretes that are exposed to freezing and thawing or deicing chemicals (Nawy, 2008).

Layered freezing is the last of the known temperature induced deterioration mechanisms. It is caused by the deicing salt concentration and temperature gradient within the concrete (high salt content and low temperature at the surface – low salt content and higher temperature in the interior part). The surface layer, because of its low temperature, and a layer at a certain depth (because of its low salt content) will freeze first. The part between these two layers freezes only

at even lower temperatures. If this happens, it can generate such high pressures on the surface layer that can spall or crack concrete.

Figure 6. Crumbling and scaling of a concrete surface after freeze and thaw cycles (Nuernberger, 1995).

Carbonation

Carbonation is a chemical reaction in which atmospheric carbon dioxide (CO_2 in air or water) reacts with compounds in the hardened cement paste and forms carbonates, primarily calcium carbonate and water. The carbonation process can be divided into two steps (Gruebl 2001):

Phase 1: Water molecules react with carbon dioxide to form carbonic acid:

$$H_2O + CO_2 \rightarrow 2H^+ + CO_3^{2-}$$

Phase 2: Carbonic acid reacts with the alkaline compounds of the concrete (cement paste) to carbonate:

$$Ca(OH)_2 + CO_2 \rightarrow CaCO_3 + H_2O$$

This reaction lowers the pH of concrete from 12.5 to between 8 and 9 and increases the drying shrinkage. The carbonation rate is largely a function of paste permeability, temperature, relative humidity, and the concentration of carbon dioxide in the surrounding atmosphere (Nawy, 2008). The depth, to which the reaction is complete, is commonly called the carbonation front. As a consequence of the depletion of $Ca(OH)_2$, the passivation of the steel becomes impaired. The carbonation front can be seen quite clearly by spraying a freshly fractured surface with a pH indicator, e.g. phenolphthalein (Figure 7). Phenolphthalein reacts with $Ca(OH)_2$ and forms a red/violet substance. Not carbonated areas remain hence, without color.

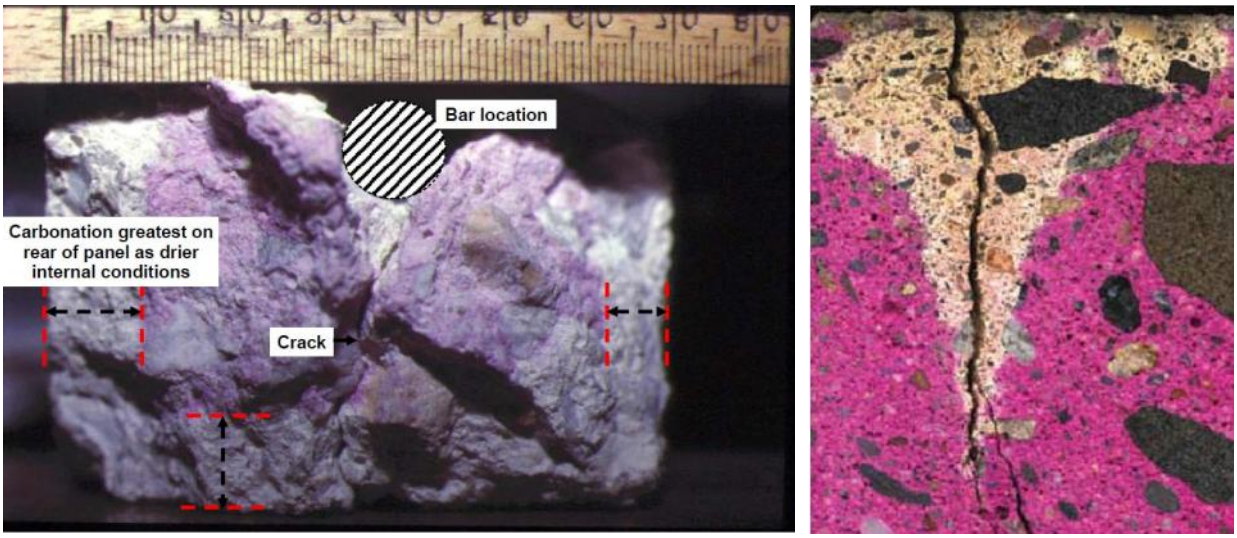

Figure 7: Carbonation depth around the bottom edge of a 7 year old precast concrete panel measured with Phenolphthalein (left) (http://www.pcte.com.au) and example of concrete carbonation in the vicinity of a vertical crack (from Jana and Erlin, 2007).

The penetration depth of a carbonation front is described by Fick's law and roughly proportional to the square root of time.

$$d_k = a\left(\frac{w/c}{f_c} - b\right)\sqrt{t}$$

with d_k being the carbonation depth, w/c the water-cement ratio, f_c the compression strength and t the time. The variables a and b reflect all other properties that affect the carbonation process. For example, concrete structures that generally are exposed to rain undergo a lesser carbonation process, because the water prevents carbon dioxide from penetrating into the structure (Hilsdorf *et al.*, 1997). If a building with a 50 year design life has a minimum cover of 20 mm, a cover reduction of only 2 mm reduces the expected life by 10 years. In an extreme case reducing the cover to 10 mm reduces the life from 50 years to 12 years. Moreover, carbonation is also largely a function of the density (resistance to diffusion) of concrete; so consequently, the water-cement ratio (w/c) plays an important role also. For concrete with w/c ratio higher than 0.6 the air permeability increases exponentially and hence, the carbonation depth gets larger (Gruebl, 2001).

Alkali-Silica-Reaction (ASR)

The ASR is an expansive reaction between reactive silica phases in aggregates and alkali hydroxides in the concrete pore solution. It produces a gel (silica gel) that swells in the presence of water causing internal and external cracking and hence, a decrease in structural safety. The reaction is going on in two steps:

Alkali + silica → gel reaction product
Gel reaction product + moisture → expansion

The alkalis potassium and sodium come mostly from cement, although in some cases they can also originate from aggregates, pozzolans, admixtures or the mixing water as well as other external sources like deicers or soils. The expansion of concrete generates two main problems: 1) the deformation of the structure impairing the serviceability and 2) the development of a crack network through the structure (Figure 8). The progression of the ASR can, however, be very different. It mostly depends on temperature, moisture level, exposure to sun/rain, reinforcement and external stresses, etc. Most of the damage is reported to occur in the concrete surface layer. Very aggressive reactants can induce cracks and surface damage within a year, whereas slowly reactive aggregates can take more than 20 years to induce visible deterioration. According to most bridge engineers, ASR deterioration is slow and therefore, the risk of unexpected, catastrophic failure due to this reaction is low. But, it must not be forgotten that surface cracking induced by ASR can easily cause severe serviceability problems and enable other deterioration processes such as freeze-thaw, deicer or sulfate damage. Testing of beams, coming from ASR affected bridge decks in the Netherlands, have shown a loss in shear capacity due to a decrease in tensile strength (Siemes and Bakker, 2000; Uijl *et al*., 2000; Uijl and Kaptijn, 2002). For most of all those elements without a three dimensional reinforcement grid, like plate type reinforced concrete bridge decks, ASR can lead to a substantial loss of structural safety (Bakker and Postema, 1999).

Both normal and high strength concrete is susceptible to ASR. To avoid these problems, Nawy (2008) suggests that:

- potentially reactive aggregates should be avoided (most effective approach),
- fly ash, silica fume, natural pozzolans or blended hydraulic cements should be used to control possible ASRs, and
- the level of soluble alkalis in the concrete should be reduced.

In some areas lacking the supply of proven nonreactive aggregates, the most effective approach of avoiding aggressive substances may not be an option for concrete producers.

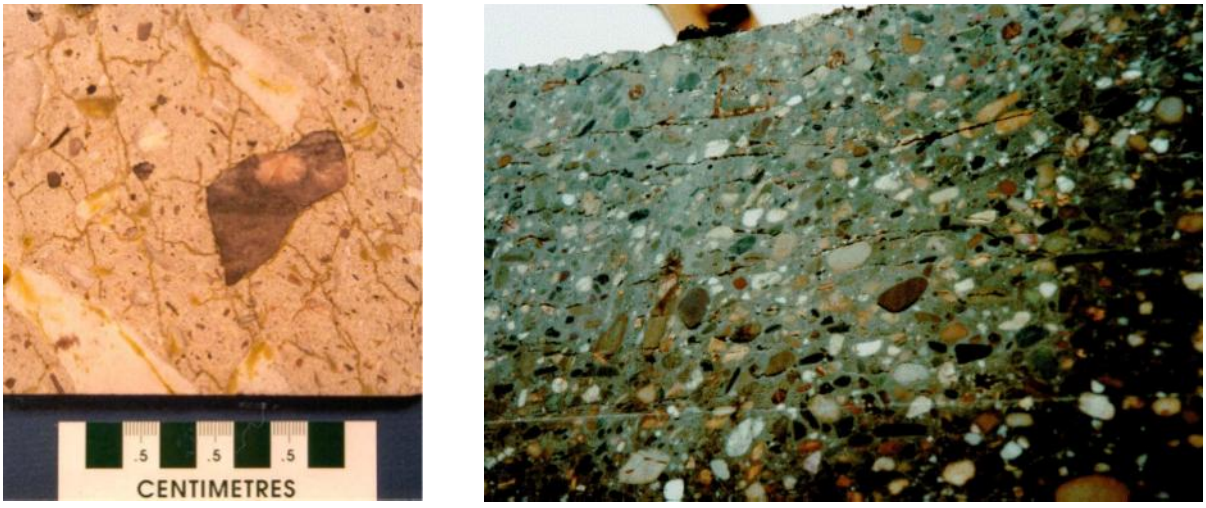

Figure 8: Thin and isotropic cracks (highlighted with epoxy impregnation) in ASR damaged dam concrete (left) (from Rivard and Saint-Pierre, 2009) and extensive internal cracking in a vertical cross-section of a concrete bridge deck (right) (Bakker and Postema, 2003).

Mechanical Stress, Overloading, Cracks

Various surveys have indicated that highway bridges are subjected to vehicular load levels and combinations far in excess of those for which they were designed. But, both reinforcement corrosion and the high vehicle loads have the largest influences on cracking and reduction of the structural capacity of the element in question or the bridge as the whole. Most common causes of cracks and their characteristics are summarized in Table 3.

Table 3: Causes of Cracks, Characteristics and Time of Development (after Brueckner, 2008)

	Cause of cracks	Crack characteristics	Time of development
1	Setting of fresh concrete	longitudinal cracks on top of the first steel layer, crack widths several mm, crack depth up to several cm	within the first hours after placement of concrete
2	Plastic shrinkage of the concrete	shallow cracks, occur often on plane structures, no preference of direction, crack width several mm, crack depth very low	like 1
3	Hydration heat	shallow cracks as a consequence of splitting and bending, crack width up to 1 mm	within the first days after placing of the concrete
4	Exterior temperature changes	splitting and bending cracks, crack width up to several mm	any time
5	Change of support conditions	splitting and bending cracks, crack width up to several mm	any time
6	Traffic load	hair line, bending, splitting or shear cracks	any time
7	Freeze-thaw cycles	mostly cracks along the reinforcement, spalling of water filled cavities	after freezing
8	Steel corrosion	cracks along the reinforcement and in edges, spalling	after several years

As long as cracks do not exceed tolerable widths, no damage has to be expected in the structure. The larger and deeper the cracks become, the more the steel protective character of concrete diminishes. Longitudinal cracks in the bridge superstructure should be particularly alarming, since they indicate loss of bonding between concrete and a very likely heavily corroded reinforcement. Hazardous substances can penetrate into the concrete and attack the passive layer of the steel; macro-elements build up diminishing later the stiffness and strength of the structure. Thresholds for crack widths are 0.3 mm in normal concrete structures and 0.2 mm in those that are subjected to deicing processes (Krieger 2006).

ACOUSTIC/ SEISMIC NDT TECHNOLOGIES

Seismic ultrasonic methods in general and impact echo in particular can overcome the inability of traditional methods of evaluation of bridge decks (e.g., chain dragging or hammer sounding) to detect early signs of delamination. Three ultrasonic seismic techniques, namely ultrasonic body-wave (UBW), ultrasonic surface-wave (USW) and impact echo (IE), have been successfully implemented in the evaluation of bridge decks (Sansalone, 1993; Sansalone and Streett 1997; Algernon and Wiggenhauser, 2006; Gucunski *et al.*, 2000 and 2008).

Impact Echo

Impact echo method can detect and assess delamination at various deterioration stages, evaluate vertical cracks, detect and characterize conditions around rebars and tendon ducts, and can be used as a material evaluation tool. While the IE evaluation is often conducted using an assumed compression wave velocity of concrete, some integrated seismic/ultrasonic devices provide complementary wave velocity determination to minimize this limitation. That velocity determination can be concurrently used as a material quality evaluation drawing its principles from pavement evaluation (Nazarian and Yuan, 1997; Rojas *et al*., 1999).

Impact echo methods have its origins in the pioneering work of Carino and Sansalone in mid eighties at the National Institute of Standards and Technology (NIST). Their research on the use of stress-wave based methods in detection of defects in concrete became known as the *impact-echo method* (Sansalone and Carino, 1986). This pioneering work was expanded and continued for more than a decade at Cornell University under direction of Mary Sansalone, developing a breadth of knowledge about the fundamental aspects and applications of impact echo, as summarized in a book by Sansalone and Streett (1997), papers by Sansalone (1997) and Carino (2001), and thesis of Peralta (1997). The research results at NIST and Cornell were an impetus for the development of a standard test method on the application of the impact-echo method in 1998 (ASTM C 1383). Sansalone (1997) described the reasons for slow adoption of the method by the agencies in the need for significant expertise in principles of acoustics, need for significant training and experience, and lack of user-friendly systems and clear instructions. A very recent comprehensive summary of IE testing was provided by Schubert and Koehler (2008).

The following sections discuss the use of impact echo and complementary ultrasonic/seismic methods in bridge deck evaluation. The discussion concentrates on the background of the method, field implementation, rationale behind the deck condition grading with respect to corrosion induced delamination and the current practice of data presentation.

Principles of IE and Complementary Ultrasonic Seismic Testing

Seismic/ultrasonic methods enable the evaluation of material properties and structural defects by measuring the velocity of propagation of elastic waves and by observing various wave propagation phenomena, such as reflections, refractions and dispersions. Of particular interest for bridge deck evaluation are three seismic/ultrasonic techniques: UBW, USW and IE. UBW and USW techniques are used to measure velocities of propagation of compression (P) and surface

(R) waves, respectively. These velocities can then be well correlated to elastic moduli. Thus, UBW and USW methods can be described as material quality control techniques. In contrast, the IE technique is primarily used to identify position of wave reflectors in a bridge deck. Thus, it is used to detect defects, objects and anomalies in the structure and can be thought of as a diagnostic tool in defect identification and characterization.

Application of UBW, USW and IE techniques in the bridge deck evaluation is illustrated in Figure 9. In the first part of the evaluation, the UBW and USW tests are conducted using an impact source and two receivers. The UBW technique is used to measure the velocity of propagation of the compression (P) waves. By measuring the travel time of the P-wave between two receivers and the first wave arrivals, the P-wave velocity (V_P) is calculated. Because it is often difficult to identify P-wave arrivals in an automated way, a more reliable procedure to estimate the P-wave velocity is through measurement of the surface (Rayleigh or R) wave velocity using the USW test, as described later. Once the R-wave velocity is determined, it can be well correlated to both compression and shear (S) wave velocities, as well as to the Young's and shear moduli.

In the second part of the evaluation, the IE test is conducted using an impact source and a single nearby receiver. Because of a significant contrast in rigidity of concrete and air, the elastic wave is practically fully reflected off the bottom of the deck back to the deck surface. The frequency of the reflection, called return frequency, can be identified in the response spectrum of the recorded signal. Finally, the depth of the reflector, in this case the deck thickness T, can be obtained from the return frequency and the previously determined P-wave velocity, as illustrated in Figure 9.

Factor β in the equation is related to section shape and to a plate like structure which is equal to 0.96. Lin and Sansalone (1997) described the correction as a result of an excitation of a particular mode of vibration in the plate, which they called the thickness mode. Later works by Gibson and Popovics (2005) related the factor to the zero group velocity frequency of the first symmetrical Lamb mode in a plate structure. Sansalone (1997) summarized the value of the shape factor β for different structural sections: plates, rectangular and circular columns, etc.

While the primary objective of the IE testing is to determine the dominant reflectors according to the approximate relationship described in Figure 9, a unique thickness or depth of the reflector can be correlated to every component of the frequency spectrum. This is illustrated in Figure 10 by a frequency spectrum, and the corresponding thickness spectrum. The thickness spectrum enables simple data interpretation, because positions of the dominant and secondary peaks clearly describe the pattern of energy partitioning, and thus the degree of delamination. Spectra for a set of points along a single test line can be combined to form spectral surfaces. As shown in the same figure, frequency spectra for one test line on a bridge deck is combined to form a frequency spectral surface and is converted into a corresponding thickness spectral surface. The frequency spectral surface emphasizes the presence of shallow delaminations, while the thickness spectrum emphasizes the presence of apparent deep reflectors along with deck zones in a serious condition that will be discussed in the following section (Gucunski et al., 2006). Because the thickness spectral surface represents a more natural choice for data viewing,

a properly selected nonlinear depth scale can provide a well-balanced image for identification of all detected reflectors.

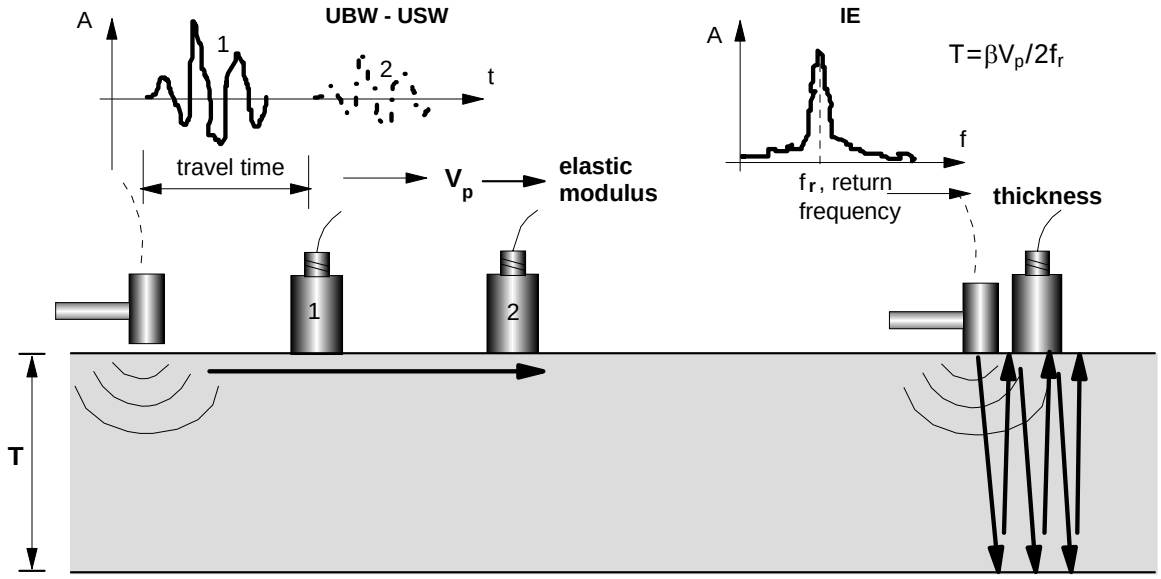

Figure 9. Measurement of bridge deck elastic modulus and thickness by USW and IE methods.

Current Practice of IE Condition Assessment with Respect to Delamination

In the case of a delaminated deck, reflections of the P-wave occur at shallower depths, causing a shift in the response spectrum towards higher frequencies. Chen and Sansalone (1995a, 1995b) have shown that a 25 μm wide crack with a sufficient length (area) can be detected by the IE method. Depending on the extent and continuity of the delamination, the partitioning of energy of elastic waves may vary. Different subjective grades can be assigned to that particular section of a deck as a part of the condition assessment process. This is illustrated in Figure 11.

In the case of a sound deck (good condition), a distinctive peak in the response spectrum corresponding to the full depth of the deck can be observed. This is illustrated by two sets of spectra under the cross section of the bridge deck. The upper spectrum in each of the four grading categories within the figure represents a schematic of the expected spectrum (graphic of spectrum shown in black), while the lower spectrum is taken from actual field testing (spectrum graphic shown in blue).

Initial delamination (fair condition), which is described as occasional separations between the two deck zones, can be identified through the presence of two distinct peaks, indicating energy partitioning from two dominant wave propagation patterns. The first peak corresponds to the reflections from the bottom of the deck, while the second corresponds to the reflections from the delamination. Lin and Sansalone (1996) have shown that IE method can be used to evaluate qualitatively the amount of unbounded fraction of an area between two deck sections. Progressed delamination (poor condition) is characterized by a single peak at a frequency corresponding to a reflector depth that is shallower than the deck thickness, indicating that little or no energy is being propagated towards the bottom of the deck.

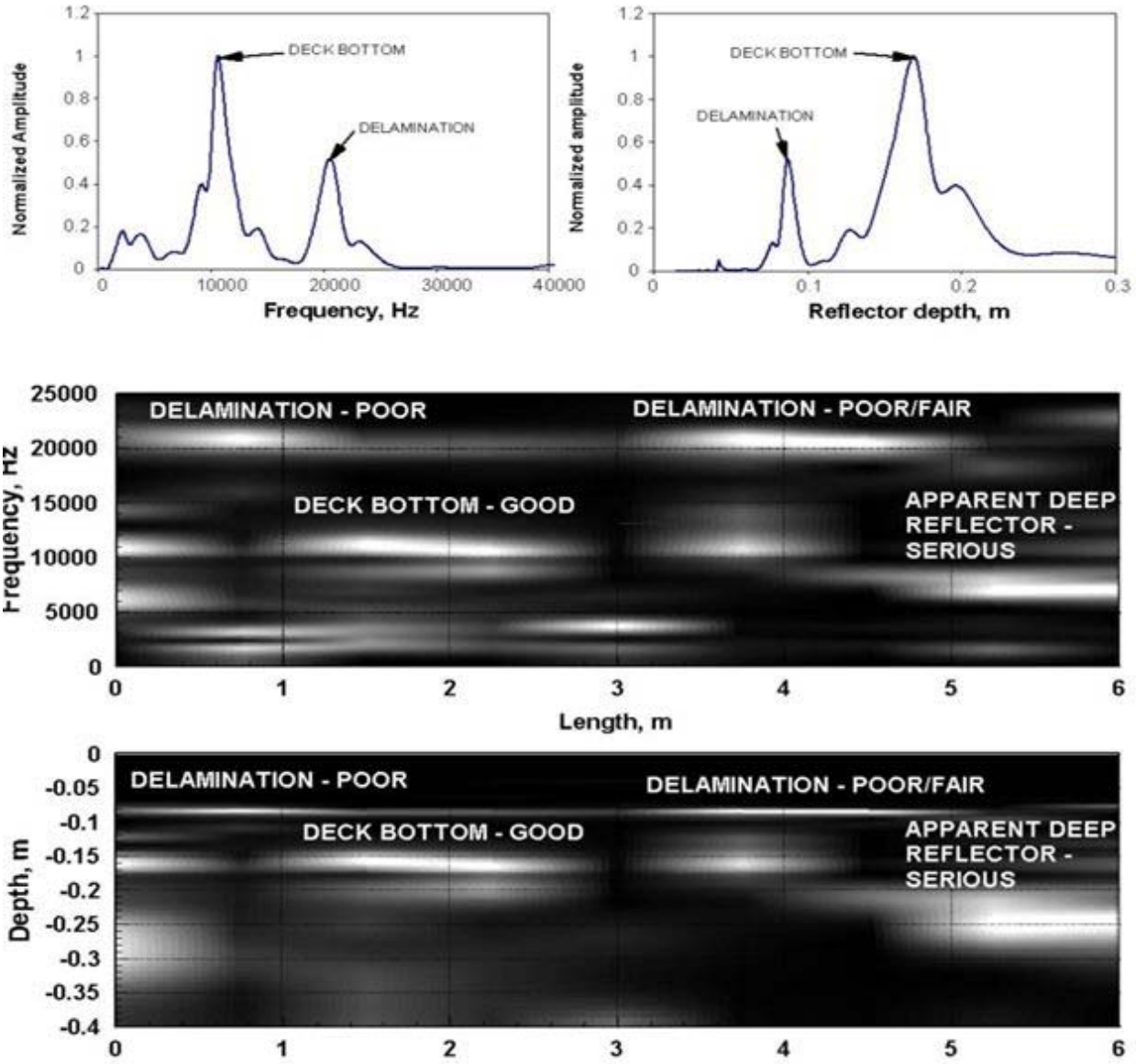

Figure 10. Frequency and thickness spectra and spectral surfaces.

Next, in a very severe case of wide or shallow delamination (serious condition), the dominant response of the deck to an impact is characterized by a low frequency response of flexural mode oscillations of the upper delaminated portion of the deck. This response is almost always in the audible frequency range, unlike response of the deck in the fair and poor conditions that may be in the ultrasonic range. The Mindlin's solution for the fundamental flexural mode of a 100 mm thick rectangular concrete slab supported on all four sides is illustrated in Figure 12. Assuming the 100 mm thickness corresponds to the delamination depth, for a size of delamination between 0.5 m x 0.5 m to 1 m x1 m, the fundamental flexural mode is going to vary between 2 kHz and 500 Hz. Shallower and smaller delaminations than those can produce oscillations in the same range frequency. Because the flexural frequency is significantly lower than the return frequency for the deck bottom, the return frequency produces an apparent reflector depth that is deeper than the deck thickness. The described scenarios have been

confirmed by the results of numerous numerical and experimental studies (Cheng and Sansalone, 1993a; Asano et al., 2003; Petersen et al., 2003). Chang and Sansalone (1993a) have also demonstrated that higher flexural modes can be excited by impacts of the center of the delamination.

Impact echo can be used for delamination detection on decks with overlays. Lin and Sansalone (1996) and Lin *et al.,* (1996) have shown experimentally that IE can be used in evaluation of decks with concrete overlays. As illustrated in Figure 13, they have shown that the frequency or reflections from the bottom of the layered deck can be accurately determined. Also, they have demonstrated evaluation of debonding between two deck layers, shown by the flexural mode and top layer frequency peaks. However, their studies have also shown that IE cannot detect weak bonding between layers, nor presence of microcracking at the interface, which can be caused for example by removal of concrete by jackhammers of hydrodemolition. Sansalone and Carino (1989) have conducted test on 15.5 cm (6 in) concrete slabs with 5.6-6.2 cm (2.2-2.4 in) asphalt overlays. They established a very good match between measured and calculated frequencies for full composite and delaminated slabs, and the thickness of the asphalt overlay. They did not report on the temperature of the asphalt overlay, which is a critical parameter for high frequency wave propagation.

Finally, in rare cases of impact echo testing on bridge decks, geometrical and boundary effects should be taken into consideration. Results of experimental and numerical studies (Carino, 2001; Pascale and Colla; 2006; Colla and Pascale, 2006) have shown that reflections from edges of finite members and modes of vibrations of structural members can significantly complicate IE data interpretation. Algernon et al., (2006) demonstrated that most of the boundary effects are coming from surface waves traveling around the element and are more pronounced on elements of regular geometry. They also stated that the effects can be effectively identified only in impact-echograms obtained from impact-echo scanning instead of point testing. Finally, they recommended in situations where the reflection effects are strong to utilize transmission mode IE (source and receiver on the opposite side of the tested surface).

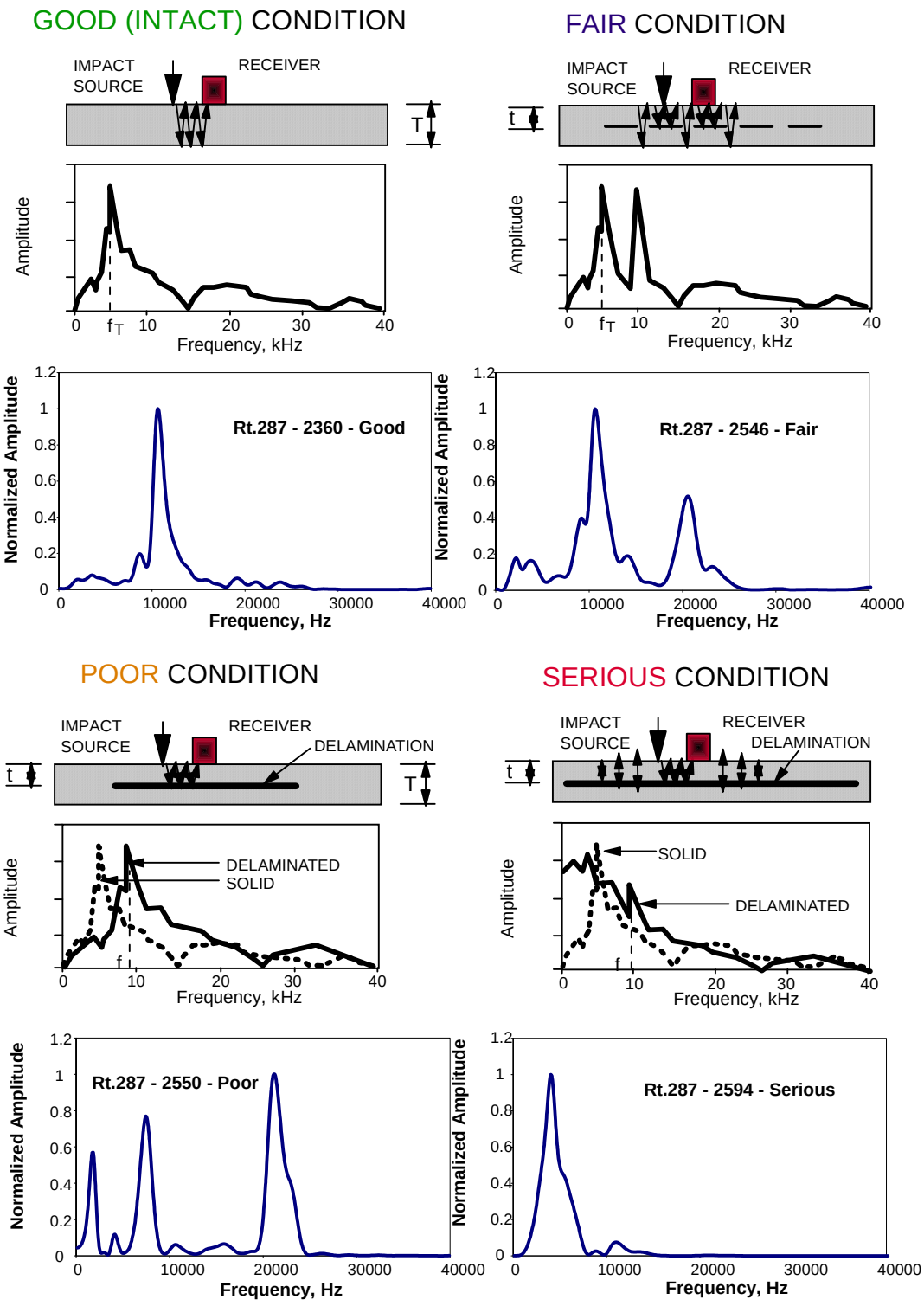

Figure 11. Grades for various degrees of deck delamination.

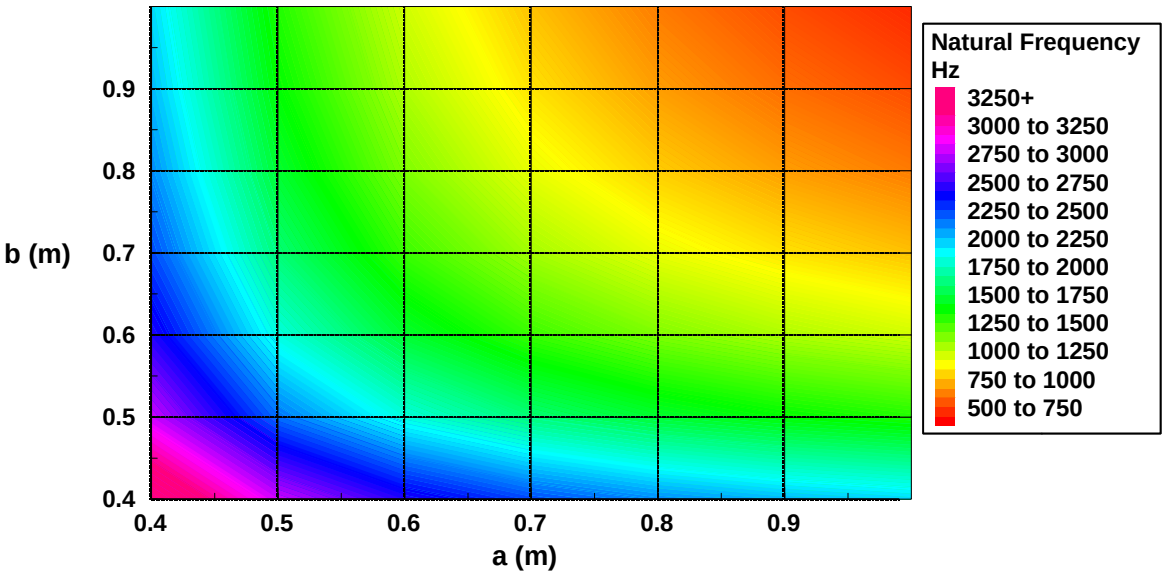

Figure 12. Fundamental flexural mode frequency for a 100 mm thick concrete rectangular slab supported on all four sides as a function of length and width.

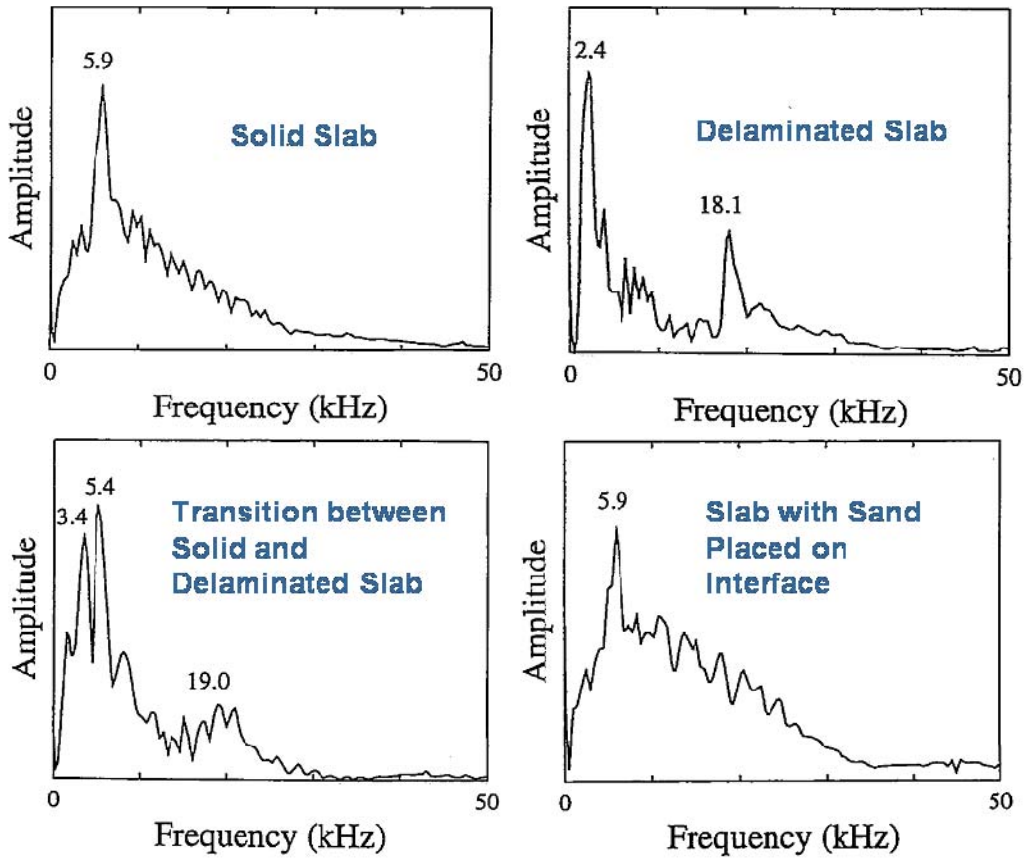

Figure 13. Response spectra for a 220 mm thick concrete slab with a 100 mm concrete overlay (after Lin et al., 1996).

Field Implementation of IE and Condition Maps

IE method is commonly implemented in deck evaluation by conducting point testing on a grid of a selected spacing. The testing is conducted using impact echo devices, which in some cases integrate other ultrasonic seismic methods. One of such devices is the portable seismic property analyzer (PSPA), shown in Figure 14, that has a sole purpose of evaluation of surface pavement layers and bridge decks. The device integrates all three previously described ultrasonic techniques (UBW, USW, IE). Bridge deck evaluation is typically done on grids of 0.6 m x0.6 m to 0.9 m x0.9 m (Figure 14). Impact echo testing is simple and typically takes less than 30 seconds per test point. On an average, about 50 m^2 of a deck can be tested per hour using a 0.9 m spacing, or about 20 m^2 using a 0.6 m spacing. The testing is relatively insensitive to traffic induced vibrations, because those are in a much lower frequency range than the IE test range, which is typically 2-30 kHz.

Figure 14. IE and USW sensor box (top) and field implementation (bottom).

A very important element in IE testing is the source used. The primary objective of a proper selection of the source is that it provides enough energy in the frequency range of interest. Cheng and Sansalone (1993a) describe the frequency requirement in terms of the wavelength: a) it should be shorter that the lateral size of the defect, and b) it should be shorter than twice the depth of the defect to be detected. A simple rule used in definition of the maximum useful frequency is the inverse of the impact duration (contact time), which is typically from 20 to 100 μs. Many IE systems utilize steel balls of different sizes as impact sources, where the maximum frequency is inversely proportional to the ball diameter. Lausch *et al.* (2001) and Motz *et al.* (2003) have studied steel balls and other impact source types and provided different measures in impact source selection.

Impact echo/seismic testing results are commonly described in terms of concrete shear and Young's moduli (or P- and S-wave velocity) distributions, as illustrated later in the discussion on the use of USW, and condition assessment distributions (with respect to the degree of delamination). This is illustrated by a condition map for a section of the Van Buren Bridge, in Dumfries, Virginia (Figure 15). The condition map is plotted in terms of the four condition grades. The deck is in a significantly deteriorated condition with zones of all four previously described conditions (grades) present. The impact echo results are compared in the figure to those of the chain drag. The comparison points to similarity of the two approaches in detection of areas with progressed delamination (poor to serious condition). The ability of the chain drag to identify those zones can be explained by the fact that the frequency response in such cases is in the audible range. On the other hand, most of the zones identified by the IE as zones of initial delamination (fair to poor grades) were not detected by the chain drag. Cheng and Sansalone (1993a) have also stated that the IE method can detect deeper delamination, while chain drag cannot. This ability to detect zones of initial delamination represents a significant advantage of the impact echo over the chain drag approach. It allows more accurate definition of boundaries of delaminated zones, better prediction of delamination progression, and leads to better assessment and timing for implementation of rehabilitation measures.

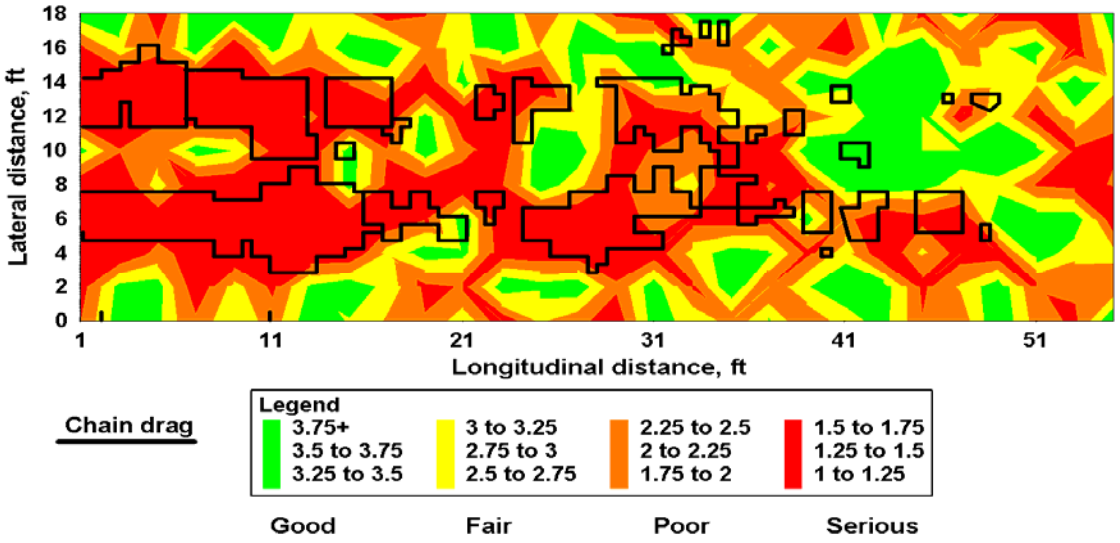

Figure 15. Condition assessment map for Van Buren Bridge.

Automation and Rapid Impact Echo Testing

As described earlier, the manual approach in impact echo data collection is a relatively slow one, conducted on a sparse grid and thus does not provide data of high spatial resolution. To overcome this limitation an automated system for data collection called Stepper was used in this project (Figure 16). The Stepper was developed at BAM (German Federal Institute for Material Research and Testing). The Stepper allows continuous data collection at a prescribed spacing between data points at a speed of about 10-15 points per minute for closely spaced points (few inches apart). In addition, the Stepper can carry and collect data simultaneously using another or multiple probes: impact echo, ultrasonic echo or GPR antenna.

Figure 16. Stepper (left) with ultrasonic (top right) and impact echo probes (bottom right).

Advantages and Limitations of Impact Echo in Delamination Detection

The strongest side of impact echo in evaluation of deterioration in bridge decks is delamination detection. IE can both detect presence of delamination and characterize its stage of development and severity of the condition. Very importantly, delaminations can be detected at very early stages, where traditional methods like chain drag and hammer sounding fail. The method works on decks with PCC and AC overlays, as long as AC temperature is sufficiently low, so that the material is not highly viscous, and there is no debonding between the overlay and the deck. Supported by right visualization tools, IE is a very intuitive method in delamination location and characterization.

The impact echo data collection for delamination detection purpose is relatively slow and requires lane closure. To accurately define boundaries of delaminations it is necessary to conduct data collection on a very dense test grid, which in most cases would be impractical. On the other hand, data analysis with respect to delamination characterization is relatively fast and interpretation in most cases is unambiguous.

Ultrasonic Surface Waves (USW)

Principle and Measurement

Seismic surface waves are a type of stress waves traveling along the free surface of a medium and usually are the predominant portion (over body waves: compressive and shear waves) in a wave train (see Figure 17), similar to waves traveling on the surface of water. Surface waves propagating in a heterogeneous medium are dispersive; that is, waves of different wavelengths or frequencies travel with different velocities. The dispersive characteristic is dependent on the elastic properties of the affected medium and thus the information of the subsurface can be obtained through the generation detection and analysis of surface waves.

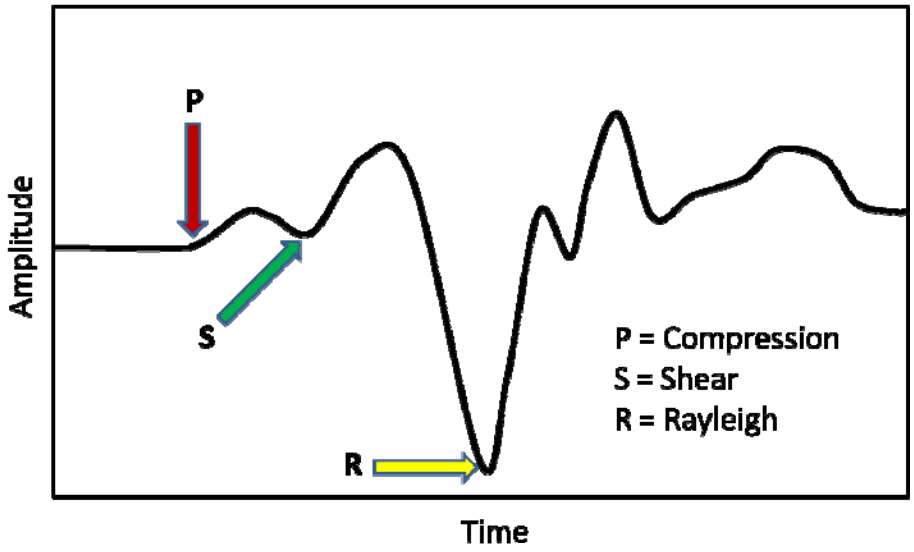

Figure 17. Typical time history and identified wave arrivals.

The USW technique is an offshoot of the spectral analysis of surface waves (SASW) test (Nazarian *et al.,* 1983; Stokoe *et al.*, 1994). The SASW method utilizes previously described phenomenon of dispersion of a surface (Rayleigh) wave in layered systems. The USW test is identical except that the frequency range of interest is limited to a narrow high frequency range where the velocity of the surface wave (phase velocity) does not vary significantly with frequency. A USW test simply consists of impacting the surface of a material, recording the time domain signals (waveforms) and processing the time signals to obtain a dispersion curve (phase velocity vs. wavelength or frequency) from the phase spectrum through FFT transformation (Nazarian *et al.*, 1993a,b). These procedures are automatically or semi- automatically achieved in the currently available USW devices. With the USW technique, the average surface-wave phase velocity of the uppermost pavement layer (e. g., concrete slab or deck) can be directly determined. As sketched in Figure 18 (top), at wavelengths less than or equal to the thickness of the layer, the velocity of surface-wave propagation is more or less independent of wavelength, if the layer or slab is uniform. The objective of the test is to determine that velocity-frequency relationship, termed the dispersion curve, and afterwards through the process of inversion or backcalculation to obtain the shear wave velocity profile. Elastic modulus profile can then be easily obtained using simple relationships between the velocity of propagation and measured or

approximated values for mass density and Poisson's ratio of different layers. Variation in the phase velocity would be an indication of variation of material properties (elastic moduli) with depth.

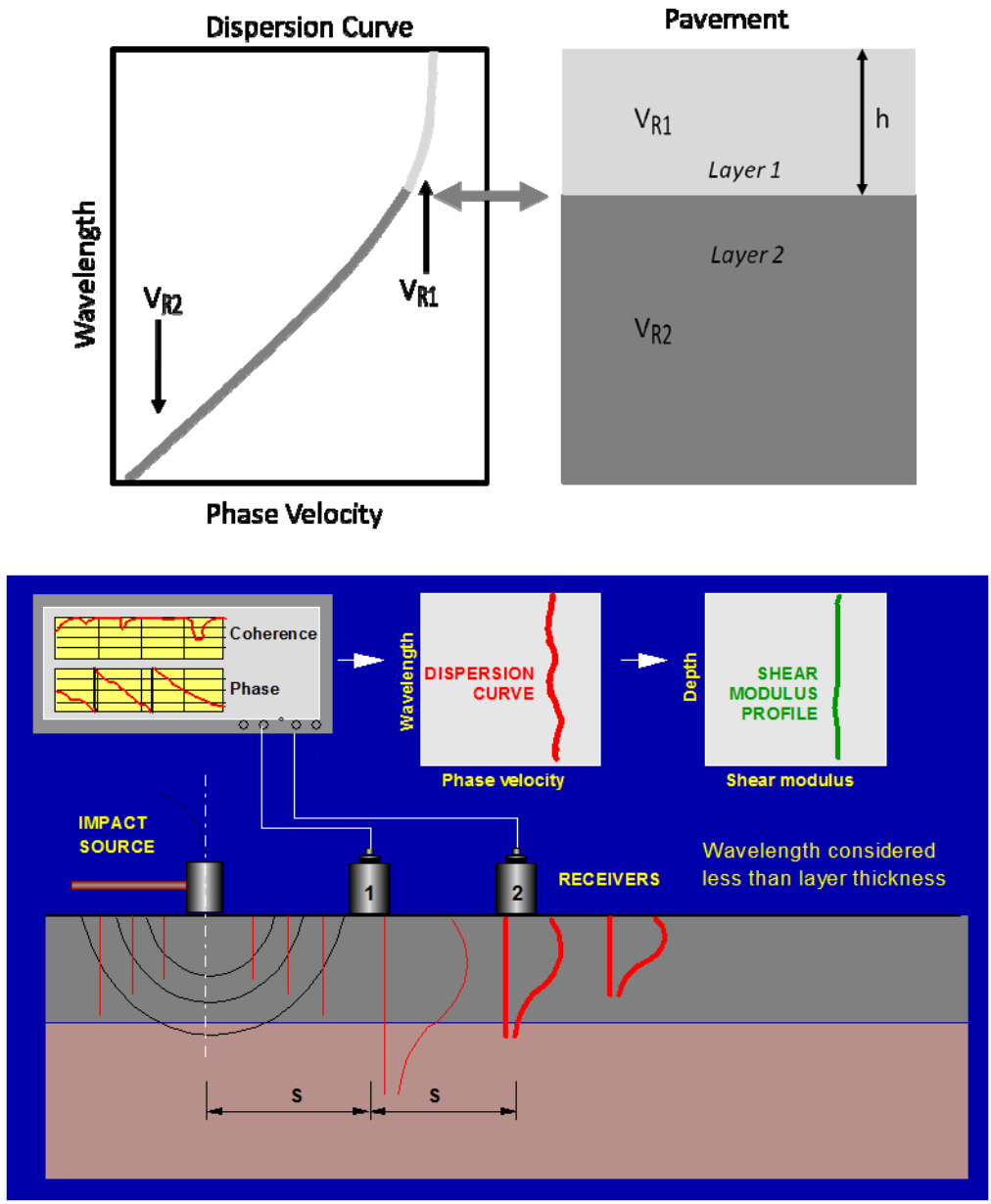

Figure 18. Schematic of surface-wave velocity vs. wavelength (top) and evaluation of a layer modulus by SASW (USW) method (bottom).

A schematic of the USW (SASW) test is shown in Figure 18 (bottom). Elastic waves are generated (by means of impacts, vibration generators or other sources), detected by a pair or an array of receivers and recorded by a transient recorder. In a case of material evaluation of a

single homogeneous layer, the SASW process becomes significantly simpler. The material modulus can be described as being directly measured instead of backcalculated.

A device shown in Figure 19 and similar to the portable seismic property analyzer (PSPA) shown in the impact echo section can be used in evaluation of concrete modulus by USW method. The device consists of an electromagnetic type impact source, on the right far end, and two receivers (accelerometers) on the left side. Once the device is placed on the ground, a series of impacts from the source is being detected by the receiver pair and recorded on a notebook size computer. Concrete modulus can be obtained directly in the field, as it is illustrated in the figure by the computer screen shot and a bridge deck modulus distribution.

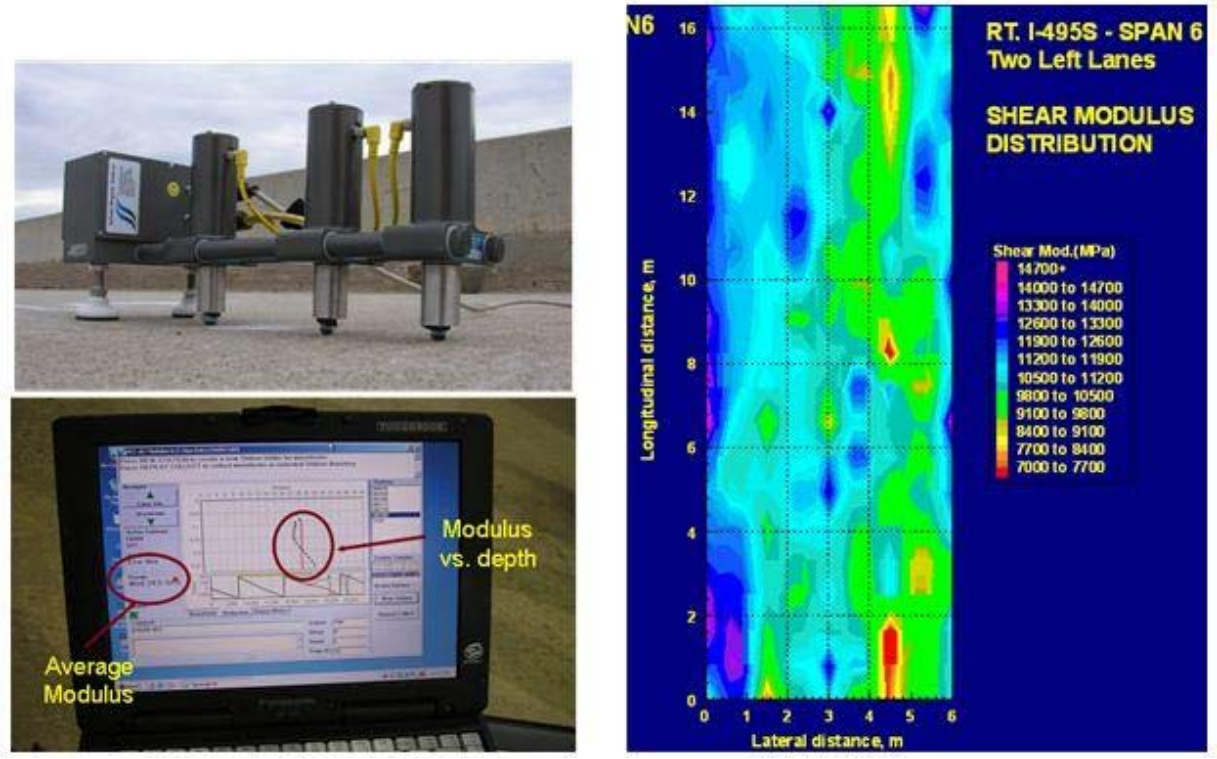

Figure 19. PSPA (top left), concrete modulus evaluation (bottom left) and concrete modulus variation (right).

With in-place calibration in the intact areas, the USW technique can be used for detecting the deterioration in a concrete bridge deck in two ways:

1. If the dispersion curve measured is smooth and relatively constant, a low average phase velocity is an indicator of weak concrete in the deck caused by fine cracking and early-age or light scaling, which does not expose the coarse aggregate on the concrete deck surface. The fine (invisible) cracking in a HMA pavement under the accelerated loading has been clearly monitored with USW measurements (Yuan *et al.*, 1999). The same principle is applicable to concrete.
2. If the average phase velocity is significantly lower (as compared to the value from the calibration measurements) and the phase spectrum/dispersion curve widely changes, it may

be an indication of delamination in the concrete deck. Figure 20 shows the comparison of field results from a reinforced concrete pavement. The rebar-induced mid-depth delamination existed in the concrete in some areas of the pavement.

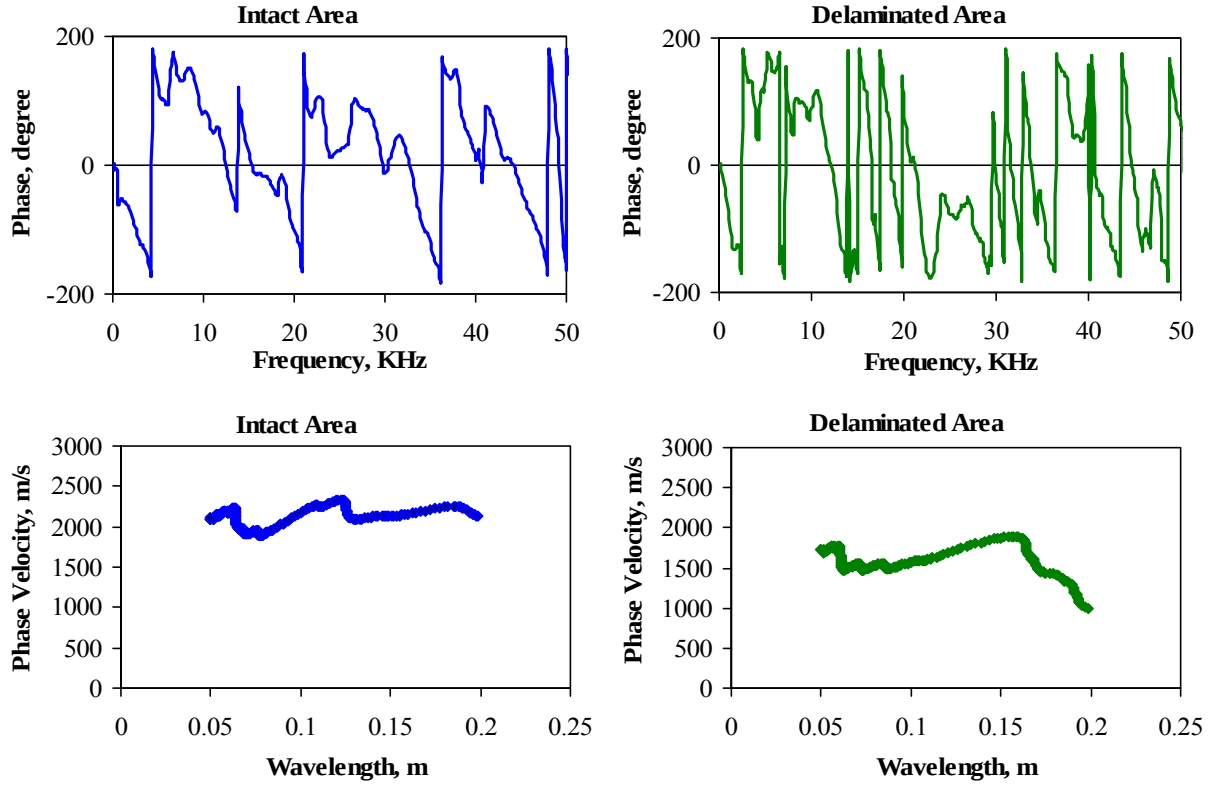

Figure 20. Comparison of USW measurements from intact and delaminated areas: phase of the cross power spectrum (top) and dispersion curves (bottom) ***(from Yuan et al., 1999)***.

Advantages and Limitations

The USW method, with suitable equipment and processing software, is an easy, simple and rapid test method to assess the properties of concrete, including the changes in modulus caused by mix design, compaction curing, fine cracking and early-age scaling. The small effect of steel reinforcement on the measurement can be ignored.

For concrete deck deteriorations such as debonding/delamination, the USW method can only play a supplemental role, and experience is required for understanding and interpreting test results.

ELECTRO-MAGNETIC NDT TECHNOLOGIES

Ground Penetrating Radar (GPR)

Ground penetrating radar (GPR) is a rapid nondestructive evaluation/geophysical method that produces graphical images of subsurface features, such as natural geological features, buried objects, as well as reflections from steel reinforcement, wire mesh or designed layered systems within engineered structures. Not only are the images themselves useful for interpreting subsurface structure and layout, but the information contained in a GPR waveform can be used for analytical measurements, as well.

Principle of Operation

Ground penetrating radar provides an electromagnetic (EM) wave reflection survey. A GPR antenna transmits high-frequency EM waves into the deck or ground. A portion of the energy is reflected back to the surface from the interface of two adjacent materials (usually layered materials such as pavement overlays, but also point targets, such as rebars) with different electrical properties (dielectric and/or conductivity contrasts) where it is received at the antenna. The remainder of the GPR energy continues to penetrate beneath this interface and additional energy is continually reflected back to the receiver from other interfaces until it is diminished. The velocity of propagation is dependent on the dielectric properties of the materials through which the GPR signal passes. The measured time of arrival of each of these signals and its amplitude are used to measure and estimate subsurface "target" depths, GPR wave propagation speed, and often subsurface concrete condition.

Electrical conductivity, as well as material dielectric properties, plays a primary role in how a GPR signal will travel through a material. Most directly, electrical conductivity (inverse of resistivity) directly affects how well GPR signals can penetrate through a material. Metals cannot be penetrated (even dense wire screens or thin foils are impermeable to GPR); most construction materials (concrete, asphalt, or engineered pavement soils—base course and subbase) are fair to good host materials for GPR. Similarly, concrete that is moist and high in free chloride ions (or other conductive materials), such as a reinforced deck that has undergone deterioration due to corrosion of the rebar, can also significantly affect a GPR signal's penetration or attenuation in a quantitative, measurable way.

GPR systems deployed for bridge deck investigations typically transmit electromagnetic pulses into the deck's surface using either vehicle-mounted, air-launched horn antennas or ground-coupled sensors to image and/or quantitatively measure specific signal responses. Those responses are caused by variations in electrical properties of the materials making up the deck – primarily contrasting signals emanating from overlays, steel reinforcement and other subsurface interfaces that reflect GPR signals. These electrical properties include electrical conductivity and relative dielectric permittivity (dielectric constant) of the host material, which respectively govern (a) the ability of GPR energy to penetrate that particular medium and (b) the speed GPR waves propagate through it. In addition, dielectric contrast between two adjacent materials through which GPR will penetrate (dielectric contrast implies that the neighboring media have

dielectric properties that are dissimilar) results in causing some of the penetrating GPR waveform to reflect back to the surface where it can be measured and recorded (Figure 21).

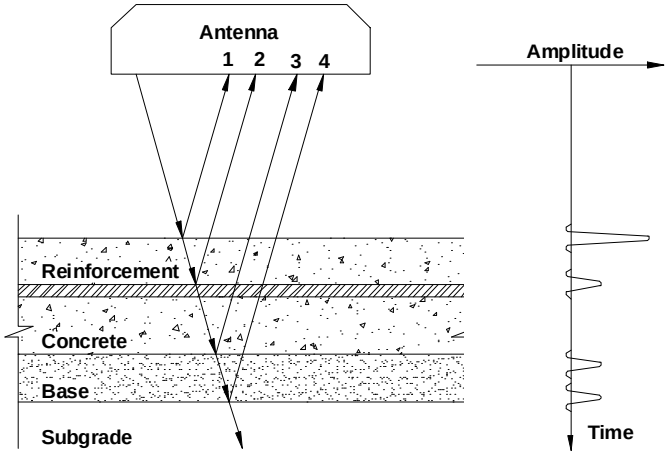

Figure 21. GPR signal transmission, reflection and measurement through layered system.

Published relative permittivity values (dielectric constant, E_r) for typical construction materials, including concrete are shown in Table 4. It should be noted that rebar (steel) is a non-dielectric (cannot store an electrical charge), thus its effective dielectric constant would exceed 10,000 making it a strong GPR reflector as a target (rebar) in virtually any other medium, or an impermeable barrier as a layer or surface feature (e.g. expansion joint). How GPR signals transmitted into a bridge deck interact with various overlays or repaired areas (if present); embedded rebars that are either in good condition or undergoing corrosion; and concrete that is either sound, deteriorated or contaminated with chlorides or corrosion products surrounding actively corroding steel; etc, will determine whether these transmitted GPR waveforms return to the GPR antenna receiver(s), how fast, and what signal properties (high amplitude or strong attenuation, signal polarity and wavelength changes, etc.) are ultimately measured.

Table 4. Dielectric Values for Construction Materials, Including Aggregates and Concrete.

Air	1	Sand	4-6
Water (fresh)	81	Gravel	4-7
Ice	4	Clay	25-40
Asphalt	4-8	Silt	16-30
Concrete	8-10	Silty sand	7-10
Crushed base	6-8	Insulation board	2-2.5

Note: Moisture can significantly increase K* (e.g. for gravel it may go from 5 to above 20 as w increases).

Transportation Applications

A general, though thorough synthesis describing GPR's ability to be exploited by the transportation community, specifically in pavement and bridge deck applications, was developed by the National Cooperative Highway Research Program (NCHRP) in 1998, as NCHRP Synthesis 255, by Morey. This synthesis and the cited references it contains continues to serve as a good starting point for those interested in applying GPR as one of several technologies that can help solve a variety of transportation-related problems. Although this NCHRP document lists many of the GPR applications, describes the fundamentals and theory related to how it works and environmental (site-specific) conditions that govern effective utilization of the technology, many additional applications have been explored since. A lot of time and painstaking effort has been dedicated to "proving" the technology to more fully understand its capabilities and limitations as the technology itself and data analysis/interpretation techniques have improved over the last decade.

More recently, other researchers have developed comprehensive literature syntheses that are broader-based, not focusing solely on bridge decks, but primarily on GPR as a technology with multiple uses in pavements, bridge decks and utility detection or mapping. These include recent investigations by both South Dakota DOT (Infrasense, 2006) and New York State DOT (Grivas, *et al.*, 2005), where the focus was on evaluating GPR capability for specific tasks. More realistic expectations of the technology's capabilities and limitations are continually being defined, documented and appreciated by both practitioners and transportation facility owners. Many specific GPR applications aid transportation infrastructure evaluations; these can generally be categorized into four types:

1. Quality Assurance (QA) inspections of new construction to verify compliance with design/build specifications.
2. Baseline condition assessments (initial GPR survey on a structure or site, whether the structure or facility is new or has been in service for some time).
3. Project-level condition assessments that do not fall into the realm of either QA inspections or baseline condition assessments since they may be one-time, stand-alone GPR investigations conducted on existing structures; solely with the intent of addressing specific project-related issues.
4. Network-level condition assessments used for the purpose of making systemic management decisions, allocating resources and prioritizing future design/rehabilitation or construction projects.

While many of these references cite validation and verification techniques applied to the specific case studies and investigations represented within their individual frameworks for discussion, as well as the capabilities and limitations examined and reported by the principal investigators within the site-specific settings explored, there are wide variations in GPR experiences for seemingly identical, or similar, applications. Therefore, the variations in scope of work, specifications for performing the investigations, and individual equipment selections and methodologies employed for designing the data collection and analytical process used for developing interpretations, maps, etc., strongly influence the reported results. Those influence

results at least as much as the quality of combined qualifications and experience of those performing the work affects the ability to design and execute successful projects and research.

Bridge Deck Evaluations

Hundreds of bridge decks have been evaluated using a variety of GPR systems and deployment configurations (Romero, Roberts, 2002a and 2002b; Roberts *et. al*, 2000; Barnes and Trottier, 2000; Alongi, *et. al.,* 1993, Maser and Rawson, 1992). Typical GPR applications include evaluations of deck thickness, concrete cover and rebar configuration, potential for delamination, concrete deterioration, and estimation of concrete properties. The GPR condition assessment is most often based on measurement of signal attenuation at the top rebar level. This provides a rational approach in characterization of the severity of deterioration of concrete and potential for bridge deck delamination based on corrosion of the reinforcing steel that is most vulnerable to chloride (or other) attack, because of its proximity to the deck surface (Figure 22). In this figure, a raw ground-coupled 1.5GHz data profile (vertical cross-section along a GPR antenna's path) reveals mostly deteriorated concrete, based on attenuated signal response from upper rebars in chloride-infused, moist concrete.

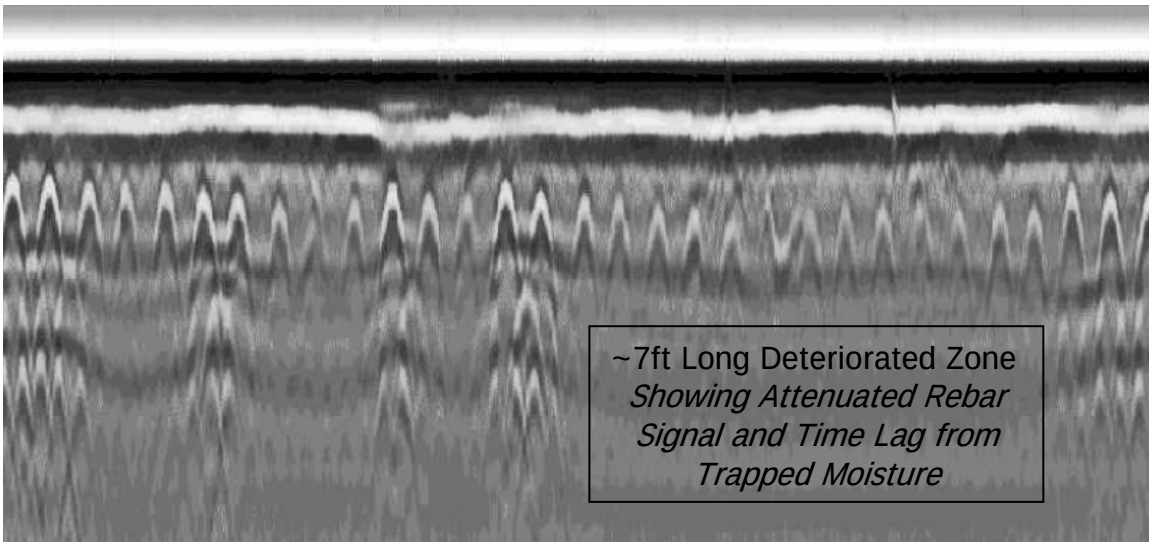

Figure 22. Raw ground-coupled 1.5GHz data showing mostly deteriorated concrete.

GPR's capabilities have been further refined, its benefits and limitations having been examined in greater detail, in a wider variety of targeted applications that include other nondestructive and traditional analysis methods. In most cases, ground truth validation of radar results is restricted to point specific areas. However, some studies have been conducted which compare full deck GPR condition assessment to those obtained from half-cell potential, chloride ion sampling and testing, impact-echo, deck resistivity, and even hammer-sounding, chain drag, or actual concrete removal quantities during repair (Cardimona *et al.*, 2000; Roberts *et al.*, 2001; Romero *et al.*, 2000; Gucunski, *et. al.,* 2005; Gucunski, *et al.,* 2009). The GPR also provides the top rebar depth measurement, or concrete cover, where the cover measurement is used to adjust the measured GPR signal attenuation that varies with depth, allowing the more accurate GPR map shown to be produced.

In general, horn (air coupled) antennas have been used in the past to primarily provide a fast overview of the condition of the deck with an attempt to also provide a detailed condition assessment. A single-polarization air-coupled antenna deployment used for a more general condition assessment is shown in Figure 23, and the limited level of detail in the quality of the GPR data when rapid deck condition assessments are performed is illustrated in Figure 24. Note that approximately 20 ft of high spatial density data are collected with a high-resolution ground coupled antenna in Figure 22, which should be compared to the approximately 200ft of more sparse, spatially sampled data shown in Figure 24, collected with a lower frequency air-coupled (horn) sensor. While ground coupled antennas provide more detailed imaging and analysis of the deck condition, one patented GPR data collection and analysis methodology employs a dual-polarization horn antenna deployment to overcome some of the limitations of lower-resolution air-coupled sensors (Romero, Roberts, 2002a and 2002b).

Figure 23. Single-polarization (1.0GHz or 2.2GHz) horn antenna deployment.

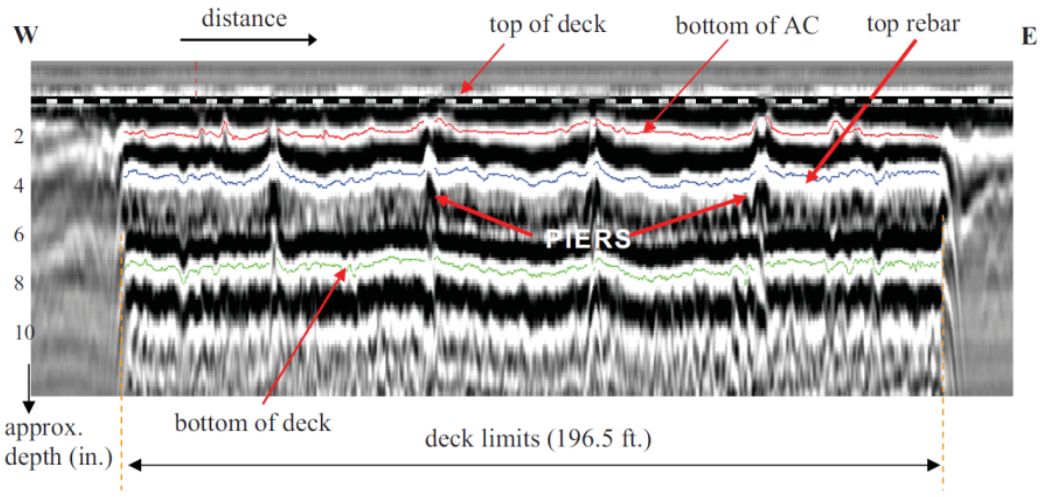

Figure 24. Sample GPR data from single-polarization sensor, with layer processing.

There have been a variety of manners in which deck condition can be assessed using GPR. The attenuation of the GPR signal at the top rebar level is used by most practitioners to directly represent the condition of the deck, though there are some variations in analyzing data warranted by either deck construct (reinforcement layout and spacing, deck thickness, etc.) or other factors (Roberts, *et al.*, 2000, Romero, *et al.*, 2000, Romero and Roberts, 2002a and 2002b; Romero and Roberts, 2004; Barnes and Trottier, 2000; Parrillo *et al.*; Maser and Rawson, 1992, Maser and Bernhardt, 2000; Maser, 1995; Alongi, *et al.*, 1993; ASTM D 6087-08). However, the predominant approach demonstrated to produce the most accurate GPR deterioration (a.k.a. condition) maps is the measurement of attenuation from the uppermost rebars oriented perpendicular to the GPR antenna path. In most cases, this implies that the GPR data collection coincides with the direction of travel, perpendicular to the transverse reinforcement in the deck. On concrete slab decks or on some newer steel girder decks, where longitudinal steel is tied above transverse steel in the upper rebar mat, the GPR antenna path should, but cannot always, be oriented perpendicular to the traffic direction. In that case GPR lines are collected at a fixed spacing, generally 2ft, across adjacent traffic lanes.

Though GPR surveys are performed routinely using both air-coupled and ground-coupled sensors, each has its inherent advantages and disadvantages. The primary advantages of air-coupled (non-contact horn) GPR antennas are minimal traffic control (attenuator truck and sign arrow) and ability to collect data on a series of bridges in close proximity, or on longer bridges, in a relatively short period of time. The primary advantages of ground-coupled antennas include greater signal-noise ratio, less disturbance from ambient radio noise, and generally both higher vertical and horizontal resolution, as well as fewer restrictions on use (FCC regulations seriously impact the ability to use any horn antennas or even data acquisition systems not manufactured prior to 2002). Restrictions on use primarily affect the ability to use non-contact (horn) antennas because lower-powered transmitters that are FCC compliant are extremely susceptible to ambient radio noise. Also, newer data acquisition systems (FCC compliant) are restricted in their pulse repetition rate (effective scan rate), meaning they no longer are able to be operated at driving speeds where they provide any significant time advantage for data collection over currently manufactured ground-coupled systems. Advantages and disadvantages of both ground coupled and air-coupled GPR systems are discussed elsewhere. Only a few studies both cite the advantages that are restricted only to the use of pre FCC-restricted air-coupled GPR sensors and data acquisition systems and also mention this as a limitation to wider adoption of air-coupled applications, in general (Wightman et al., 2003; Romero et. al., 2009).Because of these regulations on use, for the purposes of this GPR discussion, the primary focus is centered on high-resolution, ground-coupled GPR systems. These systems produce consistently more accurate GPR condition maps. The higher accuracy is achieved because of the ability to much more clearly resolve individual rebars not so much because of a higher vertical resolution (higher frequency antenna) but primarily due to higher spatial (horizontal) resolution, since ground-coupled GPR systems have both a much smaller footprint and a narrower beam width within the deck at the rebar depth, and are used with a much greater scan density (scans/foot or scans/meter) along the data collection path. This enables ground coupled GPR sensors to be used for observing low-angle cracking and other barely visible defects consistent with concrete deterioration within decks undergoing corrosion. These same subsurface features are not at all, or as clearly, visible within comparable air-coupled GPR data, as has been shown in previous investigations and will be illustrated in this report.

When the antenna is centered directly above the rebar, the highest amplitude return for the area near the rebar is obtained. This amplitude will be the highest when the deck is in a good condition. It will be weak when internal deck environmental conditions are favorable for formation of delamination and corrosion of the reinforcing steel are present, as illustrated by the results from numerical simulation of effects of concrete deterioration on GPR signal attenuation in Figure 25. Amplitudes for all points are normalized with respect to the best possible condition to obtain the plot of attenuation.

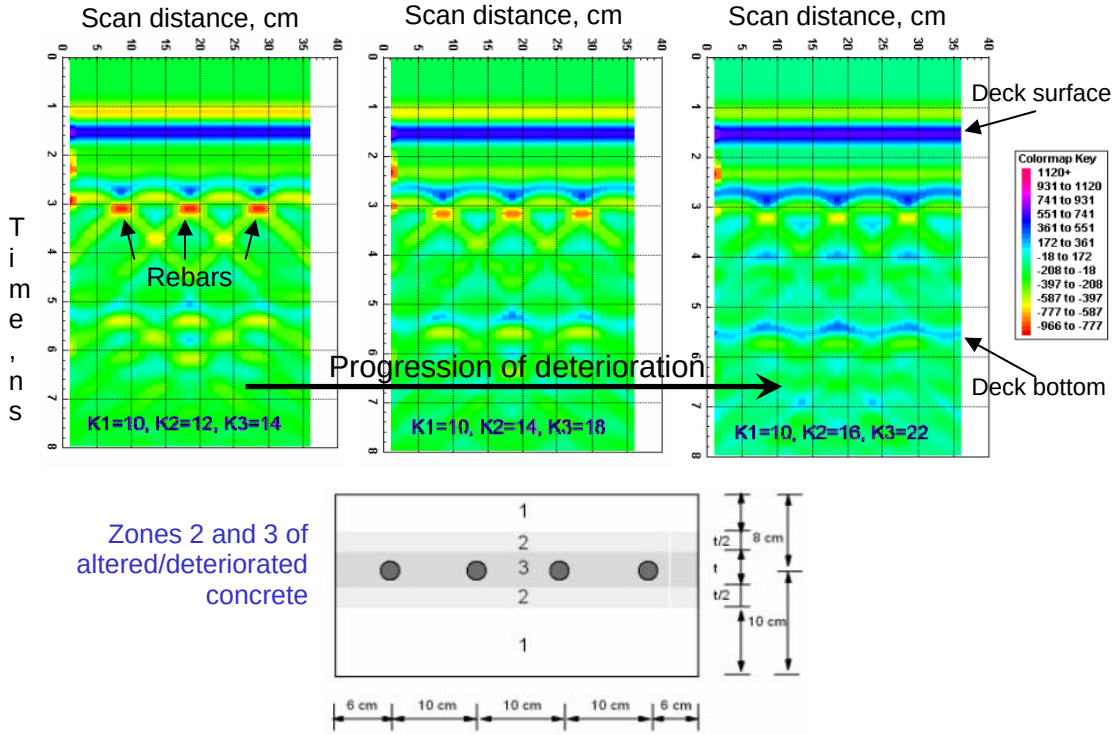

Figure 25. Results of numerical simulation of effects of corrosion on GPR signal attenuation.

The ground-coupled antenna's smaller size and higher resolution, compared with the standard, single-polarization deployment of a 1.0 GHz air-coupled (horn) antenna, give it the unique ability to accurately measure top rebar reflection amplitude without signal interference from other reflectors. These reflectors may include thin overlays, the bare deck surface when it is within 1.5 inches proximity of the uppermost deck reinforcement, or steel reinforcement tied in the upper mat but oriented in line with the GPR antenna path. Also, a ground-coupled sensor is shielded to be virtually non-susceptible to ambient radio noise that can interfere with or completely obstruct the capability of non-shielded, air-coupled (horn) antennas to collect quality data for processing, analysis, interpretation and accurate deck condition (contour) mapping. However, in some cases, particularly when antenna resolution is very high, having an ability to select between a high-resolution (e.g., 1.5GHz) sensor and a very high-resolution (e.g. 2.6GHz) antenna respectively allows for a balance to be struck between the following elements: (a) preventing signal interference from clutter that occurs when large aggregate, flaws or honeycombing in the deck generate a different type of signal interference visible only in the highest-frequency GPR data and (b) properly resolving signals between closely-spaced (vertical) layers, overlays or targets (rebar) that can often interfere with the GPR data collection objective.

Having the capability to adjust the sensor after first characterizing the signal response from the structure itself, and selecting not only the appropriate frequency but also the optimal scan line orientation (perpendicular or parallel to traffic) depending on the layout of the upper deck rebar mat, is a significant advantage of ground-coupled, high-resolution sensors. This capability allows the GPR operator to directly assess the resolution capabilities on each deck as the data are being collected and adjust accordingly (Gucunski, *et al.,* 2009), as shown in Figure 26. Otherwise, without the information available from a preliminary GPR screening of the existing internal deck configuration using a ground-coupled antenna within lane closures, the NDE practitioner and agency/owner are committing to a GPR collection strategy which may not yield optimal results once the analysis, interpretation and mapping are complete.

Unlike when ground-coupled sensors are used, swapping antennas and attempting to adjust the data collection methodology or equipment configuration to minimize unanticipated signal measurements resulting from unique variation in deck material properties (such as effects from large aggregate, sealants and/or construction defects/honeycombing, etc.), layer structure and/or deck reinforcement layout, when a commitment to using a specific air-coupled (horn) antenna deployment methodology has already been made, is a much more difficult, if not impossible option. Generally, higher-speed acquisition and limited traffic control (if any) does not allow any time to be spent performing reconnaissance of the deck's properties using the antennas, so a planned survey almost always has to be executed without (often necessary) modification. As a result, very little adjustment in an air-coupled GPR data collection strategy can be accommodated, ultimately increasing the potential to affect the accuracy of the produced results. Possible exceptions include collection using a dual-polarization methodology or perhaps using a higher-frequency air-coupled sensor and decreasing the spacing between individual GPR scan paths to 1ft instead of 2ft, so that either (a) the subtracted signals can be processed, (b) the signal from the transversely-oriented GPR antenna can be isolated for processing and analysis, or (c) the longitudinally-oriented GPR antenna signal can be used for same (Romero, Roberts, 2002a and 2002b, 2004; Romero, *et al.,* 2009) . Therefore, almost without exception it is expected that the accuracy in estimating deck deterioration quantities using the ground coupled system will be higher. Once the final interpretation is completed, a unique deterioration threshold with respect to delamination-mapping may be established using ground truth, such as cores or NDE methods like impact echo (Barnes and Trottier, 2000; Gucunski *et al.*, 2005).

ASTM D6087 – Evaluating Asphalt-Covered Concrete Bridge Decks Using GPR – covers GPR evaluation procedures that can be used to evaluate the condition of concrete bridge decks. However, it is instructive to note that the ASTM guidelines do not provide a complete procedural process required to complete a quality deck assessment because of the need to accommodate several, quite different GPR collection and analysis strategies using viable GPR technology and assessment/mapping techniques. Thorough training from the equipment manufacturers on proper use, followed by expert guidance in any of the deck data collection and analysis methodologies by established practitioners, is strongly recommended.

GPR Antenna Types and Differences in Data Quality Affecting Selection

Ground-Coupled GPR Antennas (Sensors). Data from 1.5 GHz and 2.6 GHz ground coupled antennas (Figure 26 left), taken at scan density of 79 scans/m (24 scans/foot), are shown in the upper two data sets in Figure 27. Qualitatively, at a glance it appears that the 2.6 GHz antenna provides significantly more detail compared to the 1.5 GHz sensor. Sometimes more detail is good, as when imaging for defects such as honeycombing or cracking or in attempting to resolve thin layers, such as deck overlays, so that their potential performance (condition) may be assessed and compared to GPR data indicative of concrete deterioration (Romero *et al.,* 2009). However, at other times too much high-resolution (such as the strong scatter from the aggregate, clearly visible in the 2.6GHz data, upper right of Figure 27) can obfuscate the imaging and processing of the desired signal. In this particular case accurate measurement of the strength (or attenuation) of the upper rebar/concrete interface reflection, which provides us with a clear indication of the relative degree of concrete deterioration throughout the upper portion of the deck, can be adversely affected by heterogeneous concrete material properties. This effect would be minimized, if a lower frequency sensor, say 1.5GHz, were used.

Figure 26. Data collection using 2.6 GHz ground coupled (GC) and 1.0 GHz dual polarization air coupled (AC) antennas, left and right, respectively.

To contrast the data previously referenced in the upper part of Figure 27, data from a different deck (using the same two sensors, 1.5GHz and 2.6GHz, left and right, respectively) at a sampling density of 197 scans/m (60 scans/foot) along each GPR scan path (line) are shown in the lower part of Figure 27. As shown in the lower images, typical of most decks where the deck's layer structure performance or defect detection are not the primary objectives, the relatively lower-resolution, 1.5GHz sensor often provides an additional set of benefits. Those benefits include: (a) easier ability to use the raw, non-processed data to select zones for coring and (b) the ability to see near-surface defects and low-angle cracking that are often "hidden" within the wide, dark band at the upper part of the (very high-resolution) 2.6GHz sensor's raw

signal. The 1.5GHz sensor (compared with the 2.6GHz antenna's unprocessed signal) provides clearer, uncluttered images with better contrast and clarity for immediate selection of deteriorated zones, particularly in areas displaying anomalies that appear consistent with delamination and cracking.

The down side of ground-coupled GPR data collection is that it almost always requires lane closures, because it takes time to lay out a grid when using a pushcart. Even when collecting data behind a vehicle equipped with a lane-positioning mechanism, lane closure is needed, simply because most ground-coupled operations do not exceed speeds of 5mph (typical) to 10mph (best-case). Also, GPR scan paths (lines) are generally spaced at 2ft, meaning that there are six GPR lines in a standard 12-foot lane. While there are some systems that can collect more than one channel of ground-coupled data, several GPR systems and sensors would have to be deployed simultaneously behind a vehicle, or on a wide cart. Otherwise, modifications and new designs incorporating high-resolution, ground-coupled antennas would have to be developed, tested, and proven before these operations could proceed with minimal traffic control. There are several attempts currently being made to achieve such an operation, and new designs of both time domain (pulsed) and frequency domain GPR systems are currently being developed to achieve this goal in the near future, as discussed later.

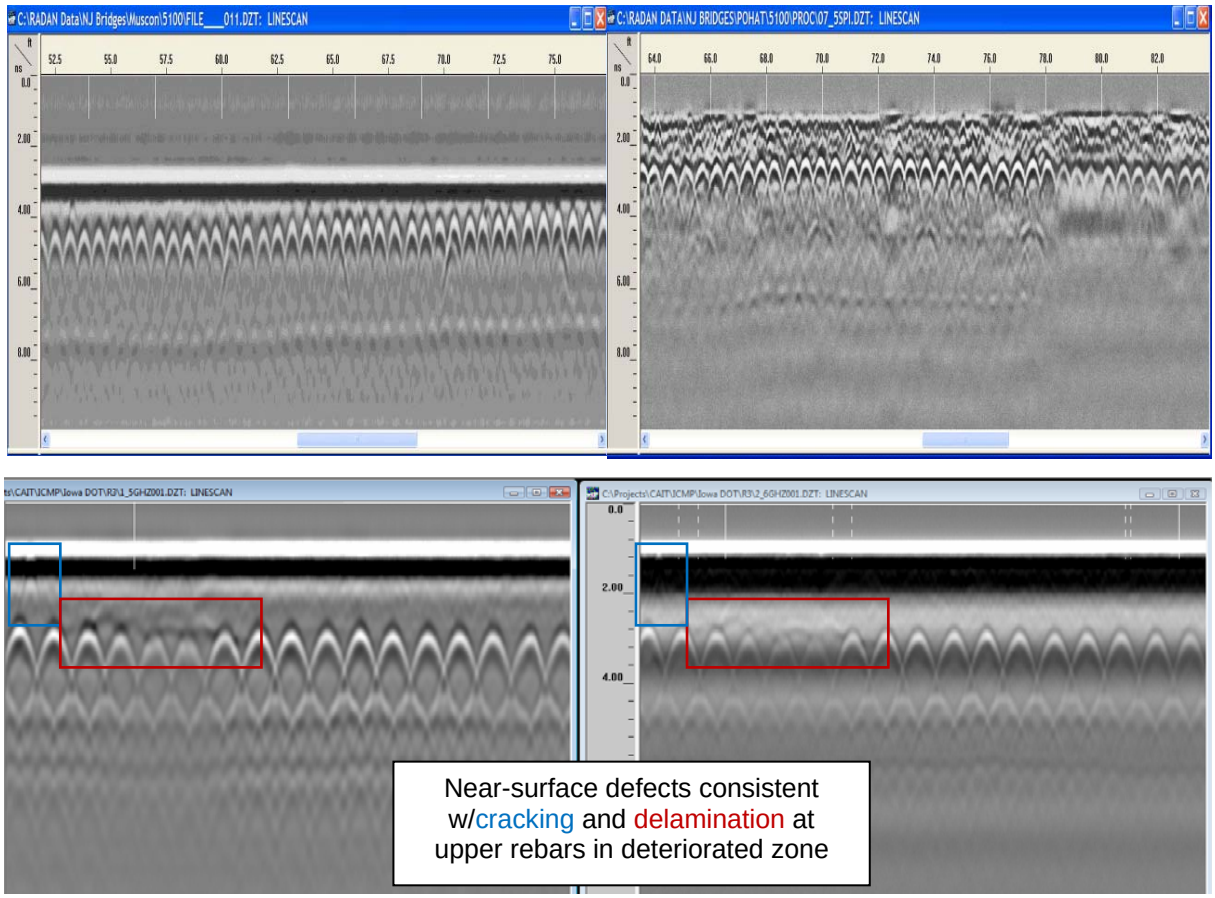

Figure 27. Raw data comparisons: 1.5GHz and 2.6GHz GC sensors, left and right, respectively.

Air-coupled GPR (Horn) Antennas. Processing data generated from air-coupled (horn) antennas is a more complex matter in many regards. Firstly, the waveform properties are affected by de-coupling the sensor from the surface of the bridge deck. Secondly, the horn antenna data requires metal plate calibration, signal normalization, and other more complex processing steps. These help counter the effects of signal amplitude variability caused by variable antenna height above the deck during data collection, ringing of the surface reflection throughout the received subsurface data, and lower spatial resolution inherent to this antenna type. Since the air-coupled (horn) antennas are suspended approximately 50 cm (20 in) above the ground surface (Figure 23 and Figure 26 right), the energy transmitted from either antenna is less focused as it reaches the surface of the deck and travels to the rebar. Consequently, rebars within the upper mat of the deck appear in the horn antenna data as a layer rather than as individual hyperbolas, typically seen in ground-coupled data. Therefore, a "rebar layer" is identified in the green box instead of individual rebars in the yellow box, respectively, as shown for a 2.0 GHz antenna (top) vs. a 1.5GHz ground-coupled antenna (bottom) at the same location (Figure 28).

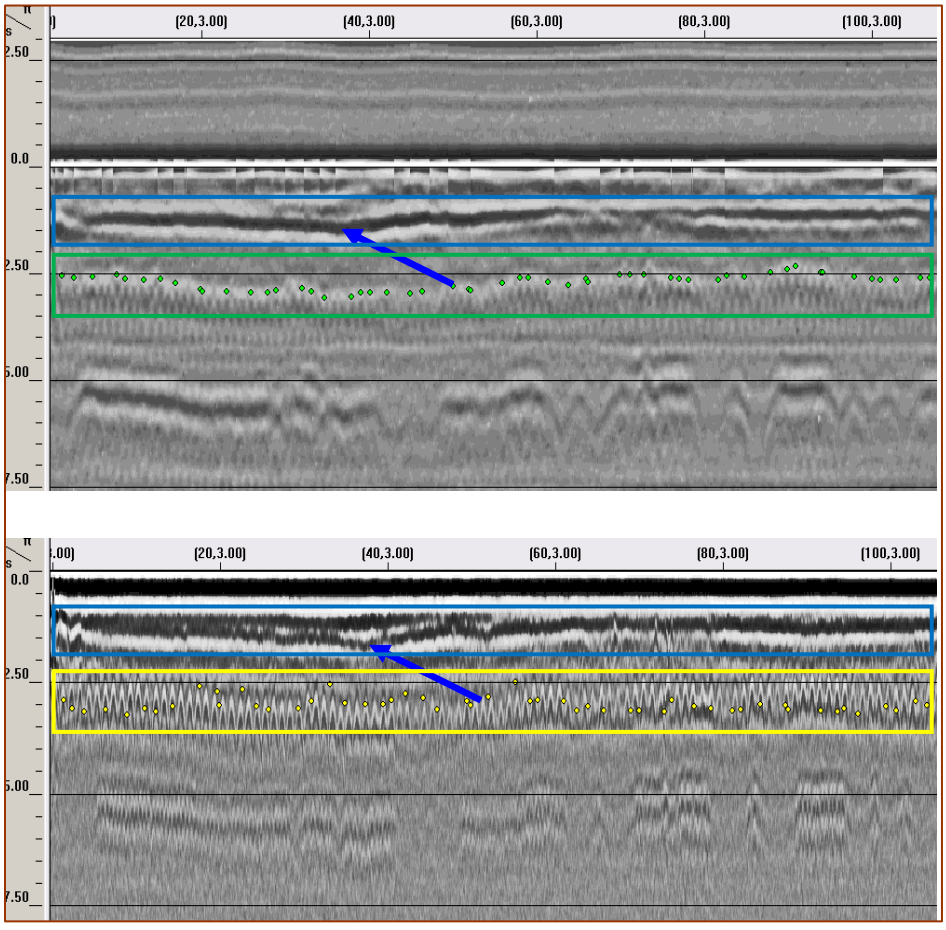

Figure 28. Processed data and automated rebar-picking from 2.0GHz horn (top) and 1.5GHz ground-coupled (bottom) sensors.

In both the upper and lower images, a very thin latex modified concrete (LMC) is seen in contact with the original deck concrete, and the LMC overlay lies beneath a hot-mix asphalt (HMA) overlay placed at the surface of the deck. Both data sets show blue boxes defining the

lateral and vertical extent of the LMC overlay between the HMA overlay and the original deck concrete, with blue arrows defining the black line (gap) within which the LMC overlay is confined. While the 2GHz air-coupled sensor provides a better vertical resolution for the layered structure across its entire length (a secondary objective for this particular survey was to determine LMC overlay performance) the 1.5GHz sensor consistently provided higher quality data for performing a deterioration assessment via top rebar attenuation mapping.

Data obtained from horn antennas is also processed and analyzed in various ways, depending on the survey objectives or specific service-provider capabilities and/or preferences. The varied analysis methods will depend on the signal characteristics of the sensors (antennas) used for the data collection and the frequency (resolution) of the antenna(s) deployed. It will also depend on whether the data collection utilizes a single-polarization or dual-polarization collection. In general, there is one patented dual-polarization data collection and analysis methodology that was developed and field-validated by GSSI and others (Romero and Roberts, 2002a and 2002b). The methodology incorporates the use of two, electronically-matched 1.0GHz horn antennas mounted in-line so that they scan along the same path and at the same sampling interval (scan density, in scans/foot or scans/m). This method provides a means of subtracting data obtained from either a longitudinally polarized T-R pair (data channel 2) from a transversely polarized T-R pair (data channel 1). In that way signal responses generated from overlays on decks that are within 1.5 to 2 inches of the upper rebar layer can be effectively removed from the targeted signal response from the upper transverse rebars. Also, effects from longitudinal steel, which is sometimes (but mostly not) immediately beneath the horn antenna path, randomly interferes in a significant way with accurate measurement of the upper transverse rebar signal reflection. This dual-polarization "subtraction" method for analyzing two-channel GPR data, when the antennas are deployed as described above (and shown mounted behind a vehicle as in Figure 26 right) has two primary benefits. It provides a means of artificially improving the vertical resolution of a lower-frequency sensor (1.0GHz horn vs. either 1.5GHz ground-coupled or 2.6GHz ground-coupled, for example), and it also lends itself to special circumstances where definitely a dual-polarization data collection and (channel subtraction) analysis method is preferred, or the selection between a transversely-polarized deployment (antenna mounted so that its long axis parallels the vehicle's centerline axis) or a longitudinally-polarized deployment (antenna mounted sideways) is chosen because it will yield a better data analysis.

A single polarization may be preferred for data analysis because (a) there is no overlay and concrete cover has been previously determined to be consistent with current design practice (minimum rebar depth of 2"), (b) typical reinforcement size consists of large diameter rebars and spacing variability (layout) within a deck structure indicates there is no need for a dual-polarization analysis, or finally (c) deck construction indicates that there is sparse reinforcement spacing and the deck thickness is such that an attenuation map based on full-depth (bottom of deck) signal attenuation is a preferred analysis strategy. Until the data have been collected it is difficult to know whether a dual-polarization approach, or a single-polarization analysis (with a definite preference in polarization during deployment) is going to provide the best results. When these are known quantities, sometimes the correct choice for single-polarization deployment can be made; however, most often some of the information is either not available for individual decks or a series of decks with variable properties are

scheduled for successive data collection on a planned route where antenna orientation (polarization) cannot be changed between accessing each of the individual structures.

When the orientation of top rebar is not known (transverse tied above longitudinal steel in the upper mat – or vice-versa), it is not clear until after the data have been collected whether a dual-polarization collection and analysis methodology (data channel subtraction) would have been preferable to a single channel (single-polarization) deployment and analysis. Certainly, the objective of the selection will be to take advantage of polarization effects so that surveys can be conducted along the direction of travel (with traffic). This cannot be achieved unless (a) two surveys, one with a single air-coupled antenna oriented in the transverse polarization and another with the sensor oriented so it is polarized longitudinally, or (b) a dual-polarization data collection takes place and both channels can be scrutinized (Romero and Roberts, 2004). Figure 29 shows GPR signal response from a deck construction that was not known until after the GPR data were collected, because the reinforcement layout (cross-sectional and plan view) were not provided until data were being processed. A peculiar reinforcement layout corresponded to negative-moment and positive-moment regions within a continuously-reinforced slab, requiring the ability to have both the transversely- and longitudinally-polarized data to analyze, for selection of the appropriate data set that would yield accurate results. Not having data from both antennas would have created a 50/50 chance that no usable data from this deck would have been generated. Without having collected dual-polarization data, and reviewing the antenna response from both channels, the "normally-selected" (dual-polarization subtraction) algorithm would have resulted in analyzing data that was not going to yield good results; instead, only the transversely-polarized signal in the upper window was analyzed once the detailed reinforcement layout and rebar size were known.

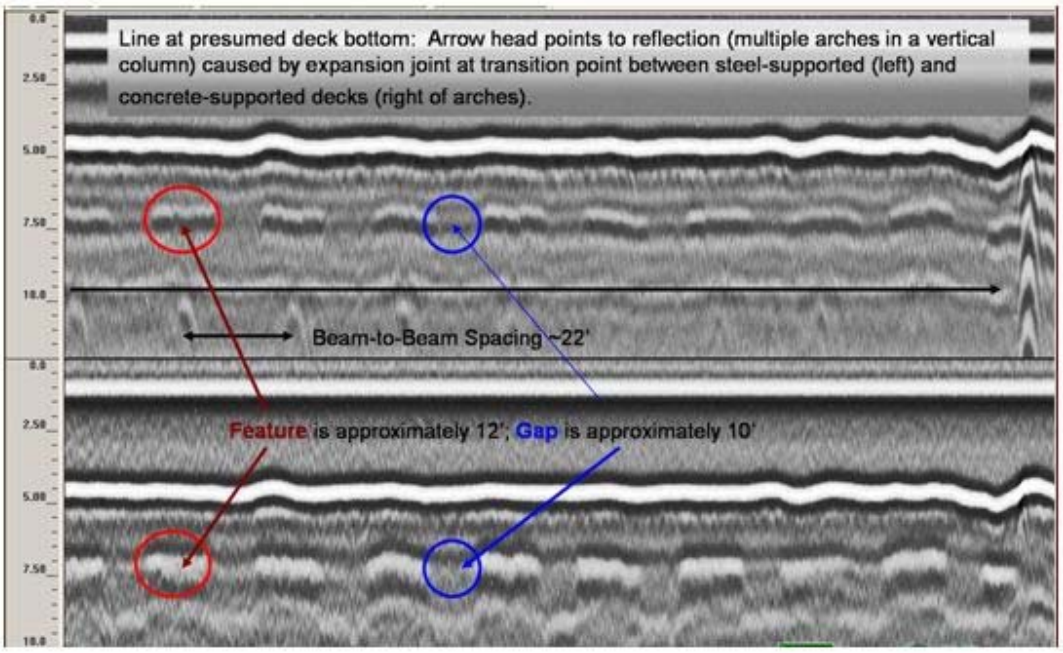

Figure 29. Raw data from transversely-polarized (upper) and longitudinally-polarized (lower) antennas confirm a difficult analysis scenario for a single-polarization deployment.

Furthermore, it is difficult, if not impossible, to resolve an air-coupled image (particularly from a 1GHz sensor, and to a somewhat lesser extent with higher-frequency 2GHz antenna) so that an analyst is able to conclude that the signal response being measured does not include artifacts from either longitudinal steel, concrete defects, shallow cover or overlays and patches within close vertical proximity. When these signal responses (potential artifacts for horn antenna data) are identified clearly in high-resolution (1.5GHz) and very-high resolution (2.5GHz) data, appropriate means can be made to extract the information sought. One approach can be to pick the portion of the signal for analysis that is consistent with the targeted object (uppermost transverse rebar, for instance), while ignoring the areas that can be negatively impacted by reflections from these objects in close proximity. The second approach is to "skip" analysis of a short-length segment of GPR data that would yield incorrect condition assessment results on a map at this problematic location. Such options are not available during an air-coupled GPR analysis because these negative effects are essentially invisible in the signal response (analyzed image), though definitely present.

The reasons mentioned above related to horizontal (spatial resolution) issues negatively impact air-coupled antennas, particularly related to the utility of horn antenna data for field selection of core locations. It is highly unlikely that appropriate core locations can be as easily picked from raw horn antenna data when both subtle signal attenuation and defects (such as those shown in Figure 27, in the red boxes, for the ground-coupled sensors) are considered as attributes used when viewing a GPR image. This is especially true when these decisions have to be made in the field. This means that a separate lane closure operation, besides whatever traffic control may be planned for the horn antenna data collection, is typically planned and staged solely for this purpose at a later date.

Despite some of these complexities, there are some advantages inherent to collecting/processing data using horn antennas. The primary one is the lower cost of data collection during the GPR survey itself, due to the ability to conduct the survey without need for lane closures. This generally means that the traffic control can be limited to an attenuator truck with a sign arrow following the GPR survey vehicle. A second advantage is that the data processing can often be less time-consuming, because the data density (scans/foot or scans/meter) is lower. The third advantage is that spacing of the GPR lines is often allowed to be wider (3ft vs. 2ft) when the GPR data is used primarily as a network-level tool to help rank deck condition, rather than to accurately delineate deterioration quantities for removal. Horn antenna surveys can present a less costly, though rarely as accurate, solution for bridge deck deterioration-mapping. Generally speaking, there are trade-offs between higher accuracy (project-level data) and lower costs (network-level information) that often drive a decision between using ground-coupled or air-coupled GPR approach, respectively, as part of a bridge deck condition evaluation process that may have either shorter-term, or longer-term, asset management or maintenance goals in mind. It is important that these benefits, limitations and tradeoffs be well understood so that client expectations can better be matched with survey results produced by the service provider, or researcher. (Romero and Gucunski, 2003, Romero *et al.*, 2009)

Data Processing and Analysis.

There are three main processing and analysis steps involved in creating a deterioration map of a deck from high-resolution, ground-coupled GPR data (Parrillo *et al.*, 2006). The first processing step, most commonly implemented in a semi-automated manner, includes time-zero correction of the surface signal, (optional) migration of the hyperbolic signals coming from the rebars, and rebar reflection picking. In the next step of the processing sequence the automatic rebar reflection picking is performed with verification of the picks using interactive interpretation. The third step is an interactive interpretation where the rebar locations may be reviewed and edited. The result of the process is a table of rebar position (depth) and amplitude of reflection, as shown in Figure 29 for rebar picking in the scan from the 1.5 GHz antenna. Zones of weak reflections or strong attenuation are clearly visible in this upper image, as in the upper right and lower images shown previously in Figure 27.

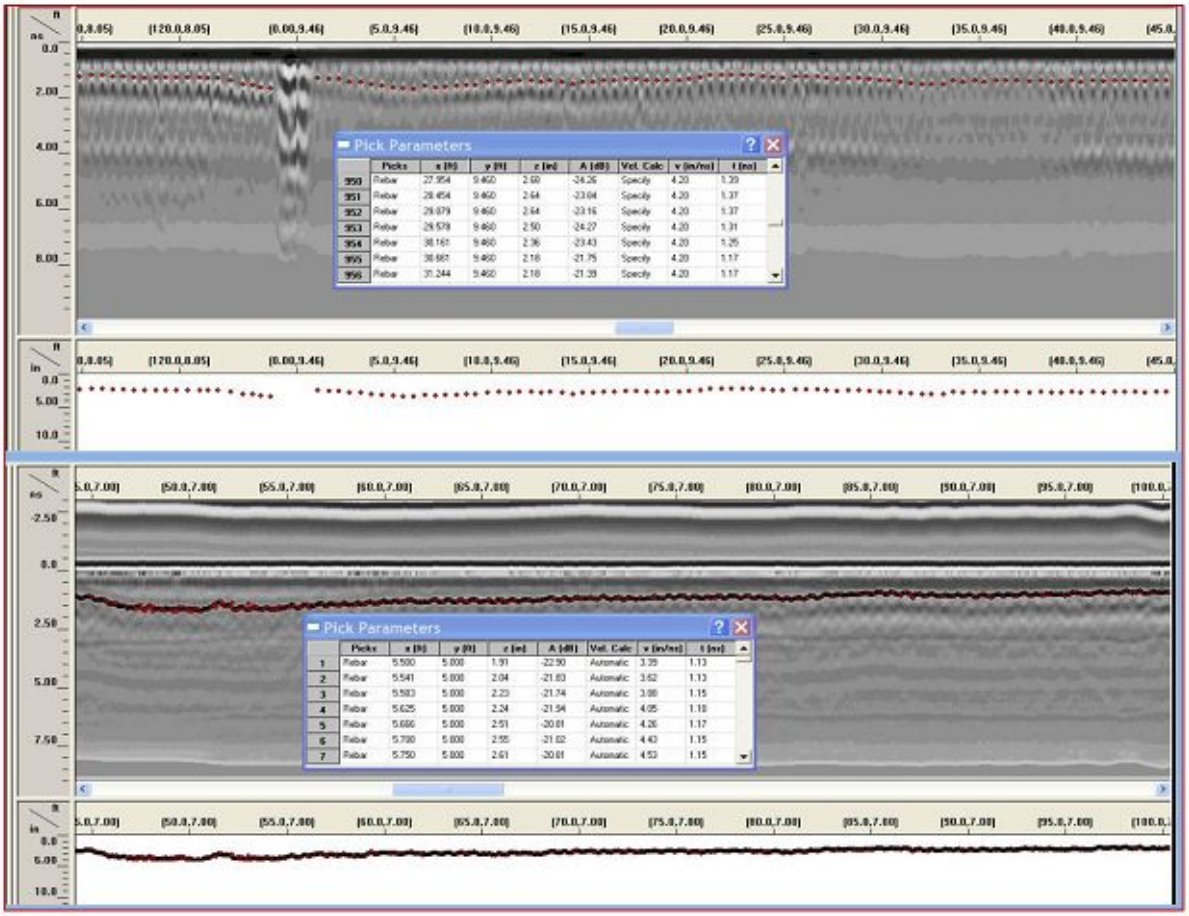

Figure 30. Processed data and rebar picking for 1.5GHz ground-coupled antenna and 2.0 GHz horn antenna, respectively, at 24 scans/foot sampling (upper and lower images).

After processing and analyzing the data the last step (either ground-coupled or horn antenna analysis) is generally the presentation of the attenuation of the signal at the rebar level, and thus relative deterioration of the deck, in the form of a contour map. Color coded contour plots are generated using the normalized or corrected amplitude of the reflection at the rebar level as the

gradient in the plot, with the most accurate maps also accounting for variations in rebar depth. Color levels represent the level of signal attenuation and, qualitatively, the severity of deterioration. Usually the hot colors (reds, yellows) represent the severest levels of deterioration and the cool colors (greens and blues, respectively) indicate a lower level of deterioration or a deck that is essentially sound, or considered to be in good condition. The contour plots for a 1.5 GHz ground coupled antenna are shown in Figure 31.

As shown in Figure 31, the uppermost contour map (not corrected for depth) displays most of the signal attenuation in areas where bars are deeper than normal. Much of this signal attenuation is simply due to excessive bar depth beyond the mean rebar cover. Thus, though this GPR signal strength decreases with increased depth to a target, this component of signal attenuation (caused by scattering or dispersion) actually has nothing to do with poor concrete quality. However, other areas which display signal attenuation include zones near expansion joints and curbs, but these areas generally do display signal attenuation indicative of corrosion-related damage, because infiltration and ponding of chlorides in these regions is common.

When compared to the depth-corrected GPR map at bottom, and to the rebar cover map and impact-echo map in between; it is obvious there is a stronger correlation to "increased deterioration with increased cover depth" than there is a correlation to damage displayed in the impact-echo map. In the areas where the concrete cover is shallowest (green and yellow/orange zones on the concrete cover map), note that these areas appear to be in extremely good condition on the GPR map without depth correction, while on the depth-corrected GPR map there are zones which fall in the "fair", "poor" and even "serious" grading levels. This suggests an inverse correlation between rebar depth and condition exists: shallower bars tend to be in more sound concrete and deeper bars tend to be more corroded, which makes no sense. In reality, areas with the most shallow concrete cover typically experience chloride ingress earlier and tend to display not only signs of corrosion that can be measured and observed, but also corrosion-related damage typically initiates in these "shallow rebar" zones. The maps in Figure 31 clearly illustrate that a better correlation exists between the depth-corrected GPR condition assessment and the impact-echo (damage) condition assessment, and that the influence of shallow or deep reinforcement is minimized by performing this depth-correction. All subsequent GPR maps in this report are provided in their depth-corrected form, since there exists in most cases good correlation between these corrected GPR maps and data obtained using other NDE methods. GPR maps that were plotted without a depth-correlation do not show anywhere near the same degree of correlation as exists on Figure 31 between the corrected and uncorrected maps, so there is no purpose for showing the inferior (uncorrected) maps in this report.

Last, attenuation plots generated from surveys using different antennas or antenna types will show similar patterns. However, attenuation ranges in those plots will be different both due to their emission patterns and any slight variations in lateral position from which the data were collected (lane wander) with respect to the surface of the deck (air or ground coupled). For this, as well as numerous other reasons: proximity of reinforcement (rebar cover), presence of joints, high density of reinforcement, etc., it is not correct to define a single unique threshold value for deck deterioration (Barnes and Trottier, 2008, Barnes, *et al.,* 2008). In general, going from the horn antenna and progressing to the ground coupled antenna in order of frequency levels, the poor quality areas of a deck are identified with higher discretion.

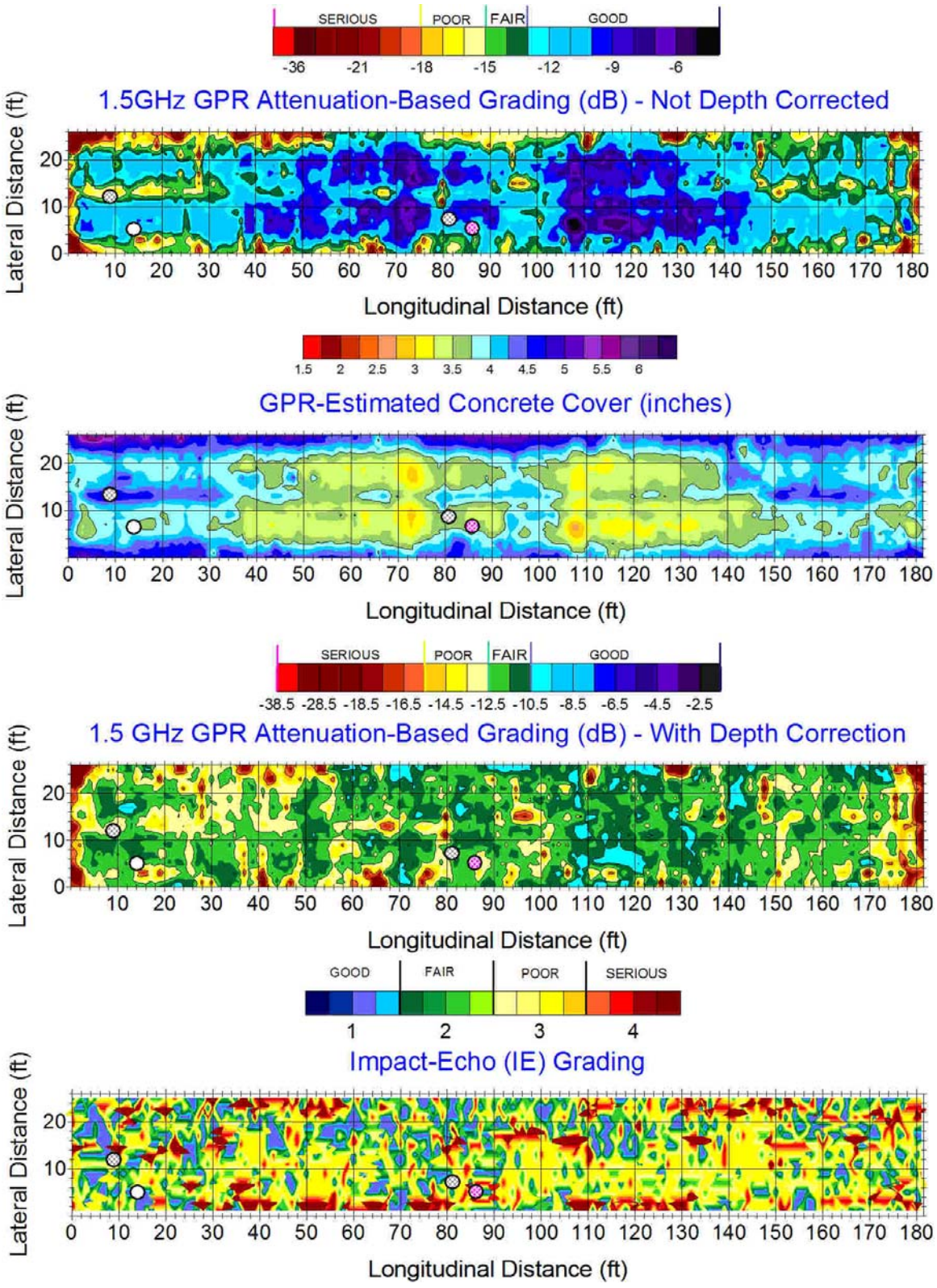

Figure 31. Deck O3 Maps show better correlation between depth-corrected GPR and IE, while GPR map not corrected for depth displays strong inverse correlation to cover depth.

Eddy Current Method

The eddy current method exploits the fact that magnetic fields cause currents in electrically conductive materials. Eddy currents are created through a process called electromagnetic induction. Alternating current applied to a conductor, such as copper wire, results in a magnetic field in and around it. This magnetic field expands as the alternating current is increased to a maximum and collapses as the current is reduced to zero. Another electrical conductor in close proximity of this changing magnetic field will experience a current. Eddy currents are induced electrical currents that flow in a circular path. They get their name from "eddies" that are formed when a liquid or gas flows in a circular path around obstacles when conditions are right.

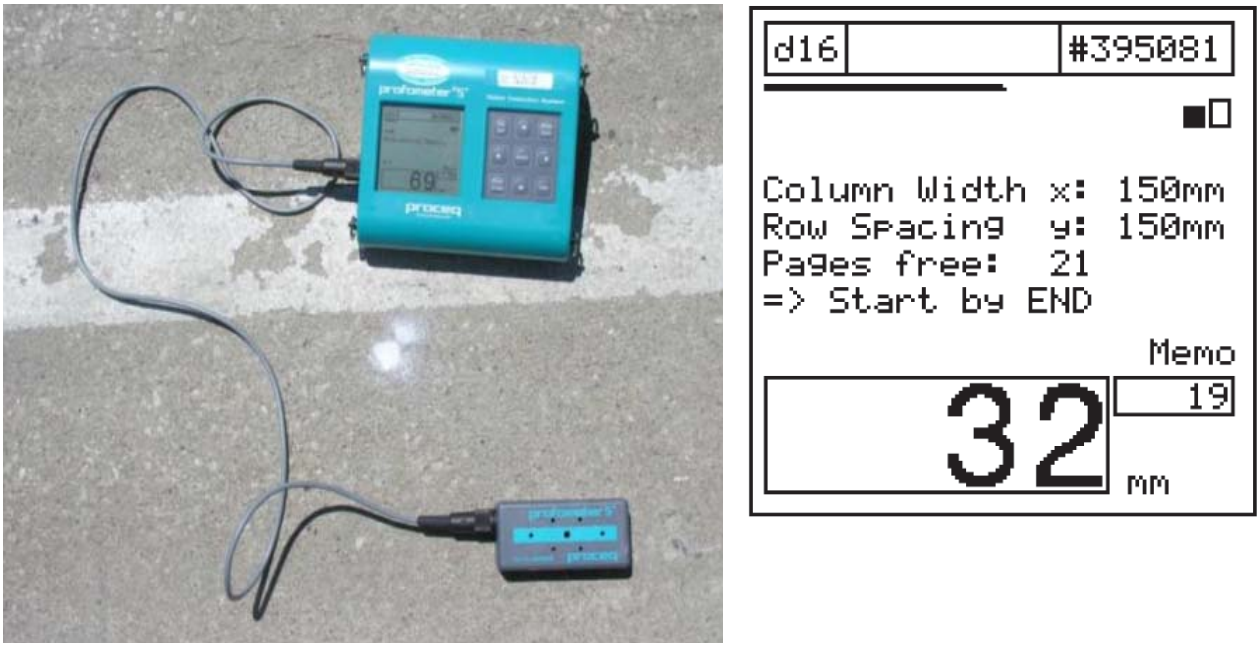

Figure 32. Eddy current cover meter device (type Profometer, Proceq, Switzerland) on a concrete bridge deck (left) and a sample screen display with estimated rebar depth (mm).

The basic principles of eddy current testing are summarized in Table 5. Eddy current devices are usually used to locate steel reinforcement. If the rebar diameter is known, its depth can be determined. Conversely, if its depth is known, the diameter can be estimated. The most basic eddy current testing instrument consists of an alternating current source, a coil of wire connected to this source, and a voltmeter to measure the voltage change across the coil. An amp meter could also be used to measure the current change in the circuit instead of using the voltmeter. An eddy current cover meter device on a concrete bridge deck is shown in Figure 32 (left). The probe (grey box) has to be moved from a starting position in one direction. The concrete cover is continuously measured and displayed or reported by an audible varying signal. The bar direction can be detected by moving the probe in the direction of its longitudinal axis along the rebar.

Table 5: Basic Principles of the Eddy Current Inspection (from http://www.ndt-ed.org/EducationResources/CommunityCollege/EddyCurrents/Introduction/IntroductiontoET.htm)

	An eddy current testing probe consists of a wire, which is formed into a coil.
	Alternating current is injected in the coil at a frequency chosen by the operator.
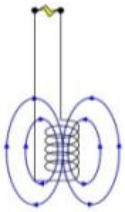	A dynamic expanding and collapsing magnetic field forms in and around the coil as the alternating current flows through the coil.
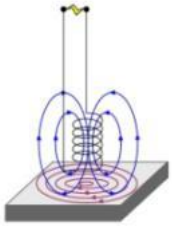	When an electrically conductive material is placed in the coil's magnetic field, electromagnetic induction will occur and eddy currents will be induced in the material.
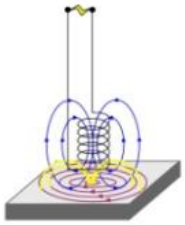	Eddy currents flowing in the material will generate their own "secondary" magnetic field, which will oppose the coils "primary" magnetic field. This entire electromagnetic induction process to produce eddy currents may occur from several hundred to several million times each second depending on the inspection frequency.
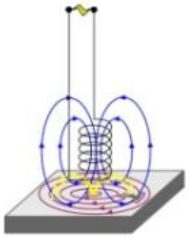	When a flaw is introduced to the conductive material, the eddy currents are disrupted.

CHEMICAL / POTENTIAL NDT TECHNOLOGIES

Corrosion monitoring systems are relatively new with the first installations carried out in the late 80s when built-in sensors for new reinforced concrete structures were developed. In the late 90s, the first post-mount sensors for existing structures were used. Today, the experience with post-mounted sensors is still limited; however, they seem promising as a tool in monitoring of the ingress of a corrosion front. Reinforcement embedded in sound concrete is covered by a passive non-corroding oxide film. Deterioration initiates when this passive layer is damaged, for example due to carbonation or ingress of aggressive substances into the concrete. This reaction involves a reduction of the half-cell potential of the rebar. While impressing a voltage across a corroding rebar, current will readily flow, but it will not when the same voltage is impressed across a passive one. The magnitude of electrical current, as well as the ability to polarize, can be measured. These properties are indicative of the corrosion state. An overview of the most commonly used electrical and electrochemical methods is given in this section. Their benefits and limitations are discussed in detail.

Half-Cell Method

The half-cell potential measurement is a well established and widely used method to evaluate the corrosion of steel reinforced and pre-stressed concrete structures. The method can be used at any time during the life of a concrete structure and in any kind of climate provided the temperature is higher than 2 ^{0}C (Elsener, 2003). Half-cell measurements should be taken on a bare concrete surface since presence of isolating layers (asphalt, coating, and paint) may make measurements erroneous to impossible. Using empirical comparisons, the measurement results can be linked to the probability of corrosion. One can measure the potential difference between a standard portable half-cell, normally $Cu/CuSO_4$ standard reference electrode, placed on the surface of a reinforced concrete element. When the reference electrode is shifted along a line or grid on the surface of a reinforced structural member, the spatial distribution of corrosion potential can be mapped. The principle of the method is depicted in Figure 33. A so-called reference electrode is connected to the positive end of a voltmeter and steel reinforcement to the negative one. The reference electrode is usually galvanically coupled to the concrete surface using a wet sponge. The input impedance of the voltmeter (Figure 33) should be in the range of $10^6 – 10^9$ Ω.

Corrosion of steel in concrete is similar to the electrochemical mechanism of corrosion of a metal in an electrolyte (Elsener, 2003). This implies that separate anodic and cathodic processes take place simultaneously on the same metal surface. At the corroding side (the anode), iron is dissolved and then oxidized to iron ions, leaving electrons in the steel ($Fe \rightarrow Fe^{2+} + 2e^-$). At the cathodic side of the reaction, oxygen is reduced and hydroxyl ions are produced ($O_2 + 2H_20 + 4e^- \rightarrow 4OH^-$). If the anodic and cathodic regions of the corrosion cell are far enough apart, that is if their spatial separation ranges between a few centimeters to meters (macro-element corrosion), they can be detected with most commercial half-cell systems. However, if the steel surface corrodes uniformly and the anodic and cathodic areas of the reaction are very small and evenly distributed (micro-element corrosion), they will most likely not be detected with standard half-cell systems (Baumann, 2008).

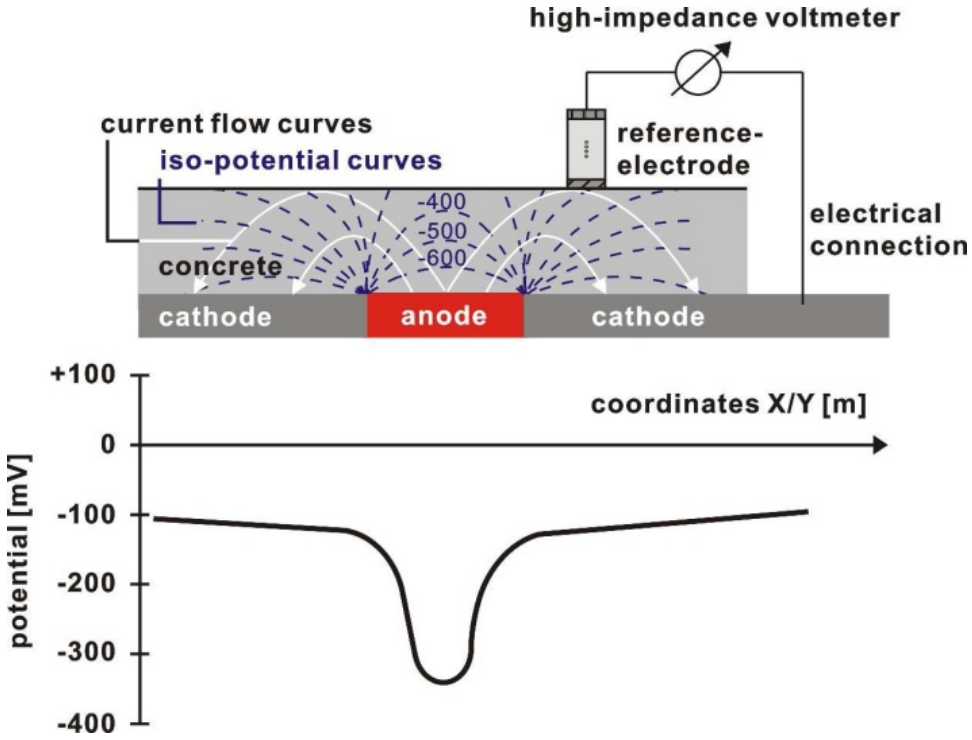

Figure 33. Schematic of the half-cell potential measurement principle (from Baumann, 2008).

Principle of Measurement

When a metal is submerged into an electrolyte, positive metal ions will solve (oxidation) leading to a surplus of electrons in the metal lattice and a net negative charge at its surface. The positive metal ions will accumulate at the metal-liquid interface, which in consequence gets positively charged. A double layer is formed. Anions, from the electrolytic solution (in concrete Cl^- and SO_4^{2-}), are attracted to the positively charged side of this double layer and accumulate there forming the so called half-cell. A potential difference between the metal and the net charge of the anions in the electrolyte builds up, and its magnitude depends on the solubility of the metal and the anions present in the solution.

When two different metals are submerged into an electrolyte (two half cells) and are electrically connected by a wire, a galvanic element is created. The two different metals will cause different electrical potentials in their half-cells, which in turn causes a current flow through the wire. The less noble of the two metals is dissolved (anode) and the more noble remains stable (cathode). In the surface layer of the less noble, the corroding metal, a surplus of electrons is formed. The potential difference between the two metals can be measured as a voltage with a high-impedance voltmeter.

ASTM C875 standard provides the general guidelines for corrosion evaluation in concrete, as shown in Table 6. According to a number of authors, however, the proposed limits for half-cell corrosion potential readings should be used with caution (Cziesielski and Marquardt 1988; Marquardt 1998; DGzfP 1990). If the majority of the half-cell readings in a potential mapping survey are low, a group of comparatively high values can still indicate a corrosion area,

even though they might not be high in the absolute sense. Elsener (1991) published a comparison of half-cell potential values measured on six reinforced concrete structures in Switzerland. Their results are presented together with the ASTM standard thresholds in Figure 34. Properties like chloride content, moisture content or concrete cover depth (more detailed information given below) can have a significant effect on the potential field and should be regarded in the interpretation. In some cases, strict adherence to the ASTM thresholds can lead to misinterpretations between actively corroding regions and areas where corrosion is considered passive, thus typical of reinforcement within sound concrete.

Table 6: Probability of Corrosion According to Half-cell Readings with $Cu/CuSO_4$ Electrodes

Half-cell potential reading vs. $Cu/CuSO_4$	**Corrosion activity**
less negative than -200 mV	90% probability of no corrosion
between -200 mV and -350 mV	increasing probability of corrosion
more negative than -350 mV	90% probability of corrosion

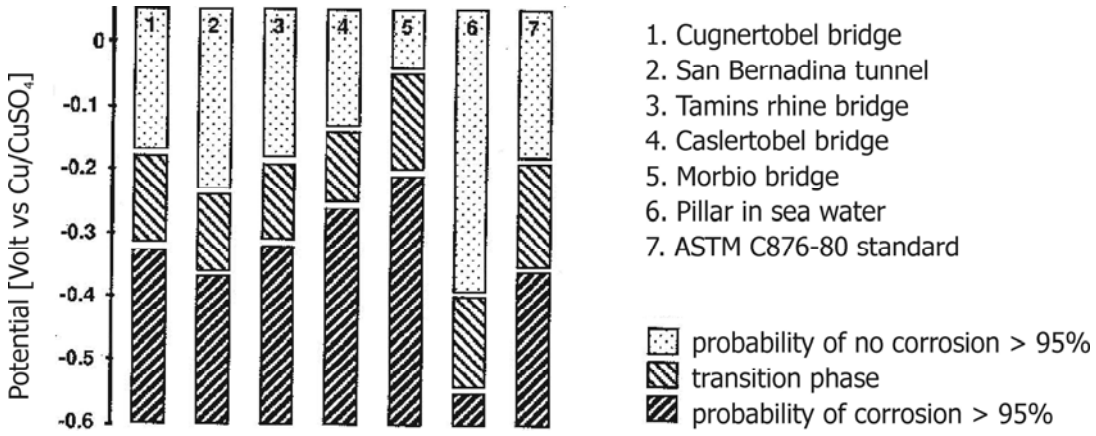

Figure 34. Half-cell potential values measured on different steel reinforced concrete structures – compared to the threshold levels reported in the ASTM standard (from Elsener, 1991).

Potential mapping is either non-destructive or destructive in the most minor sense, depending on whether there is available contact to the bare reinforcement (grounding) or not. In the best case the reinforcement is accessible at two locations far away from each other to check for electrical continuity. In this case, electrical continuity is indicated by a resistivity reading that should be below 1 Ω. The half-cell method measures the electrical potential not directly on the (possibly corroding) steel, but on the concrete surface. Though, if the cover thickness ranges between 30 and 40 mm, the measured potentials reasonably reflect the actual potential value of the steel. Change in the half-cell potential as a function of cover depth, when measured right above a corroding steel area, is shown in Figure 35. The maximum penetration depth is reported to be around 200 mm (Bien *et al.,* 2007). Obviously, the accuracy and susceptibility of the measurement decreases as the corroded area becomes deeper and smaller. The concrete temperature has only a negligible effect on the half-cell potential, as also shown in Figure 36.

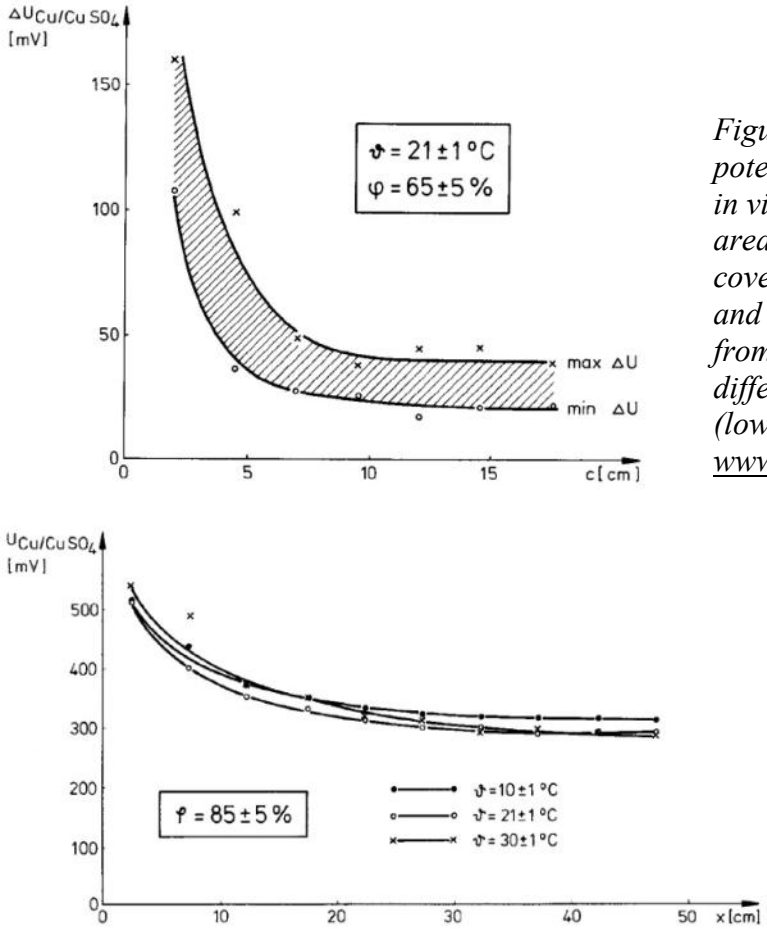

Figure 35. Change of the potential difference $V_{Cu/CuSO4}$ (a) in vicinity of a corroding steel area as a function of concrete cover thickness, c (upper figure), and (b) as a function of distance from the corroding area at different air temperatures, θ (lower figure) – link to www.fhnon.de/fbab/marquardt

The method only predicts the corrosion risk in the early phase. It is more susceptible to chloride induced corrosion than to carbonation as the former generates larger potential changes on the surface. Most important factors influencing half-cell potential data are oxygen, chloride concentration and concrete electrical resistivity, as indicated in Table 7. Dense material overlays, concrete sealers, corrosion inhibitors, chemical admixtures and cathodic protection systems confuse the issue substantially. Complementary use of other NDT methods can help to overcome these limitations. The following section summarizes the most important factors and their impact on half-cell potential surveys according to Gu and Beaudin (1998).

Oxygen Concentration

An accumulation of oxygen between the rebars and concrete has a strong impact on the half-cell potential records. A decrease in oxygen concentration at this boundary will lead to a more negative corrosion potential reading and hence, be associated with a higher probability of corrosion. For example, the corrosion potential reading would be more negative beneath a dense concrete cover having a low permeability than beneath a porous concrete with a higher permeability. However, such a negative record would not necessarily indicate a higher probability of corrosion.

Table 7: Typical Potential Ranges of Normal Steel in Concrete. Volts CSE (after Elsener, 2003)

Concrete Type	**Half-cell Potential**
Water saturated concrete without oxygen	-900 to -1000 mV
Wet, chloride contaminated concrete	-400 to -600 mV
Humid, chloride free concrete	+100 to -200 mV
Humid, carbonated concrete	+100 to -400 mV
Dry, carbonated concrete	+200 to 0 mV
Dry concrete	+200 to 0 mV

Carbonation

Concrete carbonation reduces the pH value at the steel reinforcement-concrete boundary. This reaction takes place between the carbon dioxide in the atmosphere and the calcium hydroxide in concrete and is usually observed to increase with time in most structures. If this happens, the half-cell potential will shift likewise towards slightly more negative values. This still might be misleading as sometimes even small changes in corrosion potential are associated with large increases of corrosion rates.

Chloride Ion Concentration

Chloride ions accelerate steel corrosion significantly. This kind of reaction causes a strong shift of the corrosion potential towards more negative values. This is a case that common half-cell devices and the ASTM C876 standard predict usually well.

Concrete Resistivity (moisture content)

Changes in the moisture content (e.g. by wetting of the concrete surface) cause a shift of the potential field to more negative values. Elsener (2003) reported a 100 mV shift on a bridge deck measured in dry and wet conditions after rainfall. Qualitatively, the potential map did not change, which according to him further indicates that the potential gradient is the better indicator for corroding rebars.

On the other hand, a high concrete resistivity can cause significant errors in the determination of the corrosion potential. A schematic diagram that illustrates the half-cell measurement circuit is shown in Figure 37. Half-cell devices measure the voltage difference between the two ends of the voltmeter internal resistor. Only if this internal resistor is much larger than the concrete resistance the measured half-cell potential reading will be close to the true corrosion potential of the steel reinforcement. Both decreasing the concrete resistivity and increasing the internal resistance (>20 MΩ is recommended) of the voltmeter would enhance the measurement accuracy. Moisture variations close to the surface (<2 cm) have no particular influence on half-cell potential measurements. Below a 20 mm depth, the moisture content of concrete does not exhibit a major seasonal variation. Since the concrete cover is usually thicker

than 30 mm, the moisture content of concrete should minimally influence the potential at the rebar level.

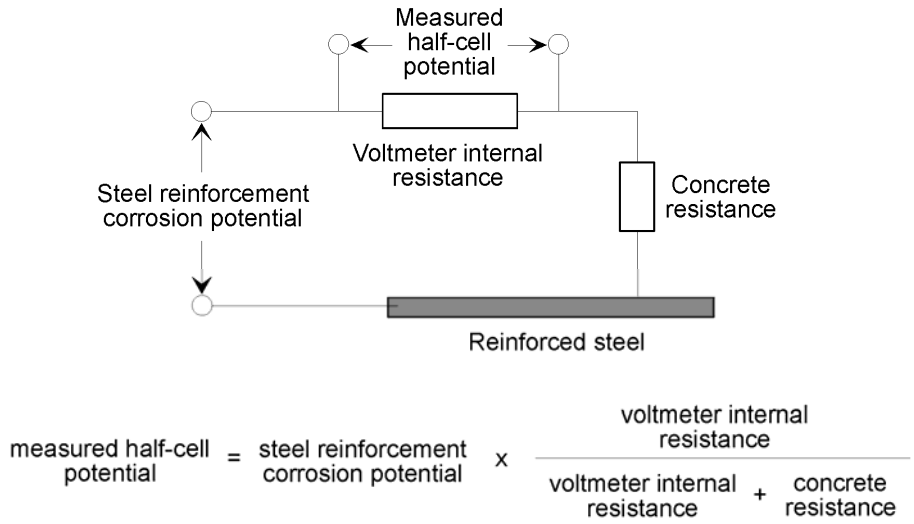

Figure 36. Schematic illustrating half-cell measurement circuit (after Gu and Beaudin, 1998).

Corrosion Inhibitors

Corrosion inhibitors can have either anodic or cathodic effects. Depending on which inhibitor is used, the half-cell potential is influenced differently. While anodic systems shift the potential toward positive values, cathodic systems shift them toward negative ones. Anodic corrosion inhibitors, like calcium nitrite, are strong oxidizing agents. As a consequence, this chemical shifts the corrosion potential toward more positive values and reduces the corrosion rate. In contrast, a cathodic inhibitor will shift the corrosion potential and reduce the severity of the steel corrosion. Many commercial corrosion inhibitors are cathodic. The mixed corrosion inhibitors are the third type of inhibitors that can influence the results in either direction in an unpredictable manner. The nature of the corrosion inhibitor is crucial to understand half-cell potential readings. In the best case, the producer of the corrosion inhibitor should be consulted before the half-cell potential measurements are carried out to clarify what is the most likely effect of the used chemical.

Epoxy-Coated and Galvanized Rebars

According to the ASTM C876, the half-cell potential method is not suitable for measurements on epoxy-coated and galvanized steel reinforcement. The former does not provide a good enough electrical connection for the measuring circuit. Even though the reading may look stable and valid, it might just have been taken on a coating defect, damaged or unprotected rebar and therefore, not be authentic. In the latter case the galvanic metal (normally zinc) protects the steel reinforcement. The measured half-cell potential reading is then no longer the corrosion potential of the steel reinforcement but a mixed potential of the steel plus zinc. Hence, a simple comparison of the reading and the data in the ASTM standard cannot be applied. Long-

term monitoring of the change of potential should be possible, provided a specialist interprets the data.

Dense Concrete Cover

A dense concrete cover has two main advantages; it provides a good physical barrier for chloride-induced corrosion and limits the oxygen diffusion process. So, the oxygen concentration at the interface of reinforcing steel-concrete can be very low and therefore, the corrosion potential could shift to more negative values without indicating a high corrosion probability.

Organic Coatings and Sealers

Due to the high resistivity of organic coatings and sealers, half-cell measurements made on such overlays tend to be inaccurate. But, readings could be taken in areas where the coatings were removed or damaged. If the coating is gas impermeable, the oxygen depletion must be regarded in the data interpretation.

Concrete Patch Repair

Most concrete repairs change the original environment in terms of electrochemical potential, which in consequence may lead to imbalances between the steel reinforcement embedded in the existing concrete and the patch. “Jumps” between the half-cell potential readings at the patch and existing areas may easily occur. Sometimes these go along with a possible acceleration of the steel corrosion.

Cathodic Protection Systems and Stray Current

Half-cell measurements on energized cathodic protection systems that cause stray currents are meaningless. On such structures, measurements should not be taken if the system is not shut down and depolarization for at least 24 hours. Large fluctuations including both high positive and high negative numbers may indicate the existence of stray currents.

The primary advantage of the method is the speed at which large areas of a structure can be tested to locate more active areas of corrosion activity, particularly when a rolling half-cell measurement system – shown in Figure 37 – is implemented. If possible the half-cell potential data should always be compared to other methods. Most useful and reliable interpretations of half-cell data will be: visual inspection, delamination survey, chloride content analysis and concrete resistivity measurements. The best results are obtained when the reinforcement is accessible and one electrode has electrical contact with it. But if the reinforcement is not accessible, the potential mapping can still be performed in a nondestructive way by using two reference electrodes. One electrode is fixed to one position, while the second one maps the surface. The drawback of this method is that it only detects spatial potential variations instead of the real reinforcement potential. Therefore, an almost uniformly corroding reinforcement would show the same small potential differences like a fully passive reinforcement.

Field Example of a Half-Cell Measurement:

A field example of half-cell potential measurements collected with a Canin+ wheel electrode (Proceq Inc.) on a concrete bridge deck is shown in Figure 37 (left). The ground electrode of the measurement device is connected galvanically to the reinforcement, and a $Cu/CuSO_4$ electrode maps the half-cell potential along the bridge surface. When records are taken along grid lines the data can be presented as contour plots. Potential values obtained on a concrete bridge deck in Iowa are shown in Figure 37 (right). Steep potential gradients and high negative potentials identify a high risk of corrosion. According to the ASTM thresholds, potentials above 350 mV indicate serious areas, where corrosion is more than 90% probable. Potentials less than 200 mV, mark sound areas with a probability of 90% for no corrosion. Intermediate potentials mark transition zones.

Figure 37. Half-cell potential measured on bridge deck (top left), example of mapped results (top right), images of control/display (bottom left) and electrode wheel (bottom right).

Advantages and Limitations:

The half-cell potential method is a fast and easy-to-use tool to detect ongoing steel corrosion in concrete. The primary advantage of the method is the speed at which large areas of a structure can be tested to locate more active areas of corrosion activity, particularly when a rolling half-cell measurement system, shown in Figure 37, is implemented. The electrodes can easily be maintained and are quite robust. Not much training is needed to carry out the measurements. The results are visualized while taking the measurements. Data processing software can usually be purchased together with the equipment, with the data plotted in a straightforward way. However, for each test object the potential thresholds have to be somewhat adjusted based on knowledge about the structure's construction and maintenance history, as well as conditions that exist during measurement. So, it is not simply recommended to accept the ASTM thresholds without considering other factors and/or combining the use of the half-cell method with other NDE methods. Even though many bridge engineers have used the half-cell potential method for years almost as a standard tool, the influence of concrete cover depth has not yet been researched thoroughly. As a consequence, correcting data for depth is not straightforward, just like it is not for moisture or salt content.

Electrical Resistivity Method

Presence and the amount of water in concrete are important parameters in assessing its corrosion state. Electrical conduction in concrete systems occurs mainly due to electrolytic current flow through the open pore system. Damaged and cracked areas, due to increased porosity, are preferential paths for fluid and ion flow. The electrical resistivity method, a well known technique among geophysicists, has been adopted for moisture and flaw detection, mainly cracks, but also for pollutions in porous media and in the field of civil engineering. Different commercially available devices for electrical resistivity surveys are on the market. Some authors report of special devices they have built to deal with particular investigation problems (e.g. Naar *et al.,* 2006).

As mentioned earlier, the higher the electrical resistivity of the concrete is, the lower the corrosion current passing between anodic and cathodic areas of the reinforcement steel will be. Resistivity surveys can be used to detect corrosion cells in tandem with another corrosion technique, like half-cell potential, to map corrosion activity (Millard, 1991; Gowers and Millard, 1999). The relationship between the electrical resistivity and normally observed corrosion rate of steel reinforced concrete is given in Table 8.

Table 8: Relationship Between Resistivity of Steel Reinforced Concrete and Corrosion Rate.

Resistivity [kohm*cm]	Corrosion rate
< 5	very high
5 – 10	high
10 – 20	moderate - low
> 20	low

In practice the voltage and current are measured at the surface of the object under investigation. Field measurement devices for civil engineering applications are adapted from the technology originally used for soil investigations. Probably the most common electrode layout in civil engineering applications is the Wenner setup (Figure 38). The Wenner layout uses four probes that are equally spaced. A current is applied between the outer electrodes and the potential is measured across the two inner ones. The resistivity is then calculated according to:

$$\rho = \frac{2\pi a\, V}{I}$$

with ρ = resistivity [ohm*m], a = electrode separation [m], V = voltage [V], I = current [A]. The inverse of the electrical resistivity is the electrical conductivity, σ [S/m].

Electrical resistivity measurements in the Wenner layout can be taken in the field or the laboratory. When taken in the field, probes, like the one shown in Figure 39 (left), can be applied that use wet foam pads at the end of the four steel rods (probes) to establish galvanic contact to the concrete surface. One example of a laboratory set up is shown in Figure 39 (right). German silver wires placed in PVC chambers serve as potential leads. Stainless steel caps at the front and end of the cell are used as current electrodes. All electrodes are coupled with agar gel to the specimen.

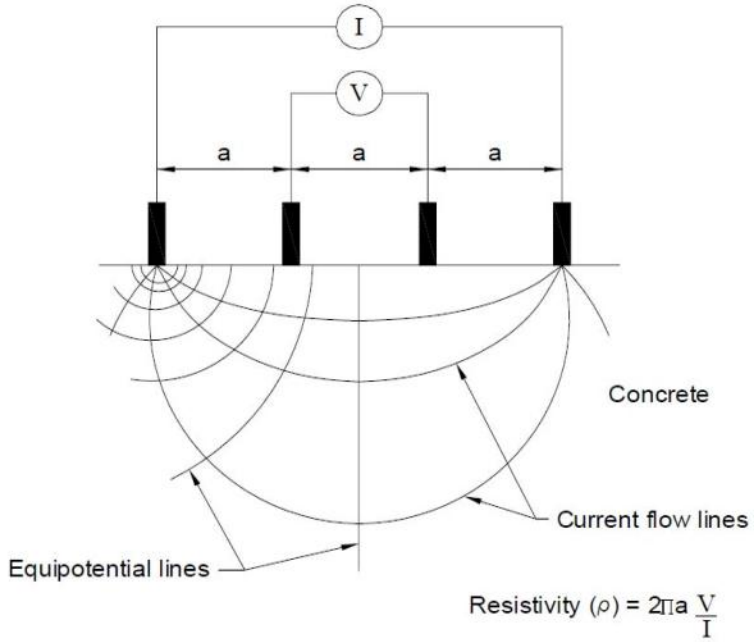

Figure 38. Commonly used four point Wenner spread applied in (geo-) electrical testing surveys (from Whiting and Nagi, 2003).

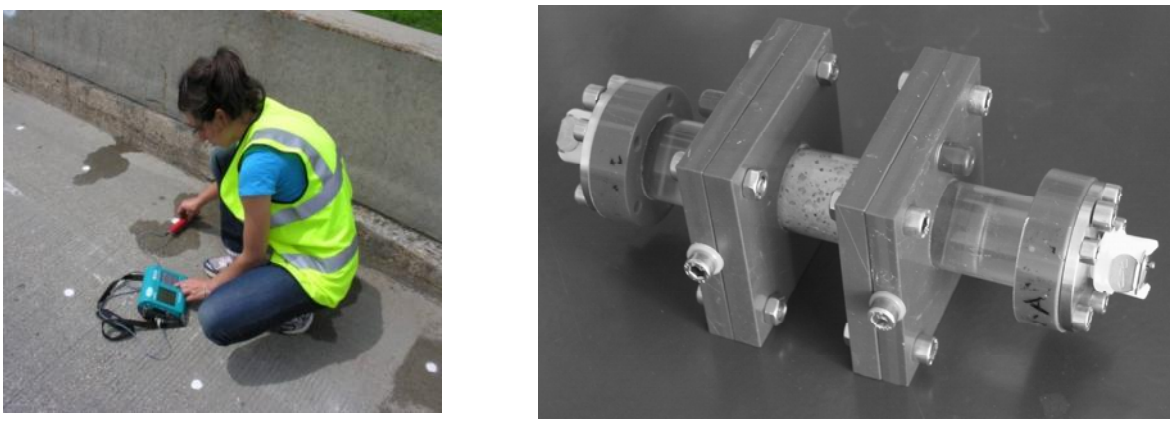

Figure 39. Resistivity measurement using Wenner probe on concrete bridge deck (left), and sample holder for CR measurements built by BAM (right) (Kruschwitz, 2007).

Electrical resistivity values in ohm*m for a variety of materials are summarized in Figure 40. Building materials like concrete, cement or wood are ion conductors, which mean that electrical conduction happens through the interconnected pore space. The resistivity of fully saturated concrete is on the order of 100 – 1000 ohm*m, depending on the conductivity of the saturating fluid. When oven dried, the electrical resistivity of concrete is as high as 10^6 ohm*m, an insulator.

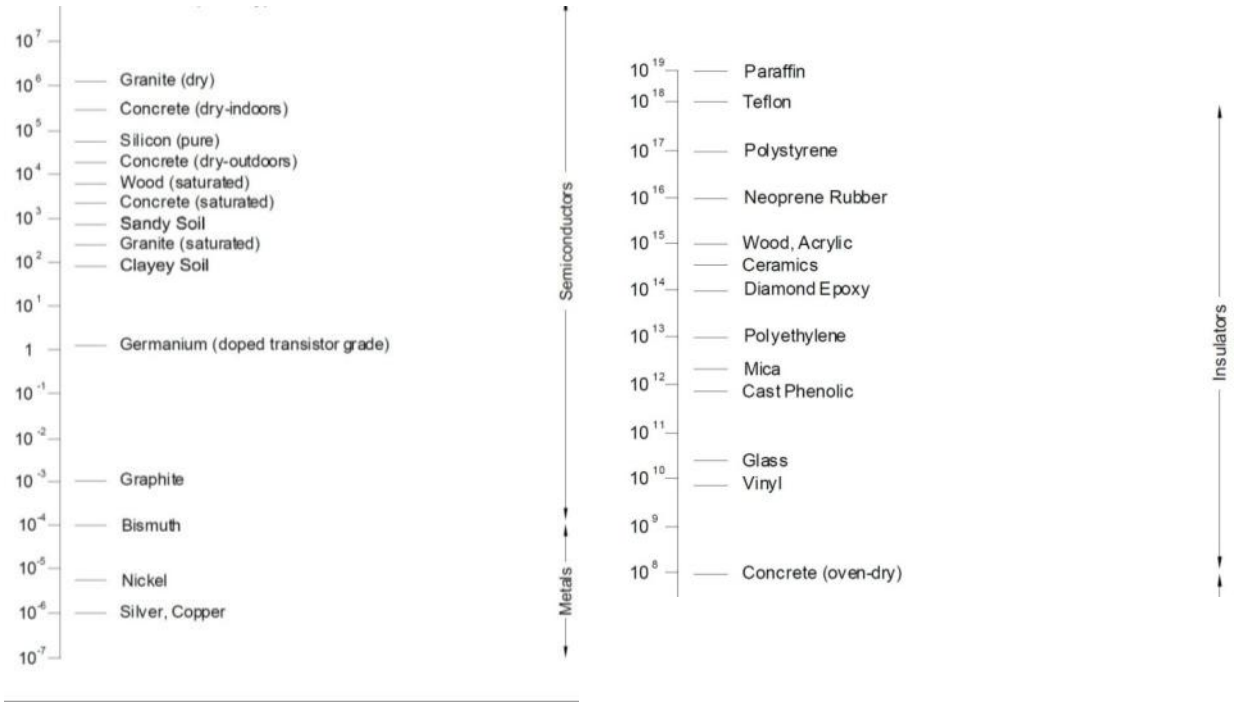

Figure 40. Ranges of electrical resistivity for a variety of materials (Whiting and Nagi, 2003).

As concrete is a composite material, its electrical resistivity will always depend upon its porosity, pore size distribution and factors such as the cement chemistry, water-cement ratio, types of admixtures etc. To a large extent it will also be a function of the ion type and content of the saturation fluid (Kruschwitz, 2007; Hunkeler, 1996; Bürchler *et al*., 1996). Phenomena like carbonation, chloride attack (deicing salts) and secondary damage like cracks also significantly influence the electrical properties of the concrete.

The effect of saturation on the electrical resistivity of different types of concrete is shown in Figure 41. The resistivity decreases with increasing water content. Gjørv *et al.* (1977) reported an inverse relationship between the water cement ratio (samples shown in red pattern) and the resulting electrical resistivity for his samples. Own (unpublished) experiments on a group of 5 concretes show similar results. Some of these samples were taken from (partly or entirely) demolished concrete bridges in Germany, others were taken from freshly made concrete.

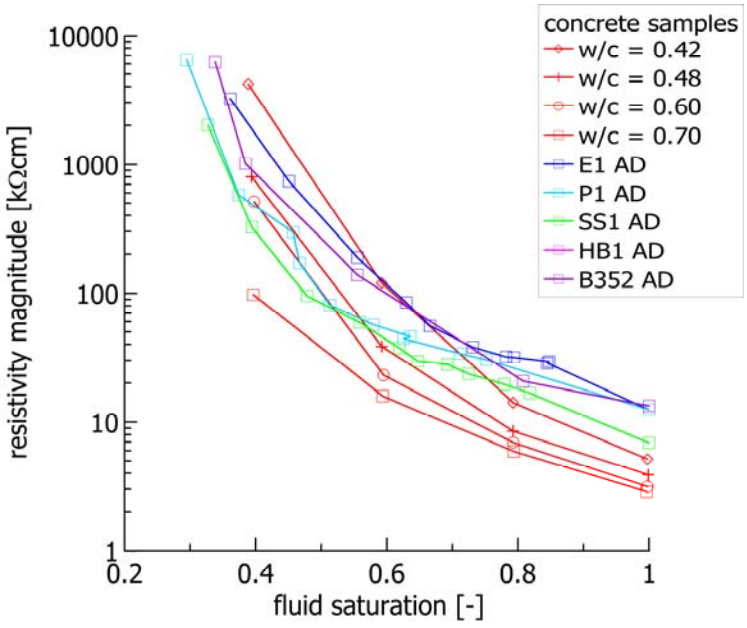

Figure 41. Effect of fluid saturation on the electrical resistivity of concrete, the graph includes data from Gjorv et al. (1977) and (own unpublished) results obtained in the laboratory.

Probably the most important parameter influencing the concrete resistivity is the fluid salinity. The results of electrical resistivity measurements for five types of concrete with different wt% NaCl solutions are presented in Figure 42. Basically, a two order of magnitude increase in the fluid conductivity decreases the resistivity magnitude of the samples by one order of magnitude. The fluid conductivity within a sample will not only depend on the saturating fluid, but also the solubility of each concrete. In electrical measurements, intimate galvanic contact has to be ensured between the electrodes and the concrete. If the surface is dry, the concrete has to be pre-wetted first with water, or contact graphite gels or pastes shall be used.

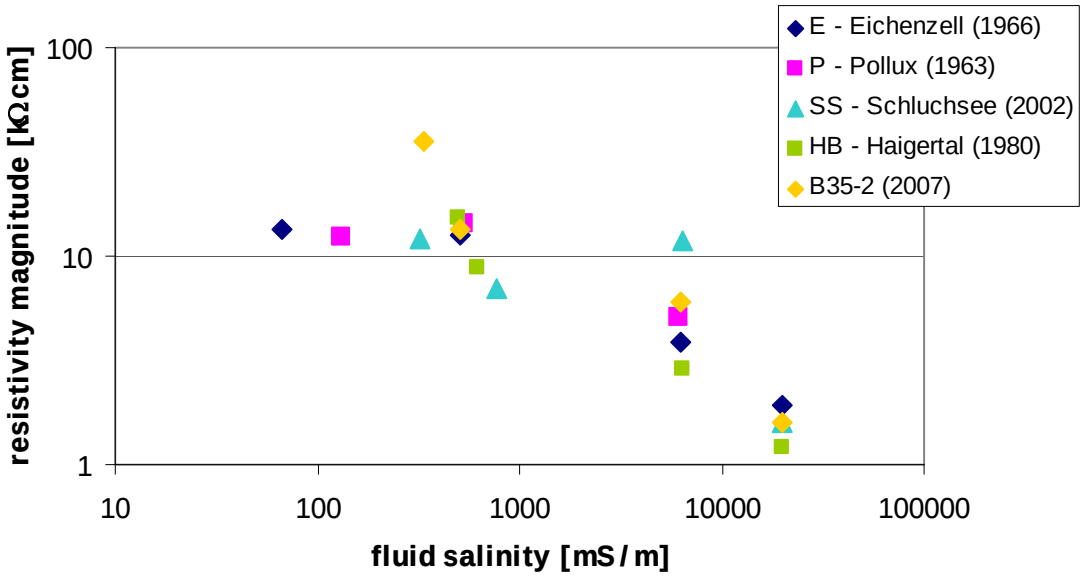

Figure 42. Resistivity magnitude of five concrete samples versus fluid conductivity (changing NaCl concentrations).

Results of a resistivity survey of a reinforced concrete bridge deck are presented in Figure 43. Low resistivity values (red and orange colors) indicate high corrosion rates and a potential serious condition of the deck. Yellow and green colors mark intermediate states while blue marks sound areas.

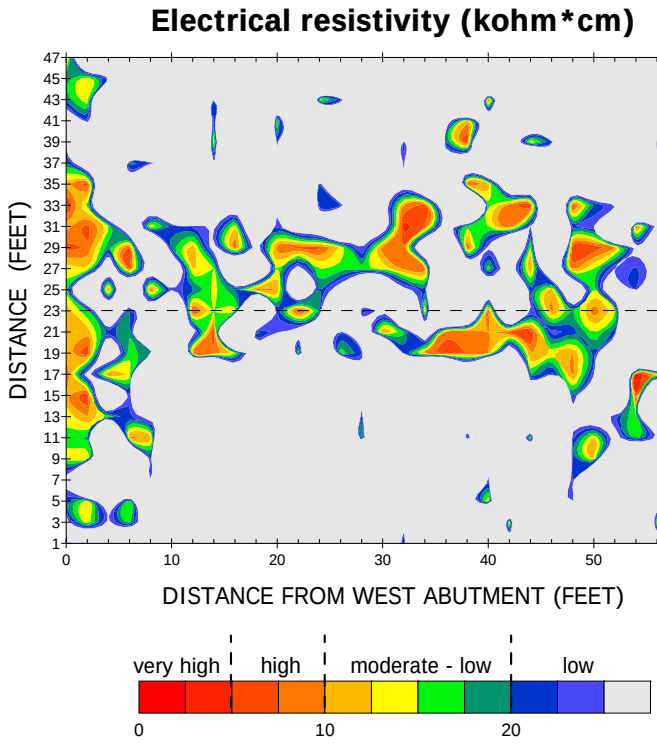

Figure 43. Electrical resistivity map obtained on reinforced concrete bridge deck, with color-coded interpretation of relative corrosion rates.

Advantages and Limitations:

The electrical resistivity method is fairly easy to use and can quickly be learned. Especially when Wenner probes are used, the data recording is very simple and the equipment is robust. Whereas, the data processing is uncomplicated and reduces pretty much to plotting the raw data, the interpretation is a bit more challenging. The reason for this observation is that the electrical resistivity depends on many material properties (e.g. moisture and salt content, porosity) and the delineation of their specific contributions to the bulk result is difficult to assess.

Despite the fact that the manageability of the equipment is straightforward, it can get wearisome when it is applied manually along a grid on a large-scale area like a bridge deck. Even though technically possible, there are no automated measurement systems for bridge deck systems available on the market as of yet. Moreover, the electrodes need galvanic coupling to the concrete and hence, the surface of a test object has to be pre-wetted. There are concerns, however, regarding "over-wetting" the deck surface which may contribute to probe-to-probe current flow along the surface, the effects of which still have to be studied in a controlled environment.

CHAPTER 3 INDIVIDUAL FIELD INVESTIGATIONS AND EVALUATIONS

OVERVIEW

The NDE methods and approaches previously described were used for field testing and subsequent condition assessment (evaluation) of nine bridge deck structures in the state of Iowa, shown on the map below (Figure 44). The primary NDE methods that were employed and evaluated on all of the decks include the following: (a) impact-echo (IE), as deployed on the robotic Stepper™ device; (b) a rolling, Proceq™ half-cell instrument and data logger; and (c) the 1.5GHz, ground-coupled (GC) ground penetrating radar (GPR) system mounted in a hand-pushed cart. Though other methods were deployed, including: electrical resistivity (ER) measurements (using a four-probe Wenner array and the same Proceq™ data logger used for the half-cell measurements), ultrasonic surface wave (USW) measurements (obtained using a portable seismic property analyzer (PSPA) instrument), and ultrasonic (US) pulse-echo data (also obtained using the robotic Stepper™ device), only the three main methods referenced in the previous sentence are discussed and reported throughout. When specific value is added to the overall evaluation of individual decks investigated as part of this report, discussion and illustration of some of the other methods is included, as warranted.

A much more expansive discussion of field procedures, analysis of field data for on-site selection of cores during data collection, and illustration of the overall analysis/interpretation process is provided for Bridge O1. Discussions for each of the subsequent bridges are less detailed, excepting critical observations unique to the individual decks; thus, organization of the Bridge O1 text is slightly different than for the remainder of the decks.

Figure 44. Location of tested bridges shown on a map of the state of Iowa.

BRIDGE O1 DECK EVALUATION

The deck on Bridge O1 is a 180’ 0” x 28’ 0”, continuous I-Beam (steel girder) structure consisting originally of a reinforced portland cement concrete deck, designed in December 1955 and constructed in 1957 (Figure 45). The structure is located on U. S. 30 over Buttrick Creek, 2.5 Miles west of Grand Junction, Iowa, approximately 2.3 miles west of Jct. Iowa #144 (Figure 46).

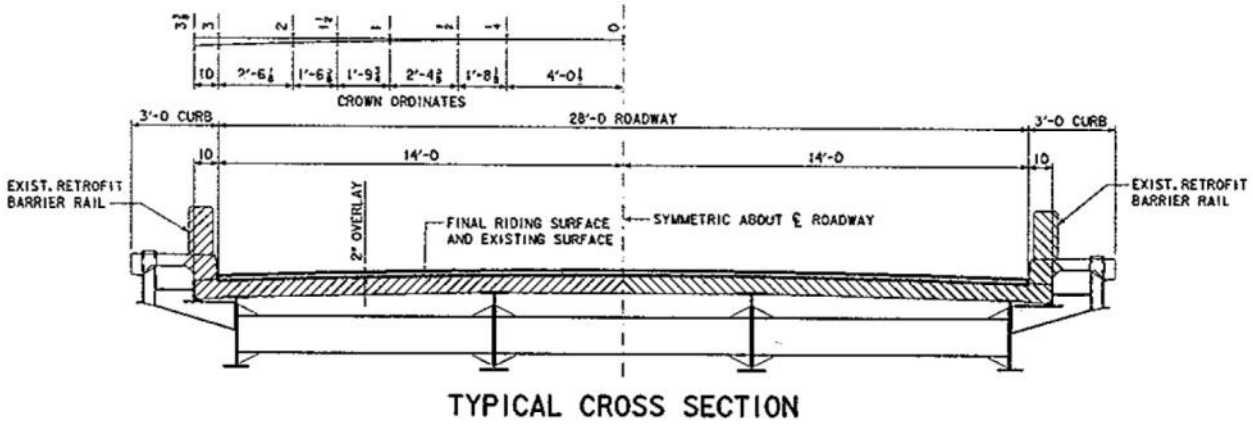

Figure 45. Cross-section of Deck O1, showing existing retrofit barrier rail and PC overlay.

Figure 46. Google Map – street view, looking east on deck (upper) and aerial view of deck on US 30 (lower).

The Bridge Condition Report for FHWA No. 25630 says the bridge deck was overlaid with dense low-slump concrete in 1983 and also that the deck had some epoxy injection in 1999. The 1983 work was as follows. Areas of proposed Class A repair were shown in the project plans based on sounding of the deck. Figure 47 defines the limits of Overlay, Class A Repair and Class B Repair. The original deck thickness was 7 1/4". The addition of the 1 3/4" overlay resulted in a top of deck surface raise of 1/2" and new deck thickness of 8 3/4". Repair concrete was placed monolithically with the overlay concrete unless an area of Class B larger than 2 square yards was encountered. If a Class B repair area larger than 2 square yards was encountered, individual concrete placement for this area occurred up to the bottom of overlay. The plans did not include a bid item for Class B because none was anticipated. However, the Standard Specifications would have provided for doing so, if it was determined during construction that it was needed. This bridge deck is recommended for a complete PC concrete repair and re-overlay, scheduled to be completed in 2009.

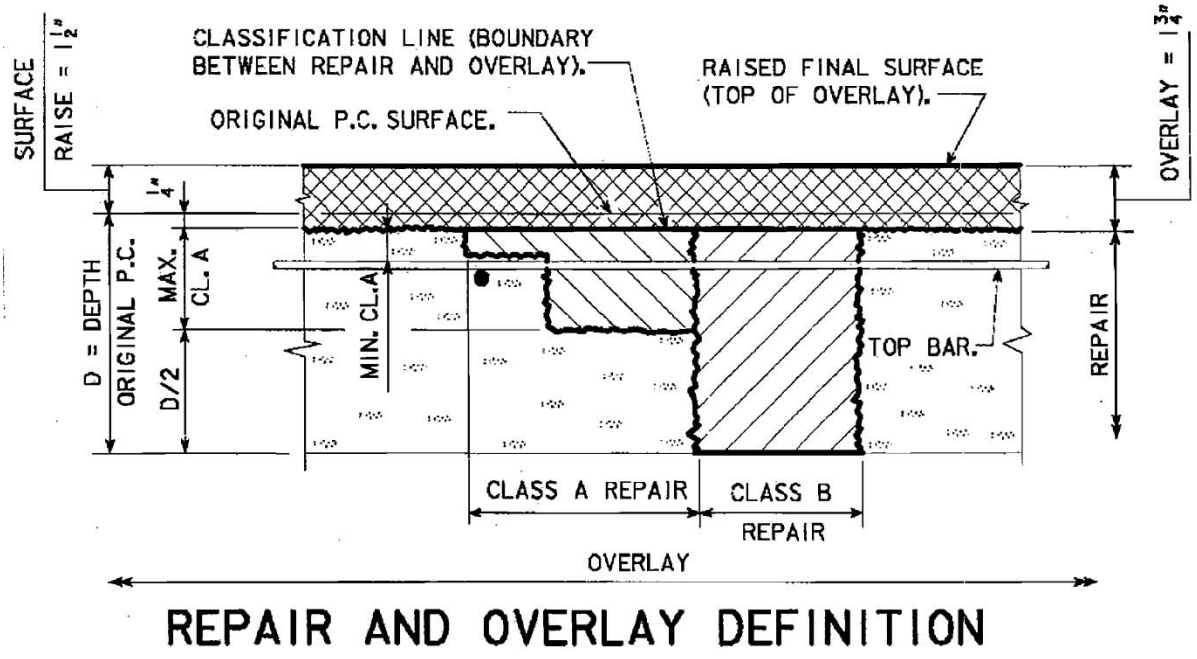

Figure 47. Schematic specifying Class A and Class B repairs and overlays.

The following discussion applies not only to Deck O1 repairs, but any other discussion about other decks included within this report indicating PC overlay or Class A, Class B repairs are recommended. Consistent with what is illustrated in Figure 47, Iowa DOT Policies and Procedures for overlay and repair are essentially as follows:

- The first ¼" of existing deck is removed.
- Concrete in areas identified as being in need of Class A or Class B repair is removed as directed by the specifications or the Engineer.
- Overlay concrete is placed monolithically with the repair concrete, except when a Class B repair area exceeds 2 square yards.
- In a Class B repair area larger than 2 square yards concrete is placed individually to the lower boundary for overlay (1/4" below the original P.C. surface).

What this procedure means is that unless an area of Class B repair larger than 2 square yards is encountered, there would be no interface between repair and overlay concrete since all the concrete is placed monolithically. If an area of Class B repair larger than 2 square yards is encountered, the concrete could be the same material as used for the overlay or an entirely different mix at contractor option. The current specifications require that these individual Class B placements be a different mix than repair concrete but none of the bridges in this study were under Iowa DOT's new 2009 Construction Specifications.

Bridge O1 differs from all the other "O" (designated for overlay) bridges because the planned work in 2009 was to re-overlay it. The process for re-overlay is not discussed because it essentially follows the same policies and procedures described in the previous paragraph. For the other "O" bridges (O2, O3, O4, O5 and O6) the work performed in 2009, following the non-destructive testing, was repair and application of the first overlay in accordance with the policies and procedures discussed previously. Bridges R1, R2 and R3 all have had previous overlay and repair done in accordance with the policies and procedures described herein; however, repair or overlay in 2009 was not planned. Except where essential, during comparison of repaired areas to NDE maps, no further discussion of the overlay/repair process will be provided.

NDE Methods Employed on Deck O1

Several NDE methods were deployed simultaneously in the field for evaluating the condition of Deck O1, using a variety of equipment. These included the combination of (a) a ground penetrating radar (GPR) system using both ground-coupled and air-coupled antennas (sensors); (b) an impact-echo (IE) device mounted on a robotic Stepper™; (c) a rolling half-cell potential measurement device with data logger; (d) a Wenner resistivity probe suitable for concrete deck electrical measurements; and (e) a portable seismic property analyzer (PSPA) used to conduct ultrasonic surface wave (USW) measurement of concrete modulus. A multi-sensor, ultrasonic instrument was also deployed on the robotic Stepper™; however, data from that instrument were too spatially sparse to have any value for the current project objectives.

GPR data were obtained from ground-coupled (GC) 1.5GHz or 2.6 GHz GPR sensors, mounted in a cart (Figure 48). A built-in distance measuring instrument (wheel encoder device) was used for triggering distance-based GPR scans by the GSSI SIR-20 acquisition system (covered w/blue raincoat to protect from light rain). Field notes and deck sketches are updated as other NDE measurements are performed in the background.

Impact-echo data collection (Figure 49, right) is also performed along longitudinal, gridded lines spaced 2ft apart, though individual impact-echo samples are taken every foot along each of these two-foot spaced lines. In this figure, the Stepper™ (robotic cart) with impact-echo (IE) is shown at (a) upper left, with the sensor lowered and the hammer (small ball) still in the "up" position and (b) lower left, with the impact hammer in the "strike" position on the tined concrete surface. At right, both the impact-echo instrument (left side of the Stepper) and ultrasonic pulse-echo (US) device (right side) are shown during deployment.

Figure 48. Ground coupled (GC) GPR data collection using 1.5GHz or 2.6GHz sensor.

Figure 49. Robotic Stepper™ with impact-echo (IE) and ultrasonic pulse-echo (US) devices mounted at left and right, respectively, during data collection on deck.

In Figure 50, ultrasonic surface wave (USW) measurements are shown being taken using two different models of a portable seismic property analyzer (PSPA). Shown on left and upper right is the original PSPA device mounted within a "lunch box"-type housing. On the lower right, the newer model of the PSPA is being used to collect USW data. Either instrument can be also used as an impact-echo device to identify deck delamination when only one sensor is used to measure the response from the impact hammer.

Figure 50. Portable seismic property analyzer (PSPA) data collection on deck, with two models of the device shown.

Figure 51 shows data collection on the same 2ft x 2ft grid on a deck, using a Proceq™ data logger and rolling, half-cell probe, as well as a hammer drill used to prepare a hole in the concrete. This allows an electrical connection to be fastened with a wire lead (alligator clamp) onto an exposed rebar located in the upper reinforcement mat. This figure shows the detail of a transparent probe housing filled with copper sulfate solution, which wets an absorbent blue strip along rolling surface. However, the blue strip itself is not in direct contact with concrete. Instead, a thicker, more absorbent strip on the rolling surface is continuously maintaining contact with concrete surface, while applying water to wet the deck. This same strip is also in contact with another absorbent dark blue strip bridging between the "copper sulfate" strip and the "water" strip. This "bridging" strip, just visible in the image at right near the location where the electrical cables mount onto the handle, provides both physical and electrical contact between the copper sulfate strip/supply reservoir and the water-soaked strip.

Together these electrically-connected strips form the $Cu/CuSO_4$ electrode that rides along the surface, measuring the electrical potential, which is displayed and stored on the logger. At a distance, which might equal the total deck length from the instrument operator, the physically connected wire lead (the alligator clamp galvanically fastened to the rebar in the drilled hole)

forms the ground electrode – as discussed previously. Voltage readings between the concrete surface and the upper rebar mat, accessed with an electrical connector (lower center image) directly attached to a rebar after drilling through the concrete (lower right), are obtained via the electrical connectors at the rolling instrument head. The connector between the instrument head and the logger feeds the data logger with potential readings (generally ranging between -100 and -800mV, on most decks) measured between the rebar cage and the deck surface at each grid node. These readings are stored on a pre-set grid matching the deck's areal dimensions, then transferred to a computer for mapping.

Figure 51. Half-cell (HC) potential measurement on deck; showing probe detail, drilled hole and wire lead connected electrically to the upper rebar mat.

Figure 52 shows electrical resistivity (ER) measurements obtained using a Wenner probe, which also feeds data into the same Proceq™ data logger used for HC measurements. Unlike the HC device, which wets the deck with a weak copper sulfate solution (as some copper sulfate is continuously absorbed by the "water-fed" strip), only a light coating of water needs to be sprayed at each grid node in order to take a resistivity measurement. The water must wet a large enough surface so that each of the four, compressible probe heads comes into direct contact with the wet concrete. Care should be taken, however, not to "puddle" the deck surface with the sprayed water

because there is concern that there may be current leakage from probe to probe, which may adversely affect the measurement. As is the case with the half-cell testing, ER measurements are collected on the same 2ft x 2ft grid and mapped using contour-mapping software.

Figure 52. Electrical resistivity (ER) measurements obtained using a four-probe Wenner array.

Air-coupled (AC) GPR data collected (Figure 53) is shown on a vehicle-mounted frame in line with the right wheel path (upper left). GPR scans are collected using two separate sensors (lower left), configured in a dual-polarization deployment and controlled by a GSSI SIR-20 data acquisition unit that is mounted inside the survey vehicle. The wheel-mounted distance measuring instrument (DMI) on the rear driver's side wheel (lower right) is used to trigger GPR scans from both antennas (sensors) at equally-spaced intervals of one inch.

Figure 53. Air-coupled (AC) GPR data collected in dual-polarization configuration.

Traffic Control/Gridding of Deck

Typically, NDE work was scheduled for two days on each deck – one day collecting data in the primary traffic direction (NB or EB) and a second day collecting data in the secondary direction (SB or WB). Traffic control consisted of a full lane closure (driving lane and shoulder) in one of the two traffic directions on the first day, with flagmen controlling the flow of traffic on the open half of the deck. A similar setup was employed the following day, except that the traffic was closed for vehicles moving in the opposite direction.

A 2ft x 2ft, orthogonal grid pattern was laid out in "dots" on the entire bridge deck using marking paint beginning with the first grid point at the expansion joint and all others 2ft apart, along a line spaced 1ft from the curb (or parapet wall). All other grid nodes are similarly spaced 2ft apart along lines that are both spaced 2ft apart and parallel to both the curbs and lane markings. In order to quickly mark the deck with a minimal number of physical measurements, a 10ft x 10ft jig was devised and built. This enabled the NDE crew to mark an orthogonal grid in 2ft x 2ft increments by simply stretching out the jig, aligning it to both the curbs and a series of

pre-measured dots spaced 10ft apart along the length of the deck on lines parallel to the curbs/lane markers (Figure 54). Because this particular deck had no skew (positive or negative), no accommodations for placement of the grid nodes on skewed portions of the deck had to be made. On skewed decks grid nodes (dots) were painted on the skewed portions of the deck so that they conformed to an orthogonal grid. This grid is based on the same convention for locating the origin at the joint and curb or parapet intersection, as defined by the primary travel direction

Figure 54. 10ft x 10ft "jig" used to quickly mark 2ft x 2ft testing grid on bridge deck.

The origin (x = 0ft, y = 0ft) for Deck O1, as shown in Figure 55, was marked at the NW corner of the deck, where the east abutment meets the curb (shoulder lane) at the expansion joint between the deck and the approach ramp. The 2ft x 2ft grid pattern was marked on the deck and labeled as follows:

1. Starting at the origin, the line closest to the curb/parapet (Line A) was marked with a series of dots placed two feet apart, with this line spaced a distance of one foot away from the curb/parapet.
2. Continuing every two feet from Line A, at distances of 3, 5, 7, 9, 11, 13ft, etc., from the curb/parapet, grid lines parallel to the curb/parapet were marked with the letters "B, "C", "D", "E", "F", "G", etc.

Figure 55. Location of origin on Deck O1 is at NW corner, where approach ramp and deck intersect the curb at the expansion joint, as shown.

Deck O1 is the only structure where the origin is not located either at (a) the west approach expansion joint-curb intersection on the half of the structure carrying EB traffic or (b) the south approach expansion joint-curb intersection on the half of the structure carrying NB traffic. On all other structures, the NDE Team followed a convention of locating the origin at the "upstream" expansion joint-curb intersection, as defined by the flow of traffic in the primary direction.

NDE Results

Plan-view maps of Deck O1 are shown in Figure 56, where GPR-estimated concrete cover (CC), impact-echo (IE) delamination assessment obtained from the Stepper™, half-cell active corrosion potential (HC), and ground penetrating radar (GPR) condition assessment results from the 1.5GHz antenna, are presented, respectively, from top to bottom. Some NDE data can be mapped, as collected (raw) as long as they are fixed to map locations (x, y grid) on the deck, e.g., readings from half-cell or resistivity measurements. Other NDE methods require analysis of the raw data, often through various processes, and normalization of the data to obtain a final, interpreted data set that can be fixed to map coordinates (gridded). For example, impact-echo (IE) records or GPR signal profiles must be modified using gain functions, standard filtering or other geophysical algorithms. Often additional analysis, normalization or interpretive processes must also be performed before a gridded data output can finally be contour-plotted as a plan-view map.

Each of the maps shown in Figure 56 is based on extracting numerical or analytical data obtained from the raw or processed NDE data, respectively; gridding the measured or interpreted data at one or two-foot intervals for the purpose of contour-mapping; and displaying the mapped data using color scales and data ranges that are sensible for each NDE technology. The NDE data (except for the GPR and impact-echo) are collected at 2ft spacing along each of the lines 2ft apart, along the entire deck. GPR data are collected at 60scans/foot and impact-echo points are collected 1ft apart on each line. The upper map (concrete cover) is displayed as a reference so that GPR, impact-echo, and half cell results can be better understood; since each of these methods is generally attempting to correlate results with what is going on at the upper reinforcement level. It also provides a basis for comparison with any field observations made during deck repair, or with the cores that were extracted on the deck.

While there are significant similarities between the condition maps, there are also differences between the various NDE methods. Those are attributed to the fact that each technology is governed by different mechanical, electromagnetic, or electrical relationships between the material being sampled (deck and embedded steel with defects or contaminants) and the instrument used to gather the information needed. None of these are physical samples, like cores or chloride data. However, the full-coverage capability of these NDE methods significantly aids in assessing the deck's condition in a holistic manner. On the other hand, the limited physical sampling can provide valuable input into determining the efficacy of the NDE results and enhance the interpretation of NDE results. Care must be taken, however, to extract physical samples at locations where NDE measurements are made. The IE map is shown again in Figure 57, overlaid by the actual repair map. Traditional sounding was used to define repair zones. Once concrete removal was underway, the contractor was instructed to continue "removing adjacent, deteriorated concrete". This has been well documented experience, that repaired zones are always larger than what was defined using traditional sounding.

Last, the ultrasonic surface wave (USW) method was employed on several of the Iowa decks as a means of obtaining information about the mechanical properties of the in-situ concrete. The portable seismic property analyzer (PSPA) was used for that purpose. Since data collection using the PSPA is slower than data collection using other technologies, USW surveys were conducted only on limited deck areas. Maps for a section of Bridge Deck O1, along with USW maps for partial areas of three different bridge decks surveyed as a part of this project, are shown in Figure 58. Since the same color scales are used on all four maps to show modulus variation, it can be easily seen that the USW results shown for Decks O1 and R1 generally show higher modulus values. Though the modulus values were lower on some decks, for example O2 and O4, in general, this does not mean the modulus reduction is due to deterioration or aging of these two particular decks or that Decks O1 and R1 are in relatively better condition than Decks O2 and O4. Rather, there may have been a significant variation in initial modulus introduced during concrete placement that would have been apparent had it been measured once the concrete was fully cured. All that can be said for certain is that these mapped modulus variations, whether distributed beneath a given deck's area or compared from one deck to another, existed as indicated at the time of testing. A separate discussion relating how modulus variation can sometimes be directly correlated to condition, as measured by other NDE methods, is included within the section on Deck O4.

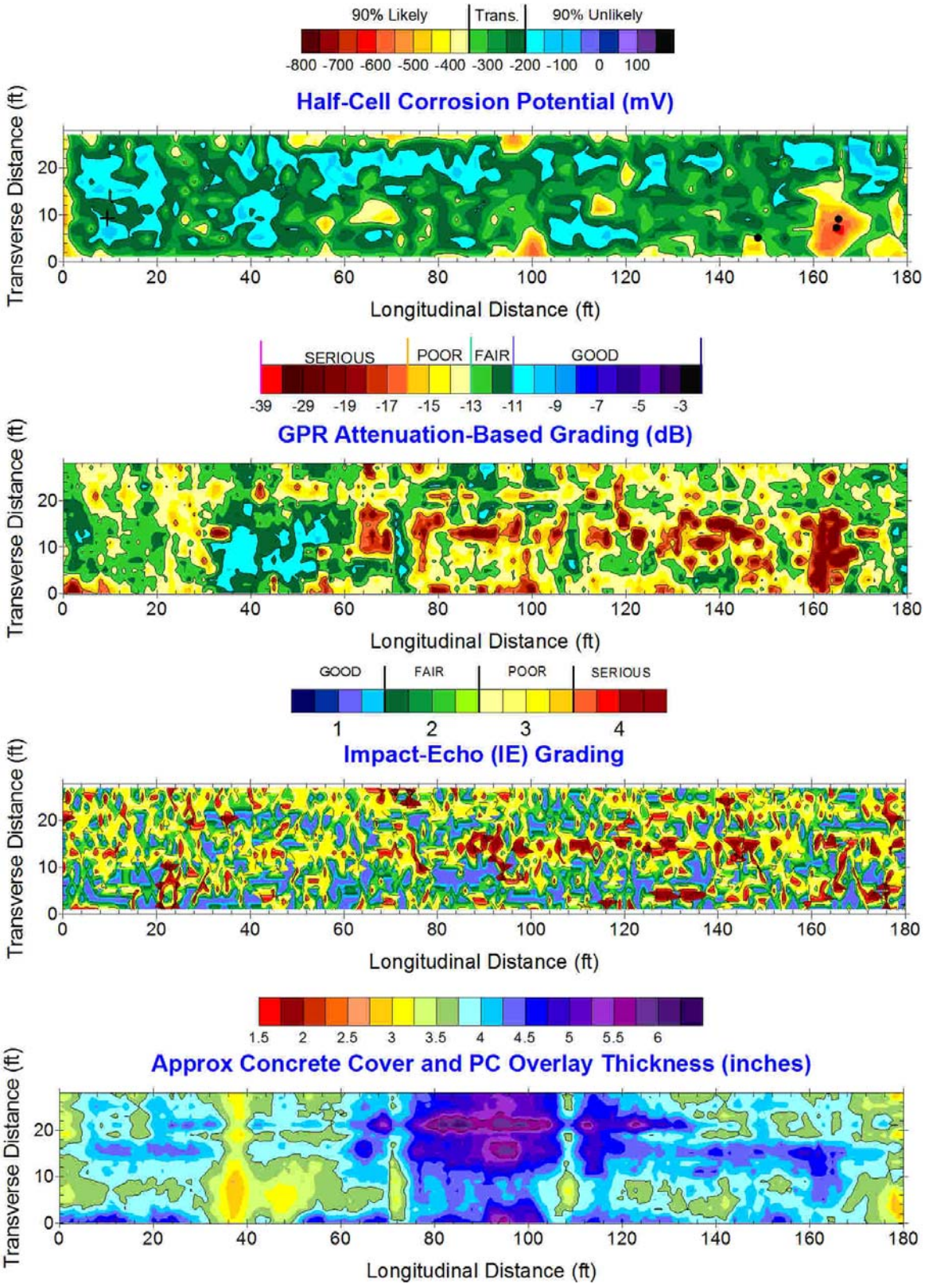

Figure 56. Concrete cover (CC), impact-echo (IE) from Stepper, half-cell (HC), and GPR maps.

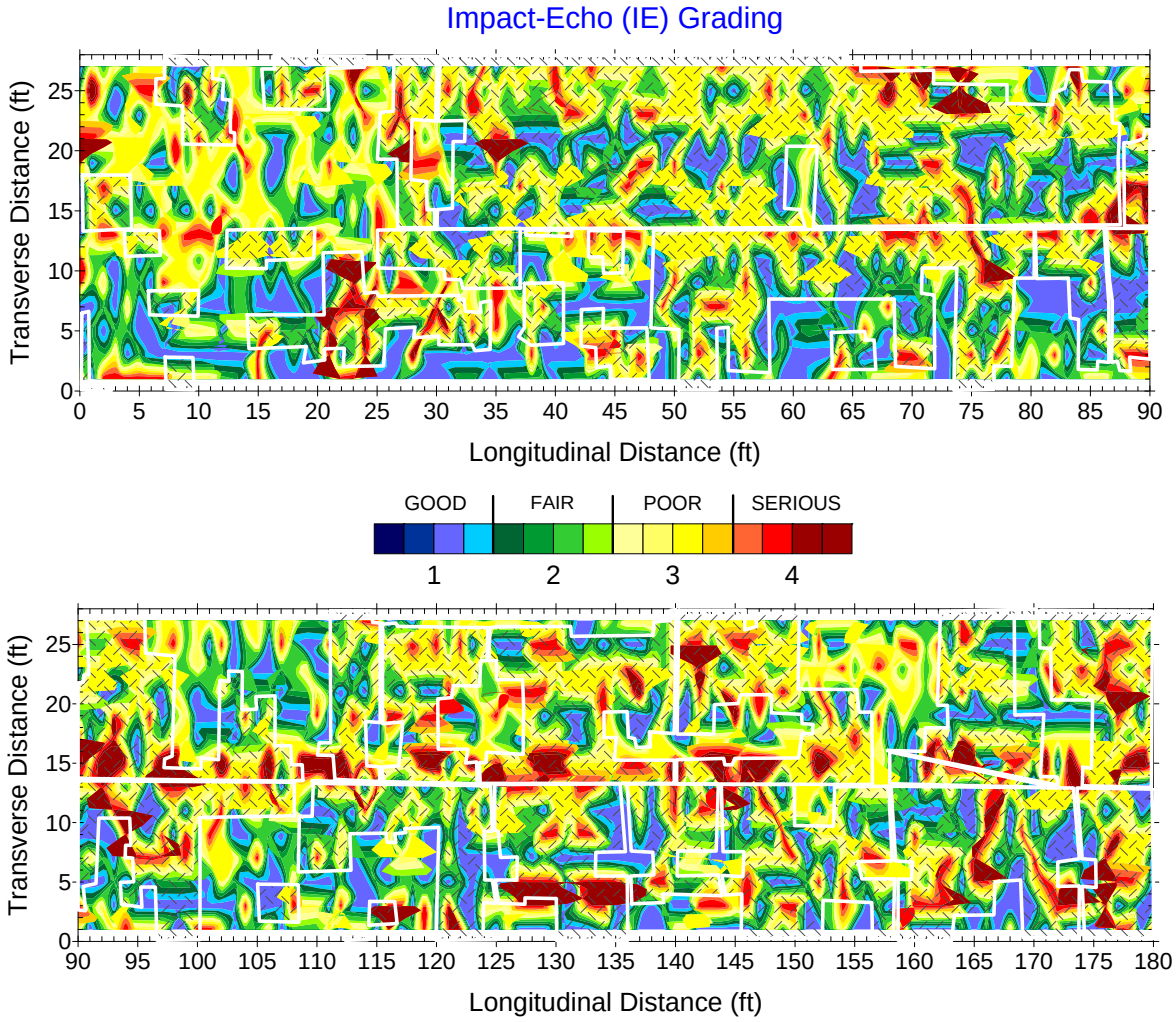

Figure 57. Impact-echo map with overlaid repair areas.

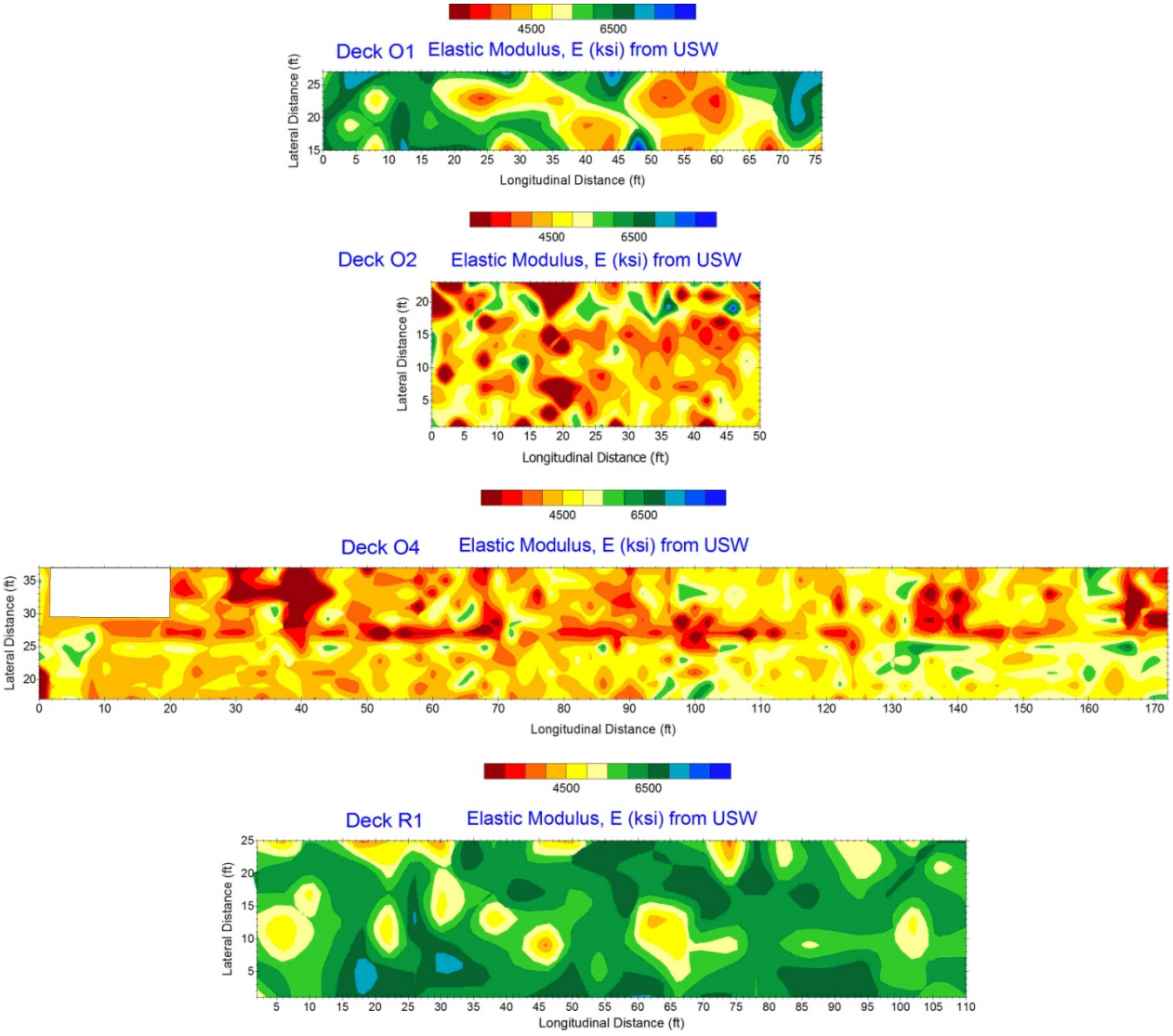

Figure 58. *USW maps showing calculated Young's Modulus from Decks O1, O2, O4 and R1.*

Validation of Field NDE Results Through Coring

Information from cores extracted immediately following part of the NDE evaluation, based on locations selected by reviewing raw GPR data, show that both the overlay and repair materials were the same. As shown in each of these figures, there is no delineation between the repair and overlay materials which were both placed in 1983. This was observed in both the GPR data and each of the corresponding core samples (Figures 59 to 67), including core/GPR data locations where repair extended well beneath the upper reinforcement mat. However, GPR data did reveal a shallow interface with fairly uniform thickness in many areas (presumed to be where the overlay was intact and no repairs were made) as well as significant areas where this same material interface (dielectric contrast) fluctuated between a few inches depth and several inches between the upper and lower reinforcement mats (Figures 61, 63, 64 and 66).

Figure 59. Core 1, showing debonding, but no obvious evidence of concrete deterioration at the rebar level, though raw GPR data used to select core location indicates such.

In addition to the core observations described above for Figure 60, this figure also illustrates part of the process used to generate a preliminary GPR map, which was later corrected for variation in rebar depth. This process is critical because either shallow or deep rebars significantly skew measured GPR signal amplitude, or signal loss (attenuation). Note that the upper (preliminary) GPR map shows significantly higher deterioration quantities in the upper, central region and a lower amount of deterioration in the upper left corner of the map, compared with the GPR map at the bottom (depth-corrected version). A visual comparison of the upper and lower GPR maps with the rebar depth map (center) shows that the area with the purple/black (deep) bars caused the uncorrected GPR map at top to display a region where it would be expected there to be extreme deterioration at the depth of the upper mat of rebars. The lower (depth-corrected) map, however, does not display the bright yellow and red colors in that same area attributed to relatively high deterioration levels on the preliminary (not depth-corrected) map.

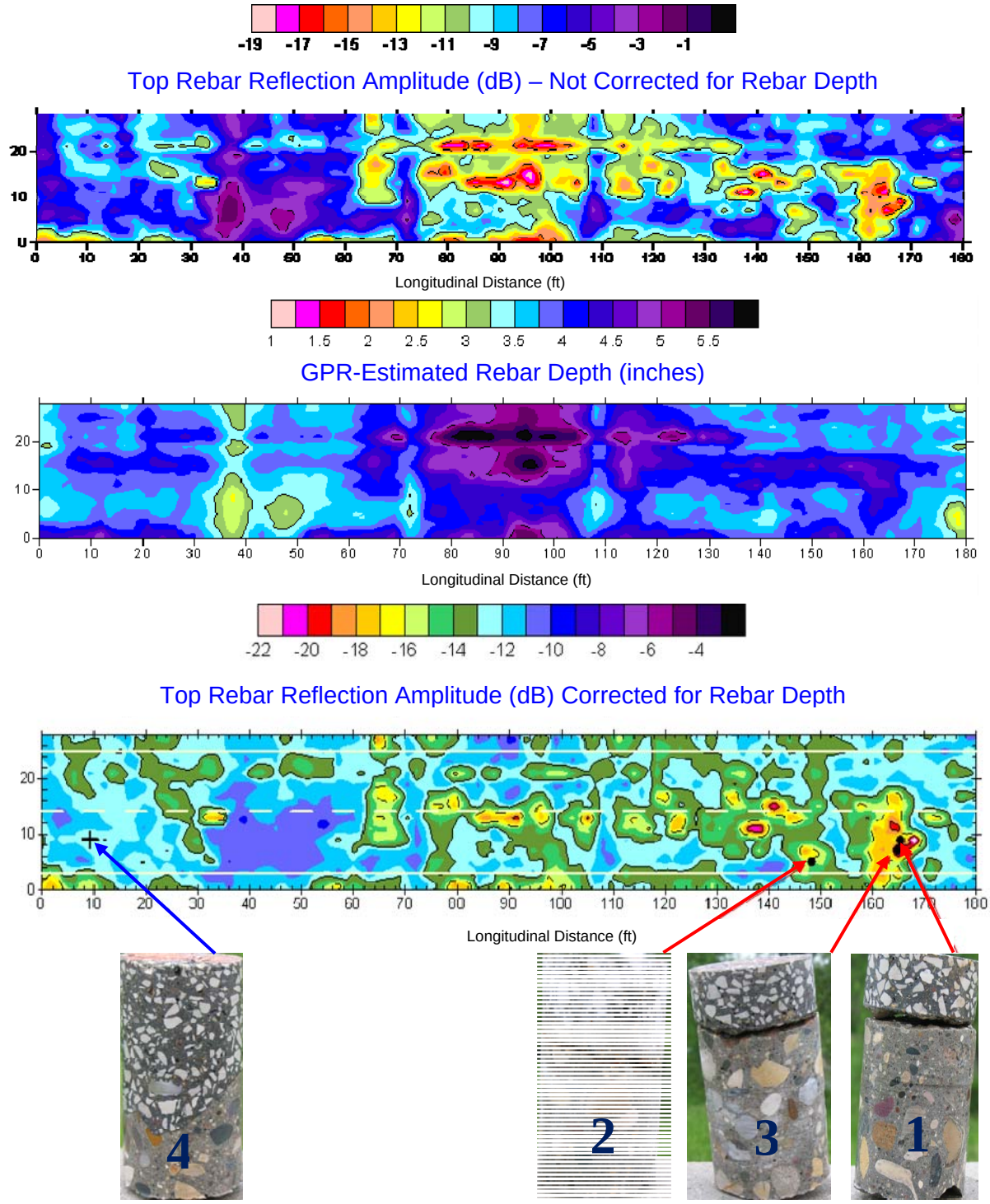

Figure 60. Deck O1 – Preliminary and depth-corrected GPR attenuation maps: extreme variation in cover illustrates impact on interpreted condition. Cores are numbered as shown.

Though the map at bottom has been corrected for depth, a final deterioration threshold (separating "sound" from "deteriorated" concrete) has still not yet been performed at this stage of

the analysis/interpretation process. This means the bottom map is still considered a "preliminary" product even though it has been depth-corrected. Thus, further analysis/interpretation will still be performed prior to finalizing a deterioration threshold. Once a final deterioration threshold (dB value separating sound from deteriorated concrete) is determined, the resulting map can at last be used for comparison to other NDE maps and for computing GPR-based deterioration quantities. Note that the cores extracted from the locations shown on the map (Figure 60) are in good agreement with the GPR data, as the preliminary map at the bottom of the figure shows.

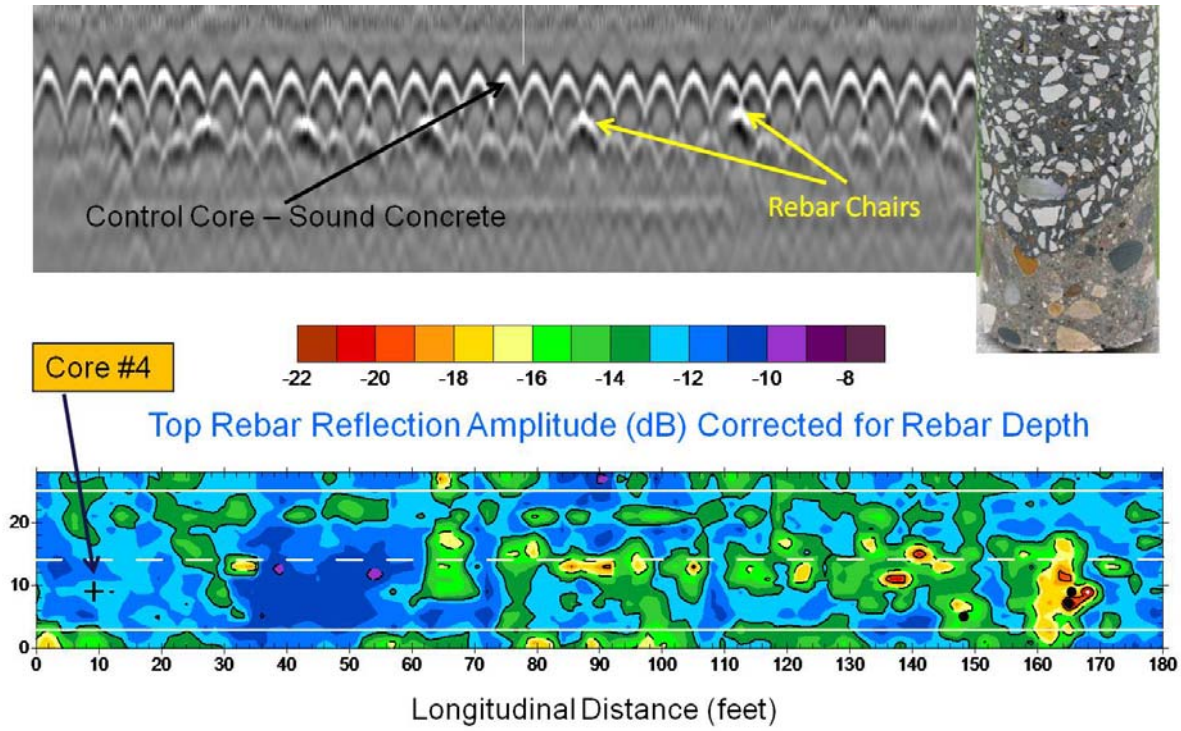

Figure 61. Raw GPR data used to select control core location (Core #4), with all four core locations marked on depth-corrected GPR map.

Core #1 is located at 165.5ft along Line E. Note the debonding of the overlay, though there is no evidence of delamination at the rebar level and none was expected. Core #1 was expected to be in a zone with significant deterioration, as evidenced by a high level of signal attenuation at the top rebar level. A lack of visible damage, though, does not rule out the likelihood that this location had both high chloride content and elevated moisture content prior to core extraction from the deck, both conditions consistent with a corrosive environment, and to which GPR is sensitive. Core #1 is, hence, a good candidate for chloride testing.

GPR was used to identify and mark all locations on bridge O1for core extraction. One of the four core locations was routinely selected as a "control" sample, ideally at a location where the concrete appeared to be in "sound" or reasonably good condition. The selection was based on the quality (amplitude and contrast) of the GPR signal visible in a raw profile (image) along one of the test lines. This core, indeed, appeared to be in good condition and it had to be broken free of the deck in order to remove it once the 6" coring depth had been reached. The core, Core #4, is shown in Figure 61 and in Figure 60 at left. Note that this particular core was at a previous

Class A repair location and the overlay at that location is not at all different from the rest of the overlay material, as indicated previously.

The other three core locations were selected for the purpose of attempting to locate concrete with either (a) visible evidence of deterioration or (b) indirectly measurable evidence of concrete degradation (high chloride content or low strength). Three of the four samples (the ones targeted as "deteriorated") indeed showed visible evidence of concrete degradation in the form of delamination at the upper steel mat, de-bonding of the epoxy-injected repair at a previously delaminated surface or an overlay/concrete boundary, or both. In addition, two of the three targeted "deteriorated" cores revealed significant corrosion of the reinforcing steel w/scaling and section loss. Only one core, targeted as deteriorated, revealed debonding but no visible evidence of corrosion (Figure 59), which may mean the GPR signal attenuation was responding primarily to an elevated chloride content in moist concrete (high electrical conductivity and reduced GPR propagation velocity).

Referring once again to Figure 61, raw GPR profile ("depth" cross-section) data used for field selection of a "control" core can be reviewed. The rebar depth here is fairly consistent, signal profile is relatively uniform, and rebar signal amplitude is high (there is good image clarity and contrast). Since the traffic control was already in place, raw GPR data had to be reviewed in the field, prior to processing or any mapping, and a core from a section of deck considered to be in "sound" condition was selected (Core #4). Several lines of GPR data were quickly reviewed and a single location, at least four feet from the lane closure and four feet from curbs/parapets, was identified as such a control specimen. Though the raw GPR data shown in Figure 61 indicates a location which appears to fit all the above selection criteria, the map below the GPR profile indicates that there is a darker blue region (higher amplitude) that would have yielded a control core with even a greater likelihood of being extracted, and confirmed as sound. It should be noted that the map shown in Figures 60 and 61 was not available in the field to aid in the selection of core locations. In any event, Core #4 was still retrieved fully intact, though it can be seen that a Class A repair had been performed there. In this sample, neither the concrete used for repair and overlay nor the parent concrete showed visible signs of either debonding or delamination/corrosion. Since this control core appears sound, it is highly likely that all other areas with higher amplitude (darker blue in color) are, likewise, sound, based strictly on acceptance of the GPR results.

The extracted Core #2, core hole and the core location on the deck are shown in Figure 62. Core #2 is located on Line C (5ft from the parapet wall) and shown at 148ft from the west abutment in Figure 63. This core is also about 6 feet away from an epoxy injection or relief hole on Line F (near the bottom of the photo on right). The core had an intact overlay. However, the epoxy-injected material, rusty color on bottom half of core shown at LHS of lower left photo, is also on the underside of the half core section on the RHS of the same photo. The orange color on the top of the core section (RHS) is simply marking paint at the top surface of the overlay, seen also around the core hole. Here, the overlay material can easily be matched with the hole in the upper left photo. Beneath the drill water the lower rebar can barely be seen running diagonally upward, left to right. Also, the epoxy-injected delamination can also be clearly seen where the core sample had split in two during extraction.

Figure 62. Photos of Core #2 location, showing extracted core, epoxy-filled delamination in core hole, and bonded overlay.

In two of the four core locations, broken pieces of discolored and de-bonded epoxy were removed with the core, which had to be extracted from the core barrel in sections. In both those locations, it was believed (prior to knowledge about the existence of a previous epoxy-injection repair) that there must have been an epoxy-injection at either de-bonded overlays or delaminations at the upper rebar level. This field interpretation was made because the GPR signal (upper image in Figure 63) indicated a continuous interface. The interface intersected depths coincident with either the upper transverse bars or the presumed location of the known overlay, the latter being visible in most of the raw data profiles. At the suspect delamination's location in the data this continuous interface also displayed a high-amplitude, negative signal polarity. It can be recognized as a black, wavy line in the cross-sectional GPR image shown in the same figure. The line, shown with the yellow and orange arrow heads, is typically indicative in GPR data of the presence of either an air-filled or plastic-filled interface, such as an air-filled delamination or one injected with epoxy (plastic). Figure 63 includes both the raw GPR profile used to select Core #2, immediately prior to its extraction, as well as its location on the depth-corrected map. "Dipping features" (observed GPR signal between yellow arrowhead and red arrowhead), on both sides of the de-bonded epoxy repair, bridge between two rebars at a delamination. This type of upward cracking is typical when delaminations form. After examining the deck where this GPR anomaly was first observed, epoxy injection and overflow holes could

be seen on the surface. Thus, the core was targeted as an epoxy-filled delamination, and the extracted sample validated the interpretation. The Core #2 photos shown in Figure 65 from three views indicate that the delamination formed at the rebar level and propagated upward toward the concrete surface (overlay interface), consistent with known behavior for delamination-induced spalls.

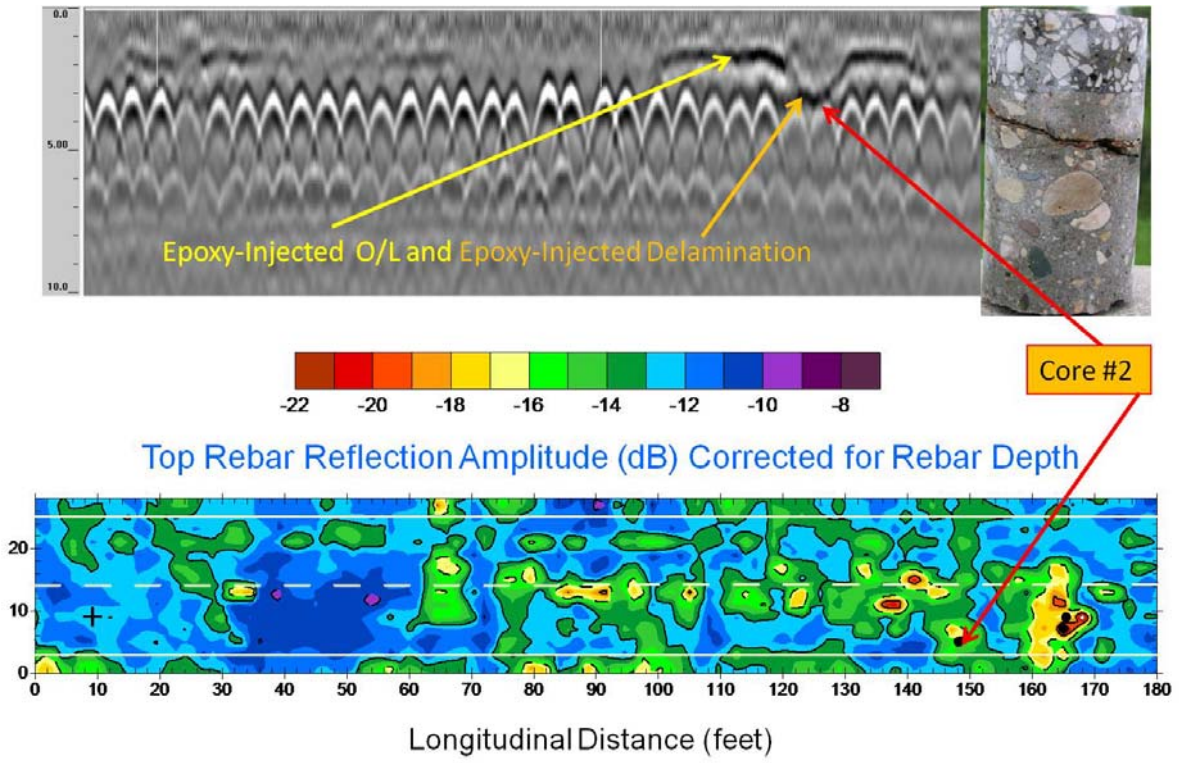

Figure 63. GPR signal indicating presence of an epoxy-filled delamination, and its location on the preliminary (depth-corrected) GPR map.

On the contrary, debonded overlays would be expected to appear on the GPR screen similar to what is shown in Figure 64, where Core #1 is shown along with its GPR signal profile and its map location. The attenuated rebars centered at the red arrowhead can be observed. They lie directly beneath a strong, nearly horizontal continuous anomaly. This signal is much higher in amplitude with either negative or positive polarity at the debonded, epoxy-filled location. Here the signal polarity is going to depend mostly on the thickness of the detachment (delamination) and whether this in-situ delamination (when imaged by the GPR) is air-filled, water-filled, or epoxy-filled. It is understood that the core will be removed in a wet condition, simply due to the use of water during extraction, so when GPR signal polarity is discussed in the context of a delamination being in an "air-filled", "water-filled" or "epoxy-filled" state, it is always to be understood that this discussion refers to the in-situ state during NDT survey. The remainder concrete/overlay interface in the GPR data shown in Figure 64 is defined by a lower-amplitude, mostly positive polarity signal.

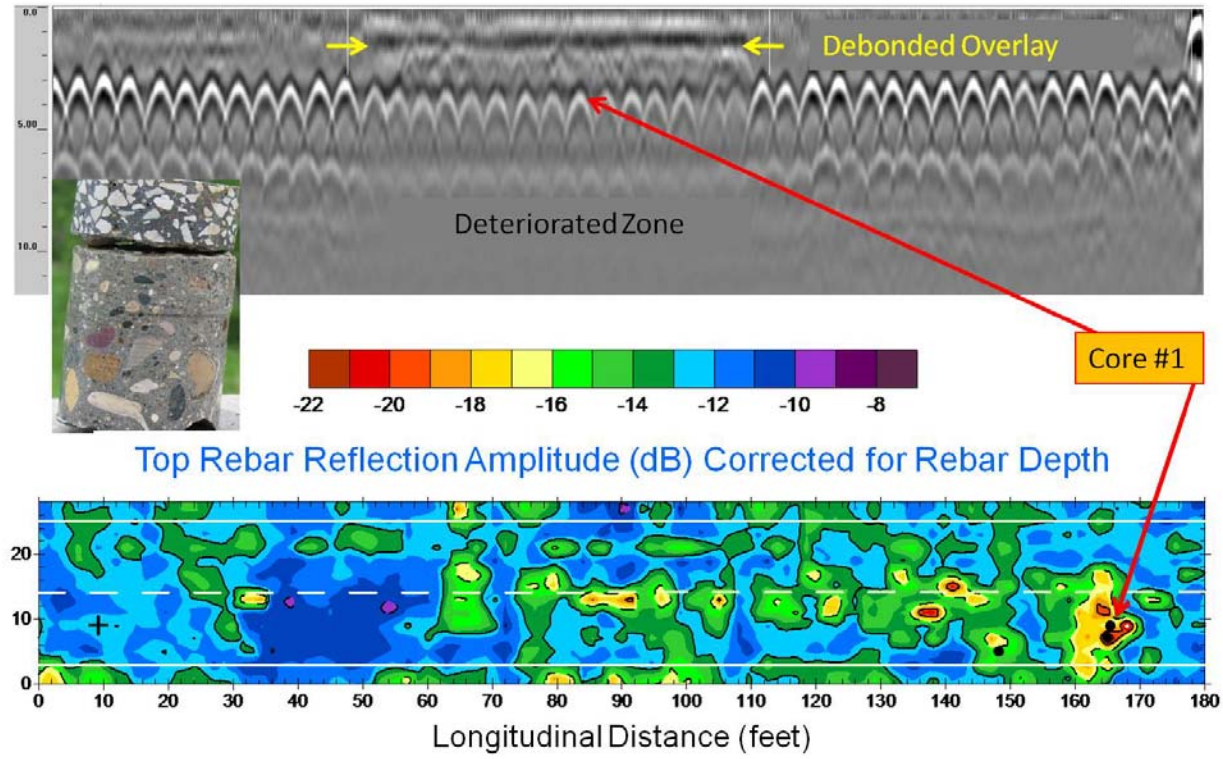

Figure 64. Core #1 and GPR data indicative of a debonded overlay above a deteriorated zone.

Figure 65. Three views of Core #2, which appeared as "epoxy-filled delamination" in field (raw) GPR data.

After a bit of field experience interpreting the unique GPR data obtained on Deck O1, it was encouraging to repeatedly identify epoxy-injected areas in the data, prior to looking at the bridge deck surface and searching for the epoxy-grouting holes. It was even more encouraging to finally see the extracted cores and identify that the depths at which these epoxy-filled anomalies were identified were correctly predicted. Those were typically at the upper rebar level, where

delaminations were epoxy-injected, or at the interface where the overlay had de-bonded from the parent concrete.

Finally, at Core #3 (identified as a potential "water-filled" delamination at the rebar level), the scan density of 60 scans/foot also provided just enough resolution to view an anomaly intersecting between two rebars. This time it was with a fairly abrupt, but positive polarity signal, which again deflected diagonally upward again from the rebars like a crack propagating toward the surface (Figure 66). Additionally, there was a strong horizontal interface at the overlay level, similar to what is shown in Figure 64 for a debonded overlay, and a strong local reflection at one of the bars where the "crack-like" interface deflected upward. This position was marked as the location for extracting Core #3. This caused the NDE Team to suspect an unusual event: an actual "sighting" in the GPR data of a water-filled deck delamination, which appeared only for a distance of about 6 in along the GPR profile before quickly propagating upward toward the epoxy overlay. On both ends of this short delamination, however, the overlay signal was very strong, appearing to be de-bonded from the concrete. The core location was marked to attempt to "hit" exactly where the black arrowhead is positioned, at the apex of a hyperbolic, rebar pattern. At this location, the upward-dipping feature quickly rose and intersected with the indication in the signal that is consistent with a debonded overlay. The hope was to extract a core that was not only debonded, but also showed delamination in the parent concrete.

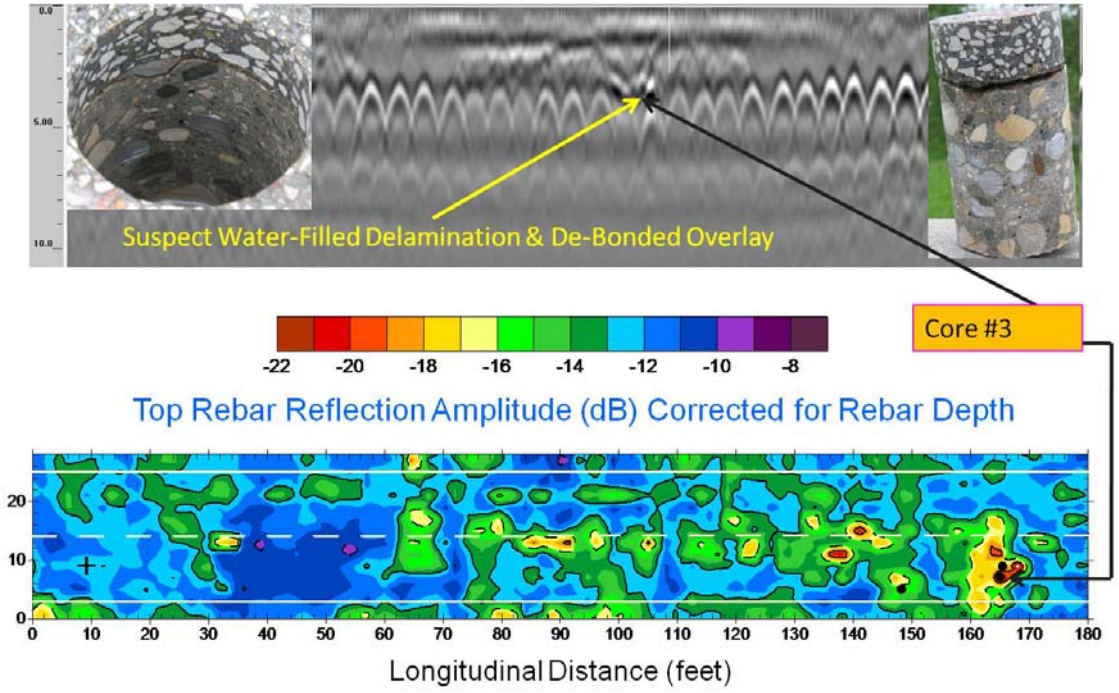

Figure 66. Core #3, field-interpreted as a suspect water-filled delamination with likely debonded overlay.

The "proof" came when this core was drilled and removed, and then the dirty water that always accompanies core extraction began to be replaced with clean water. A visible delamination just beneath the overlay was present not only in the core sample, but also within the core hole now in the deck (Figure 67), and clean water began emptying from the delamination to

quickly fill the core hole. This experience clearly showed that, based solely on a review of the raw GPR data, a water-filled delamination could actually be identified under the right circumstances and signal settings.

Figure 67. Core # 3 during extraction, where upper edge of delamination meets the debonded overlay just below the overlay, with both longitudinal and transverse rebars seen in the photo.

BRIDGE O2 DECK EVALUATION

The deck on Bridge O2 was originally constructed in 1936, 63' – 0" long with a 24' – 0" wide, two lane roadway and two 5' sidewalks. It was reconstructed in 1960 to its present configuration (Figure 68), of 63' – 0" long with a 48' – 0" wide two lane roadway and two 5' sidewalks. Both the deck surface and the underside display evidence of the reconstruction, and the GPR data also showed what appear to be "tie bars" where the old structure was evidently "spliced" to the new construction. The structure carries Iowa #93 over a small natural stream located in Sumner, Iowa (Figure 69).

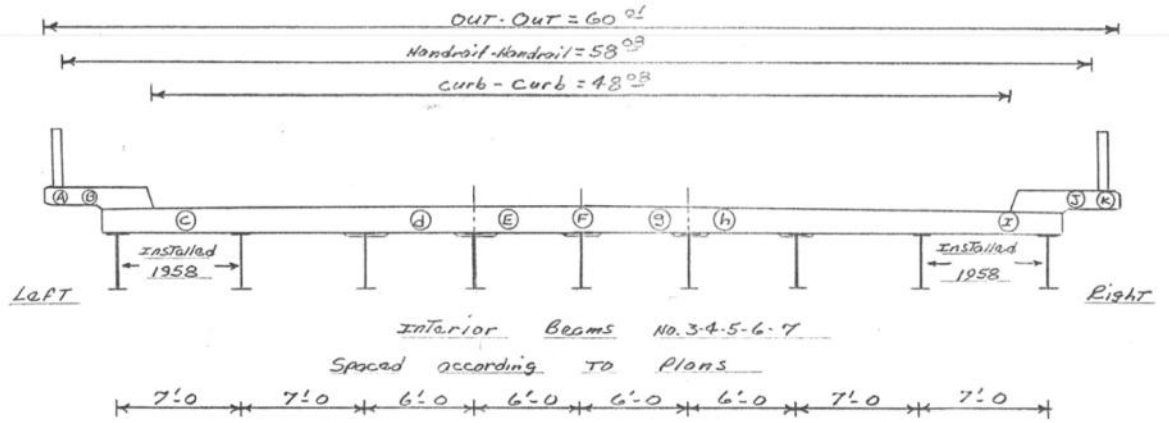

Figure 68. Cross-section of Deck O2 shows original and reconstructed (existing) structure.

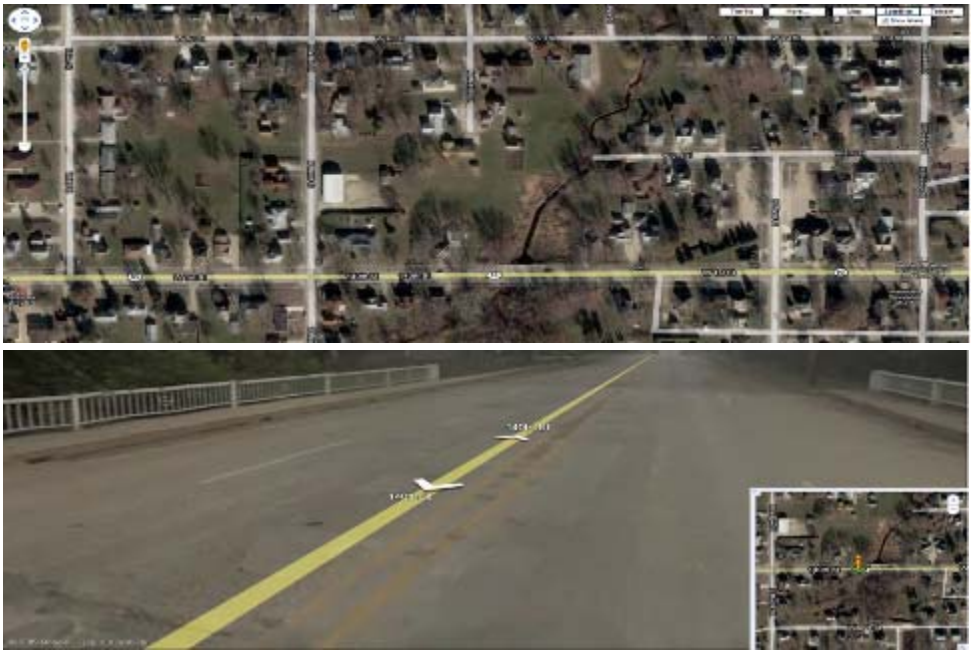

Figure 69. Google Map – Upper image shows deck location crossing creek along Iowa #93 (orange box), and lower image shows eastbound street view.

According to an Iowa DOT Bridge Condition Report (dated May 12, 2009) for FHWA No. 015740, Bridge No. 0914.5S093; this structure was recommended for a complete PC concrete overlay, scheduled to be completed by 9/25/09. The repairs followed specifications related to what was previously shown in Figure 47, in the discussion for Deck O1. Note that subsequent to NDE testing, and mapping of results, Deck O2 was repaired and these repair zones are shown overlaid above the NDE maps.

NDE Methods Employed on Deck O2

NDE methods used for collecting condition data on Deck O2 included (a) both GC and AC (ground- and air-coupled) GPR deployments; (b) the impact-echo (IE) and ultrasonic (US) devices on the robotic Stepper™; (c) the Proceq™ rolling half-cell (HC) instrument; (d) the Wenner electrical resistivity (ER) probe; as well as (e) a portable seismic property analyzer (PSPA). Some of NDE technologies deployed on Deck O2 are shown in Figure 70.

Figure 70. Simultaneous data collection on Deck O2 using various NDE instruments.

Traffic Control/Gridding of Deck

Traffic control and gridding were performed in the same manner as on Deck O1, except that the origin is located at the SW corner of the gridded deck, as shown on the upper left corner of the deck in Figure 69 There is no skew on Deck O2, so an orthogonal grid was marked on the deck surface for NDE data collection.

NDE Results and Core Extraction/Observations

Results from the GPR and HC testing, together with core locations, for Deck O2 are shown in Figure 71. There is clearly very strong correlation between the two data sets.

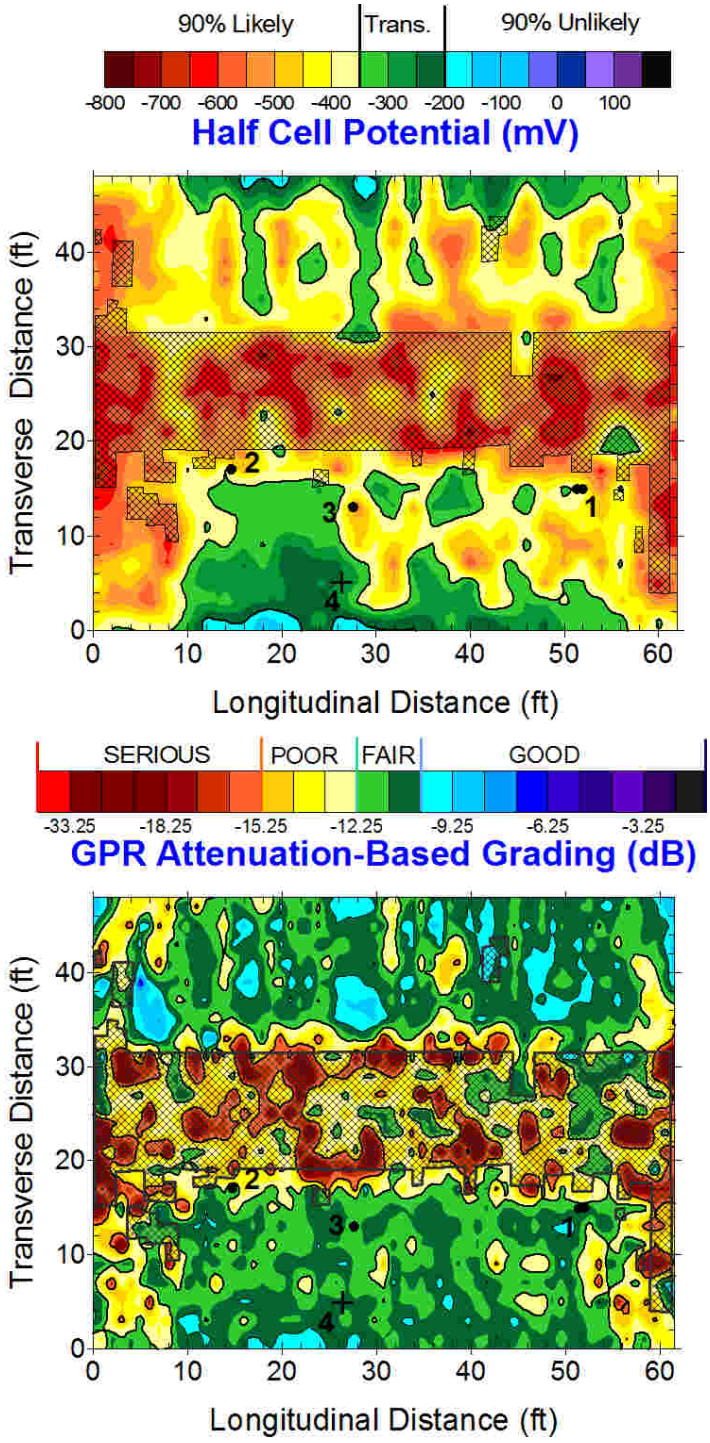

Figure 71. Cores 1 through 4 shown on the GPR and half-cell (HC) maps, with "+" sign indicating control core location and cross-hachured areas showing repairs.

Information from cores extracted immediately following part of the NDE evaluation show that the raw GPR was effective at revealing anomalies that could be identified as corrosion-induced deterioration of the concrete, including delaminations and severe steel corrosion. Cores on Deck O2 validate the GPR selections (Figure 72) by revealing expected results, as shown by typical deteriorated cores extracted as core samples 1a, 1b and 2. All cores shown in this figure were delaminated and both core samples 1b and 2 included an extremely corroded rebar. Core #2 is shown on top, along with its hole; while Core #1b is shown on bottom along with its hole. The hole for Core #1a was cut first, and then Core #1b was extracted immediately adjacent to it for a good reason: the hole at Core #1a showed slight evidence of delamination along one of the edges, but otherwise produced a fairly solid core with a coincident crack that matched the core hole. No bar was encountered in Core 1a. Confident that the raw GPR profile showed strong indications of deteriorated concrete, but also some evidence of upward-sloped cracking (consistent with a water-filled delamination as shown previously in Figure 63, Deck O1), the second core at 1b was drilled immediately above the rebar. The purpose was to determine conclusively whether there was damaged concrete or corroded steel at that location, which was believed to have been just slightly missed at the Core #1a location.

Figure 72. Core #2 and its hole (top) shown with Core #1b hole and its extracted core (bottom), immediately adjacent to the hole for Core #1a (half shown in photo).

All three cores suspected to be deteriorated broke during removal and/or were delaminated and/or split at the rebar. Also, the steel was either severely or moderately corroded. The control core

was also visibly sound and had to be broken from the deck to remove it. Cores #3 and #4, the third core targeted as "deteriorated" and the fourth as "control" core, respectively, are shown in Figure 73.

Figure 73. Cores #3 (left) and 4 (right), selected as "deteriorated" and "control" (sound) specimens for Deck O2.

Finally, a map compares impact-echo (IE) results, graded as areas where the concrete condition is considered "good", "fair", "poor" and "serious" (as explained in the Introduction) with electrical resistivity (ER) measurements (Figure 74). As was the case in Figure 71 (HC and GPR maps), the correlation between areas of concern is good between these two technologies. It can be further said that all four technologies (comparing Figures 71 and 74) correlate well. Last, there are cross-hachured areas overlaid onto both the IE and ER maps which show the repairs made by Iowa DOT subsequent to this testing, guided first by traditional sounding and then "following the damaged concrete", as previously described. On this deck, the correlation between the results points to corrosion as the likely cause of deck deterioration.

A closer inspection reveals that every single core extracted at the time of NDE data collection, including all three targeted as "deteriorated" and validated as such on-site, lies fully outside any of the repaired zones. Clearly, three samples displaying significant deterioration are shown in Figures 72 and 73, visible as delamination and either moderately or severely corroded steel. Furthermore, all these deteriorated core samples were extracted outside the repaired areas which were ultimately integrated into an overlay. This suggests that there is likely a significant quantity of reinforced concrete that probably should have been removed and replaced as repair area(s), and it supports a basis for considering use of NDE evaluations as part of the decision-making process prior to delineating removal quantities for repair.

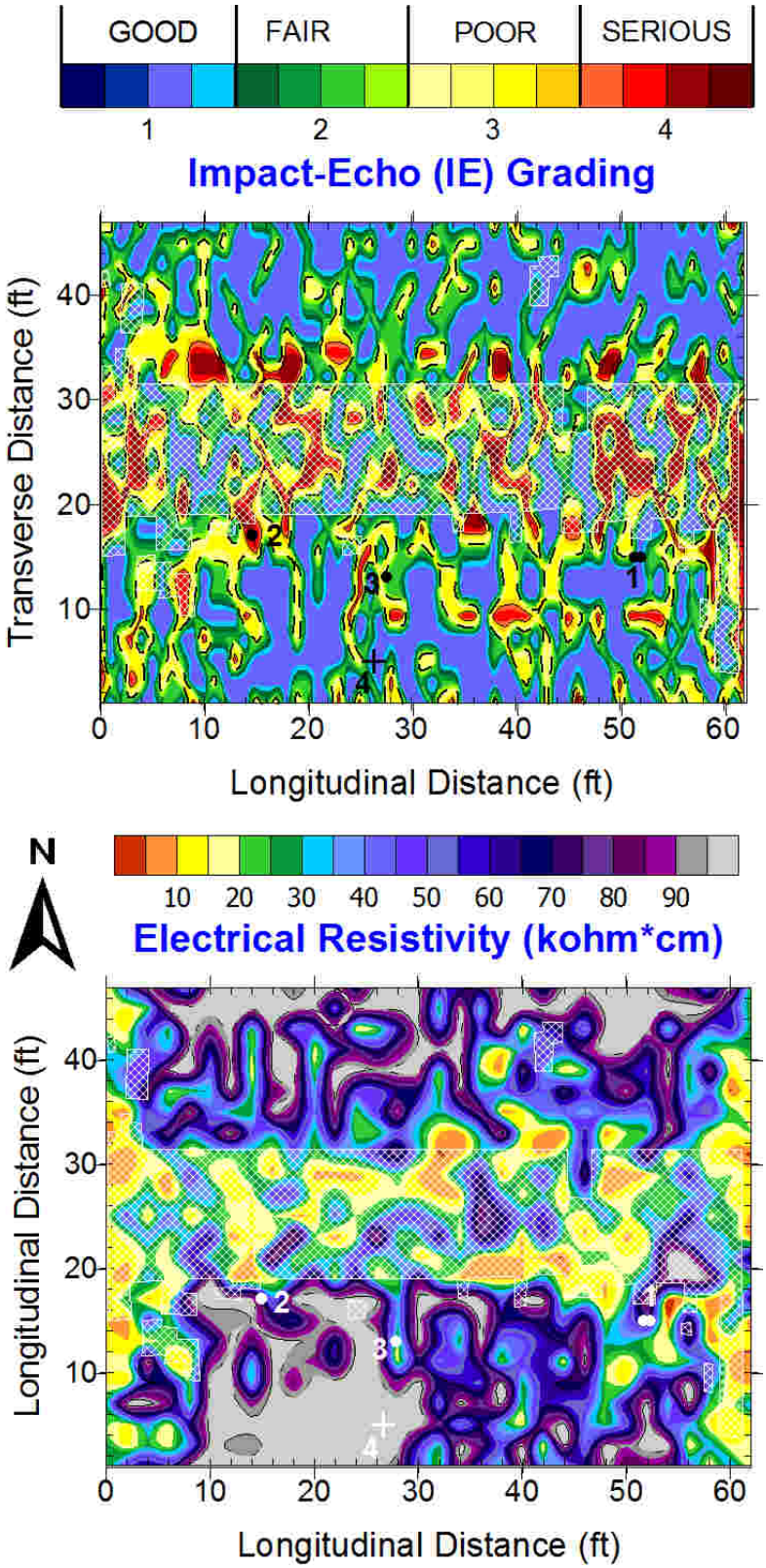

Figure 74. Repaired areas overlaid on impact-echo (IE) and electrical resistivity (ER) results.

BRIDGE O3 DECK EVALUATION

The deck on Bridge O3 consists of a 123ft x 44ft continuous concrete slab carrying Iowa #14 over Warren Grove Creek and located 5.5 miles north of Monroe, IA. . The bridge was designed in November 1969 and constructed in 1971 (Figures 75 and 76). The most recent bridge inspection report, dated May 31, 2006, indicated that the deck is PC concrete. The top of the deck has some hairline transverse, and a few hairline diagonal and longitudinal cracks. There are a few scattered small and large hollow areas and some large and small PC concrete patches. The bridge was analyzed and found to be adequate for two lane legal loads. Corrective recommendations, based on reporting of the deck spalling and deterioration, was to recommend the deck for a complete PC overlay scheduled for completion in 2009. On both figures, through-deck deterioration (rust staining) can be seen between two of the piers close to the deck centerline (shown in detail, on inset of Figure 76).

Figure 75 Side view of Bridge O3 showing full-depth (slab) deck construction between piers

Figure 76. Rust stain almost full length between piers, roughly along centerline.

NDE Methods Employed on Deck O3

NDE methods used for collecting condition data on Deck O3 included (a) both GC and AC (ground- and air-coupled) GPR deployments; (b) the impact-echo (IE) and ultrasonic (US) devices on the robotic Stepper™; (c) the Proceq™ rolling half-cell (HC) instrument; and (d) ultrasonic surface wave (USW) measurements of in-situ concrete modulus using a portable seismic property analyzer (PSPA). Simultaneous data collection using various methods took place on Deck O3, as described previously and shown in Figure 77.

GPR data collected on the deck confirmed that the shallowest steel in the upper mat of reinforcement was oriented in the longitudinal direction, parallel with traffic flow, while transverse bars are tied to the bottom of the longitudinal steel. It is well established that the best way to collect data is to orient GPR lines perpendicular to the shallowest steel in the deck, preventing erroneous data analysis and interpretation. This rebar configuration required GPR data collection across traffic lanes, in lines oriented perpendicular to traffic flow (Figure 77). Data on one-half the deck was collected up to the point where the antenna (in tub between rear and front wheels of GPR cart) could just cross the centerline, when no traffic was approaching. This mode of data collection was applied not only to Deck O3, but also the remainder of the slab decks with longitudinal steel tied on top of transverse rebars in the upper mat (O5, O6, R1 and R3). Data collection was unaffected for the other NDE methods (Figure 77, upper right), where Stepper™ is moving along Line A (1ft from curb) and PSPA data collection is taking place behind it. On this deck, exposed rebar (Figure 78) allowed steel to simply be cleaned and drilled with a small hole for a positive electrical connection during half-cell (HC) measurement preparation (not shown).

Figure 77. GPR data collection oriented perpendicular to traffic direction on slab decks, with other NDE methods unaffected by rebar orientation in upper mat.

Figure 78. Surface spall exposes rebar, simplifying half-cell preparation (equipment not shown).

Traffic Control/Gridding of Deck

Traffic control and gridding were performed in the same manner as on Deck O2, except that the region near the origin, also located at the SE corner of the gridded deck, is shown in Figure 79 (off right side of photo frame). Because of the negative deck skew (obtuse angle between the curb and abutment at the origin), an orthogonal grid the length and width of the deck surface was marked for NDE data collection using negative x-coordinates within the negatively skewed region near the south abutment.

Figure 79. Gridded area near origin, showing negative coordinates used for mapping.

NDE Results and Core Extraction/Observations

Results from the NDE testing for Deck O3 are shown in Figures 80 and 81, where core locations are marked. There is clear correlation between the data sets, particularly where each of the three methods; IE, GPR and HC; indicate, respectively, the most serious damage, deterioration or likelihood of corrosion. However, there are also large regions where the impact-echo (IE) map generally displays poor condition (yellow areas, where there are delaminations not audible to the human ear, yet detectable by the impact-echo instrumentation). In these regions the GPR generally indicates poor to fair condition, and the HC method is difficult to correlate with either method. GPR and IE are probably in better agreement since some of the damage identified by both methods exists in areas where concrete cover is either extremely shallow or deep (Figure 80). In the case of impact-echo, the method is not hindered by the ability to detect shallow or deep damage unless the damage is beyond the detection capability of the instrument. This was not the case on this deck, where IE was able to see a back wall reflection (bottom of the deck) wherever no delaminations were present. Similarly, GPR was able to image full-depth through this deck; however it is only used to report damage at the uppermost rebar level at any location on the deck. Since the GPR data are adjusted for signal attenuation (loss) variations that are depth-related, using the estimated cover measurements obtained during the GPR measurement, for the most part this method is not adversely affected by the rebar depth variation once this correction is applied.

What is described previously for impact-echo (IE) and GPR, however, does not necessarily apply to the half-cell (HC) method. It is well-documented in the literature that the half-cell method is adversely affected by both extremely shallow reinforcement or very deep rebars in the upper mat. This deck displays both: extremely shallow and very deep rebars – in other words, significant depth variation in the concrete cover. All of this rebar depth variation was part of the original construction, as there has been no overlay. However, there is obviously quite a bit of evidence of surface repair (and some spalling), as seen in previous photos and documented in other photos taken on site, which were not included as a part of this report. Spalled areas account for some of the very shallow reinforcement seen in the cover map.

Ground truth: Iowa DOT did not provide maps of repaired areas, so this information cannot be compared against the NDE results. Attempts were made to core the deck as previous, but raw GPR data in the field did not cleanly indicate regions of obvious deterioration. All cores were expected to be “good to fair”. Three had vugs, none had visible rust (Figure 82), but a good-sized vug existed in Core # 2, one of the three selected as “fair”. It would be instructive to test at least two of these cores for chloride content.

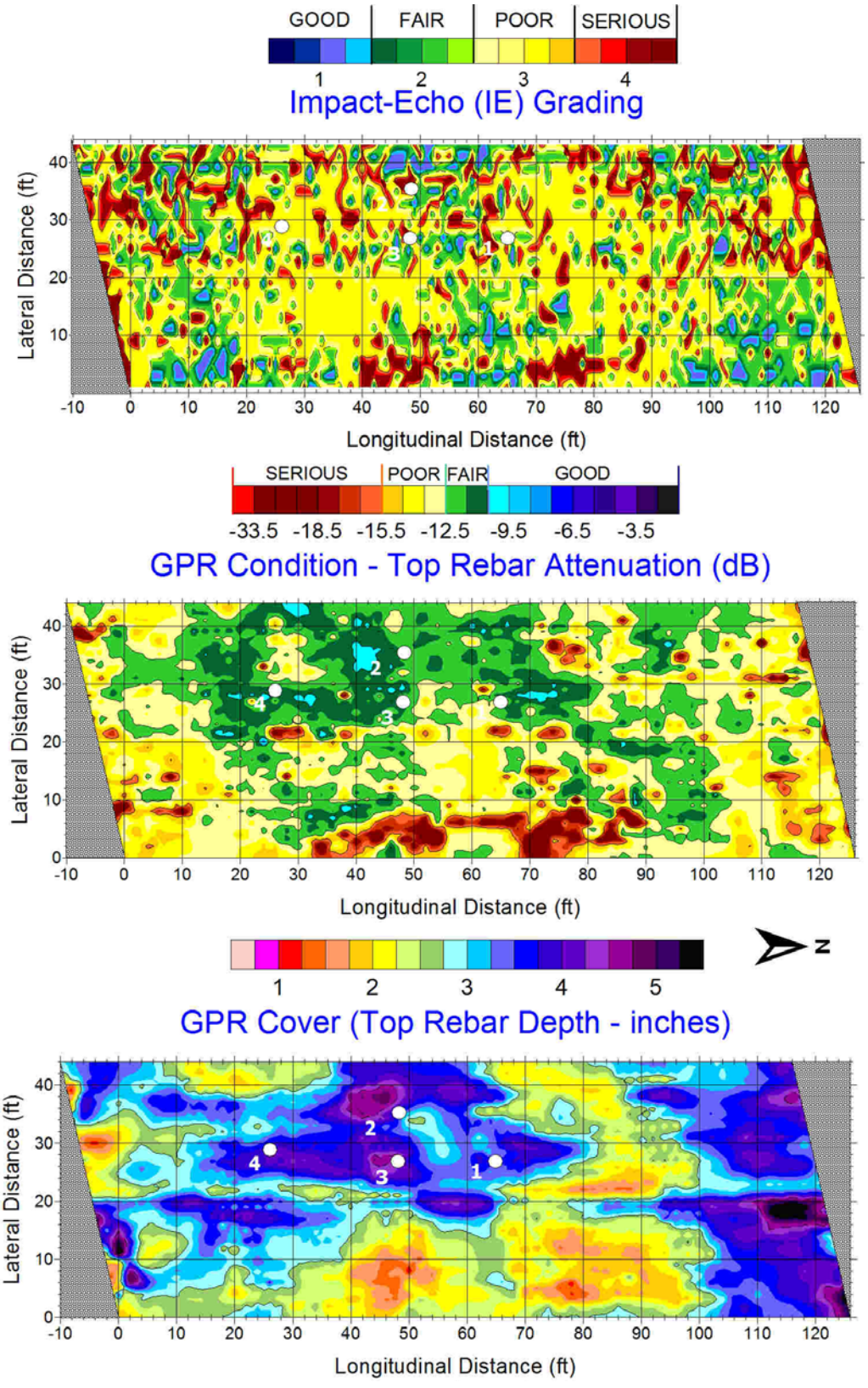

Figure 80. Results for impact-echo (IE), GPR condition, and GPR-estimated cover depth for Deck O3 – with core locations on map.

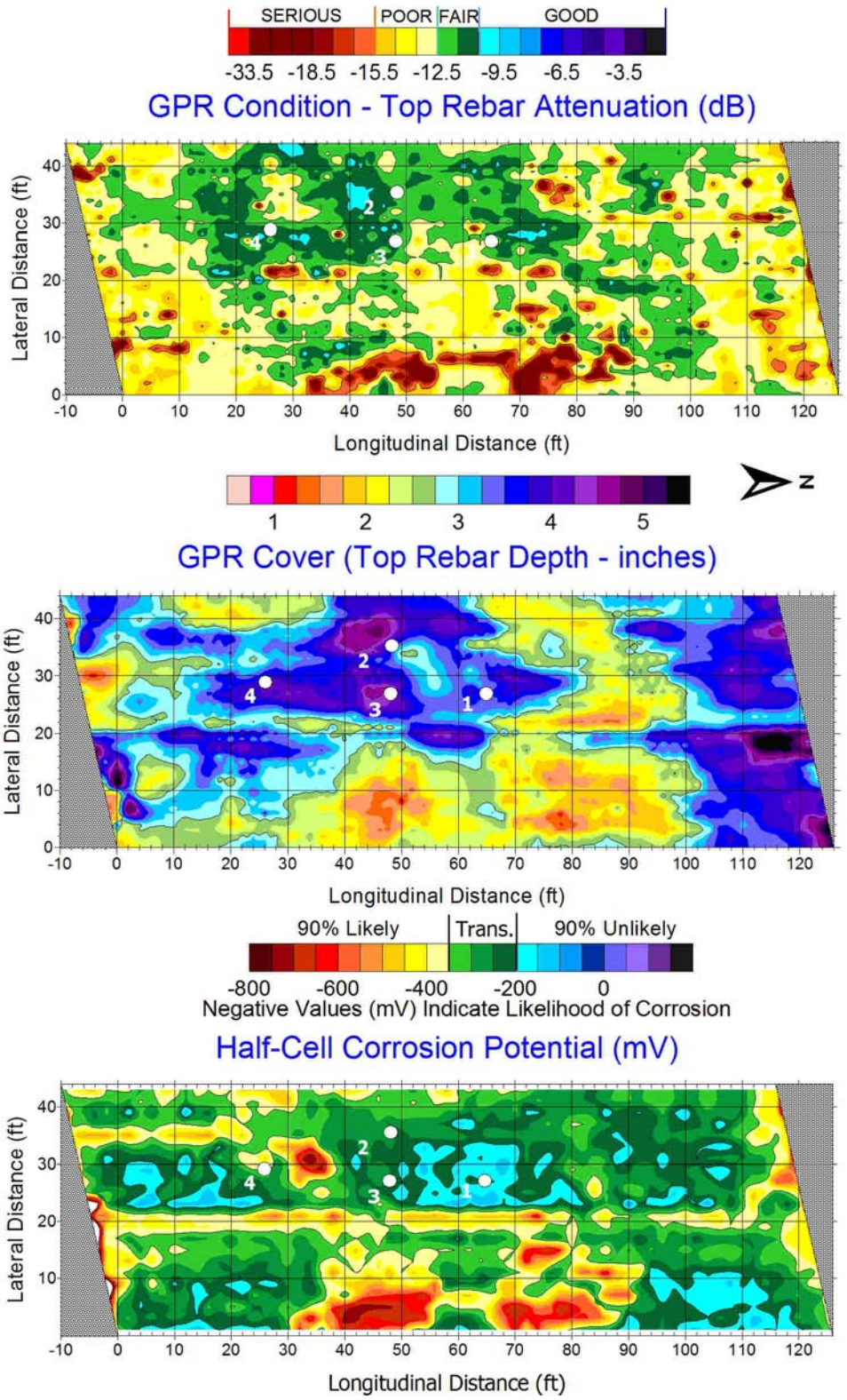

Figure 81. Results for GPR condition, GPR-estimated cover depth, and half-cell potential (HC) on Deck O3 – with core locations on map.

Figure 82. Cores 1 through 4 (left to right), where Core 1 is "control" and Cores 2 to 4 selected where GPR signal looked "slightly worse", yet not obviously deteriorated. Note pen-sized vug in Core #2.

BRIDGE O4 DECK EVALUATION

The deck on Bridge O4 is a 334ft x 52ft steel girder structure carrying US 18 over Cedar River, located in Charles City, IA (Figures 83). The bridge (FHWA No. 24970) was visually inspected as referenced in a December 30, 2008 report. The design drawings and the inspection report indicate that the structure was designed in May, 1966 and constructed in 1967. The deck is PC concrete; the top of the deck has many PC concrete patches, many narrow transverse cracks, and a few diagonal cracks. The top also has many hollow areas. Deck spalling and deterioration was reported. This bridge is recommended for a complete PC concrete overlay, scheduled for completion in 2009.

Bridge O4 is shown in Figure 83 below, using Google Map street view and aerial view. The upper portion of the figure shows the two EB lanes (right) and the oncoming traffic in the WB lanes (left). Note that in this figure and others, the dominant patching (prior to NDE inspection or subsequent repair) is visible in the WB passing lane, left of the double striped lane divider.

Figure 83. Google map street view in EB direction, on Deck O4 crossing the Cedar River.

NDE Methods Employed on Deck O4

NDE methods used for collecting condition data on Deck O4 included (a) both GC and AC (ground- and air-coupled) GPR deployments; (b) the impact-echo (IE) and ultrasonic (US) devices on the robotic Stepper™; (c) the Proceq™ rolling half-cell (HC) instrument and Wenner electrical resistivity probe; and (d) ultrasonic surface wave (USW) measurements of in-situ concrete modulus using a portable seismic property analyzer (PSPA). Simultaneous data collection using various methods took place on Deck O4, as described previously and shown in Figures 84 and 85. Data collection took place over a three day period, first on EB and WB travel (outer) lanes and then on EB and WB passing (inner) lanes. Data collection in both Figures 84 and 85 are shown in the inner (passing) EB and WB lanes.

Figure 84. Data collection during light rain using Stepper™, on EB and WB passing lanes on Deck O4.

Figure 85. Simultaneous electrical resistivity measurements being taken on east end of deck.

Traffic Control/Gridding of Deck

Traffic control and gridding were performed in the same manner as for Decks O1 and O2, with the origin located at the SW corner of the gridded deck, as shown in previous figures. There is no skew on Deck O4, so an orthogonal grid the length and width of the deck surface was marked for NDE data collection as described previously. The major difference on how this deck was gridded and marked is that traffic control was provided on outer (travel) lanes, in both the EB and WB directions. The deck width had to be pre-measured to verify where each of the grid lines (A through Z) would have to be located, since the first day of gridding would allow only marking the deck on lines H through S (inner lanes). The remainder of the deck (outer, passing lanes in EB and WB directions) would be gridded on day 2 of data collection on lines T through Z. Figure 86 shows part of the resulting grid on the northwest end of the grid across the width of the deck from the origin, as marked on day 1 of data collection.

Figure 86. Gridded area of deck near northwest corner, Stepper™ shown in foreground.

NDE Results and Core Extraction/Observations

NDE maps for Deck O4 include GPR condition assessment based on top rebar attenuation, estimated concrete cover, IE grading and half-cell corrosion potential (HC) shown in Figure 87. Note that there is good correlation among the various methods for this particular deck.

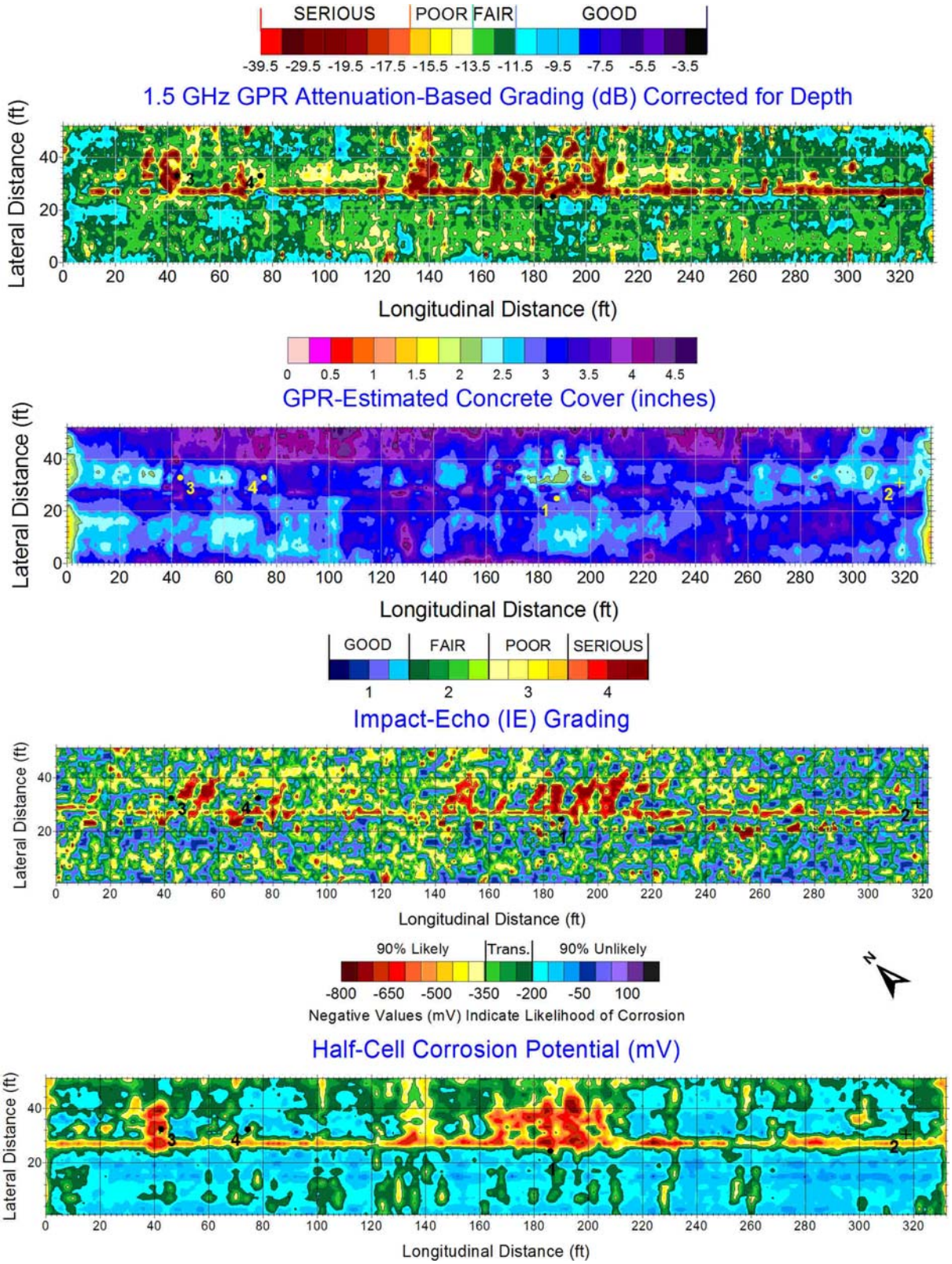

Figure 87. NDE maps for GPR condition, estimated concrete cover, impact-echo grading and half-cell corrosion potential.

Figure 88 includes NDE maps overlaid with repair zones. A field error was made by the NDE crew in laying out the grid length, and a procedural correction was made subsequent to surveying Deck O4. Note that there is a discrepancy between grid painted on the deck (324ft) and the measured deck length (332.5ft). The IE data were not distance-corrected to account for this discrepancy, as is the case with the mapped repairs overlaid onto the IE data. In other words, the IE maps are consistent with the grid marked on the deck and the marked repairs which used the deck grid for coordinate referencing, which is short 8.5ft of the measured (actual) deck length. However, the HC and GPR data were distance-corrected so that data actually cover the correct deck length, 332.5ft. Thus, the overlaid map repairs, which were hand-sketched in the field and directly digitized without benefit of the 8.5ft distance correction, are placed directly onto all three maps. On both the GPR and HC maps, it is apparent there is a cumulative distance discrepancy between these distance-corrected maps and the overlaid repairs, though the accumulated error is not necessarily linear. However, since the IE map and the digitized repair areas extend only to 324ft, and the cumulative error in each of these maps is exactly the same everywhere, IE results are expected to be a better match with regard to one-to-one comparison of all mapped areas. Nonetheless, even if the digitized repair overlay was stretched the additional 8.25ft required to match the GPR and HC map distances, the repaired areas appear to match the IE data better than they do either the GPR or HC, although there is reasonably good correlation on most deck areas between marked repairs and all three NDE data results.

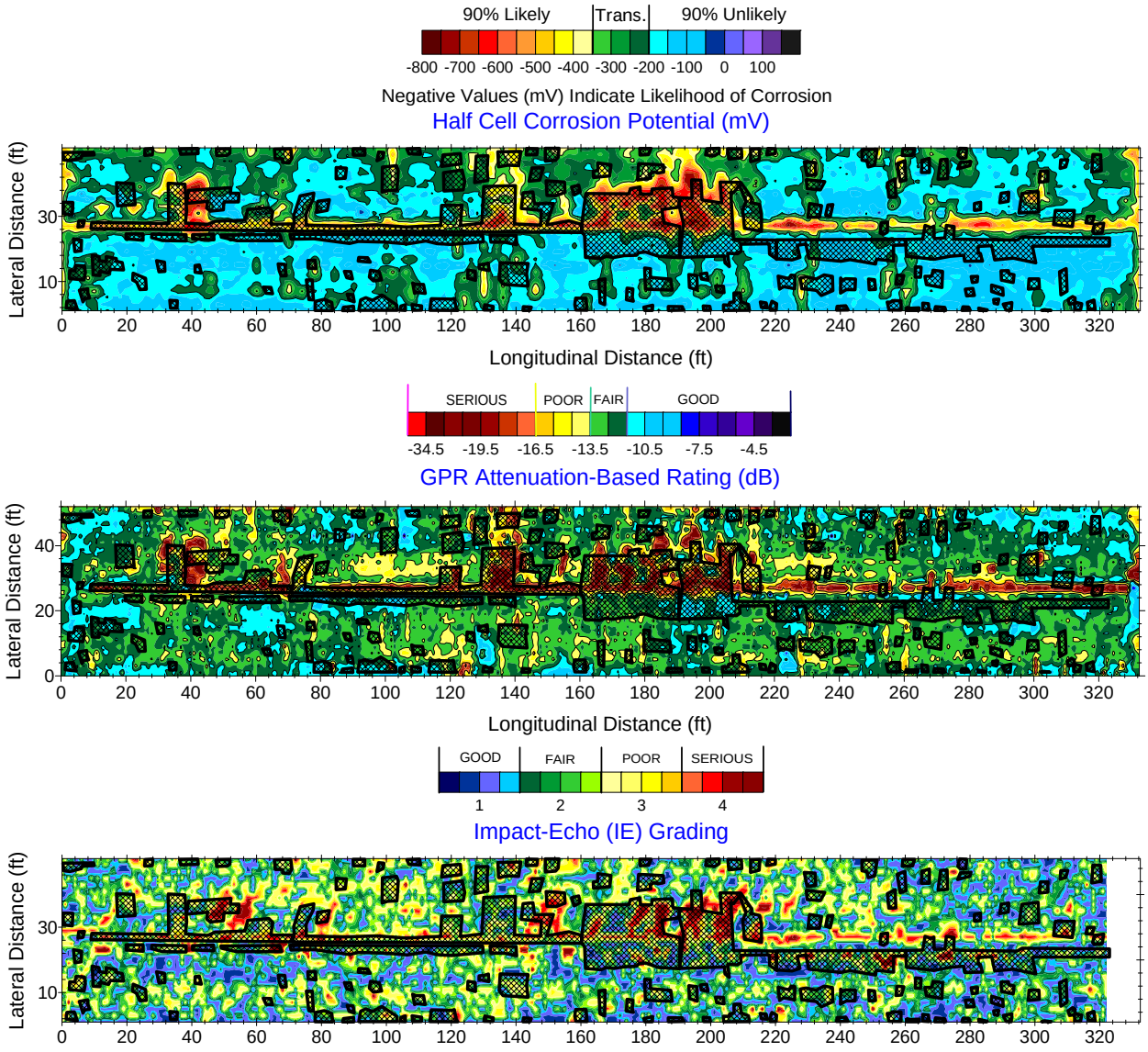

Figure 88. HCP, GPR and IE maps with overlaid repairs.

In Figure 89, a partial USW data set is compared with two other NDE maps covering the entire deck area. Again, the reason USW data is not providing complete coverage is that the method is more time-consuming, thus USW data collection on the entire deck could not be completed within the allotted traffic control duration. Though USW data were not collected as part of the required NDE research program, they were obtained nonetheless so that their value alongside other complementary methods could be gauged. Comparing the three maps shown in Figure 89 for this particular deck, it is fairly apparent that the regions with decreased elastic modulus coincide with regions displaying evidence of damage, or corrosive environment, or active corrosion as shown on the IE and GPR maps, respectively.

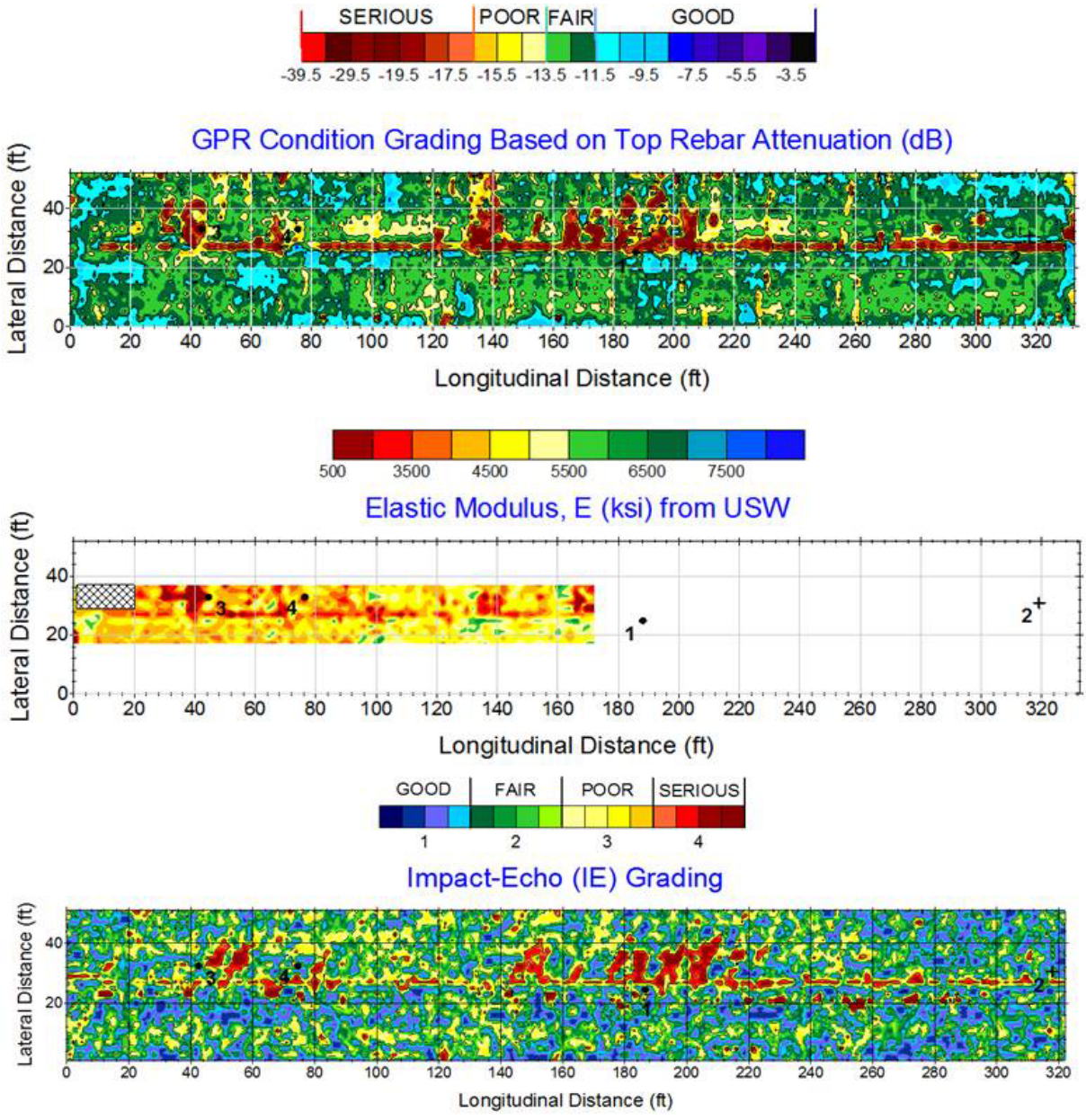

Figure 89. GPR, USW, and IE maps showing good correlation in surveyed areas.

NDE maps from this deck appear to reveal a strong correlation between reduced modulus values obtained from USW and corresponding deck areas where other NDE methods (IE, GPR and HC) also indicate either the existence of damage (delamination/cracking), along with an internal concrete environment where deterioration and corrosion, respectively, are likely to exist. Hence, there is some value in USW measurements even when no previous baseline data are available for comparison, though it would be preferable to have a baseline data set for comparison so that modulus variation due to initial construction and degradation over a structure's lifetime can be distinguished.

Cores essentially revealed deck conditions that were expected, based on using GPR field data for selecting locations. One control core was selected as "sound" and three others were targeted as "deteriorated". Figure 90 includes Core #2 (control), where GPR signal was uniform with high signal strength (no visible signal attenuation) and Core #1, where GPR showed visibly attenuated top rebar reflections – a strong indicator of deck deterioration. As seen in Figure 90, Core#2 was retrieved intact with no evidence on the core surface or within the core hole of vertical cracking, rust or delamination. On the other hand, Core #1 was retrieved in two parts, but only after prying at the core in an attempt to break it at the bottom after reaching the targeted depth of 6.5in. This certainly raises a question whether it maybe failed during the prying because of the presence of an existing or incipient crack.

Core #4 is shown in Figure 91, where the top part of the core is inverted to show a linear swath of corrosion products directly above a rebar, at the delamination (where the top portion broke just after reaching the upper rebar depth). The rust staining on the upper part of the core, which extends toward the middle of the core sample along the delaminated surface, provides clear evidence that the core was delaminated prior to retrieval. The bottom part of the core is also shown, upright, to reveal the rebar, which is corroded at top and on both sides (very obviously on top and left sides in photo). Core #4's hole also indicates that delamination had taken place prior to core retrieval (Figure 92). The rebar chair can also be observed (lower right of Figure 90, left photo), which was imaged, and interpreted as such, in the GPR data at the core retrieval location.

Finally, GPR was used to target Core #3 as a deteriorated one. The results of coring are shown in Figure 93, where the core broke apart in many pieces. Both coarse and fine aggregate, as well as crumbled mortar, were accumulated at the bottom and along the sides of the core hole.

Figure 90. Core #2 (left) selected as control, retrieved intact; Core #1 (right) retrieved in two parts.

Figure 91. Top of Core #4 (inverted, left) reveals corrosion products above delamination; core bottom (right) with corrosion products on top and sides of rebar.

Figure 92. Hole from which Core #4 was retrieved, showing delamination in both photos, rebar chair beneath bar in left photo, and rebar with corrosion at top and sides in right photo.

Figure 93. Hole and core sample (Core #3) with severe delamination and corrosion at top and sides of rebar.

BRIDGE O5 DECK EVALUATION

The deck on Bridge O5 (Bridge No. 6927.6S034, FHWA No. 037500) consists of a 127ft x 30ft concrete slab (Figure 94 and Figure 95) carrying US #34 over Indian Creek, located 1.1 miles east of US Highway 59. The bridge was designed in 1962 and constructed in 1964, according to the inspection report provided the NDE team by Iowa DOT. Cores extracted during the NDE/field work activities do not indicate that there is any overlay in place, as will be shown in subsequent figures. However, the deck surface has several concrete and asphalt patches, and there were also exposed spalls, as documented in Figure 96. This bridge is recommended for a complete PC concrete overlay, to be completed in 2009.

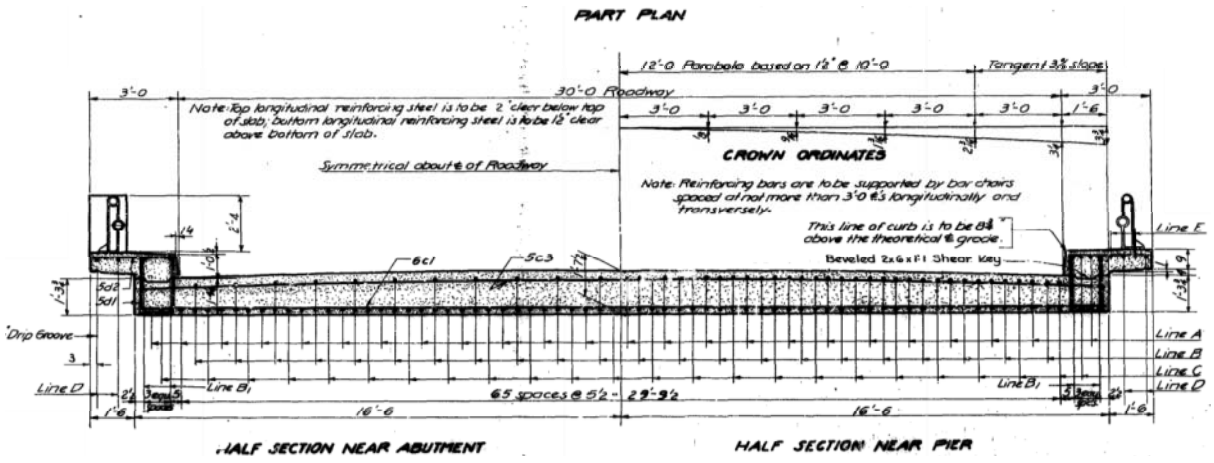

Figure 94. Deck half-sections near abutment and pier, showing reinforcement layout.

Figure 95. Side view of Bridge O5 showing full-depth (slab) deck construction between piers.

Figure 96. Perspective view of Deck O5, showing patches and spalls; also, repaired settlements in approach slab (foreground).

NDE Methods Employed on Deck O5

NDE methods used for collecting condition data on Deck O5 included (a) both 1.5GHz and 2.6GHz GC GPR deployments; (b) the impact-echo (IE) and ultrasonic (US) devices on the robotic Stepper™; (c) the Proceq™ rolling half-cell (HC) and electrical resistivity (ER) instrument; and (d) ultrasonic surface wave (USW) measurements of in-situ concrete modulus using a portable seismic property analyzer (PSPA). Simultaneous data collection using various methods took place on Deck O5, as shown in Figure 97.

GPR data collected on the deck confirmed that the shallowest steel in the upper mat of reinforcement was oriented in the longitudinal direction, parallel with the traffic flow, while transverse bars are tied to the bottom of the longitudinal steel. Once again, this rebar configuration required GPR data collection across the traffic lanes, in lines oriented perpendicular to the traffic flow (Figure 97). Data on one-half of the deck was collected up to the point where the antenna (in tub between rear and front wheels of the GPR cart) could just cross the centerline, when no traffic was approaching. This mode of data collection was to all the slab decks with the longitudinal steel tied on top of the transverse rebars in the upper mat (O3, O6, R1 and R3). Data collection was unaffected for other NDE methods (Figure 97, upper left), where

Stepper™ is moving along Line C (5ft from the curb), rolling half-cell (HC) data are being collected on Line D, and PSPA data collection is taking place near the west abutment (near the passing semi-truck).

Figure 97. GPR data collection oriented perpendicular to traffic direction on slab decks, with other NDE methods unaffected by rebar orientation in upper mat.

Traffic Control/Gridding of Deck

Traffic control and gridding were performed in the same manner as on Deck O2. The region near the origin, also located at the SW corner of the gridded deck, is shown in Figure 98. Because of the positive deck skew (acute angle between curb and abutment at the origin) on Deck O5, an orthogonal grid the length and width of the deck surface was marked for the NDE data collection, but did not require using negative x-coordinates as did Deck O3.

Figure 98. ER measurement on EB lane along Line C (5ft from curb), 10ft from west abutment, near origin.

NDE Results and Core Extraction/Observations

Results from the NDE testing for Deck O5 are shown in Figure 99, where core locations are marked using circular symbols denoting predicted core condition, as determined in the field using the GPR instrument. The circular symbols include a crosshair dividing the symbol into four equal pie-shaped areas, with either blue (control), yellow (fair to poor), or red (serious) quadrants within the symbols used to denote predicted condition. Cores 1 to 4 are shown from left to right on the NDE maps using the yellow, blue, red, and red descriptors indicated previously. The four core locations (Core #'s 1 to 4, left to right, respectively) are most visible in the concrete cover map (upper map in Figure 99), and are located in that particular map with red arrows. Each of the symbols representing a core sample is also visible in the other NDE maps, though not labeled. All four maps are in agreement that there should be expected deterioration (GPR), likely corrosion (HC) or delamination (IE) where the yellow and red-colored circular symbols are marked. There is also full agreement among the maps that the control core location should produce either a "good" or "fair" core, which is highly likely to be extracted intact.

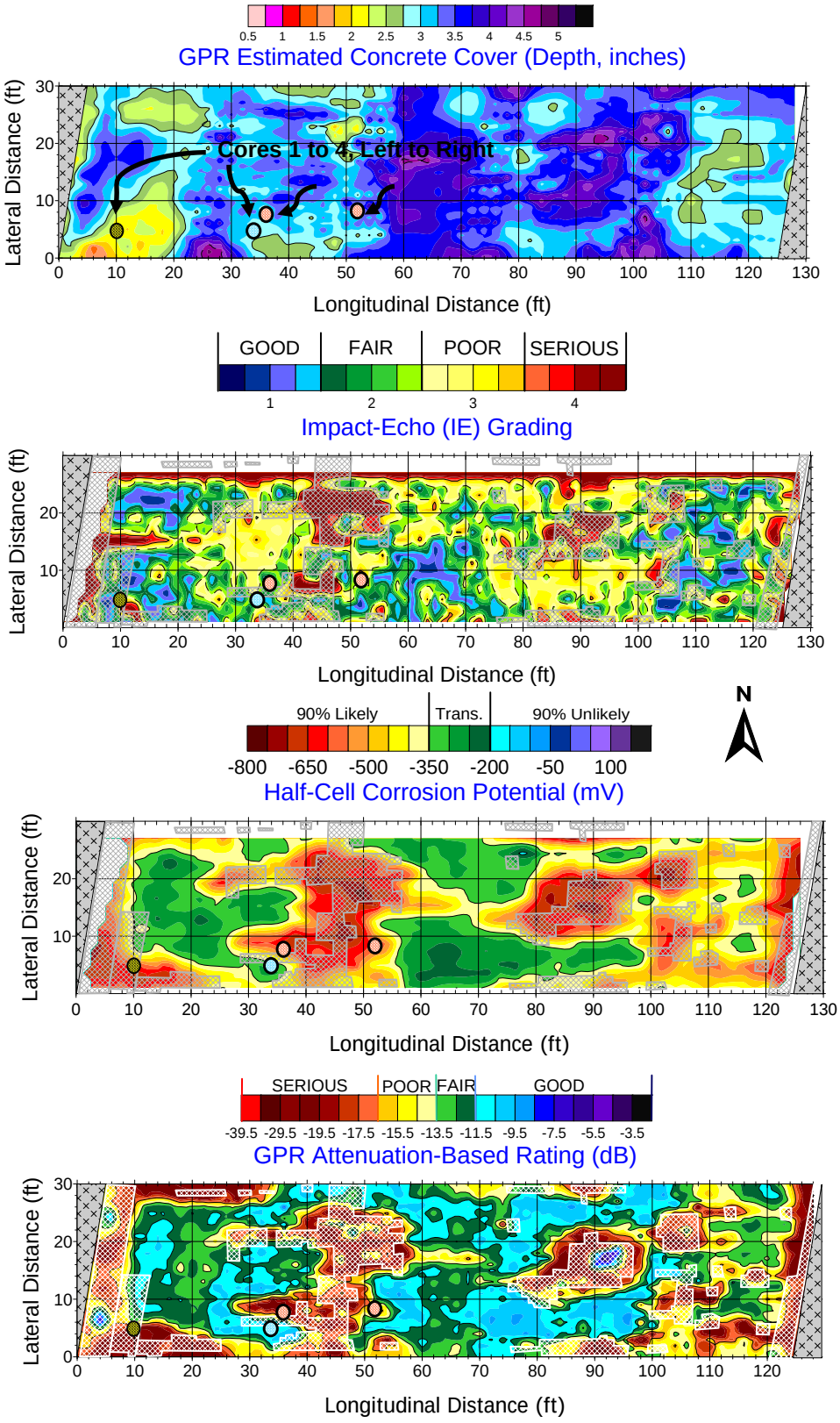

Figure 99. GPR-estimated cover depth, impact-echo (IE), half-cell potential (HC) and GPR condition maps shown on Deck O5 with cores (#'s 1 to 4, left to right) and repairs.

Figure 99 also shows cross-hachured (mesh overlay) areas where Iowa DOT performed repairs after the NDE testing was performed, again not using the NDE results for guidance, rather for comparative purposes (previously discussed). There is clear correlation between the data sets, particularly where each of the three methods indicates, respectively, the most serious damage, deterioration or likelihood of corrosion. However, there are some discrepancies between what each of the methods is predicting, as is to be expected for the previously discussed reasons.

GPR was used in the selection of core locations. Cores ranged from "good" (control) to "fair-to-poor" and "serious". The results are shown in Figures 100 and 101. A "fair to poor" rating using impact-echo indicates that there is some evidence of damage that was measured at the Core #1 location, since the signal included both a high-frequency response from a crack or initial (incipient) delamination and a portion of energy reflected back from the deck's bottom. As can be seen in Figure 100, Core #1 (inverted) was also expected to be "fair to poor" based on its IE grading shown on the map within Figure 99 (IE was not used for field-selection of the core) and was extracted intact, with a delamination extending 2/3 of the way around the sample's circumference. The core hole also showed a "nicked" rebar with corrosion products surrounding the steel and along a good part of the delamination. Some rust discoloration (corrosion products) embedded within the delamination, bonded to the crack's interior surface. Since the IE signal response represents a response of a larger deck volume, in comparison to the core sample, the IE ranking may slightly differ from the condition observed on the core.

Figure 100. Core #1 – expected to be "fair to poor" – shows delamination, and core hole reveals "nicked" rebar, delamination and corrosion.

Cores #2, #3 and #4 are shown in Figure 101 (respectively, left to right), where Core #2 is the "control" specimen and Cores #3 and #4 were field-predicted by GPR to be in serious condition, with regard to what was visible in the raw data. Core #2 (control) is shown inverted at

left and was extracted fully intact, with no visible signs of deterioration within the concrete or corrosion surrounding the transverse and longitudinal bars exposed in the core sample. The core hole also showed no signs of deterioration. Core #3 was predicted to be in serious condition (reference circular dot with two red quadrants indicating same, Figure 99), and though it was removed intact there were a number of horizontal cracks that nearly cut through the entire specimen. This included one major delamination that was propagating toward the surface from the top of the cut rebar (cut piece of rebar shown in front of the inverted core specimen, at center of Figure 101), which fell off the left side of the core (see rebar imprint on the core at the center of the figure). The core hole also showed a delamination surrounding most of its circumference, just above the top rebar, with other intersecting horizontal cracks (delaminations) propagating elsewhere along the core hole. Finally, Core #4 was extracted in two pieces and is shown at right where the upper right photo shows the fully-delaminated (bottom portion) of the core sample with an embedded rebar that has corroded and generated corrosion products that have moved outward into the delamination. The photo at lower right shows the upper section of the core placed on top of the lower portion (core not inverted), including the embedded rebar that corroded and likely generated the delamination shown. The core hole for this sample also shows a fully delaminated deck at that location, with horizontal cracks matching those seen in the sample and rust-staining embedded within the open delaminations (not shown). Though many of the observations described for NDE and core results include discussions about the condition of cores and the holes where they were extracted, not all photos can be possibly included within the report. Project photos, however, are archived and used to support any reported observations that may not be fully evident within the cited figures.

Figure 101. Cores 2, 3 and 4 are shown left to right, respectively, with control (good) core at left.

Based on the comparison of all the NDE maps to the core results, there are different recommendations that can be made for chloride sample profiling:

- Core #3 could be evaluated, since it is the only one that falls within a mapped zone where GPR, IE and HC are slightly in disagreement (IE shows "fair" condition and other methods indicate a significantly higher likelihood of deterioration).
- Alternately, the control core (Core #2) could be checked for chloride content to further validate that it is sound – or to refute the physical evidence, since sometimes a core that physically looks good can exhibit high chloride levels.

Both (or all) cores could certainly be examined, depending on how many cores Iowa DOT wants to perform a chemical analysis, or chloride profile. An argument could be made for testing any core where only physical condition is used to assert that it is, indeed, "sound". The opposite is not true for cores which display evidence of corrosion or delaminations induced by a corrosive process.

BRIDGE O6 DECK EVALUATION

The deck on Bridge O6 consists of an 83ft x 44ft continuous concrete slab (Figures 102, 103, 104 and 105) carrying US #71 over a small stream, located 0.8 miles north of North Junction Secondary Road, J20. The provided plans and inspection report indicate that the deck was designed in 1971 and constructed in 1972. Inspection reports include an analysis that the deck was found adequate for two lane legal loads. Finally, the deck surface was reported to have been randomly sounded and had previously been repaired (about 5% of the deck area) using PC patches, based on an inspection report generated in November 2007. A number of visual underside inspections over the years, coupled with the reported repairs, surface spalling and deterioration, etc. included in the most recent inspection report; caused the deck to be recommended for a complete PC concrete overlay, scheduled to be completed in 2009.

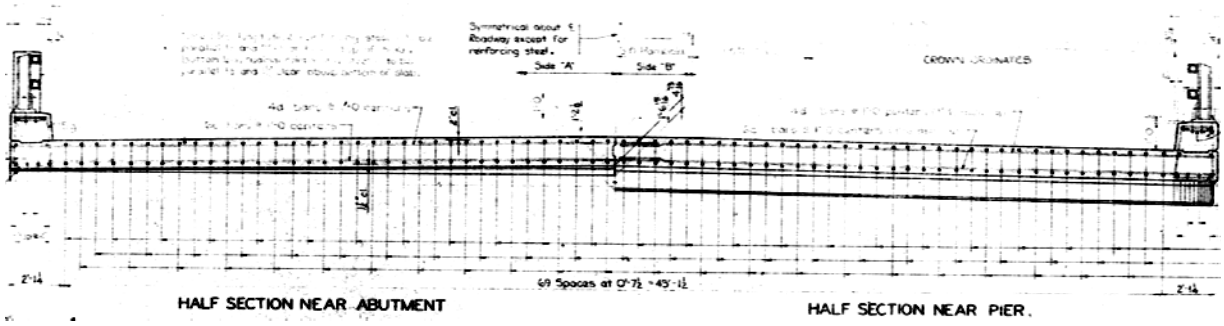

Figure 102. Deck O6 half-sections near abutment and pier, with rebar layout for continuous slab.

Figure 103. Perspective view of Deck O6, looking southbound, shows PC patches and spalls.

Figure 104. Side view of Deck O6 showing continuous slab construction on east face.

Figure 105. Bottom view of Deck O6 (continuous slab) shows rust staining, efflorescence and swallow nests along entire deck underside at pier.

NDE Methods Employed on Deck O6

NDE methods used for collecting condition data on Deck O6 included (a) both GC and AC (ground- and air-coupled) GPR deployments; (b) the impact-echo (IE) and ultrasonic (US) devices on the robotic Stepper™; (c) the Proceq™ rolling half-cell (HC) and electrical resistivity (ER) instrument; and (d) ultrasonic surface wave (USW) measurements of in-situ concrete modulus using a portable seismic property analyzer (PSPA). Simultaneous data collection using various methods took place on Deck O6 on June 5 and 6, 2009 (NB and SB lanes, respectively), as described previously and shown in Figure 106.

Again, the rebar configuration required GPR data collection across traffic lanes, in lines oriented perpendicular to traffic flow (Figure 106, far distance), as previously described. Data collection was unaffected for other NDE methods (Figure 106), such as half-cell (HC), Stepper™ (IE and ultrasonic pulse echo), and PSPA (foreground, left to right). Though there were spalls, the deck was drilled with a small hole for a positive electrical connection during half-cell (HC) measurement preparation (not shown). Gridded areas outside the lane closure were collected the day prior (June 5, 2009), on the NB lanes. Though provided design maps show positive deck skew, negative skew was encountered in the field (see NDE maps at end of Deck O6 write up). This was also verified in field notes and using Google Map image, shown in Figure 107, though dimensions of bridge and plans matched.

Figure 106. Multiple NDE methods collected in longitudinal direction on SB lanes, with GPR data collection across lanes.

Figure 107. Google Map (photo taken in 2009) showing Deck O6 repairs underway on NB lanes, confirming negative deck skew.

Traffic Control/Gridding of Deck

Traffic control and gridding were performed in the same manner as on Deck O2, except that the region near the origin, also located at the SW corner of the gridded deck, is shown in Figure 108. Because of the negative deck skew (obtuse angle between curb and abutment at the origin), an orthogonal grid the length and width of the deck surface was marked for NDE data collection, and required using negative x-coordinates as did Deck O3.

Figure 108. PSPA and GPR (left), PSPA and electrical resistivity (ER) data collection near south abutment in NB lanes.

NDE Results and Core Extraction/Observations

Results from the NDE testing for Deck O6 are shown in Figure 109, where core locations are marked using circular symbols denoting predicted core condition, as determined in the field using the GPR instrument. The field-predicted results, using GPR, were as follows: Core #1 (control) – good; Core #2 – serious; Core #3 – poor to serious; Core #4 – poor to serious. There is clear correlation between the data sets, particularly where each of the four NDE methods; IE, GPR, ER and HC; indicate, respectively, the most serious damage, deterioration, likelihood of active corrosive environment (ER), or likelihood of corrosion (HC). However, there are some discrepancies between what each of the methods is predicting. This is to be expected since each is based on a technology that differs with respect to what is being measured. There were no maps provided by Iowa DOT showing repairs, which took place later in the 2009 construction season (refer back to Figure 107).

As can be seen in Figures 109 and 110, Core #1 was expected to be "good" and was extracted intact, with no indication of delamination but some rust on the extracted core. A sliver of steel (upper rebar) was also extracted from the core hole, which fell from the core wall at the right side of the photo at left. The rust on the sample was not "fixed" to the core surface, but appeared to have been rubbed onto the specimen from the surface rust that was on the inside of the core bit. This may be the case, as (a) it was the first core extracted that day and (b) there is surface rust only on this sample's severed rebars, though these exposed bars showed no evidence of corrosion products around them. This sample would be a good potential candidate for chloride profiling, but only if it is believed by Iowa DOT that physical core condition is not enough information to deem the concrete in that location as sound, consistent with its rating as "good".

Core #2 (Figure 111) was extracted in two pieces (left photo), where both the bottom part of the core (bottom left) and the top (inverted) show mated faces with significant rust staining. No reinforcement was cut at this location, though the delamination was sloped toward the direction on both the top and bottom sections where there is the most rust staining. The core hole showed the same indications (rust-infused delamination), coinciding with the "deep" side of the core, closest to the nearest rebar in the deck. This core was ranked as "serious".

Cores #3 and #4 were both field-predicted to be "poor to serious", based on the GPR signal response, though Core #3 was located directly on a crack above a longitudinal rebar. Results are shown in Figure 110 (Core #3) and Figure 111 (Core #4). Extraction of Core #3 showed that it was not only split but also delaminated, as the upper portion immediately separated and had to be removed. Continued coring revealed that the remaining (longer) part of the core, extracted from the bottom of the hole, was likewise delaminated and split – but in four pieces, instead of two. The photos in Figure 110 display the reassembled core at left, the upper pieces at the top, middle pieces at the center right, and lower three pieces (below rebar) at the bottom right. The extracted bar is marked in solid ovals, while severe rust staining and corrosion products are outlined in dashed boxes. Matching vertical splits and horizontal delaminations, including a through-crack at its bottom, were seen in the hole and in project photos.

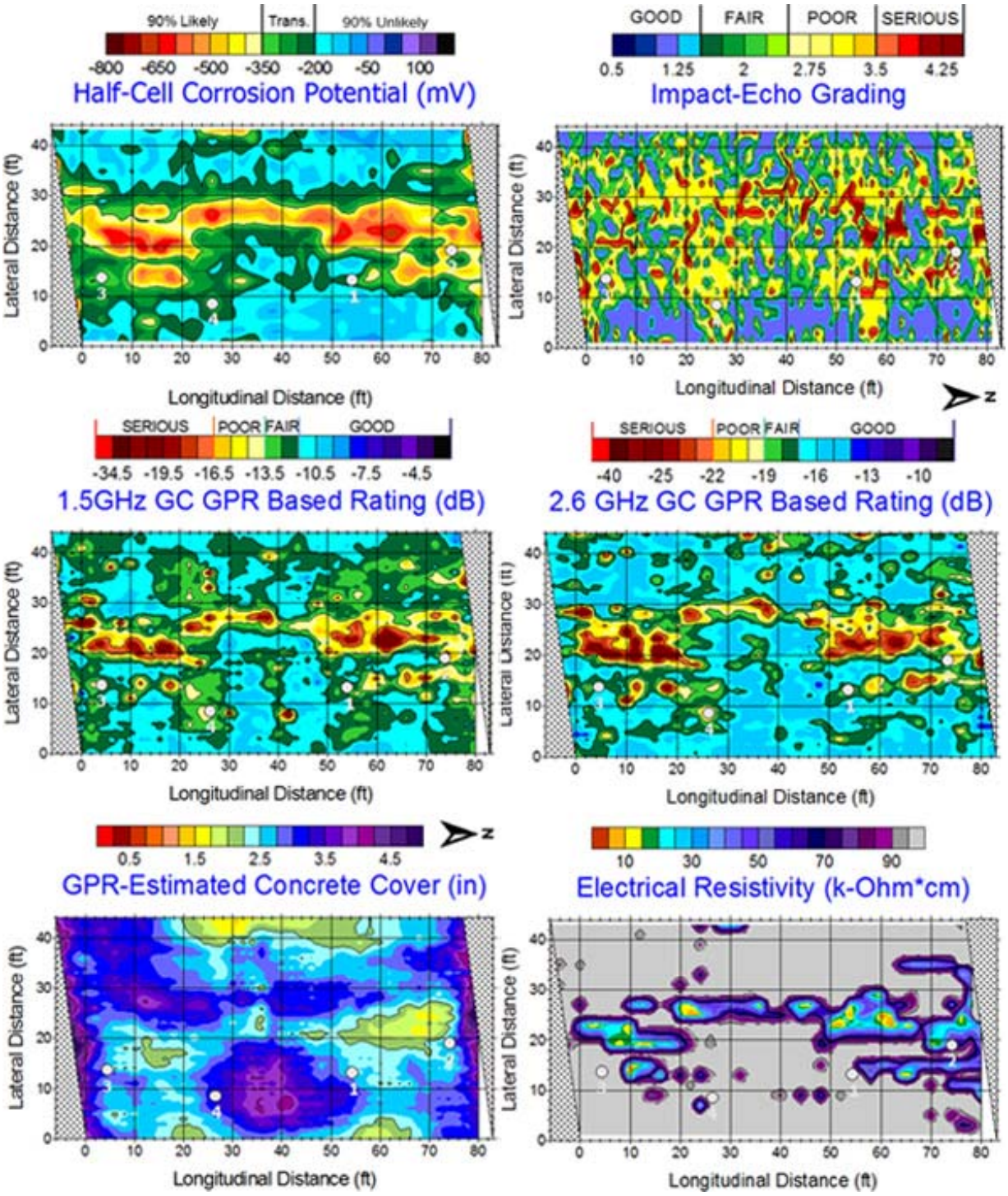

Figure 109. HC, IE, GPR, Concrete Cover, and ER Maps, with core locations marked. GPR data is shown twice with a comparison between 1.5GHz and 2.6GHz GC results.

Core #4, on the other hand, was expected to be retrieved in "poor to serious" condition based on review of the raw GPR data. Though Core #3 was located at a crack, coincident with both the orientation and position of a longitudinal rebar, this was not factored into the prediction so as not to bias the expected results. With the exception of the vertical crack, which could be seen in the raw GPR data profile at Core #3's location, the raw data at both core locations was similar. Thus, the GPR-based rating (used for core selection) was the same for each. As poor as Core #3 appears in every manner of description, it would be expected for Core #4 to look similar once extracted from the hole if only the GPR data were taken into account. The fact that it was not is indicative that a GPR signal is responsive to "conditions coincident with a corrosive environment" at both sites, not actual deck damage. Comparing Cores 3 and 4 using either chloride profiling, petrography, or both would probably be more beneficial than testing Core #1 simply to see whether there is evidence of high chloride content in an area where GPR sees no evidence of a corrosive environment and the core also reveals no visible damage, since they were rated the same. However, since both cores #1 and #4 appear to be undamaged (though GPR indicates significant differences in in-situ conditions related to a condition assessment), there is justification for including core #1 in this comparison. Again, it depends on how exhaustive an effort Iowa DOT believes the supplemental chemical testing and analysis should be in order to better understand all the variables in play.

Figure 110. Core #1 – rated "good" – reveals no damage; core hole shows part of sliced upper rebar along with imprint of lower rebar.

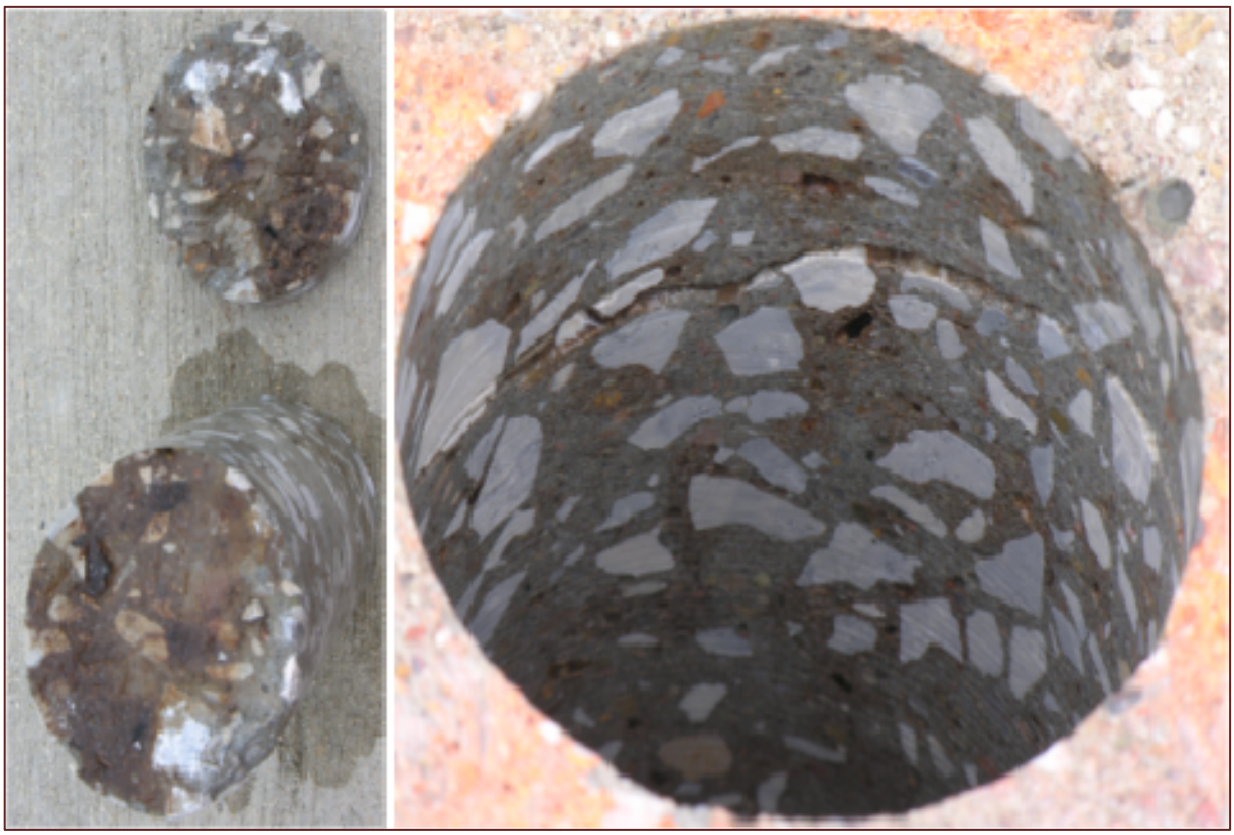

Figure 111. Core #2 and hole, showing rust-coated delamination (coated w/rust stains).

Figure 112. Core #3, retrieved in six pieces, extracted above longitudinal bar at surface crack.

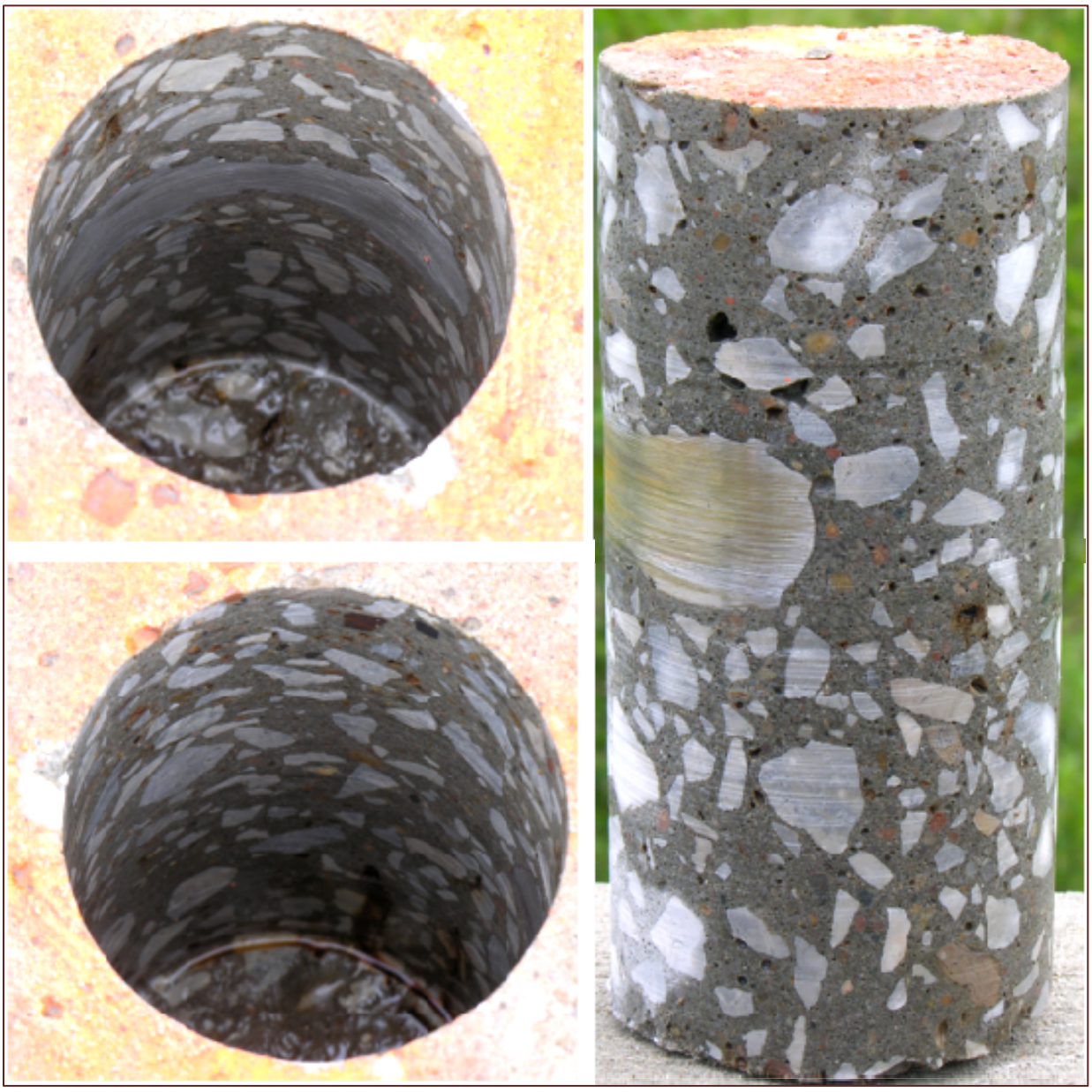

Figure 113. Core #4 shows little evidence of deterioration, with exception of some rust staining along small cracks, vugs and splits along the sides and bottom of the core and its hole.

BRIDGE R1 DECK EVALUATION

The deck on Bridge R1 consists of a 113ft x 28ft, three-span continuous concrete slab structure (Figures 114, 115 and 116) carrying US #30 over Yankee Creek, located 1.9 miles west of Lowden, Iowa. Deck R1 half-sections near the abutments and piers; and partial plan views near centerline (C/L) of piers, C/L of abutments and C/L of deck areas between; are shown in Figure 114 for this concrete slab deck. The provided plans and inspection report indicate that the deck was designed in 1953 and constructed in 1955. The deck is PC concrete overlaid with dense, low-slump PC concrete in 1979. A December, 2005, inspection report includes an analysis that the deck was found adequate for two lane legal loads. Also, the deck surface was reported to have been randomly sounded, with hollow areas reported, a number of them which had begun to crack and breakup. A number of visual underside inspections over the years, coupled with the condition of the deck after previously reported repairs, surface spalling and deterioration, etc. were included in the most recent inspection report. The combined analyses, along with recognition of other deficiencies at or near deck boundaries, and with the presence of deck spalling and deterioration, triggered a corrective recommendation to declare the deck as a candidate for a complete re-overlay. Figure 117 shows typical underside deterioration.

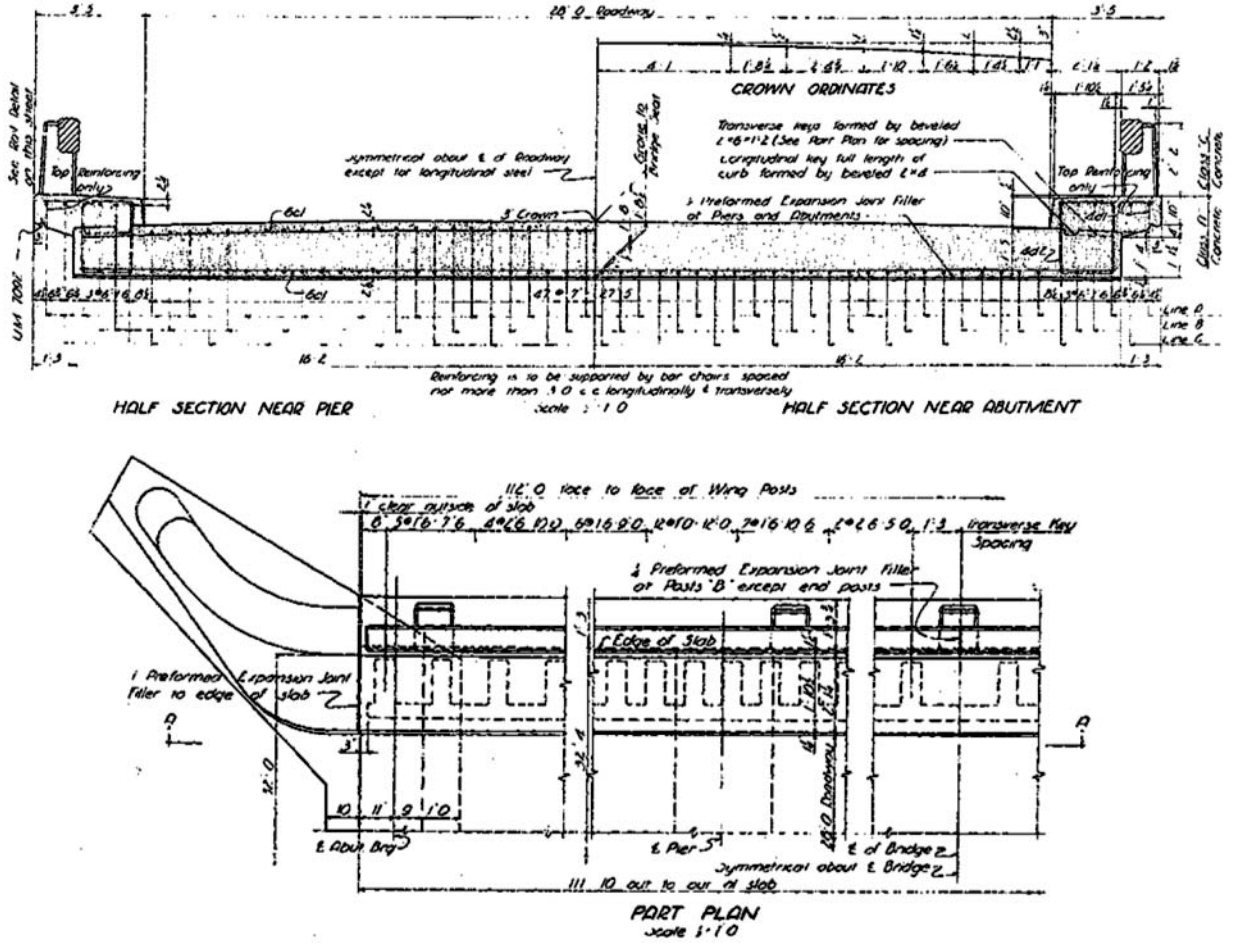

Figure 114. Deck R1 half-sections and partial plan views.

Figure 115. Perspective view of Deck R1, looking down eastbound lane of US Highway 30.

Figure 116. Side view of Deck R1 showing continuous slab construction on east face.

NDE Methods Employed on Deck R1

NDE methods used for collecting condition data on Deck R1 included (a) both 1.5GHz and 2.6GHz GC GPR deployments; (b) the impact-echo (IE) and ultrasonic (US) devices on the robotic Stepper™; (c) the Proceq™ rolling half-cell (HC) and electrical resistivity (ER) instrument; and (d) ultrasonic surface wave (USW) measurements of in-situ concrete modulus using a portable seismic property analyzer (PSPA). Simultaneous data collection using various methods took place on Deck R1 on August 10 and 11, 2009 (EB and WB lanes, respectively), as described previously and shown in Figure 118.

Figure 117. Bottom view of Deck R1 (continuous slab) with rust staining, efflorescence and crack running between pier and abutment.

Once more, the rebar configuration required GPR data collection across traffic lanes, in lines oriented perpendicular to traffic flow, as previously described. Data collection was unaffected for other NDE methods (Figure 118), such as Stepper™ (IE and ultrasonic pulse echo) and half-cell (HC) in the foreground, and PSPA at the west end of the deck. Here, GPR is used to determine rebar orientation, since the first sixteen feet near either abutment had no rebars in an upper mat. This was verified by Iowa DOT personnel who compared these field observations with additional deck plans. Once bars were confirmed to be oriented in the longitudinal direction, for the middle section of the deck, all GPR lines had to be collected across lanes at 2ft intervals. A small hole was prepared for a positive electrical connection during the

half-cell (HC) measurement, where the blue roll of insulated wire rests on the concrete powder drilled from the deck.

Figure 118. Multiple NDE methods collected on WB lane.

Traffic Control/Gridding of Deck

Traffic control and gridding were performed in the same manner as previously with the origin at the SW corner of the deck (Figure 119, upper left). The deck is not skewed.

Figure 119. Stepper at far left (curb) near west abutment; GPR near patches on EBL.

NDE Results and Core Extraction/Observations

Results from the NDE testing for Deck R1 are shown in Figure 120, where core locations are marked using circular symbols denoting the Impact-Echo (IE) grading levels assigned to each IE record, as determined in the field by the impact-echo operator. The field-predicted results, using IE, were as follows: Core #1, ranked "Serious" was delaminated; Core #2, ranked "Good" was intact and sound with no evidence of deterioration or corrosion; Core #3, ranked "Serious" was also delaminated; and Core #4, ranked "Fair to Poor" showed incipient crack and corroded steel. A summary of the ground truth for this deck, field-predicted using impact-echo for the first time during this project, was impressive as shown in Table 9. Cores #1 through #4 are shown (left to right, respectively) on Figure 120, and their tabulated locations likewise indicate respective grid locations.

Table 9 Results from cores graded and selected in the field using impact-echo measurements.

Core locations for Bridge R1 selected on the basis of Impact-Echo (IE) Data			
Drilled August 11, 2009			
Sample	**Location**	**IE Grading**	**Core Observation**
Core1	K24	Serious	delaminated
Core2	L56	Good	good condition
Core3	J65	Serious	delaminated
Core4	I85	Fair to Poor	Incipient crack and corroded steel

There is clear correlation between the data sets, particularly where each of the four NDE methods; IE, GPR, ER and HC; indicate, respectively, the most serious damage, deterioration, likelihood of active corrosive environment (ER), or likelihood of corrosion (HC). Some of the NDE maps are incomplete, however. The blank areas at the west and east ends of the deck (left and right) represent the areas where there was no shallow reinforcement, only bottom reinforcing steel in the thick slab. Thus, the GPR was not able to measure anything in either location, and GPR-based deterioration and concrete cover maps cannot be generated near the abutments. In addition, the half-cell measurements were unable to remain recorded on the data logger for the EB lane, so the lower half of the deck area (plan view) includes no HC data at all. Though half-cell data were collected along the entire WB deck surface, the fact that there is no reinforcement in the 16ft zones nearest the abutments, with perhaps the exception of occasional stirrups used for shear resistance in the slab, means that the HC data in the cross-hachured areas ought to be viewed as "suspect", because the deck reinforcement in these regions is very deep (about 20in beneath the surface).

The NDE maps show some correlation between the impact-echo and GPR, particularly where serious damage (red colors) is predicted using impact-echo (IE) or where a serious/poor deck deterioration grading (reds/yellows) are mapped using (GPR). Once again, there is a good correlation between what is graded as "Poor" using impact-echo (yellow colors) and what is generally graded as

"Fair" (green) using the GPR. There is some discrepancy from these general observations, as should be expected since the methods operate on very different principles and detect different deterioration or causes of deterioration.

Likewise, there is some agreement in the contour boundaries defined by both the GPR and HC results, when data are compared in the regions where both instruments were able to provide data for their respective maps. Thus, in general, GPR-predicted deterioration somewhat reflects areas identified using HC as 90% probable of deterioration where GPR shows any grading between "fair" and "serious". Within the transition zone for HC results, , the GPR generally indicates deck conditions that are graded "Good". However, there is some overlap between the transition and "90% Unlikely" zones in the HC map and the "Good" or "Fair" regions along the GPR deterioration scale.

There tends to be some correlation between corrosion potential predictions generated by HC maps and IE predictions, though the IE and HC results either generally agree well in some areas and somewhat well to hardly at all in others. The GPR seems to correlate better to either the IE or the HC – in different areas, probably where corrosion is the primary mechanism for deck deterioration – than the IE or HC correlate to one another. Furthermore, they don't all correlate well as a group, necessarily, in the same locations from one map area to the next. It needs to be considered, however, that there are limited areas where the HC can be compared with either method (one single lane, and highly suspect in the areas where reinforcement is very deep). Similarly, there are two ends of the deck where the GPR cannot be compared with any other data simply because deep rebars were not able to be imaged (detected) at all.

Regardless, "where it counted," at the four core locations identified using the IE results available in the field, all three methods were in fairly good agreement. Looking at the core locations on the map, samples 1 through 4 were selected at the locations shown with results of the observed core extractions noted previously in Table 9. Taking those physical core observations and looking at each of the mapped core locations, each of the NDE maps show the core location right at the boundary of, or within, a zone colored "90% Likely" (HC), "Serious" (IE), or "Serious/Poor" (GPR). Likewise, all three methods show the "control" core (rated good by IE, "transitional" using HC, or "Fair" using GPR. All three methods show Core #3 in "Serious" (IE), "90% Likely" (HC) or "Poor" (GPR); and only on the last core do the HC and IE compare better than the GPR and the other two methods. For core #4, IE indicates "Fair to Poor", HC indicates "90% Likely" and GPR maps as "Good to Fair". All but the control core, though, were located in areas within close proximity to highly variable measurements – as can be readily seen near steep contour gradations.

On a highly deteriorated deck such as this, where highly damaged (delaminated) areas are interspersed throughout, there are generally good global agreements within the data sets but highly localized discrepancies, as well. This is to be expected, as the NDE methods employed are truly complementary and should be used together, instead of alone, whenever possible.

Core results (photos) can be seen in Figure 121 and Figure 122 where Cores #1 and #2 are shown in Figure 121, and Cores #3 and #4 are seen in Figure 122. Core #1 is fully delaminated below the overlay; Core #2 is fully intact and visibly sound. Core #3 is seriously split and delaminated with a great deal of corrosion products surrounding the top rebar, and was retrieved in 5 pieces (three split at top, three split at bottom with the upper rebar as the boundary between upper and lower portions).

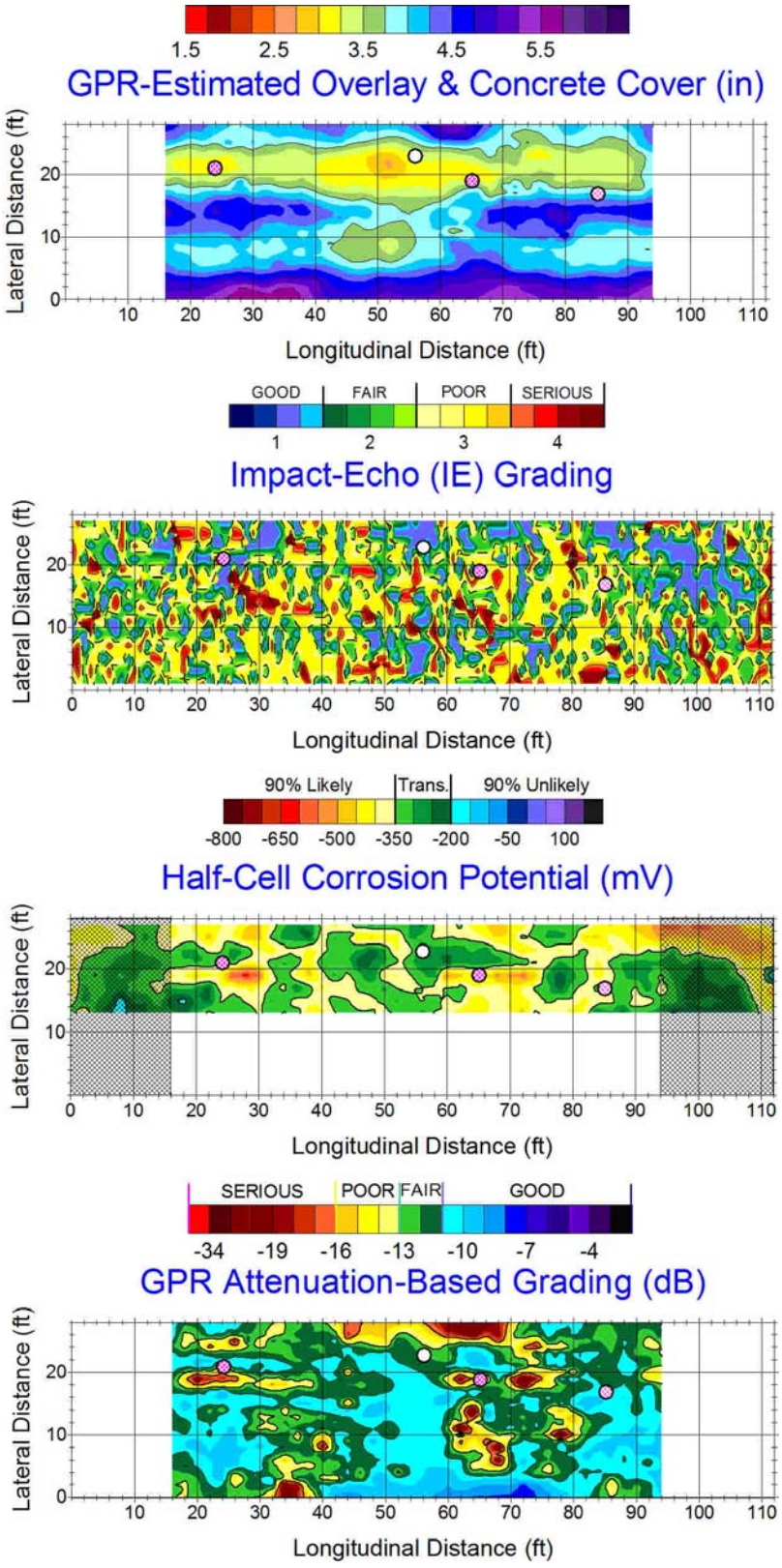

Figure 120. Concrete Cover, IE, HC, and GPR Maps, with core locations marked (Cores #1 through #4, left to right, respectively).

Though Cores #1 and #3 may appear visibly different, in an IE analysis the frequency response used for grading both areas as 'serious' is virtually the same. Additional cracking (vertical) beneath the delamination, or steel corrosion itself (seen in Core #3), is not something IE can be expected to detect as no energy is effectively penetrating beneath the near-surface delamination (evident in both Cores #1 and #3). Core #4, on the other hand, is showing early indications of corrosion around the exposed steel, with both horizontal and vertical cracking emanating from the corroded bar, though the core was retrieved intact.

No re-overlay has been performed on Deck R1, so there is no basis for comparing the NDE results with completed repairs.

Figure 121. Cores 1 & 2 (left and right), graded "serious" (delaminated) and "good" (intact) using IE.

Figure 122. Cores 3 (upper) and 4 (lower), graded "serious" and "fair to poor" with IE.

BRIDGE R2 DECK EVALUATION

The deck on Bridge R2 consists of a 331ft x 28ft, four-span reinforced concrete structure supported by steel beams (Figures 123 through 127) carrying US Highway 6 over IAIS Railroad and located 1.6 miles east of East Junction Iowa #21. Deck R2 half-sections near the abutments and at a typical intermediate deck location are shown in Figure 123. A longitudinal section showing piers and abutments, as well as a situation (plan) view of the deck showing the same are included in Figures 124 and 125. The provided plans and 2008 inspection report indicate that the deck was designed in April, 1954 and constructed in 1956. The deck was PC concrete overlaid with dense low-slump concrete in 1978. The inspection report includes an analysis that the deck was found adequate for two lane legal loads. The top of the deck has several narrow transverse, random, and longitudinal cracks and many small to very large hollow areas (sounding), with some spalling and delamination of the PC concrete deck overlay reported. The curbs have some spalled/scaled areas and the bottom of the deck has several random and transverse cracks with some leaching. There is a full depth PC patch along both ends, and both overhangs have some small hollows and spalls. The final recommendation is that PC concrete deck patching and epoxy injection should be done as needed.

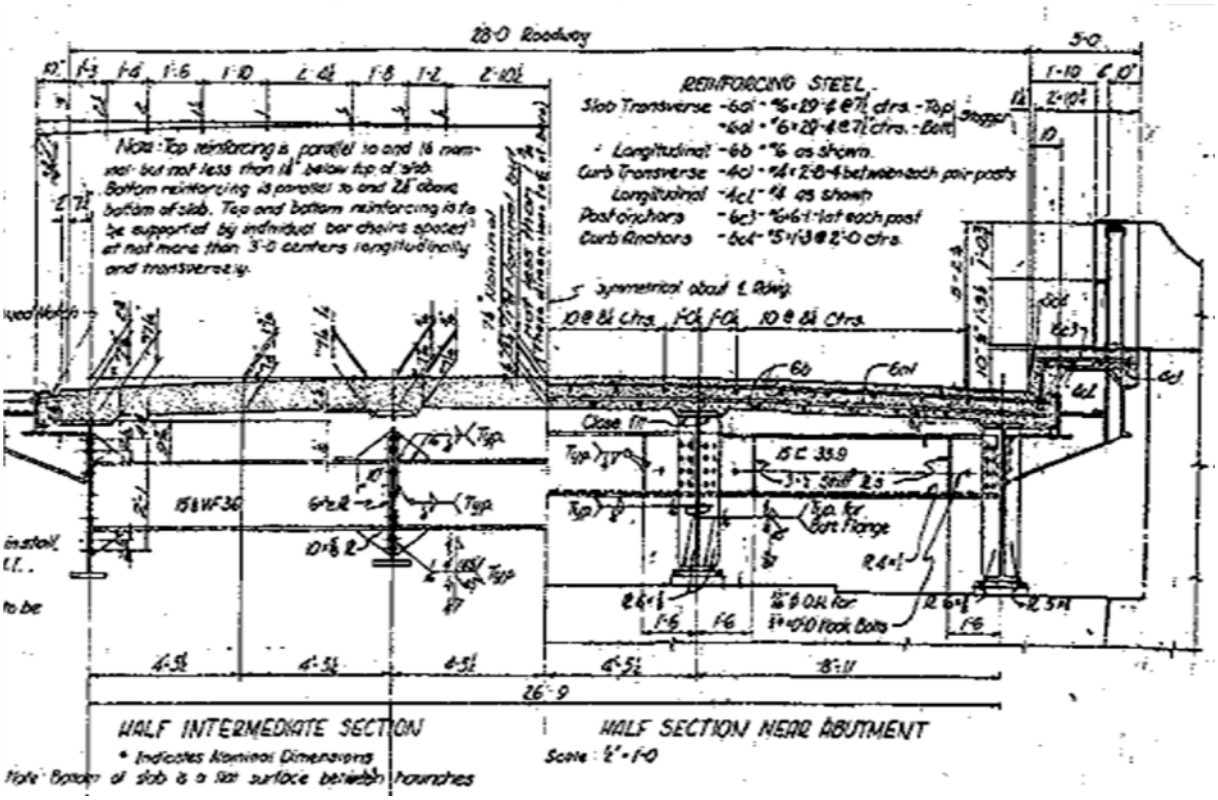

Figure 123. Deck R2 half-sections near abutment and at intermediate section.

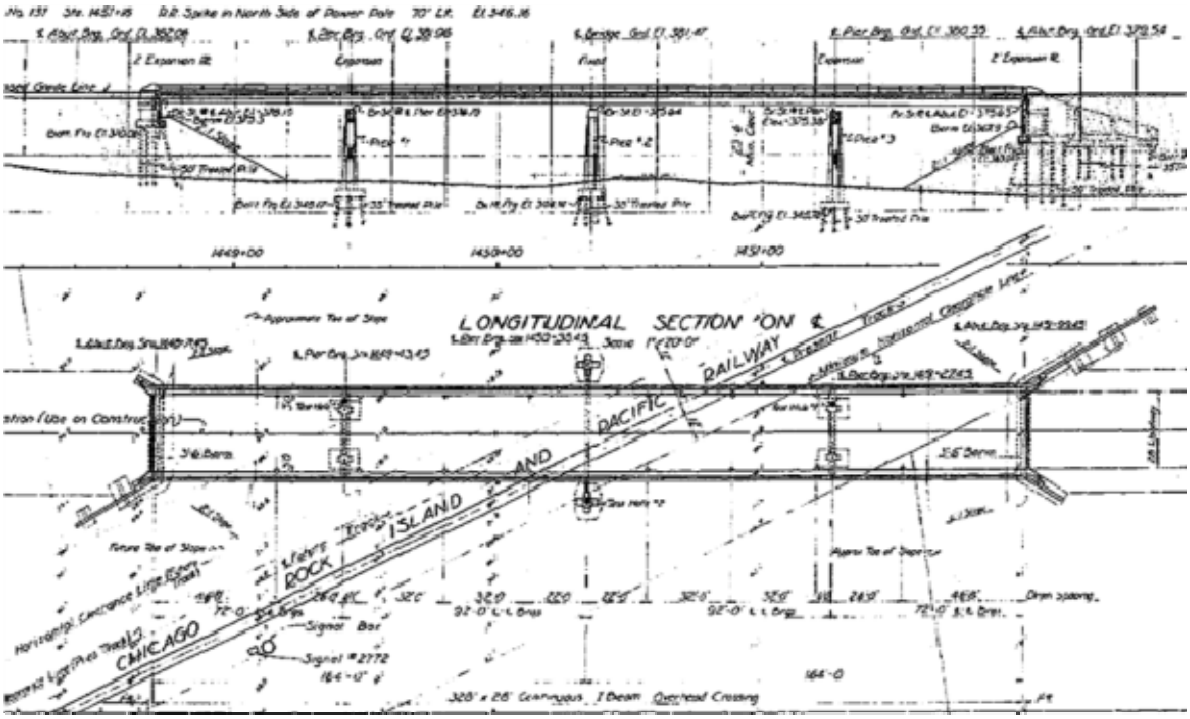

Figure 124. Bridge R2 longitudinal section, and situation (plan) view showing railroad beneath.

Figure 125. Perspective view of Deck R2, looking eastward along US Highway 6.

Figure 126. Side view of Bridge R2 showing steel girder construction on south face.

Figure 127. Bridge R2 superstructure as seen from deck underside.

NDE Methods Employed on Deck R2

NDE methods used for collecting condition data on Deck R2 included (a) both GC and AC (ground- and air-coupled) GPR deployments; (b) the impact-echo (IE) and ultrasonic (US) devices on the robotic Stepper; (c) the rolling half-cell (HC); and (d) ultrasonic surface wave (USW) measurements of in-situ concrete modulus using a PSPA. Simultaneous data collection using various methods took place on Deck R2 on June 11 and 12, 2009 (EB and WB lanes, respectively), as described previously and shown in Figure 128. On this steel girder deck, the rebar configuration allowed GPR data collection along lines oriented with traffic.

Figure 128. PSPA, HC and Stepper (IE and US) collection on EB lane.

Traffic Control/Gridding of Deck

Traffic control and gridding were performed in the same manner as previously with the origin at the SW corner of the deck (Figure 128, upper left). The deck is not skewed. The remainder of the EB lane is seen in Figure 129, from approximately X = 50ft to the far end where the coring crew is preparing to extract samples.

Figure 129. Grid on EBL, showing HC lead connected to rebar through small hole (foreground).

NDE Results and Core Extraction/Observations

Results from the NDE testing for Deck R2 are shown in Figure 130, where core locations are marked using circular symbols and sample numbers, as determined in the field using GPR. The field-predictions, using GPR, were as follows: Cores #1, 2 and 3 were ranked "Serious" (deteriorated) and Core #4 was selected as the control (good) core. The locations of these cores were recorded in the notes and marked directly on the grid without taking into account the discrepancy between the actual measured deck length and what was recorded on the instrument's DMI. This meant that the core locations recorded in the notes and marked as such on the deck are slightly off in the longitudinal direction, with accumulated measurement error moving eastbound on the deck from the west to east abutments. Therefore, it was expected that some of the core predictions may be slightly off, especially those farther from the west abutment. The actual locations on deck are marked on each of the NDE condition maps shown in Figure 130. It should be noted that for the purpose of being able to see the maps more clearly in the printed report, Figure 130 was stretched (top to bottom) so that the deck's lateral distances appear longer than corresponding longitudinal ones. Thus, the aspect ratio for the x- and y-axes is not constant.

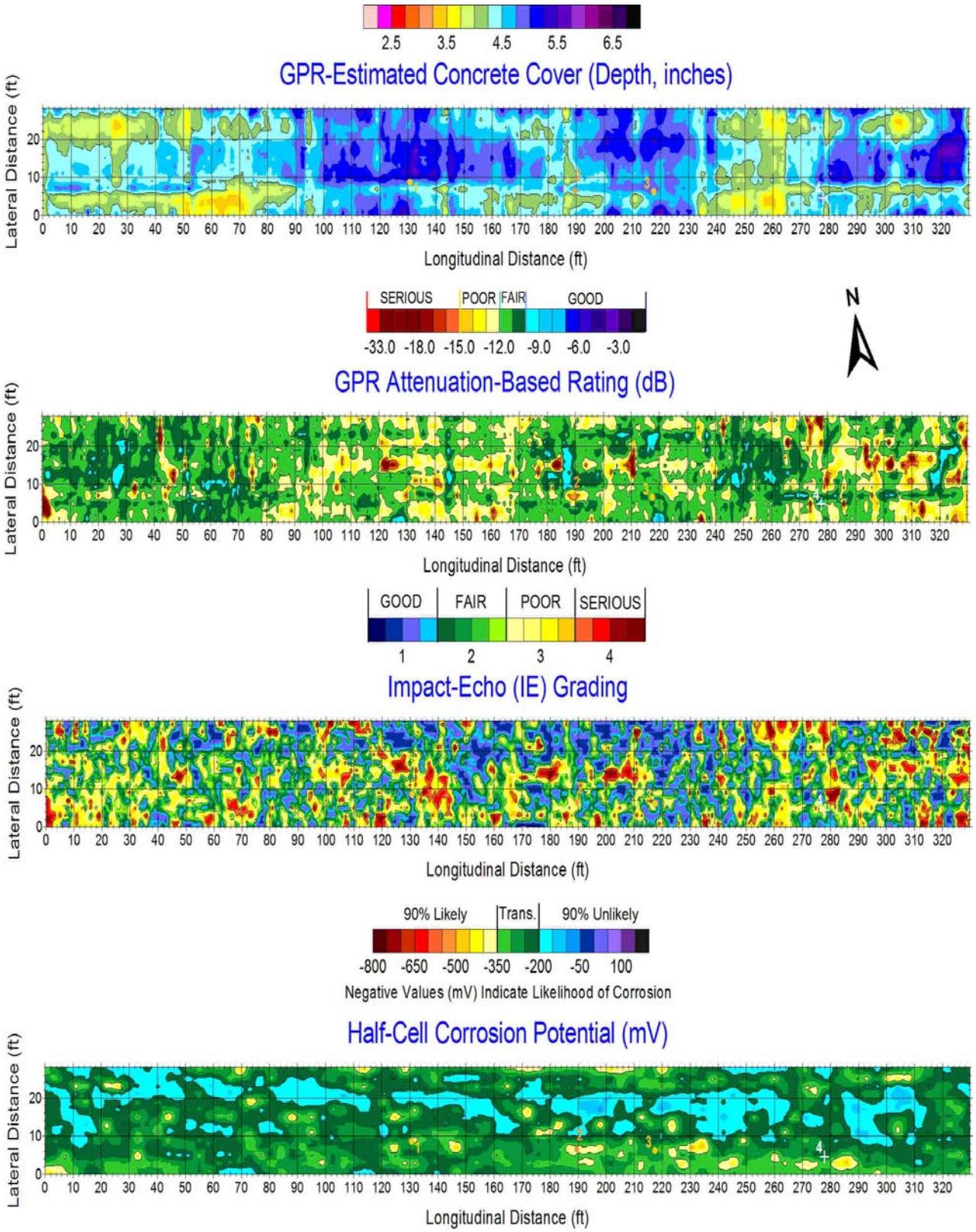

Figure 130. Concrete cover, IE, HC, and GPR Maps, with core locations marked.

There is some correlation between the data sets, particularly where each of the three NDE methods; IE, GPR, and HC indicate, respectively, the most serious damage, deterioration, or likelihood of corrosion (HC).

The NDE maps show some correlation between the impact-echo and GPR, particularly where serious damage (red colors) is predicted using impact-echo (IE) and where a serious/poor deck deterioration grading (reds/yellows) are mapped using (GPR). There is also correlation between what is graded as "Poor" using impact-echo (yellow colors) and what is generally graded as "Fair" (green) using the GPR. The impact-echo (IE) seems to be predicting considerably more damage than the GPR is predicting "serious" deterioration, looking one-to-one at only the "serious" grading level. Also, the GPR seems to be more liberal in its prediction of deteriorated concrete than what the IE indicates is present (when all three grading levels of "serious" to "fair" – everything except "good") in terms of damage.

Similarly, there tends to be some correlation between corrosion potential predictions generated by HC maps and IE predictions, though the IE and HC results either generally correlate well only at the worst areas ("serious" IE vs. "90% Likely" HC) and at the best areas ("Good" on IE map and "90% Unlikely" on the HC map).

The four core locations identified for coring can be seen in Figure 130, marked with yellow dots at the locations where Core #1 and Core #3 appeared to be in fair-to-poor condition based solely on viewing the on-screen GPR data. Similarly, Core #2 was marked in orange since the raw GPR data indicated a more serious (poor) condition was expected. None of the cores were expected to be in "serious" condition, so none of the dots was colored red on the map. However, the "control" (Core #4) was expected to be in good condition based on the raw GPR data on-screen, and was marked on the GPR map with a white cross.

Core #1 (Figure 131, left) showed no evidence of damage at the upper steel, where GPR showed moderate signal attenuation. It should be noted that the selected GPR location for Core #1 was centered diagonally between two isolated deteriorated spots on lines spaced a few feet apart, in an attempt to show that the two locations could potentially be connected. The GPR map does show two yellow areas with orange/red spots in them on either end of the Core #1 location, but the core location itself is mapped on a green color (fair condition grade) while the raw data itself was reviewed along the two lines on either side of where the core was extracted. Impact-echo (IE) at that location indicated that the core would be sound, rated "good", and HC showed similar results to the GPR map. Ultimately, Core #1 was marked within the transition zone, located between two small dots on the map that were barely above the 90% likely threshold for corrosion activity.

A lesson learned on this deck was not to mark the deck for core extraction at any location where NDE sampling did not occur, as was the case between test lines (Core #1 location), since there is no real basis for determining whether the core is expected to be sound, or deteriorated, at an interpolated location between test lines.

Figure 131. Cores 1 & 2 (left, right), were graded "serious" in the field. Core #1 is inverted, showing bottom of core, broken purposely to retrieve it.

Core #2, selected within a long segment of attenuated GPR signal, was marked close enough to the desired location that the measurement discrepancy did not matter. This can be seen on the map, where the Core #2 "dot" is marked right on a yellow zone with orange/red in the middle. The IE map shows the location of Core #2 to be directly on an area graded as "poor", which means it is delaminated, but likely not detectable by chain drag. This is reasonable, because the core, though highly deteriorated, delaminated and split (there was also a longitudinal crack at the surface where the core was drilled), had the overlay and some parent concrete above. This would be considered a "deep" delamination. The core hole did not show a large gap, though there was a crack where the core had separated into two pieces during removal. The HC map shows Core #2 to be located just above the 90% deterioration threshold, indicating likelihood of active corrosion. Thus, all three NDE maps were in agreement regarding the predicted/observed condition of this core. The core itself is shown in Figure 129, at right.

Core #3 falls on a transition zone between "fair" and "good" for IE (just missing a small hot spot that would be graded "serious"), and within the "fair" grading on the GPR map. The HC map shows Core #3 to be in the transition zone, no closer to the 90% likely zone than the 90% unlikely zone (between -250mV and -300mV).

Despite using the GPR to select this core location, field-viewing the raw data apparently supported this selection but the distance-corrected GPR map does not. Thus, it is not unexpected that the extracted core, in general, appears to be good (Figure 132) since the mapped NDE data all indicate a "fair to good" (IE), "transitional" (HC) or "fair" condition (GPR) – and all the maps have been corrected for cumulative distance error. Unfortunately, the marked grid on the deck was used to directly locate the spot where the core was to be retrieved, and no distance-

correction for cumulative marking error had yet been discovered. As such, no distance-correction, taking into account actual (measured) deck length, was applied to the GPR-measured field data which simply recorded apparent distance as measured by the cart-mounted DMI.

Figure 132. Cores 3 (left) and 4 (right), graded "deteriorated" and "good" with GPR.

Core #4 (control) fell on locations where all maps were in agreement (transition for HC, "fair" for IE, and "good" for GPR), and the field-reviewed GPR data at the selected location in the data confirmed the same. The core was also extracted intact (Figure 132), with no visible signs of corrosion or damage/cracking. Fortunately, at this location, the mapped GPR data appears "good to fair" for a fairly long distance (6ft or so) along the line over which the field GPR data was reviewed to look for "sound concrete". This meant that the applied distance correction did not seem to impact whether the field extraction was slightly misplaced on the deck, with regard to the desired sample location. Thus, in this particular case a sound core would have been removed from the deck even if a 2 to 3ft measurement discrepancy in the x-coordinate for the core, along the measured GPR line, would have resulted.

No re-overlay has been performed on Deck R2, so there is no basis for comparing the NDE results with the completed repairs. Lessons learned from this deck included some improvements on the process used to select core locations, similar to what was learned on Deck O3, which was surveyed just prior to this deck. It also created a field QC improvement applied on all future decks to measure each deck length at center line and along both curb lines, so that the measured data length could be properly adjusted to the actual deck length.

BRIDGE R3 DECK EVALUATION

The deck on Bridge R3 consists of a 184ft x 26ft, a three span continuous steel beam structure with a reinforced concrete deck (Figures 133 through 136) carrying Iowa #1 over Old Man's Creek, located 7.1 miles south of Junction US Highway 6. Deck R3 half-sections near the abutments and at a typical intermediate deck location are shown in Figure 133. The provided plans and 2004 inspection report indicate that the deck was designed in 1948 and constructed in 1949. The deck is PC concrete overlaid with dense low-slump concrete in 1986.

The inspection report includes an analysis that the deck was found adequate for two lane legal loads. The top of the deck has several hairline transverse and longitudinal cracks, a few 1/16 inch narrow longitudinal cracks and a few hairline diagonal cracks. There were also several spalls on Span #1 and some medium to large hollow areas (sounding), some along the near end deck joint. Recommendations are to perform Portland cement concrete patching and epoxy injection as needed.

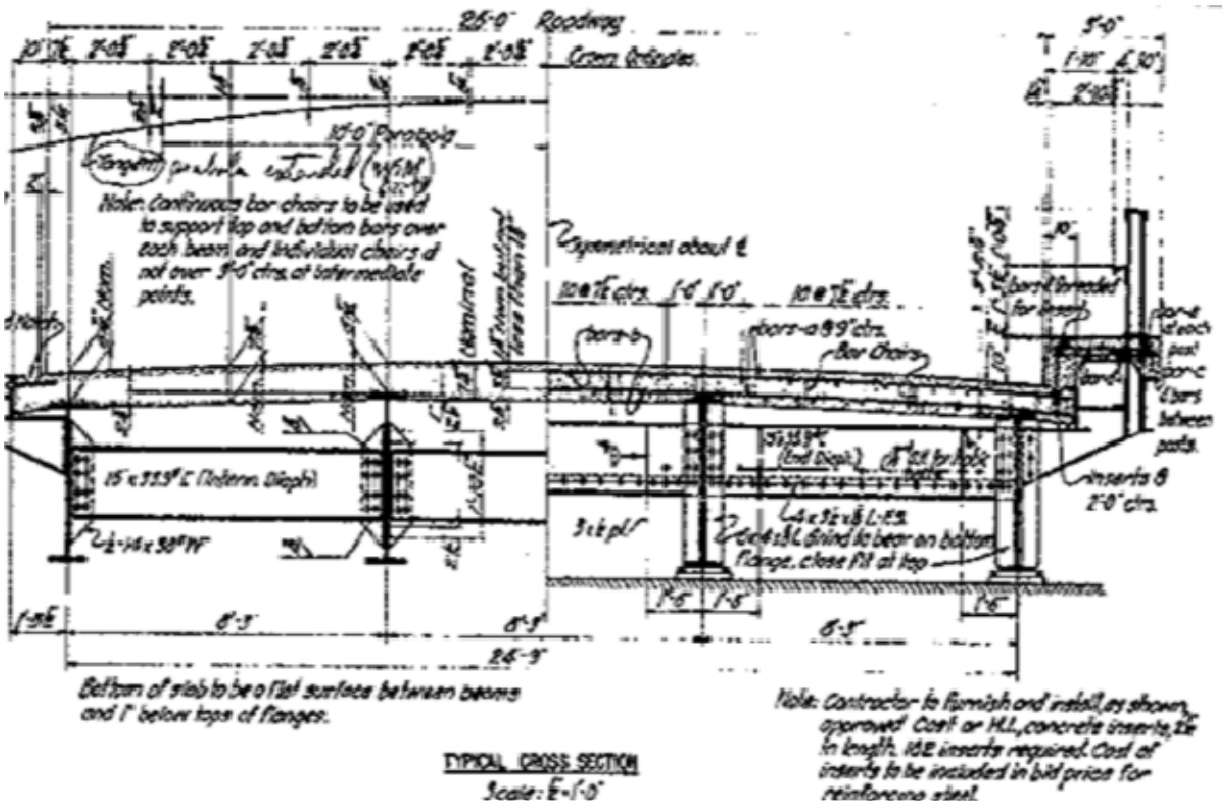

Figure 133. Deck R3 half-sections and partial plan views.

Figure 134. Perspective view of Deck R3, looking SW down northbound lane of Iowa #1.

Figure 135. Side view of Deck R1 showing continuous slab construction on east face.

Figure 136. Bottom view of Deck R3 with rust staining, cracking and efflorescence at abutment.

NDE Methods Employed on Deck R3

NDE methods used for collecting condition data on Deck R3 included (a) both GC (ground coupled) GPR antennas, 1.5GHz and 2.6GHz; (b) the impact-echo (IE) and ultrasonic (US) devices on the Stepper; (c) the rolling half-cell (HC); and (d) ultrasonic surface wave (USW) measurements of in-situ concrete. No horn antenna (GPR) or electrical resistivity (ER) data were collected.

Simultaneous data collection using various methods took place on Deck R3 on August 13 and 14, 2009 (EB and WB lanes, respectively), as described previously and shown in Figure 134. On this steel girder deck, the rebar configuration allowed GPR data collection along lines oriented with traffic.

Figure 137. Checking for electrical continuity between deck rebar (drilled hole) and old rail posts built into the deck edge, outside of barrier rail.

Traffic Control/Gridding of Deck

Traffic control and gridding were performed in the same manner as previously with the origin at the SW corner of the deck (Figure 134, upper left). The deck is not skewed, and though the roadway runs north/south, the northbound traffic is actually oriented almost directly east at this bridge's location.

NDE Results and Core Extraction/Observations

Results from the NDE testing for Deck R3 are shown in Figure 138. There is clear correlation between the data sets. Particularly, it is between IE, GPR and HC in the areas of the most serious damage, deterioration, or likelihood of corrosion (HC).

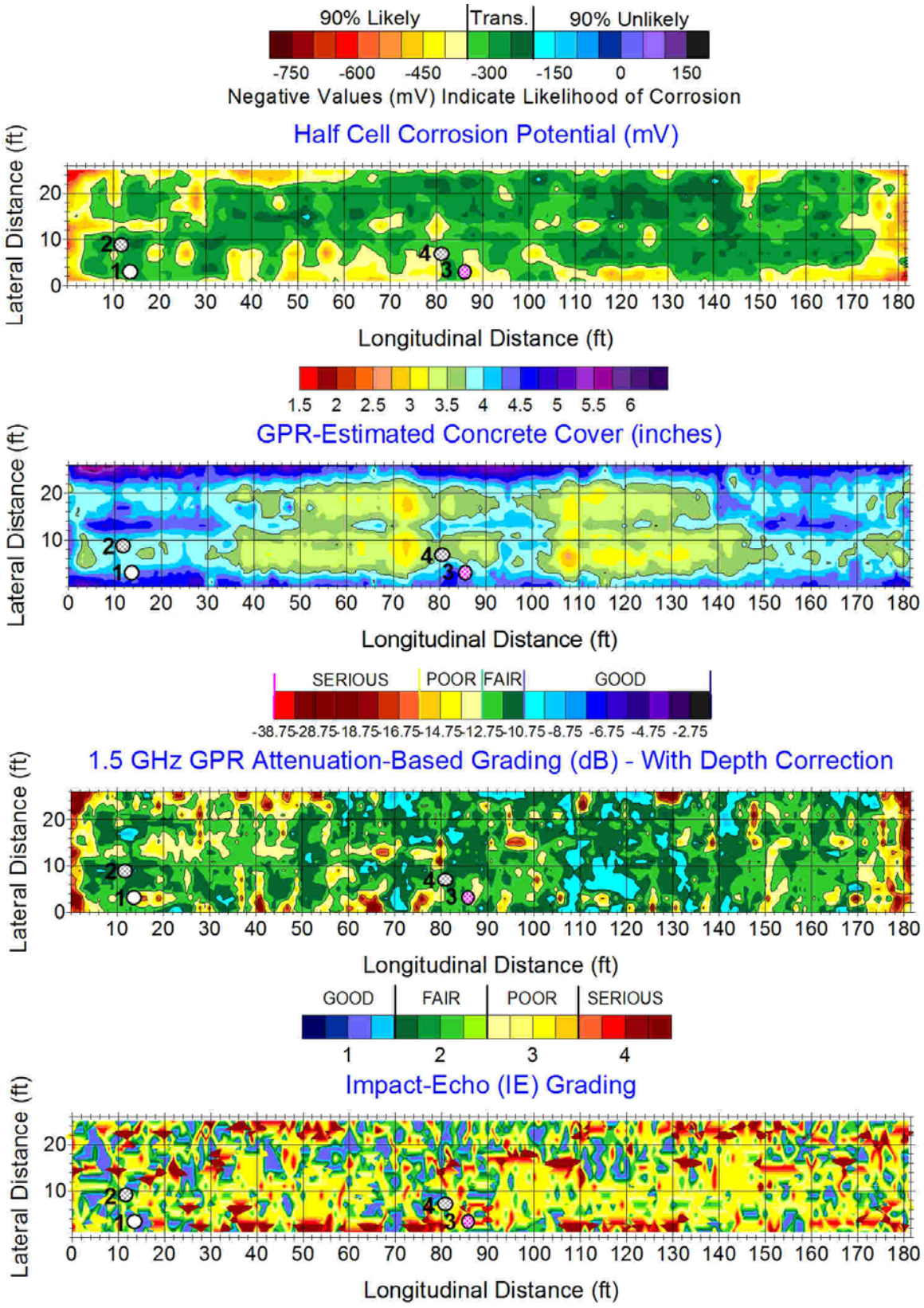

Figure 138. HC, CC, GPR and IE maps.

The NDE maps show a good correlation between the impact-echo and GPR, particularly where serious damage (red colors) is predicted using impact-echo (IE) or where a serious/poor deck deterioration grading (reds/yellows) are mapped using (GPR). Once again, there is a good correlation between what is graded as "Poor" using impact-echo (yellow colors) and what is generally graded as "Fair" (green) using the GPR. There is some discrepancy from these general observations, as should be expected since the methods operate on very different principles.

Likewise, there is fairly good agreement in the contour boundaries defined by both the GPR and HC results in the areas where HC is showing active corrosion and GPR deterioration is either "Serious" or "Poor", regions generally considered in a GPR survey to be worthy of repair. Thus, in general, areas identified using HC as 90% probable of deterioration are where GPR shows any grading between "poor" and "serious". Within the transition zone for HC results, the GPR generally indicates deck conditions that are graded "Fair". However, there is some overlap between the transition and "90% Unlikely" zones in the HC map and the "Good" or "Fair" regions along the GPR deterioration scale.

Similarly, there tends to be reasonably good correlation between corrosion potential predictions generated by HC maps and IE predictions, though the IE and HC results generally correlate well in the areas where HC is above the 90% active corrosion threshold and the IE is graded as "Serious".

On a highly deteriorated deck such as this, where highly damaged (delaminated) areas are interspersed throughout, there are generally good global agreements within the data sets but highly localized discrepancies, as well. This is to be expected and, therefore, the NDE methods are employed in a complementary manner.

No re-overlay has been performed on Deck R3, so there is no basis for comparing the NDE results with completed repairs.

The IE was used to identify core positions based on the review of the data while being collected in the field. Core #1 was selected to be in the sound zone of the deck, Cores #2 and 4 to be in transition zones (fair to poor), while Core #3 to be in a clearly delaminated zone. Positions of the four cores were marked in Figure 138. Once the IE condition map was completed, it became obvious that all four locations were actually in the zones of transition from one condition level to another. In summary, Cores #1 and #3, predicted correctly good condition and delamination, respectively, while Cores #2 and #4 did not show clear damage, in terms of visible delamination or cracking.

Core results (photos) can be seen in Figures 139 and 140, where cores 1 and 2 are shown in Figure 139 (left and right, respectively), and cores 3 and 4 (left and right, respectively) are seen in Figure 140.

Figure 139. Cores 1 & 2 (left, right) graded "good" (intact) and "fair" by IE.

Table 10 Results from Cores Graded and Selected in the Field using Impact-Echo

Core locations for Bridge R3 selected on the basis of Impact-Echo (IE) Data			
Drilled August 13, 2009			
Sample	**Location**	**IE Grading**	**Core Observation**
Core1	C14	Good	good condition
Core2	E12	Fair	good condition
Core3	C86	Serious	delaminated
Core4	D81	Fair to Poor	good condition

Core #3 is fully delaminated below the overlay; core #2 is intact and visibly sound. Core #3 is seriously split and delaminated with a great deal of corrosion products surrounding the top rebar, and was retrieved in 5 pieces (three split at top, three split at bottom with the upper rebar as the boundary between upper and lower portions). Core #4 is showing early indications of

corrosion around the exposed steel, with both horizontal and vertical cracking emanating from the corroded bar, though the core was retrieved intact.

Figure 140. Cores 3 (left) and 4 (right), graded "serious" and "fair to poor" with IE.

CHAPTER 4 SUMMARY OF FINDINGS AND CONCLUSIONS

The report provides a comprehensive review of the NDT technologies used in this project and their implementation in evaluation of nine bridge decks in Iowa. The review includes the description of principles of operation, field implementation, data analysis and interpretation, and implicitly provides information regarding their advantages and limitations in practical bridge deck evaluation and condition monitoring. The chapter on the evaluation of nine bridge decks provides results of the evaluation obtained using the five NDT technologies and their comparison to ground truth data obtained from coring and deck "autopsies" for bridges O1 – O6 during the 2009 bridge deck overlay projects.

A number of conclusions regarding the technologies can be stated at the end of the project. The following are the most important ones:

1) A number of technologies can provide detailed and accurate information about a certain type of deterioration or defect. However, comprehensive condition assessment of bridge decks, at this stage, can be achieved only through a complementary use of multiple technologies.
2) Impact echo provides reliable and comprehensive delamination detection and characterization. Delamination can be detected in both advanced and early stages of delamination, and thus impact echo provides significant advantages over chain drag and hammer sounding. It works on both decks with PCC overlays and decks with AC overlays, if the testing is conducted at lower temperatures. (The conclusion regarding the decks with AC overlays comes from other studies.) Delamination characterization can be automated and results presented in an intuitive way.
3) Half-cell potential is fast, precise and reliable method to detect active steel corrosion. It requires little trained personnel and equipment is robust and relatively inexpensive. Data analysis is straightforward, while interpretation requires some experience. The cost of half-cell surveys is low.
4) Electrical resistivity is a reliable, comprehensive and easy to use measurement of electrical resistivity of concrete, which can be correlated to the corrosion rate. Measurements are precise and accurate, and require little trained personnel. The equipment is robust and relatively inexpensive. Electrical resistivity can complement half-cell potential analysis.
5) Ground penetrating radar provides overall deterioration condition mapping, concrete cover, reinforcement and duct layout and depth, and defect characterization. In many instances there are strong correlations with impact echo in delamination detection, especially in the zones of progressed delamination, and with half-cell or resistivity in identification of zones of active corrosion. It is reliable, repeatable and data collection is rapid, especially if air-coupled systems are used. GPR works on both bare and overlaid decks.
6) Ultrasonic surface waves method is a simple and reliable way to measure in situ concrete modulus. A single measurement provides only the baseline measurement, since concrete modulus variation can be simply a result of the variability of the material and construction practice used. Concrete deterioration, thus, can be detected and characterized from the subsequent periodical measurements through modulus

degradation. In many cases, the USW method detects delamination through strong fluctuations in the dispersion curve.

7) Validation of NDT results using cores and to a minor extent comparisons with the records from the conducted overlay projects, confirms the ability of the NDT technologies to detect deterioration in bridge decks. It is critical that the cores be taken to exactly match the points of NDT records. Ideally, cores should be extracted after the condition maps have been developed, since some technologies sense presence of deterioration in their proximity (order of several inches).
8) Evaluation of bridge decks with the NDT technologies used in this project can be conducted at rates of about 2500 to 3000 square feet per work day for a 2 by 2 foot survey grid about for about 6 hours actual data collection. The ranking of the technologies by speed would be: GPR, ER, HC, IE and USW. Further discussion regarding speed of different GPR methodologies is included in the Appendix.
9) To improve the speed of data collection on bridges where traffic interruptions (lane closures) have to be minimized, the described technologies provide two options. The first option is using multiple devices, which would require larger workforce. The second option is using multiple probes. For example, the Stepper could be modified to carry three IE probes, or HC device is available with multiple probes. Implementing such measures could probably bring the speed above 7000 square feet per day. Finally, significant improvements were made in the past few years and it is expected that new devices will provide further speed improvements.
10) Three technologies: GPR, IE and USW require moderate to significant level of training, especially in data analysis and interpretation. Two technologies: HC and ER require small to moderate level of training.
11) Considering the current dominant practice of the Iowa DOT's bridge deck rehabilitation procedure relying on detection of delamination using chain drag and hammer sounding, impact echo is the technology recommended as an equivalent. However, impact echo also provides information regarding the initial to progressed delamination, which is often missed by chain drag and hammer sounding.

In summary, the approach to bridge deck evaluation and monitoring by NDT technologies should be by targeting the use of a group of complementary technologies. The selection of those should be based primarily on the accuracy of information they provide regarding the most important deterioration and defect types. Those technologies should also meet or exceed certain criteria of the Iowa DOT regarding the speed, ease of use and cost.

APPENDIX COMPARISON OF GPR METHODOLOGIES: GROUND-COUPLED (GC) VS. AIR-COUPLED (AC)

All of the bridge decks were surveyed using both ground-coupled GPR antennas (1.5GHz and 2.6GHz), but some of them were also surveyed using a dual-polarization, air-coupled (horn) GPR antennae deployment. GPR survey results from all of the bridge decks are shown within this Appendix so that:

a) 1.5GHz GC antenna results (shown previously for all decks) can be compared with results obtained using a 2.6GHz GC antenna (sensor), and
b) Results obtained using air-coupled (AC), or "horn", antennas can be compared with results obtained using the other two ground-coupled methods.

Next, results obtained using various air-coupled (horn) antenna deployment and analysis methodologies will be compared and contrasted, for the following reasons:

- Most often only a single-polarization data collection and analysis approach is used by practitioners, yet it is generally not known for certain in advance whether the selection of the deployed polarization is going to yield optimal results. This is because there are generally unexpected field conditions that deviate from as-built and other drawings/structure plans.
- There are significant deviations from GC and AC deployment and analysis methodologies, which often result in obtaining unwittingly erroneous GPR condition assessment maps produced when only a single-polarization AC method is employed.
    - Lane closures allow the appropriate GC GPR survey line orientation (transverse, or parallel to traffic flow) to be determined based on upper steel rebar mat construction. However necessary, GPR data collection perpendicular to traffic flow is simply not an option with AC antennas.
    - Atypical structures like the slab deck (R1), where longitudinal bar spacing is highly variable in the upper mat and also nonexistent within 15ft of either abutment, are not only better served with GPR lines collected across lanes using a GC antenna; but also AC (horn) data collection simply would have been ineffective in identifying existence of unknown structural configurations within the reinforcement that critically impacted how data should be analyzed. Unfortunately, AC data was not collected for Deck R1, which was surveyed during the second field deployment when no decks were assessed using air-coupled GPR methods.

Some detailed discussion related to each of the above comparisons is provided in the 'Ground Penetrating Radar' section of this report where electromagnetic technologies are reviewed within Chapter 2. Relevant similarities or differences seen in the generated maps are discussed in appropriate detail, as they pertain to concepts summarized above.

Deck O1 GPR Maps

The GPR deterioration maps from the 2.6GHz and 1.5GHz ground-coupled (GC) antennas (first and second maps, top to bottom) for Deck O1 can be compared in Figure 141 to the previously presented results from the IE survey. The fourth (bottom) map shows top rebar depth (concrete cover) as measured using the 2.6GHz antenna (sensor). Previously, Figure 60 included the top rebar (cover) map at top, as measured by the 1.5GHz sensor. Note that there are only slight variations between the cover maps generated using the two sensors.

Particularly where the deeper bars are identified and mapped slightly differently near the upper, middle section on both maps at a transverse distance of approximately 21ft from the curb, there are some significant localized differences in the GPR condition maps produced by the two different GC sensors. There is similarly a significant discrepancy along the entire upper portion of the two maps along the curb, where the 2.6GHz data set indicates significantly more deterioration. These two localized regions where there is significant deviation appear to be in greatest due to either: (a) an errant GPR data collection path or (b) a processing error such as including data from a single GPR line at two y-coordinates within the map, or most likely (c) swapping two GPR lines inadvertently while generating the 3D GPR file for the 2.6GHz data set. When comparing both maps, it appears as if the GPR lines at y = 21ft and y = 27ft were inadvertently "swapped" when the 3D GPR file was constructed. This can be more easily seen, if Figure 60 is printed alongside Figure 141 so that both the GPR condition maps, and the cover maps, are compared.

There is additional reason to believe the 2.6GHz analysis generated the discrepancy: The 1.5GHz data set, as a matter of routine QA, and because it was compared against the other NDE methods during the production phase of the data analysis/interpretation in preparation for the report, was more carefully scrutinized. Only a cursory QA review of the 2.6GHz data analysis process was provided, as the comparative data were collected primarily as a value-added attempt to compare/contrast the results as a means of evaluating the performance of the two GC sensors.

Note that though there are slight discrepancies between the two maps, both are generally in agreement with regard to: (a) defining the range of concrete cover (rebar depth) and (b) delineating deterioration boundaries which were ultimately well-correlated to the other NDE results, shown previously. Both maps are also similar in terms of defining the zones where serious and poor condition concrete is identified, as well as areas determined to be in either fair or good condition. As indicated previously, though the 1.5GHz antenna produces GPR profiles that are easier to interpret in the field, particularly in bright sunlight and because of a better ability to see near-field defects, both antennas serve the purposes for which GPR antennas are used on decks. Either of the two GC antennas is ideal for field collection where lane closures can be provided, and core extraction is planned during the same closure. Even though on Deck O1, where there were epoxy-injected repairs (overlays and filled delaminations) which were better identified using the 1.5GHz sensor, a much quicker selection of core locations can be made using the raw 1.5GHz data.

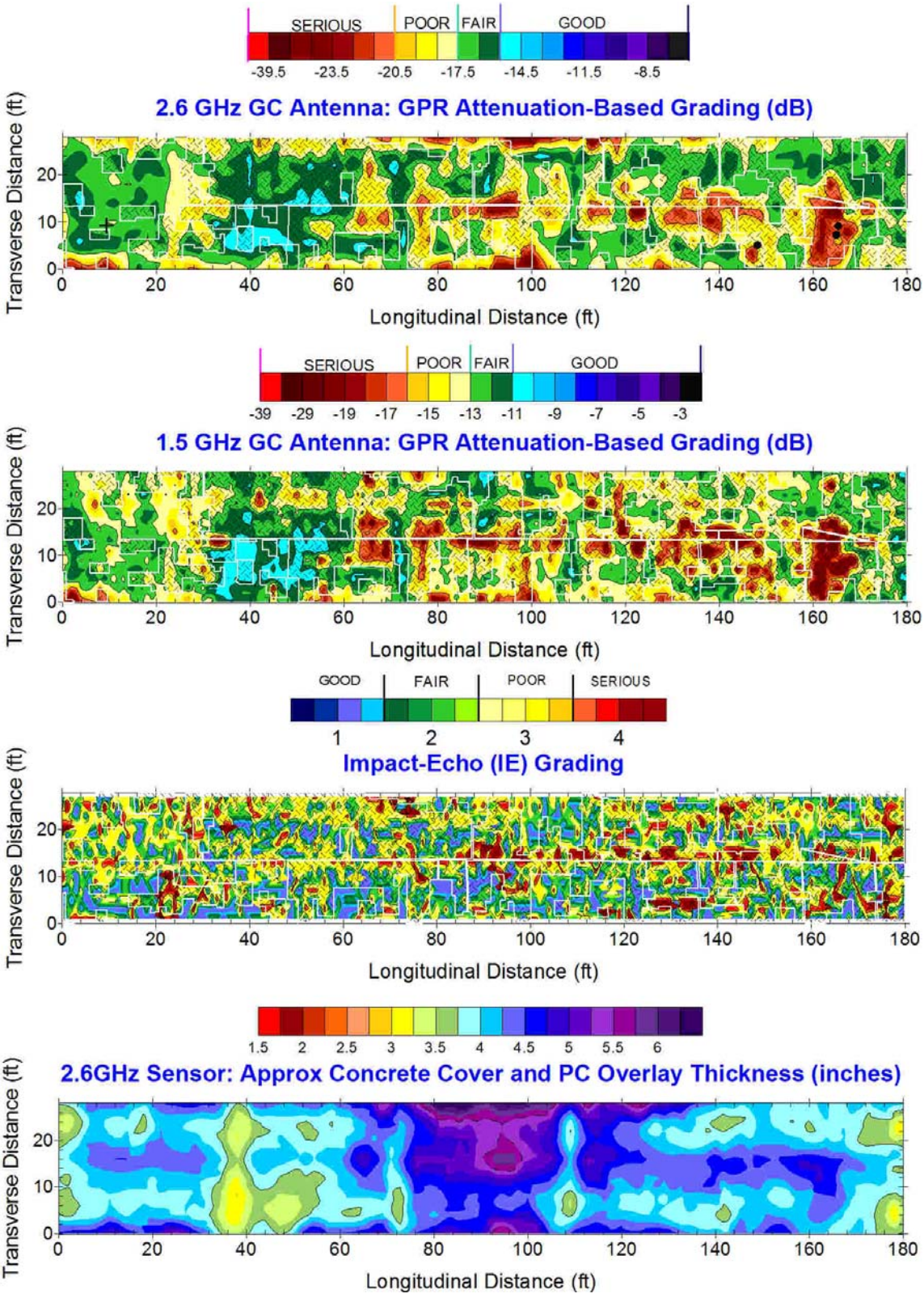

Figure 141 - Ground-coupled (GC) 2.6GHz and 1.5GHz deterioration maps, respectively, are shown, top to bottom, with IE and concrete cover map generated from 2.6GHz antenna.

GPR data was collected using the AC (horn) antennas, but unfortunately there was a problem tagging with the appropriate GPR filename generated by the acquisition system. Lines A through N were collected out of order, however the vehicle could be navigated either around the NDE instruments or in the lane open to traffic. Even following several attempts to reshuffle the order of the GPR lines during processing, it was impossible to determine their original sequence.

Deck O2 GPR Maps

For Deck O2, a comparison of the GPR maps resulting from data obtained using the 1.5GHz and 2.6GHz ground-coupled (GC) antennas (left and right, respectively) is seen in Figure 142, where top rebar depth (concrete cover) is shown on top and GPR condition assessment maps are shown on bottom.

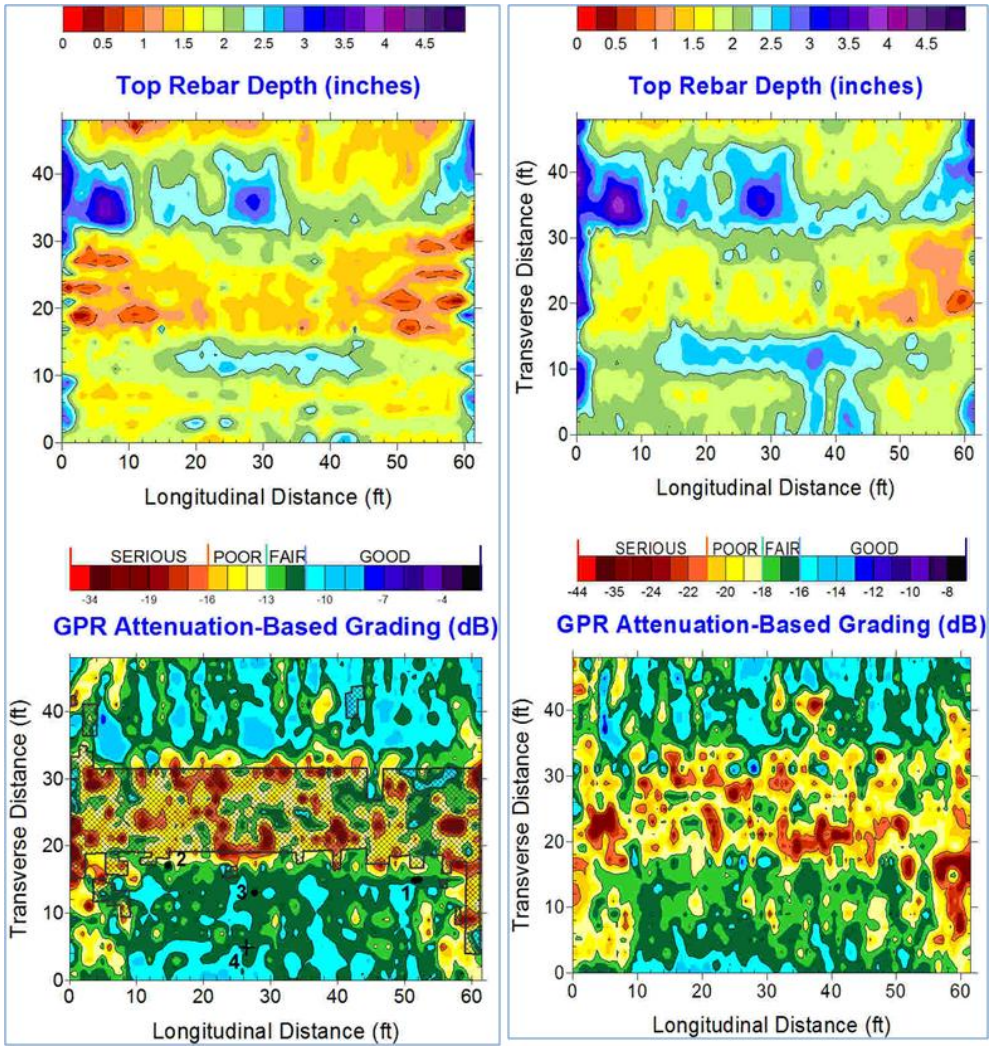

Figure 142 – 1.5GHz and 2.6GHz ground-coupled (GC) GPR data, left and right, respectively.

Note that though there are slight discrepancies between the two maps, both are generally in agreement with regard to: (a) defining the range of concrete cover (rebar depth) and (b) delineating deterioration boundaries, which were ultimately well-correlated to the other NDE results, shown previously. Both maps are also similar in terms of defining the zones where serious and poor condition concrete is identified (red and yellow colors), as well as areas determined to be in either fair (green) or good (blue) condition.

Because there was rain that became heavy at the close of the second day of data collection, no dual-polarization AC (horn) antenna data were collected for Deck O2. Note that while a light rain, or even a fairly wet deck is not an issue when collecting ground-coupled GPR data, provided data are not collected in standing water, GPR data collected with AC (horn) antennas can be significantly impacted when the deck surface is not surface dry. A saturated, surface dry (SSD) condition is probably all right for horn antenna GPR work, but any minor pooling of water or surface 'sheen' that is inconsistent among different areas of the surveyed deck can have a significant impact on the measured rebar amplitude readings. Since most of the ground-coupled (GC) antenna energy is actually loaded directly into the deck, and a significant amount of energy is not reflected from the surface (as is the case with the AC (horn) antennas), slight variations in surface wetting does not affect signal amplitude measurements in any appreciable way. Care still has to be taken, however, not to collect GC GPR data when data on part of the deck are collected in dry conditions and data on other sections of the deck (in a two-day data collection process, for example) are obtained when the surface is significantly wet or is slightly puddled.

Deck O3 GPR Maps

For Deck O3, GPR data were collected using both GC antennas (1.5GHz, shown previously in the report, and 2.6GHz) as well as using a dual-polarization (DP) 1.0GHz deployment. As was seen on both Deck O1 and Deck O2, the 1.5 GHz and 2.6GHz GC antenna data produced similar maps. The only major difference was the deterioration threshold (attenuation, dB level) used to separate fair quality concrete from poor/serious (deteriorated) concrete. Figure 143 includes the IE and the 1.5GHz GPR data previously shown in Figure 80, as the first two maps on the left side of the figure. On the right side of Figure 143, the two upper maps are the HCP (shown previously in Figure 81) and the 2.6GHz GC data showing comparable deterioration quantities as the 1.5GHz map just to its left.

Immediately below the two GPR maps are a third set of maps (left and right). Those show, respectively, concrete cover as measured using the 1.5GHz GC sensor and the subtracted, dual-polarization GPR data obtained using the electronically matched 1.0GHz AC (horn) antennas. Though there are not significant differences in the cover maps produced by the AC antenna and the map produced by the lower resolution (of the two GC antennas), it can be immediately seen that for very shallow steel the 1.0GHz sensors are not able to as accurately map cover depth. The same was true with the previous comparison between 1.5GHz and 2.0GHz GC antennas. The higher resolution GC antenna is more accurate in measuring near-surface targets (very shallow cover).

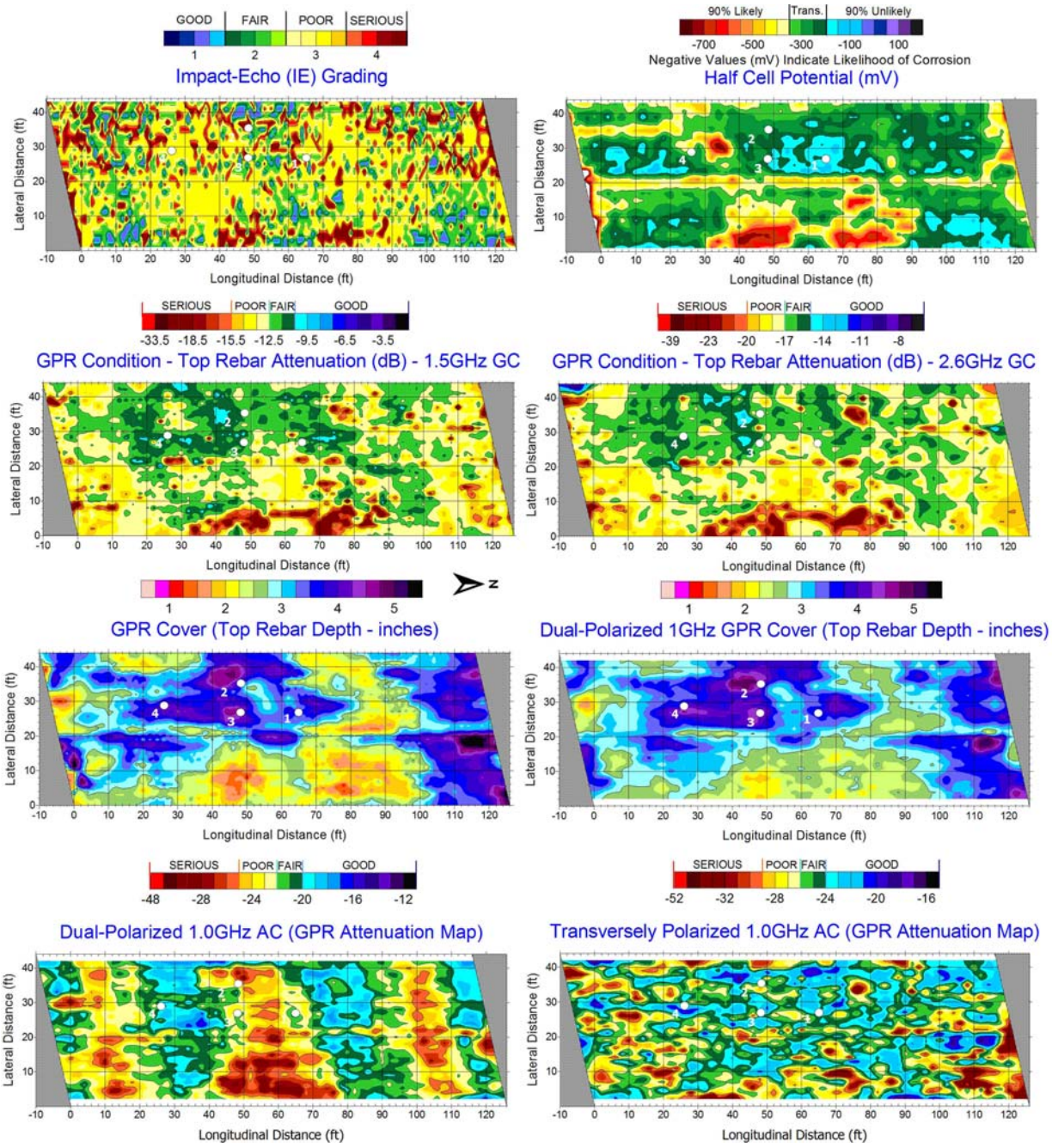

Figure 143 - Deck O3 maps comparing three different GPR sensors and/or deployment techniques (data from both AC and GC antennas shown) with IE and HCP.

There are two additional maps shown on the bottom of Figure 143: At lower left there is a map produced using a subtracted signal, as specified by the dual-polarization, 1.0GHz AC analysis methodology. At lower right is a map produced by a single-polarization, 1.0GHz AC antenna analysis, where only the transversely polarized antenna data are shown. As can be seen in this particular example, data from the slab deck (Bridge O3) were more consistent among the GPR surveys when the single, transversely-polarized antenna data were analyzed. This is not

generally the case, however, when data from concrete or steel girder decks are analyzed. More often than not, the dual-polarization, 1.0GHz analysis produces results most close to the more accurate 1.5GHz and 2.6GHz GC maps. For purposes of keeping the comparison fairly basic, maps obtained from data analysis of the longitudinally-polarized antenna measurements are not shown, as they did not at all correlate with any of the other GPR maps.

Deck O4 GPR Maps

Deck O4 was surveyed using 1.5GHz and 2.6GHz GC antennas, as well as both the transversely and longitudinally polarized antennas (channels 1 and 2, respectively) configured in an in-line, Dual Polarization deployment. Data were analyzed for all five antenna configurations: (a) 1.5GHz GC (shown previously in Figures 87 through 89), (b) 2.6GHz GC, (c) 1.0GHz Dual-Polarization AC (horn), (d) 1.0GHz Transverse (Single) Polarization AC (horn), and (e) 1.0GHz Longitudinal (Single) Polarization AC (horn). Figures 144 through 148, respectively, are used to display both the GPR condition assessment map and the estimated concrete cover obtained using the five configurations.

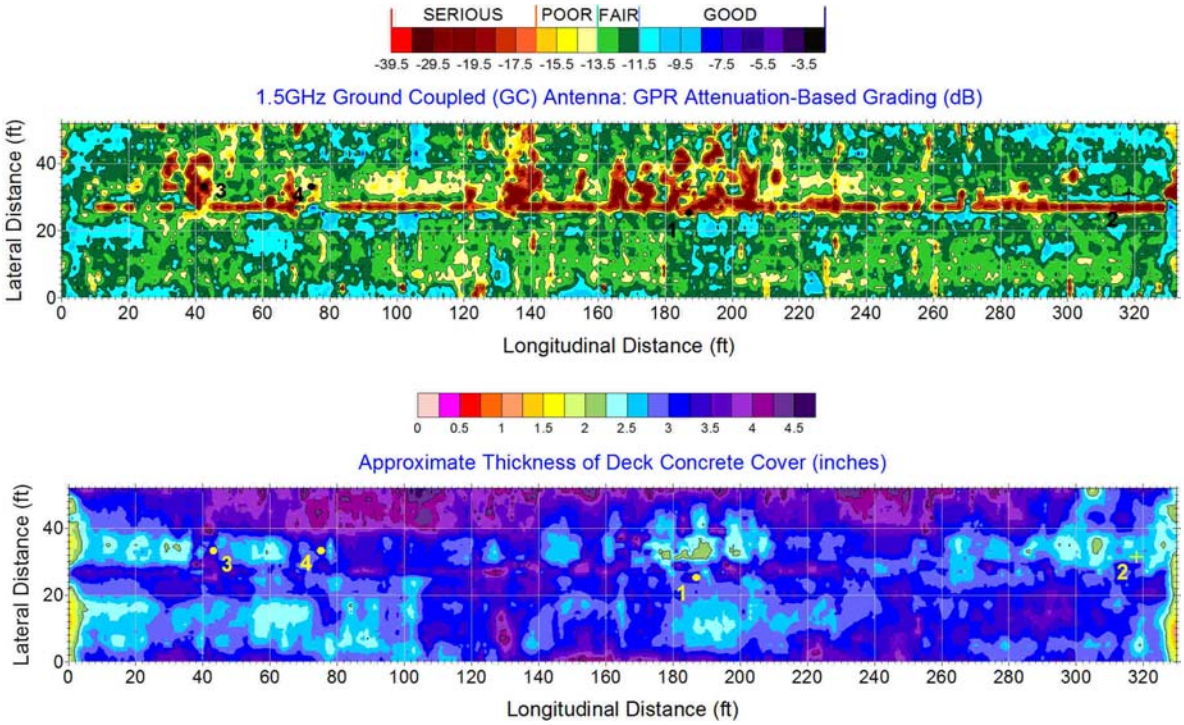

Figure 144 - 1.5GHz GC maps of GPR condition (top) and estimated concrete cover (bottom).

Comparing Figures 144 through 147, it is obvious thatboth GC methods and the two AC methods which incorporate use of the transverse rebar measurement provide similar maps for approximating the concrete cover on the deck. However, the concrete cover map shown on Figure 148 does not at all resemble the other cover maps. This is reasonable since the longitudinally polarized sensor is more attuned to picking up the rebar reflections from the longitudinal rebars in the upper reinforcing mat, which are tied beneath the transverse bars. Since longitudinal steel GPR reflections are often masked by transverse steel, but often are

intermittently imaged more accurately when the antenna path is directly above a longitudinal bar, this happening more often in negative moment regions above and on either sides of piers, a different concrete cover map is expected, at the very least.

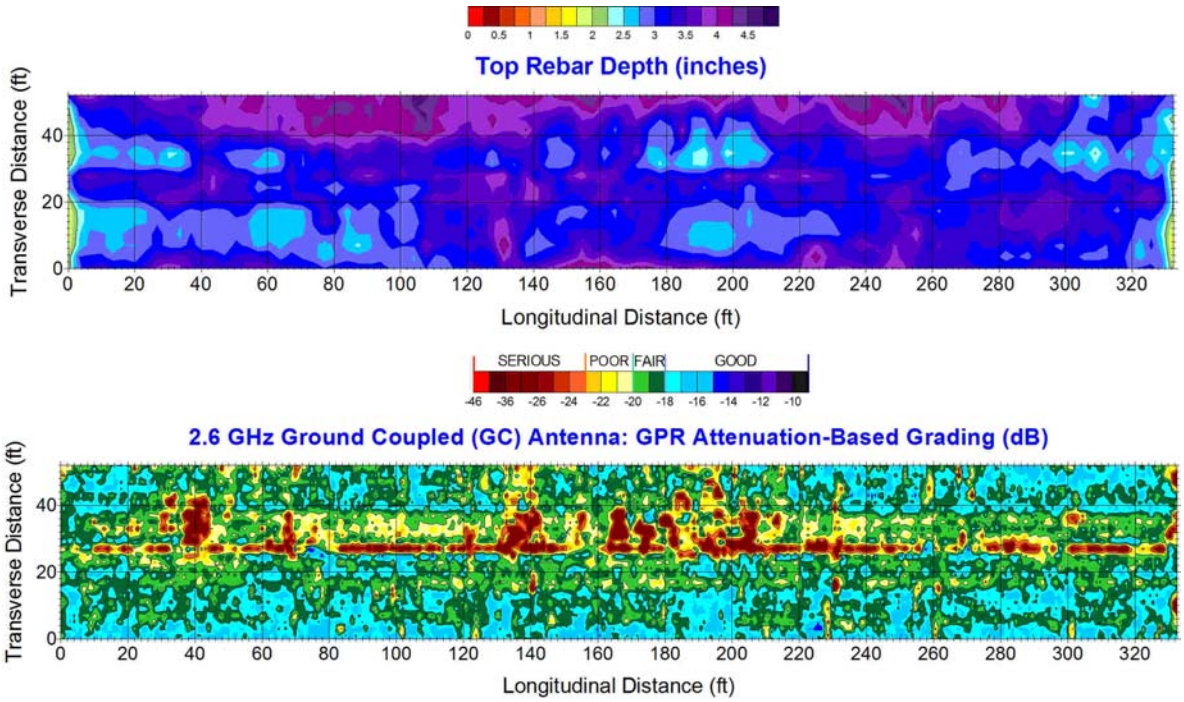

Figure 145 - 2.6GHz GC maps of estimated concrete cover (top) and GPR condition (bottom).

Looking next at the GPR condition maps, the following observations can be readily made. Results for 1.5GHz GC and 2.6GHz GC antennas shown in Figures 144 and 145 provide virtually identical maps, both in terms of GPR condition assessment and GPR-estimated concrete cover. There are minor discrepancies, both due to differences in antenna frequency and transmit signal strength. However, even differences in the signal attenuation thresholds used to delineate deterioration quantities on either map do not take away from the fact that both GC sensors are essentially producing the same condition assessment. The primary difference between these two maps is that the 2.6GHz sensor produces results indicating that a bit more of the deck area falls within the "good" grading, as opposed to the "fair" category. The 1.5GHz sensor produces the opposite results.

Differences between GC and AC sensor results can be obtained by comparing either of Figures 144 and 145 to Figures 146 and 147. Figure 146 is the result of mapping data obtained from a dual-polarization deployment of two, electronically matched, in-line 1.0GHz antennas (sensors). Data processed from a dual-polarization configuration is produced by subtracting the data obtained by the longitudinally polarized antenna from that of the transversely polarized antenna. The intent is to minimize effects of horizontal layers (overlays, patches, or shallow cover less than 2" in thickness), but also to compensate for some of the negative effects that can result from having a lower resolution antenna that vertically "smears" the signals reflecting from the transverse and longitudinal antennas within the upper mesh. This problem is most

pronounced when the rebars in the upper mat are small diameter, but not so critical when rebars are larger sized. Thus, the difference between the maps shown on Figures 146 and 147 are not that different from one another, with some minor exceptions in some of the boundaries between "serious", "poor", "fair" and "good" gradings.

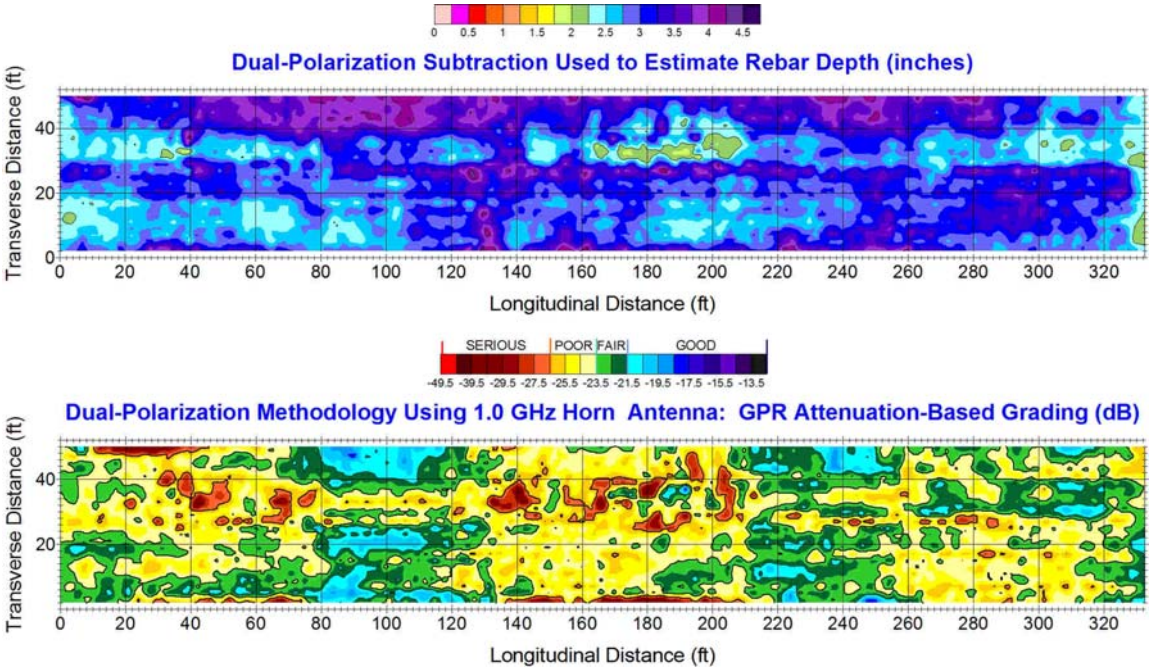

Figure 146 - Dual Polarization 1.0GHz GPR cover (top) and condition assessment (bottom).

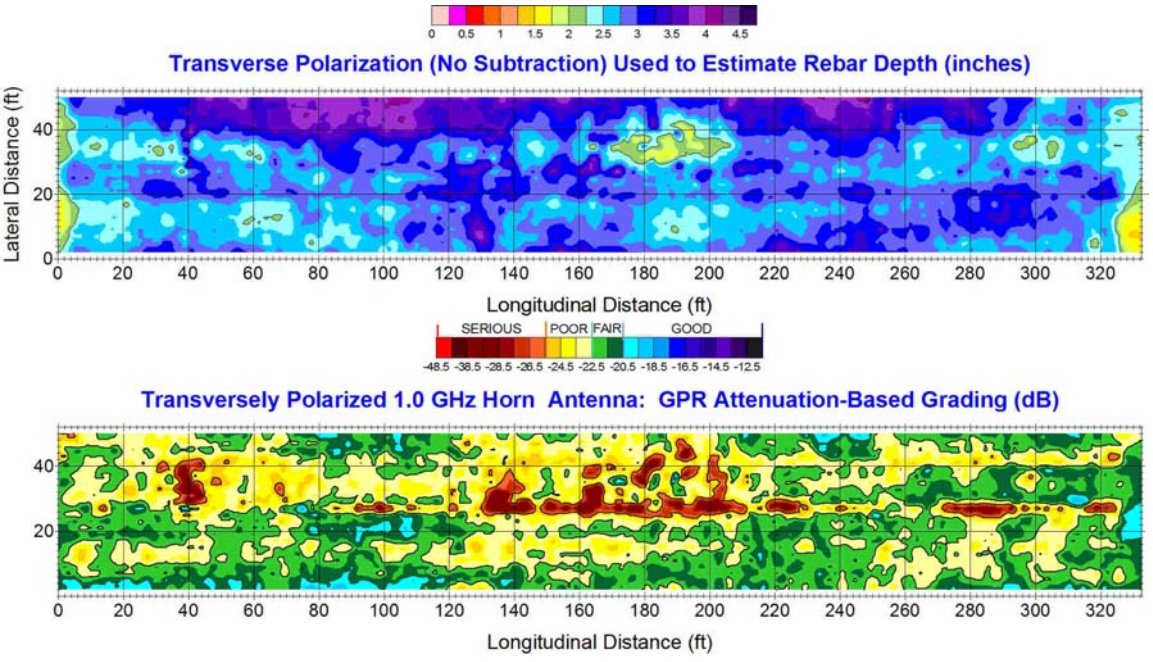

Figure 147 - Transversely Polarized 1.0GHz GPR cover (top) and condition assessment (bottom).

There are significant differences, however, when contrasting Figures 144 and 145 to 146 and 147. Each of these maps was assigned a deterioration threshold that would result in approximately the same quantity of bridge deck area that would fall within the "serious" grading category (red colors). GPR deterioration maps from Figures 144 and 145 show a much smaller percentage of the deck categorized (graded) as "poor", areas colored yellow, than do Figures 146 and 147. Thus, both the GC maps show lower quantities of deck area considered to be in serious-to-poor condition, and both AC maps indicate that a significantly large percentage of the deck area (greater than 50%) is considered to be in serious-to-poor condition. Very little of the deck, in either of the AC maps, is considered to be in good condition. However, almost none of the deck area is considered "good" when the transversely polarized antenna is used by itself.

Finally, a GPR condition assessment map obtained from processing the 1.0GHz data obtained using the longitudinally polarized antenna is shown in Figure 148, along with the estimated concrete cover. There is virtually no correlation to the other GPR condition maps. In this particular case, there is no value in processing GPR data obtained from an AC (horn) antenna during field deployment. However, as this may be the case for the particular deck being examined, there are some instances where AC data obtained in the longitudinal orientation provide better results than what can be obtained from either the dual-polarization or the single-polarization, transversely polarized methodologies. Results such as these have been cited in previous papers submitted by one of the co-authors of this report, and generally exist on continuously-reinforced concrete decks or decks with slab construction where longitudinal rebars are both large in diameter and very closely spaced. Such a sample can be seen later in this Appendix within the maps and related discussion for Deck O6.

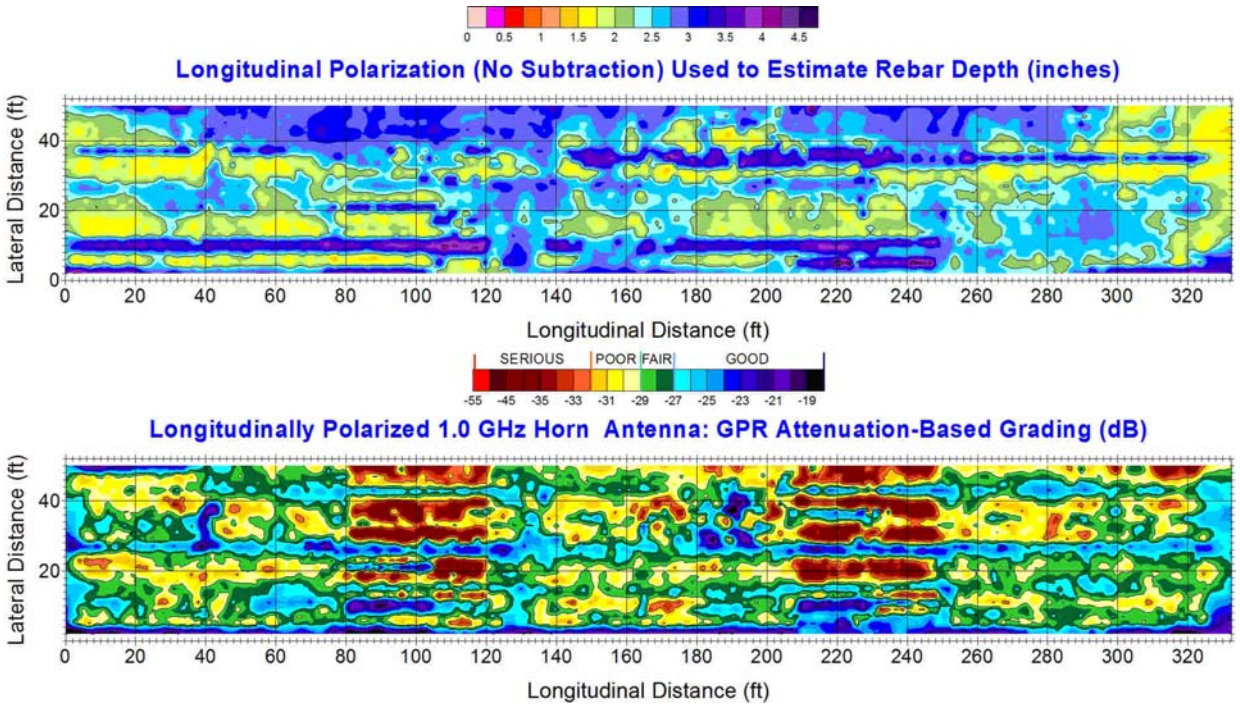

Figure 148 - Longitudinally Polarized 1.0GHz GPR cover (top) and condition assessment (bottom).

Deck O5 GPR Maps

Maps from only 1.5GHz and 2.6GHz GC data for Deck O5 are shown in Figures 149 and 150, respectively.

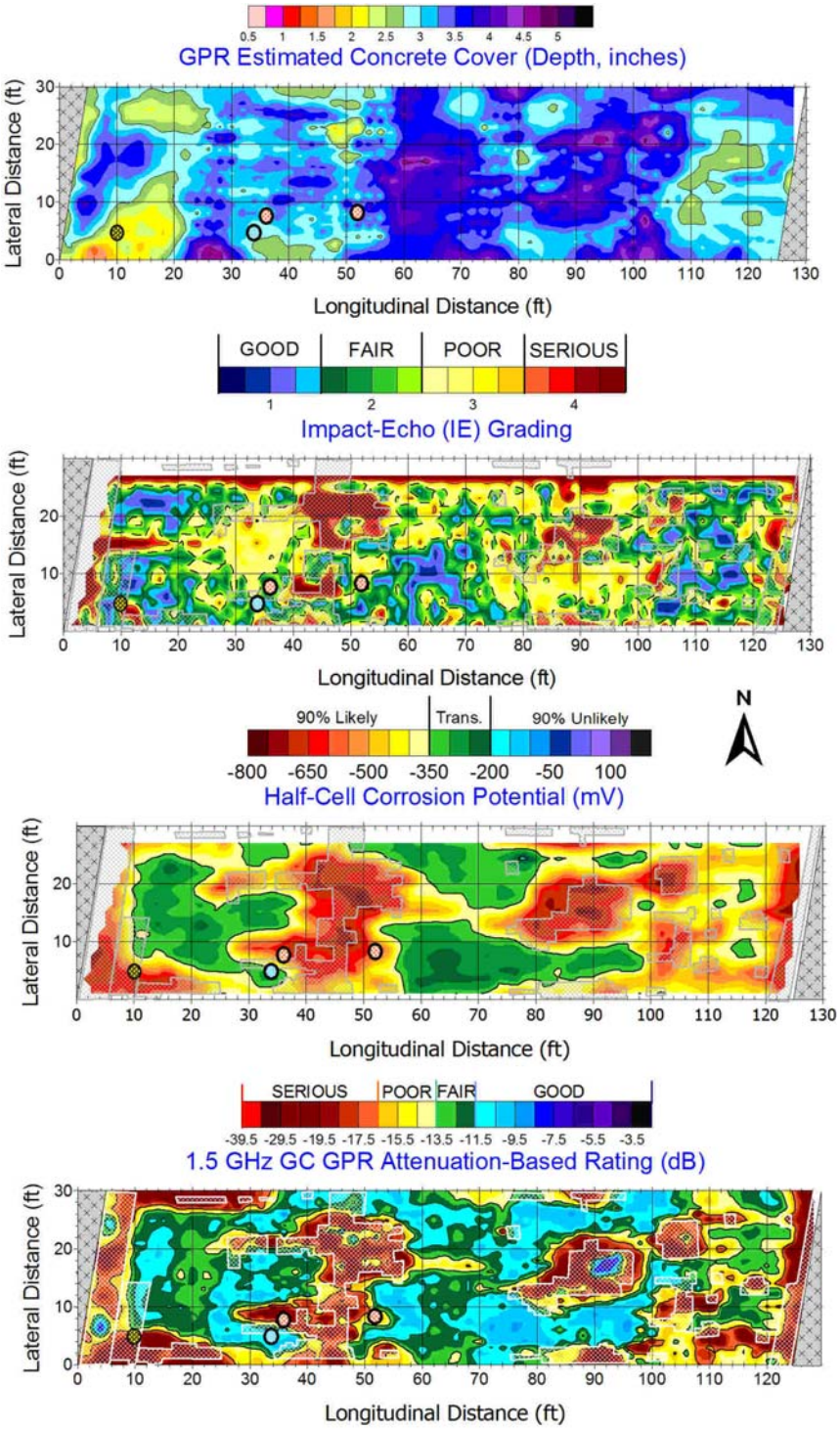

Figure 149 - 1.5GHz GPR condition and cover maps shown with HCP and IE.

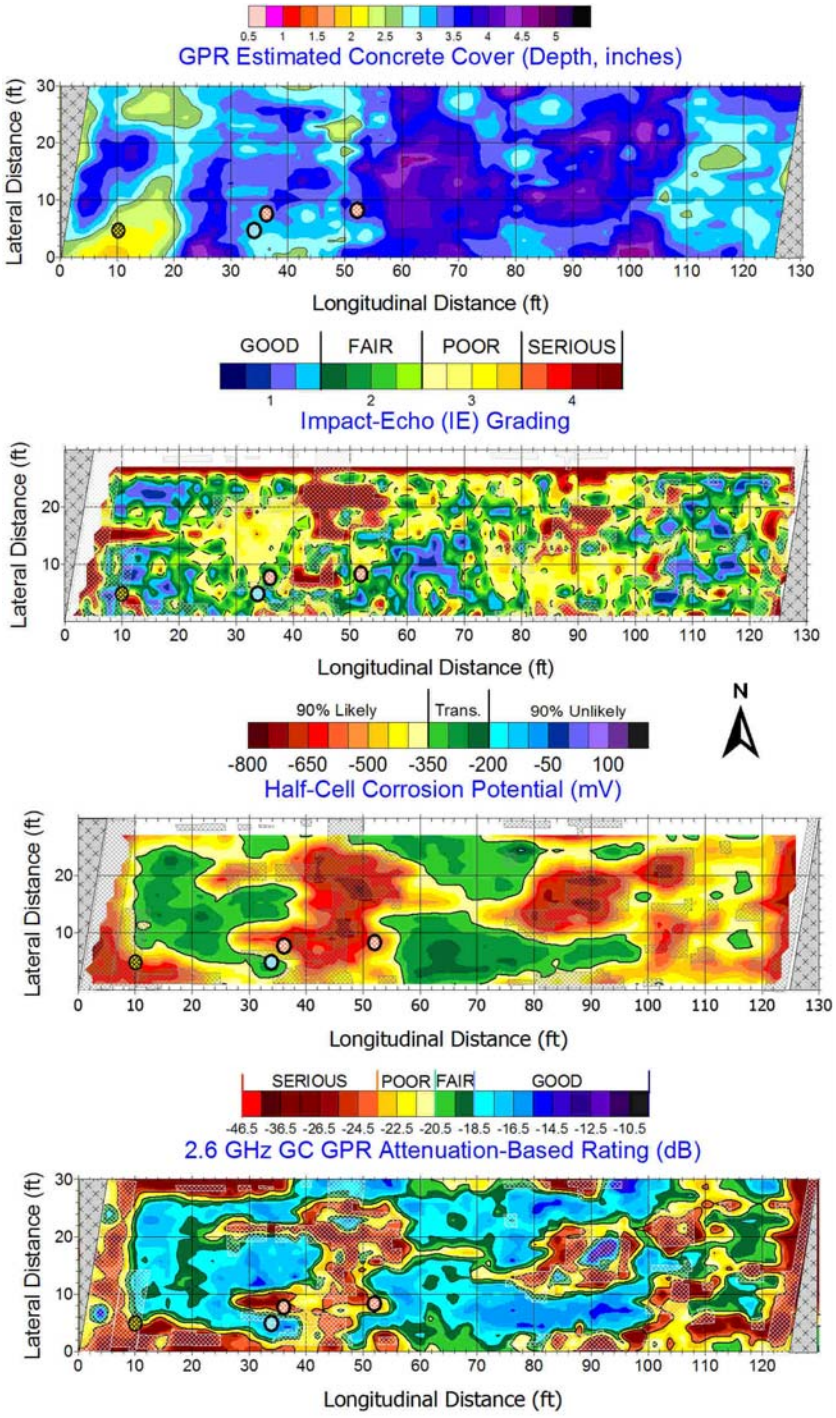

Figure 150 - 2.6GHz GPR condition and cover maps shown with HCP and IE.

Figure 149 is the same as Figure 99, shown in the main body of the report for Bridge Deck O5, which is based on analysis of 1.5GHz GC data. It is straightforward to see the similarity between the GPR maps for both concrete cover (top) and GPR attenuation-based rating (bottom),

Deck O6 GPR Maps

Deck O6 GPR results include maps from 1.5GHz GC and 1.0GHz AC (horn) antennas collected and processed using a dual-polarization configuration deployment of two, electronically matched 1.0GHz AC (horn) antennas. Additionally, the individually processed and mapped transverse and longitudinal data obtained from the two separate AC GPR channels in the same dual-polarization deployment are also shown. The results are shown in Figure 151, with the 1.5GHz GC data set shown alongside results from all three 1.0GHz AC methods.

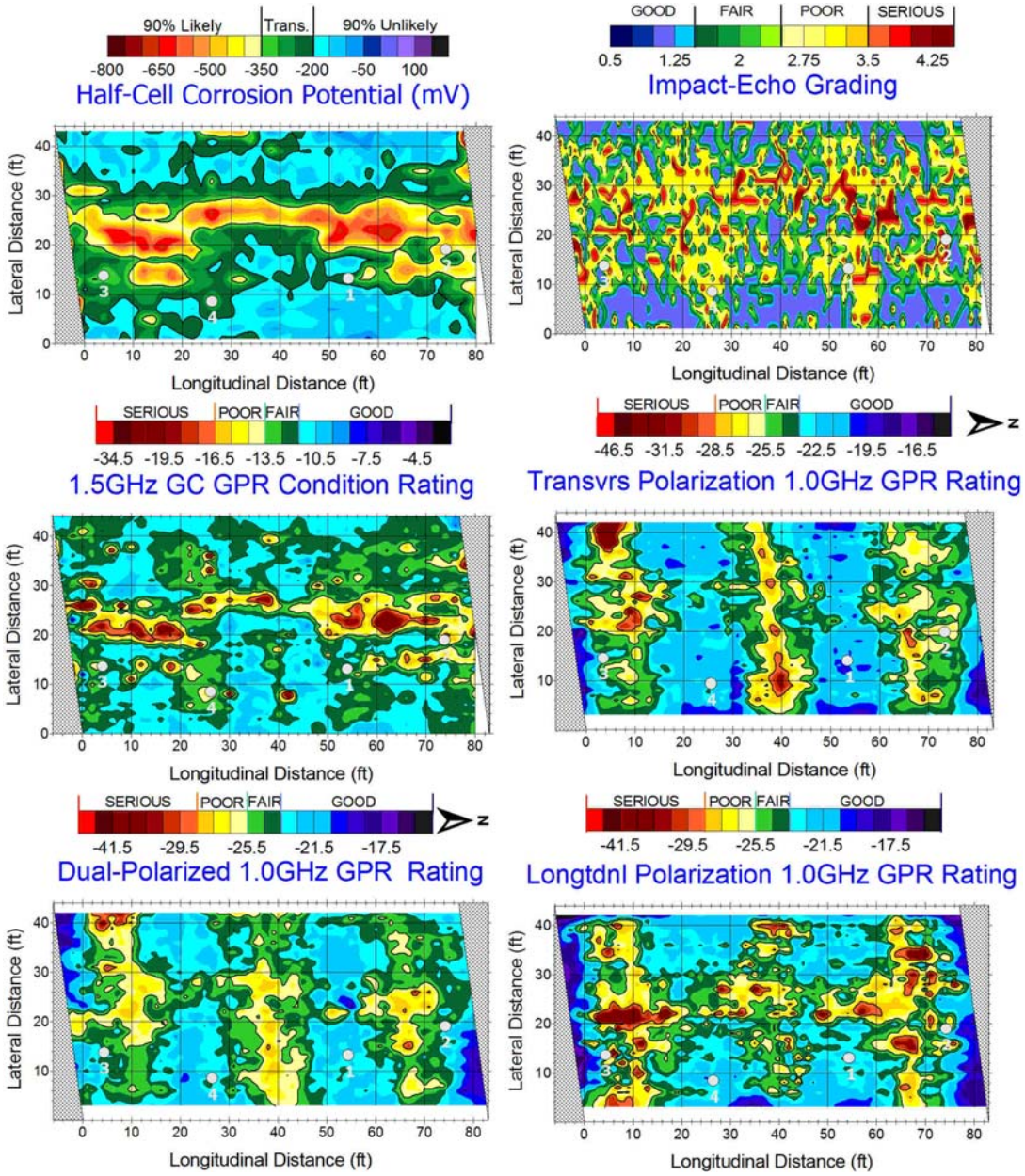

Figure 151 - NDE maps including HCP, IE, two unique 1.0GHz AC analyses, 2.6GHz GC and 1.5GHz GC GPR data (clockwise from upper left).

Though the 2.6GHz data are not shown in this figure, the 1.5GHz GC and 2.6GHz GC data correlate as closely for this deck as they do for all others.

Common to the previous figures in the report are the two maps at top (HCP and IE), as well as the left, center map showing the 1.5GHz GC GPR data. As indicated previously, there is significant correlation between the HCP, 1.5GHz GPR and IE maps, as there was also strong correlation between the HCP and ER maps (Figure 109). The results from the analysis of the longitudinally polarized GPR data set (lower right), for this particular deck, show the most agreement (a) with data from the 1.5GHz GC analyses, and (b) with the other NDE data from Deck O6. As can be easily seen, the 1.0GHz AC correlates reasonably well with the 1.5GHz GC results, with the main difference being the quantity of deck area that is graded as either "serious", "poor", fair" or "good" using data from either sensor.

There is not much agreement between the 1.5GHz GC data map or either the 1.0GHz dual-polarization AC or 1.0GHz transverse polarization maps. As indicated previously, there are some situations where one or the other polarization produces better results with AC antennas than a dual-polarization AC configuration. This is one of those situations, on a slab deck, where the longitudinally polarized (single-channel) AC data would produce the best AC results; however, in the field this configuration is rarely used by any practitioners.

The fundamental problem with collecting data using AC antennas at high speed without lane closures is the following. Without knowing which is the best way to collect data (in advance of collecting the data and comparing to GC results), it is obvious that the AC collection and analysis methods can all fall short of satisfactory in many instances. Deck O6 is a prime example of that.

Deck R1 GPR Maps

GPR maps for Deck R1 are shown in Figure 152. Concrete cover maps are generated from 1.5GHz and 2.6GHz data (top two maps, respectively) and GPR condition assessment (deterioration) maps are generated from 1.5GHz and 2.6GHz GC data (bottom two maps, respectively). There are minor differences between maps generated using data obtained from the two GC GPR sensors. Once again, there is a notable difference in the attenuation level (signal strength) at which the deterioration threshold, the boundary separating "poor" from "fair" concrete on the deck, is selected for either data set.

Since no air-coupled (AC) GPR data were collected on Deck R1, no results are shown. However, it is highly unlikely that survey results from AC sensors, regardless of configuration, could produce anything better, or more repeatable, than what was obtained using the GC antennas. This is particularly true because of the variable nature of the spacing between the longitudinal rebars within the deck, something which would not have been observed in the lower-resolution AC antenna data.

A suitable strategy for determining the best data collection methodology, after confirming rebar layout in the construction drawings, would not have developed (as was, conversely, the case with both the 1.5GHz and 2.6GHz GC data). Data collected using AC antennas would have

simply been collected at 2ft spacing, and it would have been very difficult to decide how to analyze the data with respect to the polarization. Industry-wide experience with collecting, analyzing and interpreting GC and AC data sets on slab decks is recognized as difficult, particularly when reinforcement layout is highly variable or undeterminable.

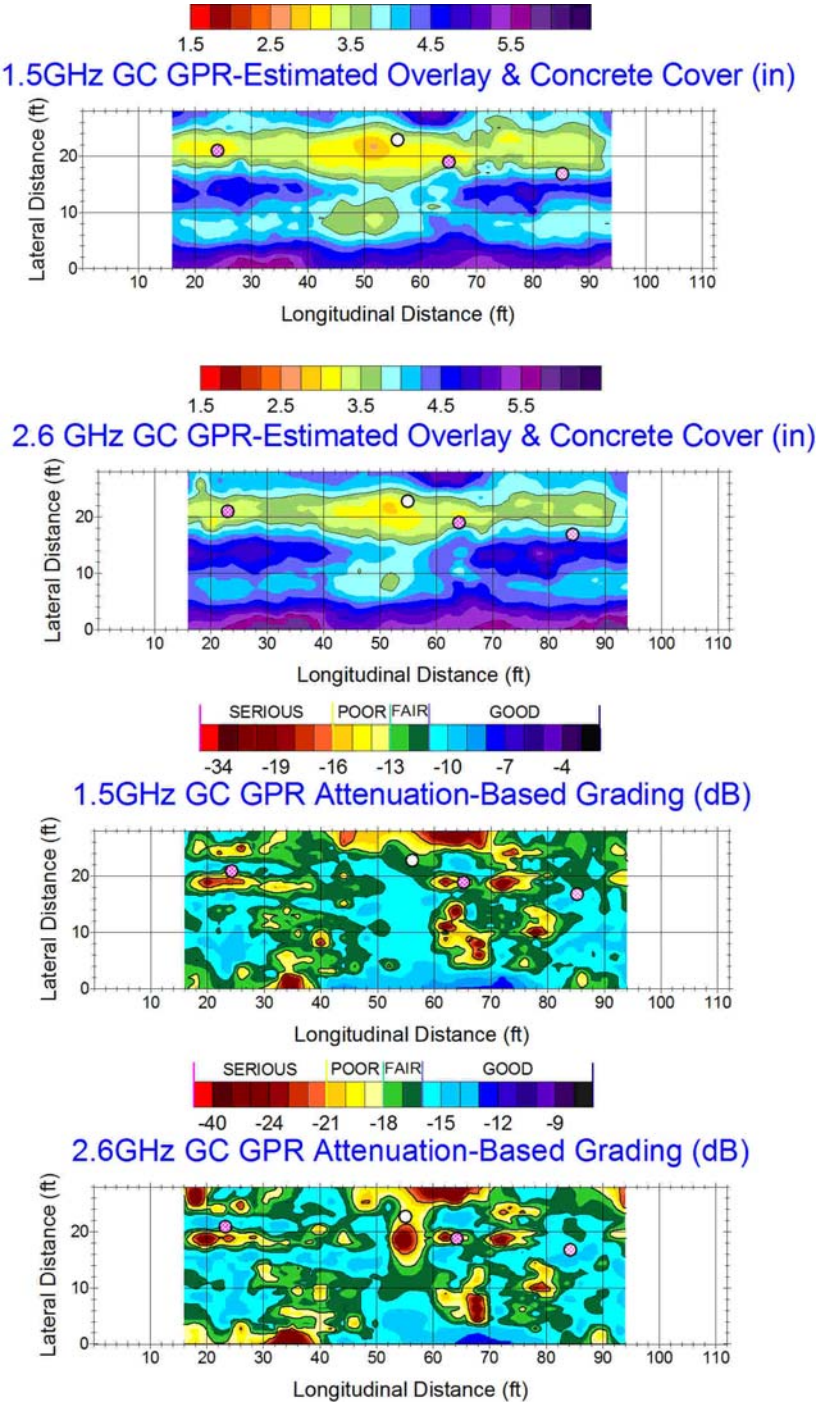

Figure 152 - Deck R1 maps comparing data obtained using 1.5GHz & 2.6GHz GC antennas (sensors).

Deck R2 GPR Maps

Ground-coupled (GC) and air-coupled (AC) GPR maps for Deck R2 are shown in Figure 153 and 154, respectively.

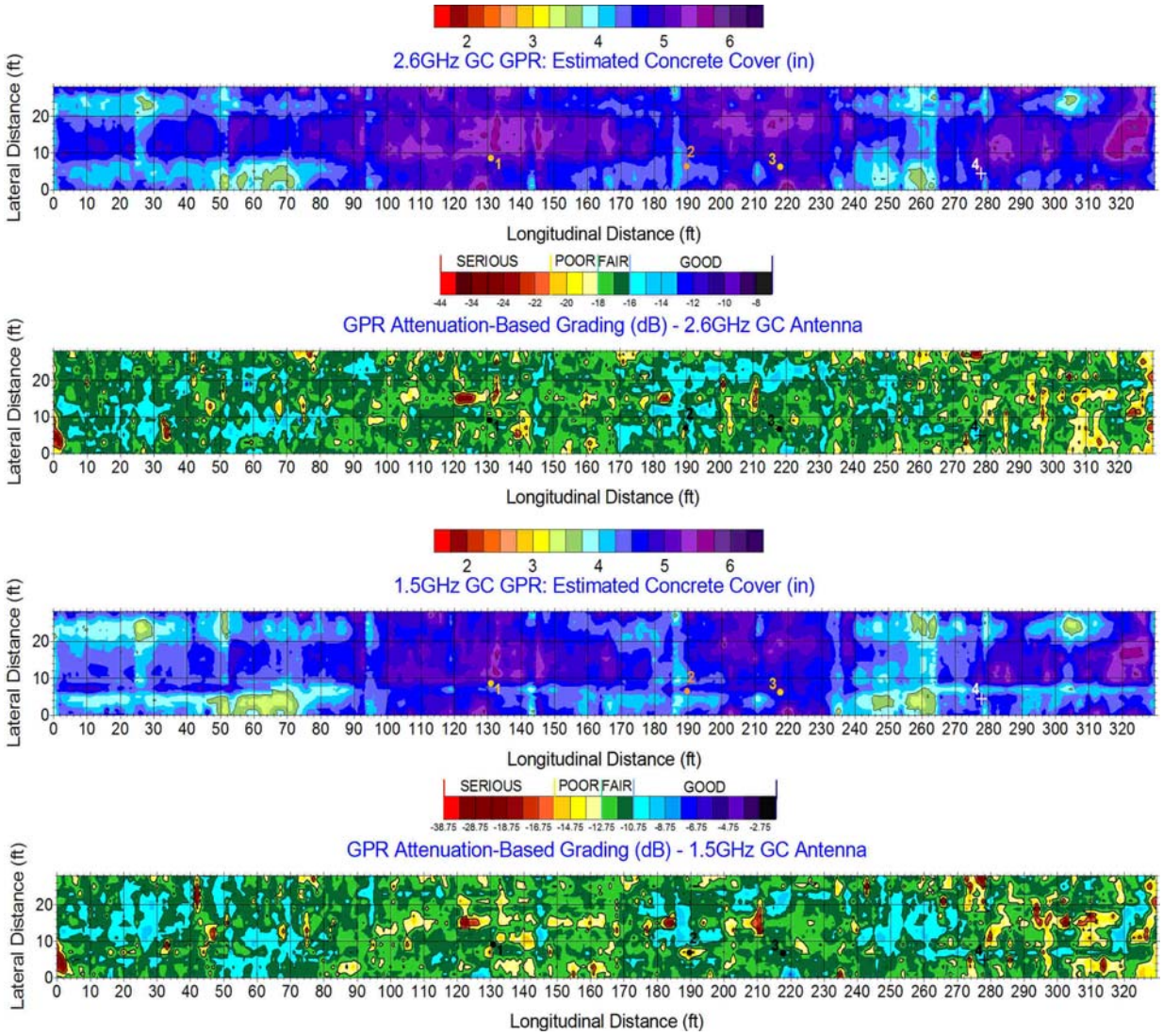

Figure 153 - 1.5GHz and 2.6GHz GC maps showing GPR-estimated concrete cover and GPR condition assessment.

As has been shown on all previous decks, there are only subtle differences between GPR-estimated cover depth or GPR deterioration grading (serious, poor, fair or good) when either the 1.5GHz or 2.6GHz antennas are used (Figure 153). The same cannot be said for the various air-coupled (AC) GPR methods, as presented in Figure 154, except for the estimated cover depth of the top rebars, which is essentially the same for the dual-polarization or the single-polarization (transversely oriented) data. This is to be expected, since both methods are essentially targeting

the shallowest steel, which in this case was transverse rebars tied above longitudinal rebars in the upper reinforcing mat. In Figure 154, only the concrete cover from dual-polarization (subtracted) data is shown, though the GPR condition assessment maps (GPR Attenuation-Based Grading) are provided for all three methods: (a) dual-polarization analysis method, based on subtracting longitudinal channel data from data obtained by the transversely oriented antenna, (b) single-polarization analysis of data obtained from the transversely oriented antenna (sensor), and (c) single-polarization analysis of data obtained from the longitudinally oriented sensor. Note that in this and previous discussions, and in Figure 154, the words "antenna", "channel" or "sensor" are somewhat loosely interchanged.

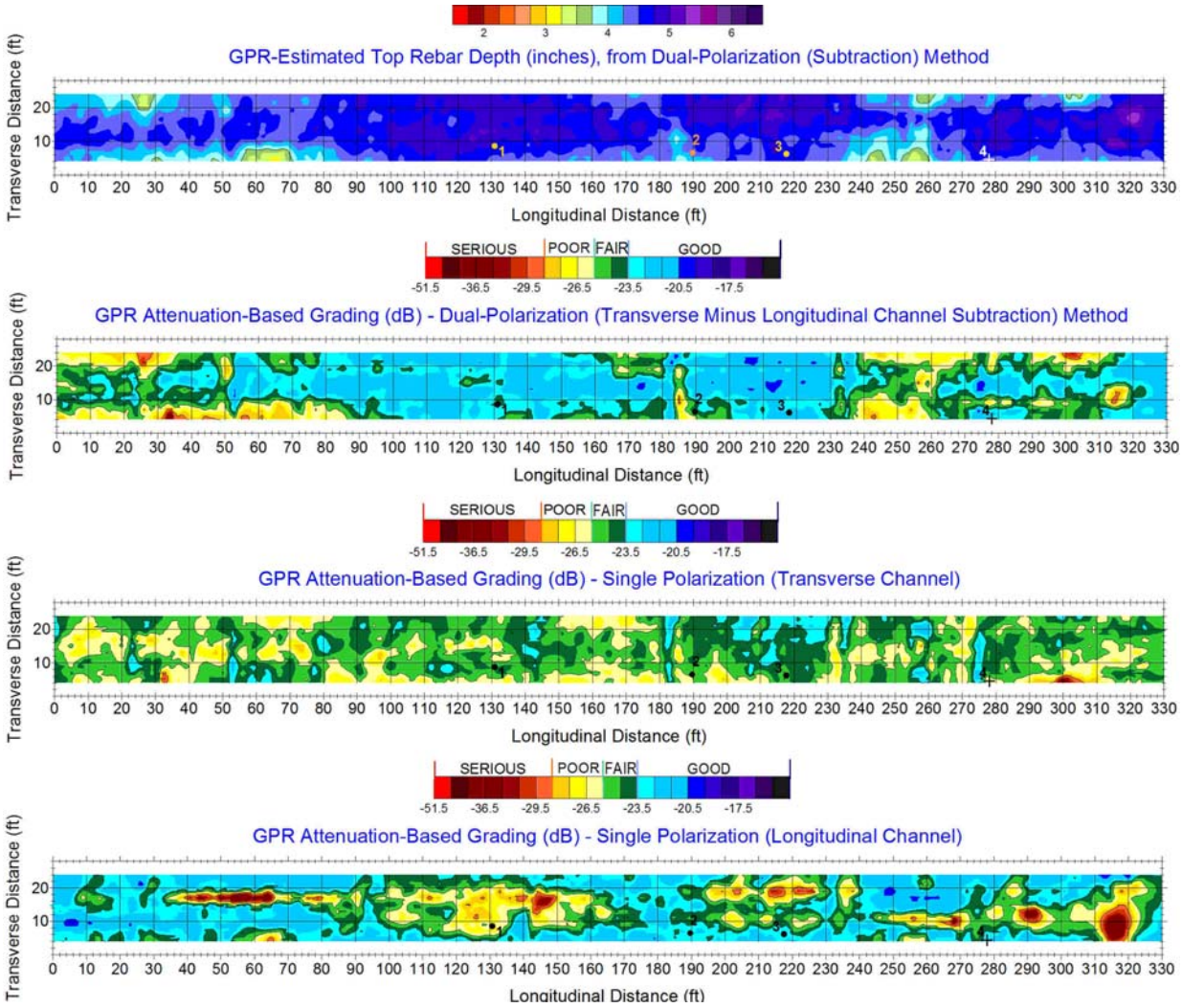

Figure 154 - GPR cover and attenuation-based grading using three different 1.0GHz AC deployment and analysis methods.

Comparing the various AC GPR maps, if the mapped data are normalized so that the areas graded as "serious" and "poor" are separated from "fair" and "good", once again there is a fairly huge discrepancy. There is little agreement between the dual-polarization AC map and the map generated using the single polarization attenuation methodology with data obtained by the longitudinally oriented sensor. In fact, the two almost produce inverse results. For this particular deck, though there are not very many areas which directly correlate. At least the two GC GPR

methods produce a map that looks somewhat like the map obtained by the transversely oriented 1.0GHz AC antenna in that the "serious" and "poor" regions (added together) on the deck, the "fair" sections, and the "good" sections are somewhat proportional.

Deck R2 was the last of the bridge decks where the 1.0 AC (horn) antennas was deployed alongside the two, GC sensors. Since it is well beyond the scope of this report to compare results from core sampling with each of the various GPR data collection and analysis methodologies, it is left to the reader to refer back to the main body of the report where ground truth (cores) is discussed alongside NDE results.

Deck R3 GPR Maps

Ground-coupled (GC) GPR maps generated from the analysis of 1.5GHz and 2.6GHz data are shown in Figure 155. Clearly, there is a strong correlation between the two GPR data sets with regard to the condition maps produced. Though not shown, the estimated concrete cover (rebar depth) correlates as well as any of the previous maps where 1.5GHz and 2.6GHz GC data were presented. Last, for Deck R3 the comparison between both GPR maps and the impact-echo (IE) and half-cell potential (HCP) maps once again supports the value of a complementary NDE approach, where there is either a strong correlation among all data or there can be explanations for some of the discrepancies.

For the purpose of comparison to previous discussions (and Figure 138) in the main body of the report, core locations are marked as circles on Figure 155:

- Core 1 is marked by a white circle ringed with black (considered to be sound, as rated in the field using IE),
- Core 2 is marked by a gray-hachured pattern in a circle ringed with black (fair-to-poor condition, as rated in the field using IE),
- Core 3 is marked by a red/white circle ringed with black (predicted as delaminated, as rated in the field using IE), and
- Core 4 is marked again using a gray-hachured pattern in a black-ringed circle (fair-to-poor condition, as field-rated using IE).

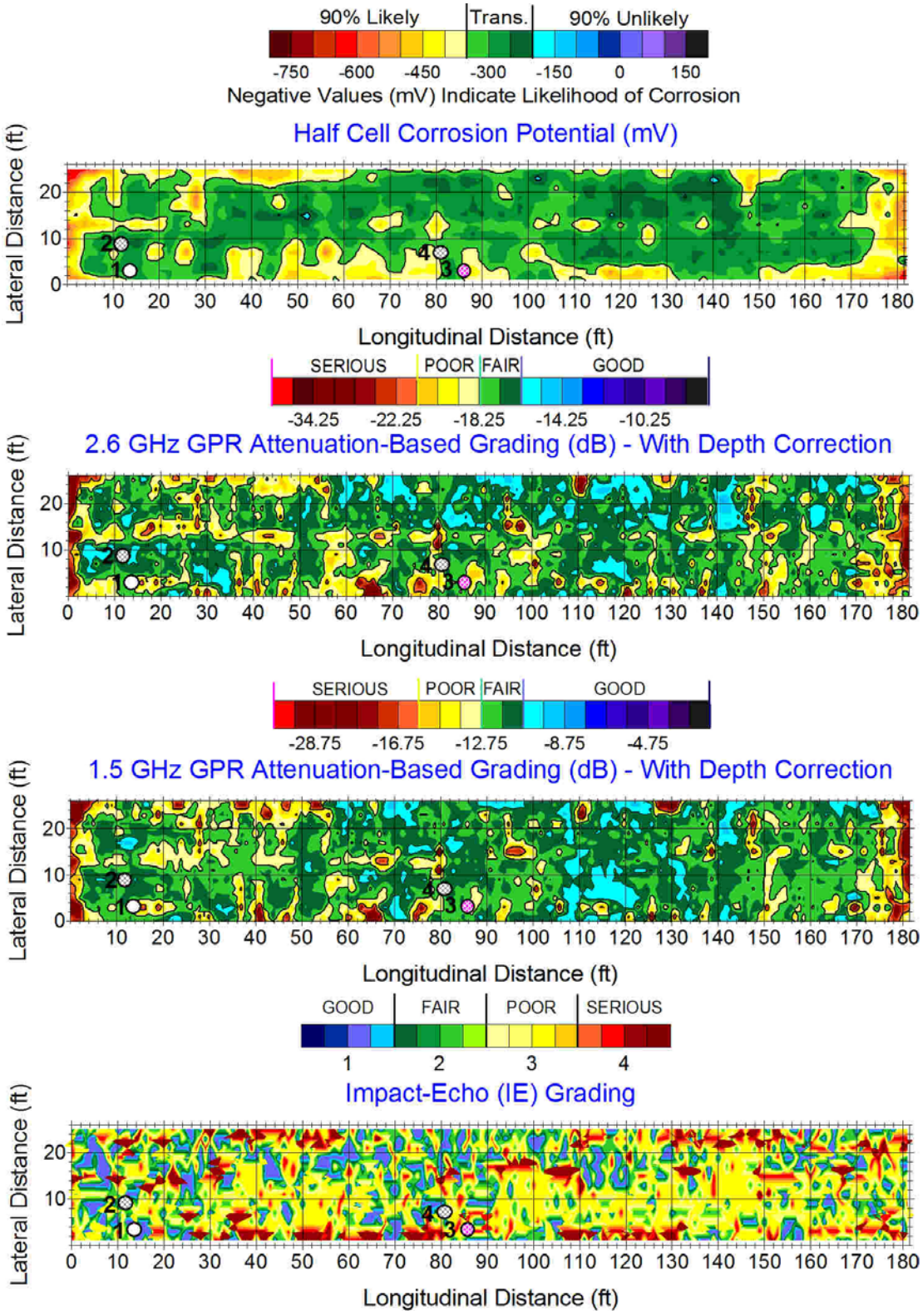

Figure 155 - Comparison of 2.6GHz & 1.5GHz GC GPR data to HCP and IE data, with core locations shown.

REFERENCES

Algernon, D. and Wiggenhauser, H., "Impact Echo Data Analysis" ASNT's NDE Conference on Civil Engineering, St. Louis, MO, USA, Proceedings (August 14-18, 2006) on CD.

Algernon, D., Wiggenhauser, H. and Schubert, F., "A New Approach for the Investigation of Geometry Effects in Impact-Echo Measurements – Experimental Results and Numerical Simulations" 9th ECNDT, Berlin, Germany, Proceedings (June 25-29, 2006) on CD.

Alongi, A.J., Clemena, G.G., and Cady, P.D., *Condition Evaluation of Concrete Bridges Relative to Reinforcement Corrosion – SHRP C-101 – Volume 3: Method of Evaluating the Condition of Asphalt-Covered Decks*, Strategic Highway Research Program Report SHRPS-325, Washington, D.C., USA, (1993).

Asano, M., Kamada, T., Kunieda, M., and Rokugo, K., "Impact Acoustics Methods for Defect Evaluation in Concrete" International Symposium on NDE in Civil Engineering, Berlin, Germany, Proceedings (September 16-19, 2003) on CD.

ASTM C 1383, "Test Method for Measuring the P-Wave Speed and the Thickness of Concrete Plates Using the Impact-Echo Method," *2000 Annual Book of ASTM Standards*, Vol. 04.02, ASTM, West Conshohocken, PA, USA.

Bakker, J. D. and Postema, F. J., "Monitoring of ASR in concrete structures: a "smart structure" project"International Non-Destructive Testing in Civil Engineering Conference, ISBN 3931381-49-8, Berlin, Germany, Proceedings (2003).

Barnes, C. L., and Trottier, J.-F., "Ground Penetrating Radar for Network Level Concrete Deck Repair Management," *ASCE Journal of Transportation Engineering,* Vol. 126. No. 3 (2000), pp. 257-262.

Baumann, K., "Practical Example of interpretation of half cell measurements on r.c. structures" 12th International Conference on Structural Faults and Repair, Edinburgh, UK, Proceedings (2008).

Baumann, K., "Practical Example of interpretation of half cell measurements on r.c. structures" 12th International Conference on Structural Faults and Repair, Edinburgh, UK, Proceedings (2008).

Bien, J., Elfgren, L. and J. Olofsson (Eds.), *Sustainable Bridges – Assessment for Future Traffic Demands and Longer Lives*, (TIP3-CT-2003-001653) within the 6th Framework Programme of EU, ISBN 978-7125-161-0, Wroclaw, Poland (2007).

Bien, J., Elfgren, L., Olofsson, J. (Eds.), *Sustainable Bridges – Assessment for Future Traffic Demand and Longer Lives*, Dolnoslaskie Wydawnictwo Edukacyjne, Wroclaw, Poland (2007).

Bjegovic, D., "Advantages and disadvantages in new technologies of rebar protection in concrete" 9th International Conference on Structural Faults and Repair, London, UK, Proceedings (2001).

Böhni, H. And B. Elsener, B., Früherkennung von Bauwerkskonstruktionen: Potentialfeld-messung und galvanostatische Impulstechnik, in: Zerstörungsfreie Prüfung im Bauwesen, Tagungsbericht Int. ZfPBau-Symposium Feb, 27 - March, 1, 1991, Berlin; Ed: Schickert, G., BAM, DGZfP, Berlin, Germany, 1991, 101 – 122.

Braml, T. and Keuser, M., "Beurteilung der Tragfaehigkeit von geschaedigten Stahlbetonbruecken auf der Grundlage der Ergebnisse einer Bauwerkspruefung," *Beton und Stahlbetonbau* Vol. 104, No. 5 (2009).

Broomfield, J.P. , Davies, K and Hladky, K., "The use of permanent corrosion monitoring in new and existing reinforced concrete structures," *Cement and Concrete Composites*, Vol. 24, (2002), pp. 27-34.

Brown, M. C., *Corrosion Protection Service Life of Epoxy-Coated Reinforcing Steel in Virginia Bridge Decks*, PhD thesis, Virginia Polytechnic Institute and State University, Blacksburg, VA, USA (2002).

Bürchler, D. Elsner, B. and Böhni, H., Electrical resistivity and Dielectric Properties of Hardened Cement and Mortar, Institute of Materials Chemistry and Corrosion, Swiss Federal Institute of Technology, ETH Hönggerber, CH-8093 Zurich, Switzerland (1996).

Cardimona, S., Willeford, B., Romero, F., Wenzlick, J., and Anderson, N., *Ground Penetrating Radar Applied to Bridge Deck Condition Studies: A Comparison of Two Instruments and Methodologies*, Report for the Missouri Department of Transportation, UMR Department of Geology and Geophysics Contribution, (May 1999).

Carino, N.J., "The Impact-Echo Method: An Overview," Structures Congress and Exposition, ASCE conference, P.C. Chang (Ed.) Washington, D.C., USA, Proceedings (May 21-23, 2001) 18 pp.

Cement and Mortar, Institute of Materials Chemistry and Corrosion, Swiss Federal Institute of Technology, ETH Hönggerber, CH-8093 Zurich, Switzerland (1996).

Cheng, C. and Sansalone, M., "Determining the Minimum Crack Width That Can Be Detected Using the Impact-echo Method, Part I: Experimental Study," *RILEM Journal of Materials and Structure,* Vol. 28, (1995a).

Cheng, C., and Sansalone, M., "Determining the Minimum Crack Width That Can Be Detected Using the Impact-Echo Method, Part II: Numerical Fracture Analysis," *RILEM Journal of Materials and Structure,* Vol. 28 (1995b).

Cheng, C.C., and Sansalone, M., "Effects of Impact-Echo Signals Caused by Steel Reinforcing Bars

and Voids Around Bars," *ACI Materials Journal*, Vol. 90, No. 5, (1993b), pp. 421-434.

Cheng, C.C., and Sansalone, M., "The Impact-Echo Response of Concrete Plates Containing Delaminations: Numerical, Experimental and Field Studies," *Materials and Structures*, Vol. 26, No. 159, (1993a) pp. 274-285.

Chiaw, C. C. and Harik, I. E., *Performance Evaluation of Concrete Bridge Decks Reinforced with MMFX and SSC Rebars*, Research Report KTC-06-02/FRT 113-01-1F, Kentucky Transportation Center, Lexington, KY, USA, (2006).

Clear, K.C., *Reinforcing Bar Corrosion in Concrete: Effect of Special Treatments*. Special Publication 49. American Concrete Institute, Detroit, MI, USA, (1975) pp. 77–82.

Clemeña, G. G., *Testing of Selected Metallic Reinforcement Bars for Extending the Service Life of Future Concrete Bridges: Summary of Conclusions and Recommendations*, Final Report (No. VTRC 03-R7), Virginia Transportation Research Council, Charlottesville, VA, USA, (2002).

Colla, C., and Pascale, G., "Non-Destructive Defect Location and Sizing in Concrete Columns and Masonry Pillars from Impact-Echo Testing" International Conference on Structural Faults and Repair, Edinburgh, UK, Proceedings (June 13-15, 2006) on CD.

Cziesielski, E. and Marquardt, H., "Auffinden korrodierender Bewehrung mit der elektrochemischen Potentialdifferenzmessung," *Bautechnik* Vol. 65, No. 7, ISSN 0932-8351, (1988) pp. 226 - 232.

El-Safty, A., "Behaviour of RC bridge deck slabs and girders strengthened with CFRP laminates" 12th International Conference on Structural Faults and Repair, Edinburgh, UK, Proceedings (2008).

Elsener, B., "Half-cell potential measurements – Potential mapping on reinforced concrete structures," *Materials and Structures*, Vol. 36 (2003) pp. 461-471.

Gibson, A., and Popovics, J.S., "Lamb Wave Basis for Impact-Echo Method Analysis," *Journal of Engineering Mechanics,* Vol. 131, No. 4 (2005) pp. 438-443.

Gjørv, O. E., Vennesland, Ø, and El-Busiady, A. H. S., "Electrical Resistivity of Concrete in the Oceans" 9th Annual Offshore Technology Conference, Houston TX, USA, Proceedings (May 25, 1977) pp. 581-588.

Gowers, K. R. and Millard, S. G., "Measurement of Concrete Resistivity for Assessment of Corrosion Severity of Steel Using Wenner Technique," *ACI Materials Journal*, Vol. 96, No. 5, (1999) pp. 536-542.

Grimm, C. T., "Demolish Charleston's Brick Walls Because There Is Chloride in the Mortar?," *Journal of Materials in Civil Engineering*, American Society of Civil Engineers, Reston, VA, USA,

Vol. 9, No. 3, (August 1997), 160 pp.

Gruebl, P., Weigler, H. and Karl, S., *Beton; Arten, Herstellung und Eigenschaften*. Ernst & Sohn Verlag fuer Architektur und technische Wissenschaften GmbH, Berlin, Germany (2001).

Gu, P. and Beaudoin, J. J., Obtaining Effective Half-Cell Potential Measurements in Reinforced Concrete Structures, 1998, Construction Technology Update No. 18, National Research Council of Canada.

Gucunski, N., Antoljak, S. and Maher, A., "Seismic Methods in Post Construction Condition Monitoring of Bridge Decks," *Use of Geophysical Methods in Construction,* Geotechnical Special Publication No. 108, Eds. S. Nazarian and J. Diehl, Geo Institute, ASCE (2000) pp. 35-51.

Gucunski, N., Consolazio, G.R. and Maher, A., "Concrete Bridge Deck Delamination Detection by Integrated Ultrasonic Methods," *International Journal Material and Product Technology*, Special Issue on Non-Destructive Testing and Failure Preventive Technology, Vol. 26., No. ½ (2006) pp. 19-34.

Gucunski, N., Feldmann, R., Romero, F., Kruschwitz, S., Abu-Hawash, A., and Dunn, M., "Multimodal Condition Assessment of Bridge Decks by NDE and Its Validation" Mid-Continent Transportation Research Symposium 209, Ames, IA, USA, (August 20 – 21, 2009), Proceeding on CD.

Gucunski, N., Rascoe, C., Huston, D., and Jalinoos, F., "Condition Assessment of Bridge Decks by Complementary Impact Echo and Ground Penetrating Radar Approach" 17th Annual ASNT Research Symposium and Spring Conference, Anaheim, CA, USA, Proceedings (March 31-April 4, 2008b) on CD.

Guide to Durable Concrete (ACI 201.2R-92), ACI Committee 201, American Concrete Institute, Farmington Hills, MI, USA, (1992, reapproved 1997) 41 pp.

Hilsdorf, H. K., Schoenlin, K. and Tauscher, F., *Dauerhaftigkeit von Beton*. Beton-Verlag GmbH, Duesseldorf, Germany (1997).

Hunkeler, F., "The resistivity of pore water solution – a decisive parameter of rebar corrosion and repair methods," *Construction and Building Materials*, Vol. 10 No. 5 (1996) pp. 381-389.

Infrasense, SD2005-05-F, *Feasibility of Using Ground Penetrating Radar (GPR) for Pavements, Utilities, and Bridges*, South Dakota Department of Transportation Office of Research, (August 2006).

Jana, D. and Erlin, B., "Carbonation as an Indicator of Crack Age," *ACI Concrete International*, (May 2007), pp. 39-42.

Krauss, P.D. and Rogalla, E. A., *Transverse Cracking in Newly Constructed Bridge Decks*, Report 380, National Cooperative National Highway Research Program (1996).

Krieger, J., "Erhaltungsmanagement der Bundesfernstrassen, Bedeutung und Perspektiven der ZfPBau-Verfahren" Conference DGzfP Fachtagung Bauwerksdiagnose, Berlin, Germany, Proceedings (2006).

Kruschwitz, S., *Assessment of the complex resistivity behavior of salt affected building materials*, PhD thesis, Technical University Berlin, Germany (2007).

Lausch, R., Knapp, J., and Colla, C., "Influence of Impact Source Frequency on Impact-Echo Data from Testing of Concrete Structures" International Conference on Structural Faults and Repair, London, England, Proceedings (July 4-6, 2001) on CD.

Lemieux, M., Gagné, R., Bissonnette, B. and Lachemi, M., "Behavior of Overlaid Reinforced Concrete Slab Panels Under Cyclic Loading—Effect of Interface Location and Overlay Thickness," *ACI Structural Journal*, (2005).

Lin, J. M., and Sansalone, M., "A Procedure for Determining P-wave Speed in Concrete for Use in Impact-Echo Testing Using a Rayleigh Wave Speed Measurement Technique," *Innovations in Nondestructive Testing*, SP-168, S. Pessiki and L. Olson, Eds., American Concrete Institute, Farmington Hills, MI, USA (1997) pp.137-165.

Lin, J.M., and Sansalone, M.J., "Impact-Echo Studies of Interfacial Bond Quality in Concrete – Part 1-Effects of Unbonded Fraction Area," *ACI Materials Journal,* Vol. 93, No.3 (1996) pp. 318-326.

Lin, J.M., Sansalone, M.J., and Poston, R., "Impact Echo Studies of Interfacial Bond Quality in Concrete – Part 2-Effects of Bond Tensile Strength," *ACI Materials Journal,* Vol. 93, No. 4 (1996) pp. 394-405.

Marquardt, H., "Locating Rebar Corrosion in Concrete Walls by Potential Measurements" IABSE-Colloquium "Saving Buildings in Central and Eastern Europe", Zurich: IABSE/AIPC/ IVBH 1998, Report 77, Proceedings (June 4 - 5, 1998) pp. 38 - 39, ISBN 3-85748-094-8

Maser, K.R., and Rawson, A., "Network Bridge Deck Surveys Using High Speed Radar: Case Studies of 44 Decks (Abridgement)," *Transportation Research Record: Journal of the Transportation Research Board*, No. 1347, National Research Council, Washington, D.C., USA, (1992) pp. 25-28.

Millard S. G. and Gowers, K. R., *The influence of surface layers upon measurement of concrete resistivity*. In: Malhotra VM (Eds). SP126: Durability of Concrete. Detroit, Michigan, USA CANMET/ACI (1991).

Millard, S. G., "Reinforced Concrete Resistivty Measurement Techniques" The Institution of Civil Engineers Part 2 - Research and Theory, Vol. 91, Proceedings (1991) pp. 71-88.

Motz, M., Haller, P., Krueger, M., Grosse, C.U., and Beutel, R., „Impact-Echo: New Developments Regarding Hardware and Software“ International Symposium on NDE in Civil Engineering, Berlin, Germany, Proceedings (September 16-19 2003) on CD.

Naar, S., Sirieix, C., Breysse, D. and X. Derobert, Assessment of water saturation in a reinforced concrete structure: non destructive testing of Tarbes' precast duct, RILEM International Conference on Concrete and Reinforced Concrete, September 5-9, 2005, Moscow, pp. 673-679.

Nawy, E. G. (Ed.), Concrete *Construction Engineering Handbook*, 2nd Edition, CRC Press, Taylor & Francis Group, FL, (2008).

Nazarian, S. and D. Yuan "*Evaluation and Improvement of Seismic Pavement Analyzer*," Research Project Report 7-2936, The Center for Highway Materials Research, The University of Texas at El Paso, El Paso, USA (1997).

Nazarian, S., Baker, M., and Crain, K., *Development and Testing of a Seismic Pavement Analyzer*, Report SHRP-H-375, Strategic Highway Research Program, National Research Council, Washington, D.C., (1993).

Nazarian, S., Baker, M.R. and Crain, K., *Development and Testing of a Seismic Pavement Analyzer*, Report SHRP-H-375, Strategic Highway Research Program, National Research Council, Washington, D.C. (1993a).

Nazarian, S., Stokoe, K. H., II, and Hudson, W. R., "Use of spectral analysis of surface waves method for determination of moduli and thicknesses of pavement systems," *Transportation Research Record*, No.930, National Research Council, Washington, D.C. (1983), pp. 38-45.

Nuernberger, U., *Korrosion und Korrosionsschutz im Bauwesen*, Issue 1, Bauverlag Berlin, Germany, (1995).

Page, C. L., Bamforth, P. B. and Figg, J. W. (Eds.), *Corrosion of Reinforcement in Concrete Construction*, Royal Society of Chemistry, Cambridge, UK, (1996).

Pape, J. and Fanous, F., "Impact of Bridge Deck Cracking on Durability" Transportation Conference, Proceedings (1998).

Parrillo, R, Roberts, R and Delea, D. "Comparison of 2 GHz Horn Antenna and 1.5 GHz Ground Coupled Antenna for Bridge Deck Condition Assessment Using GPR" International Conference on Structural Faults and Repair, Edinburgh, UK, Proceedings (June 13-15, 2008) on CD.

Pascale, G., and Colla, C., "Wave Propagation Based Assessment of Cylindrical Concrete Elements," 9th ECNDT, Berlin, Germany, Proceedings (June 25-29, 2006) on CD.

Peralta, D.F., *Non-Destructive Evaluation of Bridge Decks,* Master of Science Thesis, Massachusetts Institute of Technology, Department of Civil and Environmental Engineering, USA, (1997) 101 pp.

Petersen, C.G., Davis, A., and Delahaza, A., "Impact-Echo Testing for Delaminations in the Walls of a Marine Structure" International Conference on Structural Faults and Repair, London, UK, Proceedings (July 1-3, 2003) on CD.

Pincheira, J. A., Aramayo, A. A., Kim, K. S., and Fratta, D., *Corrosion Protection Performance of Epoxy-Coated Reinforcing Bars*, Final Report, Minnesota Department of Transportation, St. Paul, MN, USA, (2008).

Rivard, P. and Saint-Pierre, F., "Assessing alkali-silica reaction damage to concrete with non-destructive methods: From the lab to the field," *Construction and Building Materials*, Vol. 23, (2009) pp. 902-909.

Roberts, G. E., and Amrol, J. J., *Concrete Cover Determination Using Ground Penetrating Radar (GPR*), United States Department of Transportation (Federal Highway Administration—FHWA) Priority Technology Program, Project No. NH1997-01, State of New Hampshire Department of Transportation, Bureau of Materials & Research Final Report; (August, 1999).

Roberts, G., E., Roberts, R., L., and Tarussov, A., "Identifying Concrete Deterioration using Ground Penetrating Radar Technology" Annual ASNT Fall Conference, Proceedings (November 2001).

Roberts, R. L., and Romero, F. A., "High-Resolution GPR Bridge Deck Evaluation Surveys" International Conference on Corrosion and Rehabilitation of Reinforced Concrete Structures, FHWA-SA-99-01, Proceedings (December 7-11, 1999).

Rojas, J., Nazarian, S., Tandon, V. and Yuan, D., "Quality Management of Asphalt-Concrete Layers Using Wave Propagation Techniques," *Journal of Association of Asphalt Paving Technologists*, Vol. 68 (1999) pp. 450-478.

Romero, F. A., and Roberts, R. L., "Data Collection, Processing and Analysis Challenges—GPR Bridge Deck Deterioration Assessment of Two Unique Bridge Deck Systems" Symposium on the Application of Geophysics to Engineering and Environmental Problems (SAGEEP), Colorado Springs, CO, USA, Proceedings (February 2004) Paper #223

Romero, F. A., and Roberts, R. L., "Mapping Concrete Deterioration: High-Speed Ground Penetrating Radar Surveys on Bridge Decks Using New Analysis Method Based on Dual-Polarization Deployment of Horn Antennae" International Bridge Conference, Pittsburgh, PA, USA, Proceedings (June 10-12, 2002).

Romero, F. A., and Roberts, R. L., "The Evolution in High-Resolution Ground Penetrating Radar

Rosenberg, A., *How to prevent corrosion in precast concrete, Technical section – manufactured concrete*, National Precast Concrete Association, Indianapolis, USA, (1999).

Sansalone, M. J. and W. B. Street, *Impact-Echo - Nondestructive Evaluation of Concrete and*

Masonry, Bullbrier Press, Ithaca, New York (1997).

Sansalone, M. J., "Detecting Delaminations in Concrete Bridge Decks with and without Asphalt Overlays Using an Automated Impact-Echo Field System" British Institute of Non-Destructive Testing International Conference *NDT in Civil Engineering* Liverpool, U.K., Proceedings (April 14-16, 1993) pp. 807-820.

Sansalone, M., and Carino, N.J., "Detecting Delaminations in Concrete Slabs with and without Overlays Using the Impact-Echo Method," *Journal of American Concrete Institute,* Vol. 86, No.2 (1989) pp. 175-184.

Sansalone, M., and Carino, N.J., *Impact-Echo: A Method for Flaw Detection in Concrete Using Transient Stress Waves*, NBSIR 86-3452, National Bureau of Standards, (September 1986) 222 pp.

Sagues, A. A., Lee, J. B., Chang, X., Pickering, H., Nystrom, E., Carpenter, W. Kranc, S. C., Simmons, T., Boucher, B., and S. Hierholzer, Corrosion of Epoxy Coated Rebar on Florida Bridges. Final Report, Florida Department of Transportation, 1995.

Schubert, F. and Koehler, B. "Ten Lectures on Impact-Echo," *Journal of Nondestructive Evaluation,* Vol. 27 (2008) pp. 5-21.

Siemes, A.J.M., and J. D. Bakker, "Evaluation of the Institution of Structural Engineers Procedure on Concrete Structures with Alkali-Silica Reaction in the Netherlands" 11th International Conference on AAR in concrete, Quebeck City, Canada, Proceedings, (2000) pp. 1195-1214

Smith, J. L. and Virmani, Y. P., *Performance of Epoxy Coated Rebars in Bridge Deck*, Report FHWA-RD-96-092, Federal Highway Administration, Washington D.C., USA, (1996).

Sohanghpurwala, A.A. and Scannell, W.T., *Condition and Performance of Epoxy-Coated Rebars in Bridge Decks, Public Roads*, Federal Highway Administration, Washington D.C., USA, (1999).

Surveys from Ground-Coupled to High-Speed, Air-Coupled Evaluations" Structural Materials Technology V: An NDT Conference, Cincinnati, *OH,* USA, Proceedings (Fall 2002).

Uijl J.A. and Kaptijn, N., Structural consequences of ASR: an example of shear capacity, HERON, Delft, The Netherlands, Vol. 47, No. 2, (2002) pp. 125-139.

Uijl, J. A., Kaptijn, N. and Walraven, J. C., "Shear Resistance of Flat Slab Bridges Affected by ASR" 11th international conference on AAR in concrete, Quebeck City, Canada, Proceedings, (2000) pp. 1129-1138.

Vittery, J. P. and Pearson-Kirk, D., "Sulfate induced deterioration of above ground components of highway structures" 12th International Conference on Structural Faults and Repair, Edinburgh, UK, Proceedings (2008).

Whiting, D. A. and Nagi, M. A. (Eds.), *Electrical Resistivity of Concrete – A Literature Review*, PCA R&D Serial No. 2457, Portland Cement Association, Skokie, IL, USA, (2003) 57 pp.

Whitman, W.E., Jalinoos, F., Sirles, P., and K. Hanna (2003), "Application of Geophysical Methods to Highway Related Problems," Publication No. FHWA-IF-04-021, Federal Highway Administration, Office of Bridge Technology, Washington, D.C., 742 pp.

Wiolet, A. P., Weyers, R. E., Weyers, R. M., Mokarem, D. W.Zemajtis, J. Sprinke, M. M., and Dillard, J. G., *Field Performance of Epoxy-Coated Reinforcing Steel in Virginia Bridge Decks*, Final Report (VTCR 00-R16), Virginia Transportation Research Council, Charlottesville, VA, USA (2000).

Yuan, D, Nazarian, S. Chen, D, and Hugo, F., "Use of Seismic Pavement Analyzer in Monitoring Degradation of Flexible Pavements Under Texas Mobile Load Simulator (A Case Study)," *Transportation Research Record*, No. 1615, Washington, D.C., (1999) pp. 3-10.

Websites:

http://www.e-archives.ky.gov/Pubs/transportation/TC_Rpt/KTC_06_02_FRT_113_01_1F.pdf (As of August 2009)

http://www.dot.state.fl.us/research-center/Completed_Proj/Summary_SMO/FDOT_805a.pdf (As of August 2009)

http://www.pcte.com.au/Lecture-Slides.aspx (As of August 2009)